

Copyright Notices

Notice 1

Under the Copyright Act 1968, this thesis must be used only under the normal conditions of scholarly fair dealing. In particular no results or conclusions should be extracted from it, nor should it be copied or closely paraphrased in whole or in part without the written consent of the author. Proper written acknowledgement should be made for any assistance obtained from this thesis.

Notice 2

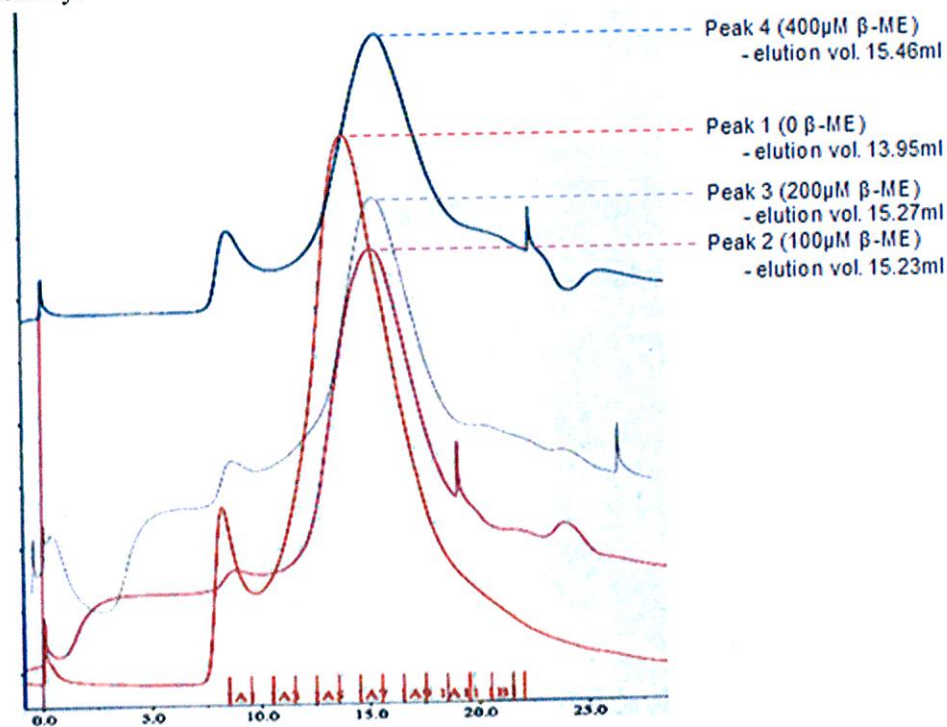
I certify that I have made all reasonable efforts to secure copyright permissions for third-party content included in this thesis and have not knowingly added copyright content to my work without the owner's permission.

ADDENDUM

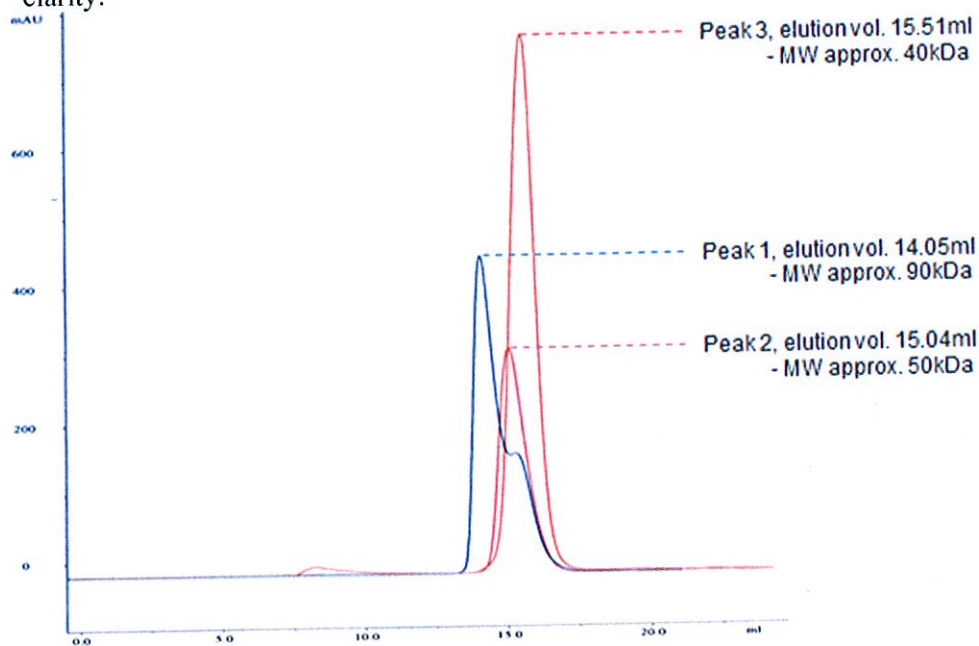
Page 48, lines 16 & 17: Delete "KPO₄" and read "potassium phosphate". Comment: At the pH specified, potassium phosphate buffer will be comprised of K₂HPO₄ and KH₂PO₄.

Page 62, column 2, para 4: "T_m", representing melting temperature, should read "apparent T_m". This amendment also applies at Page 64, column 1, para 1 and Page 64, Figure 7.

Page 81, figure 4.9: The body and labels of this figure should appear as follows for improved clarity:



P100, figure 5.4C: The body and labels of this figure should appear as follows for improved clarity:

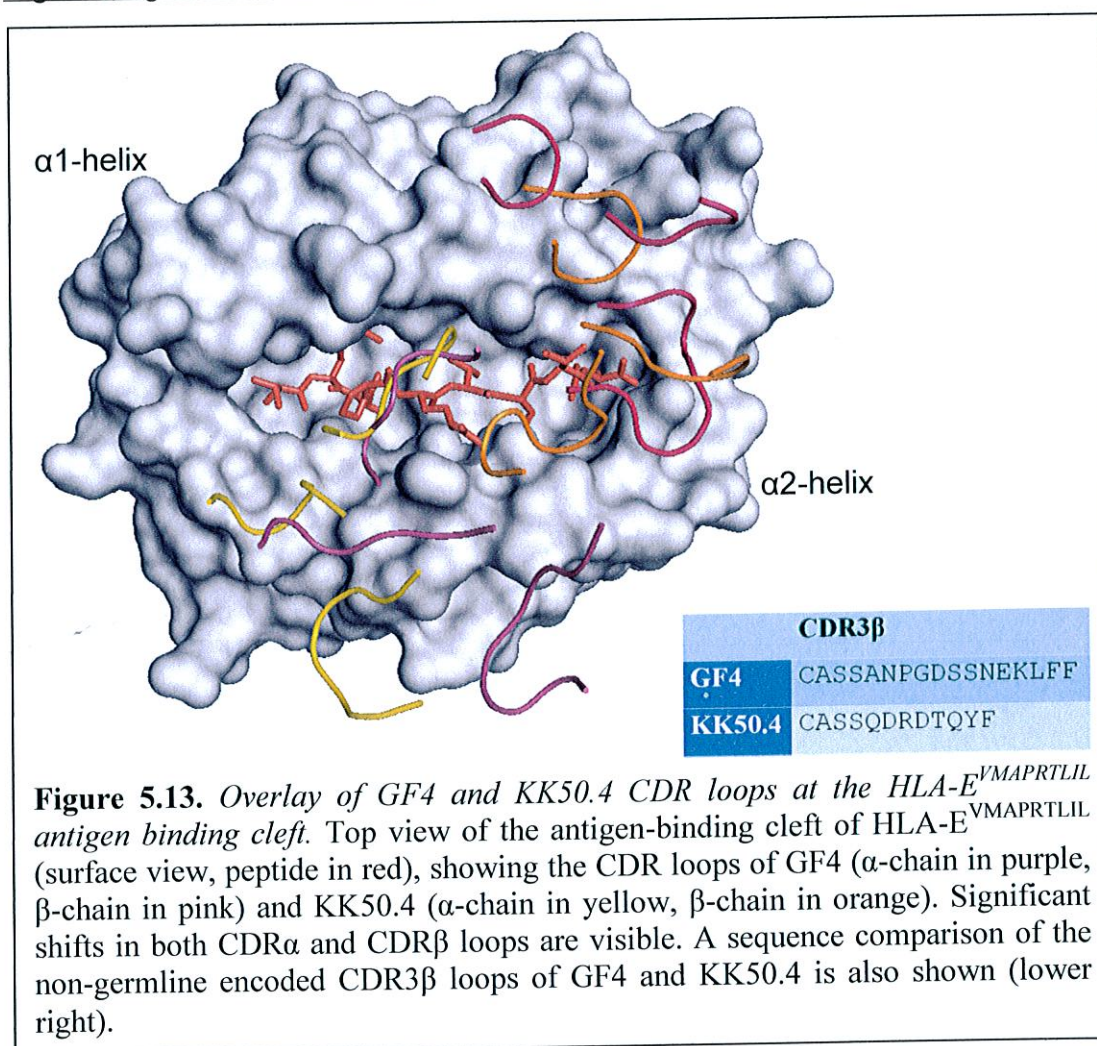


Page 104, line 8: Comment: All Matthews coefficients mentioned were calculated using the 'Matthews' cell content analysis program from the CCP4 suite (*Collaborative Computational Project, 1994*). This comment also applies to Page 104, para 2, line 4 as well as Page 115, line 16 and Page 115, para 2, line 8.

Page 116, para 4: Delete this paragraph, which continues on Page 117. The paragraph should read instead:

"Successive rounds of maximum-likelihood refinement were carried out using the REFMAC5 program in the CCP4 suite (*Collaborative Computational Project, 1994*), with the same parameters as for GF4:HLA-E^{VMAPRTLVL}. These parameters are described above in *Structure Solution and Refinement of GF4:HLA-E^{VMAPRTLVL}*. The finalised GF4:HLA-E^{VMAPRTLIL} structure was analysed using MolProbity (*Chen et al., 2010*), the CONTACT and AREAIMOL programs from the CCP4 suite (*Collaborative Computational Project, 1994*) and PyMOL (version 1.3) (*Schrodinger LLC*). The parameters within which these programs were used are also described above in *Structure Solution and Refinement of GF4:HLA-E^{VMAPRTLVL}*."

Page 121, figure 5.13: The whole figure should appear as follows for improved clarity:



A Structural Investigation of Human Class Ib Major Histocompatibility Complex Molecules in Innate and Adaptive Immunity

Nicholas George Walpole

Bachelor of Science (Science Scholars Program) (Honours)

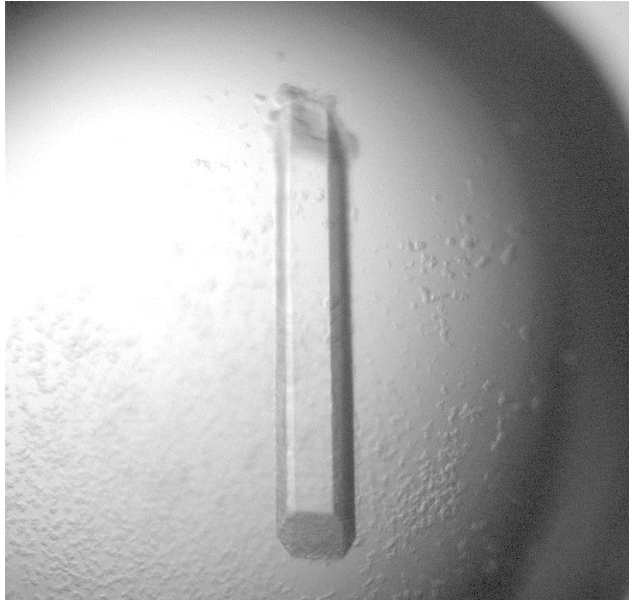
Submitted to comply with the requirements of the degree of Doctor of Philosophy
18th of April 2012

Submitted with amendments
22nd of August 2012

Department of Biochemistry and Molecular Biology
School of Biomedical Sciences
Faculty of Medicine, Nursing and Health Sciences



MONASH University



*It is important that students bring a certain ragamuffin,
barefoot irreverence to their studies; they are not here to
worship what is known, but to question it.*
Jacob Bronowski in *The Ascent of Man* (1975)

Table of Contents

Table of Contents	iii
Thesis Summary	vi
Declarations	viii
Copyright Notices	x
Acknowledgements	xi
List of Abbreviations	xii
List of Figures and Tables	xvi
Publications arising from this PhD	xviii
 Chapter One – Introduction	 1
<i>Introduction to the Human Innate and Adaptive Immune Responses</i>	1
<i>Introduction to Human Leukocyte Antigen (HLA)</i>	2
<i>Introduction to HLA-G</i>	6
<i>HLA-G in Pregnancy</i>	8
<i>HLA-G in Cancer and Organ Transplantation</i>	10
<i>HLA-G: Peptide Binding and Structural Considerations</i>	11
<i>Introduction to HLA-E</i>	17
<i>Role of HLA-E in Innate Immunity</i>	19
<i>HLA-E: Peptide Binding and Structural Considerations</i>	19
<i>Receptors of Class Ib MHC</i>	21
<i>Receptors of HLA-G</i>	22
- <i>KIR2DL4 and the KIR family</i>	22
- <i>Leukocyte Ig-like Receptors (LILRs)</i>	28
<i>Receptors of HLA-E</i>	30
- <i>CD94/NKG2 Receptors</i>	30
- <i>$\alpha\beta$ T-cell Receptors (TcRs)</i>	32
<i>Class Ib MHCs in Adaptive Immunity</i>	36
- <i>HLA-G</i>	36
- <i>HLA-E</i>	37
- <i>Other Class Ib MHC</i>	39
 Chapter Two – Materials and Methods	 41
<i>DNA</i>	41
- <i>Plasmid preparation</i>	41
- <i>Sequencing</i>	41
- <i>Restriction endonuclease digestion and cloning</i>	42
<i>Transformation</i>	42
- <i>Preparation of electrocompetent cells</i>	42
- <i>Transformation by electroporation</i>	42
<i>Production of KIR2DL4</i>	43
- <i>Insect cell expression system - Preparation and amplification of viral stocks</i>	43
- <i>Insect cell expression system - Expression of recombinant KIR2DL4</i>	43
- <i>Mammalian cell expression system</i>	44
<i>Production of MHC HC, β_2-m, TcR α- and β-chains</i>	45
- <i>Protein expression</i>	45

- Isolation of inclusion bodies	46
Generation of correctly folded protein	46
- pMHC complexes	46
- $\alpha\beta$ TcR	47
Crystallisation	49
Crystallography	50
Biophysical Analysis Techniques	51
- Circular Dichroism (CD) Spectrum Analysis	51
- Small Angle X-ray Scattering (SAXS)	51
Chapter Three – The effect of peptide binding on HLA-G	53
Commentary	53
Publication: <i>The Structure and Stability of the Monomorphic HLA-G Are Influenced by the Nature of the Bound Peptide</i>	55
Chapter Four – Characterisation of KIR2DL4	69
KIR2DL4 Production using a Baculoviral Expression System	70
Crystallisation of Baculovirus-Expressed KIR2DL4	73
KIR2DL4 Production using a Mammalian Cell Expression System	76
Deglycosylation of Mammalian-Expressed KIR2DL4	79
Biophysical Analysis of Baculovirus-Expressed KIR2DL4	79
- Dimerisation and Oligomerisation of Recombinant KIR2DL4	79
- Association with HLA-G	85
Small Angle X-ray Scattering (SAXS) of Baculovirus-Expressed KIR2DL4	86
Discussion	93
Chapter Five – Structural Investigation of an HLA-E restricted T-cell response	95
HLA-E and GF4 TcR Production and Copurification of the Ternary Complexes	96
Crystallisation of GF4:HLA-E ^{VMAPRTLVL} and Data Collection	101
Structure Solution and Refinement of GF4:HLA-E ^{VMAPRTLVL}	105
Major Features of the GF4:HLA-E ^{VMAPRTLVL} Structure	107
Recognition of pHLA-E by the GF4TcR	112
Crystallisation of GF4:HLA-E ^{VMAPRTLIL} and Data Collection	114
Structure Solution and Refinement of GF4:HLA-E ^{VMAPRTLIL}	115
Major Features of the GF4:HLA-E ^{VMAPRTLIL} Structure & Comparison with GF4:HLA-E ^{VMAPRTLVL}	117
Discussion	119
Comparison with KK50.4 TcR:HLA-E ^{VMAPRTLIL}	119
Comparison with TcR recognition of MHC-Ia	123
Concluding Remarks	126
Chapter Six – Discussion and Future Directions	127
Peptide Presentation by Class Ib MHC	127
Roles of Class Ib MHC in Adaptive Immunity	127
Future Directions	130
- pHLA-G Structural Studies	130

- <i>KIR2DL4</i>	130
- <i>TcR Recognition of pHLA-E</i>	132
<i>Concluding Remarks</i>	133
Bibliography	134
Appendix 1 – Commercial 48- and 96-well Crystallographic Screens	150
<i>The Sigma-Aldrich Basic Grid for Proteins (Sigma-Aldrich) (48-well)</i>	150
<i>The PEG/Ion Screen (Hampton Research) (48-well)</i>	151
<i>The PACT Suite (Qiagen) (96-well)</i>	153
<i>JCSG+ (Qiagen) (96-well)</i>	156

Thesis Summary

While the Human Leukocyte Antigen (HLA) locus is the most polymorphic region in the human genome, Major Histocompatibility Complex Class Ib (MHC-Ib) molecules display far less polymorphism and variation than the structurally similar MHC Class Ia (MHC-Ia) molecules. From an evolutionary perspective, the polymorphism of MHC-Ia stems from the advantage conferred by a heterozygotic MHC-Ia genotype, due to the recognised role of antigen presentation to clonotypic $\alpha\beta$ T-cell receptors (TcRs) in the adaptive immune system. In contrast, the primary roles of the various MHC-Ib molecules are in the regulation of the innate immune system, roles which are generally independent of allele variation. Indeed, the two most extensively studied Class Ib molecules in humans, HLA-G and HLA-E, are essentially monomorphic at the amino acid level, though a limited number of polymorphisms have been found in healthy individuals.

The role of HLA-G in regulating the innate immune response to the semi-allogeneic foetus in pregnancy has been a recent focus of research in reproductive biology. Little is known about the role of the peptide presented by HLA-G in this context, though the crystal structure of HLA-G presenting the endogenous peptide RIIPRHLQL, has been determined in both monomeric (*Clements et al.*, 2005) and dimeric (*Shiroishi et al.*, 2006a) forms. It has been proposed that the nature of the bound peptide may influence binding to Natural Killer (NK) cell receptors of the Leukocyte Immunoglobulin-like Receptor (LILR/LIR/ILT) family, as well as KIR2DL4, a member of the Killer Immunoglobulin-like Receptor (KIR) family of NK receptors. Therefore, the structure of HLA-G was determined with two further endogenous peptides, KLPAQFYIL and KGPPAALTL, in order to investigate the effect of the bound peptide on the conformation of HLA-G. KIR2DL4, which also displays significantly less polymorphism relative to other members of the KIR family, was expressed recombinantly and studied using biochemical techniques including circular dichroism (CD) analysis and small angle x-ray scattering (SAXS) as part of the wider aim of solving the crystal structure of this NK receptor.

HLA-E performs a distinct role in regulating the innate immune response, mediated by the presentation of related peptides, derived from the leader sequence of MHC-I

molecules, to NK receptors of the CD94/NKG2 family. This role forms part of the ‘missing self’ reaction, with downregulation of pMHC-I (peptide/MHC-I) production (for example, in infected or damaged cells) resulting in downregulation of pHLA-E presentation and knockout of signals inhibiting NK cell-mediated lysis. Constitutive, activatory signals present in the NK cell are then able to mediate lysis of the infected or damaged cell.

While the structure of HLA-E has been solved with several peptides and also in complex with CD94/NKG2A, a role in the adaptive immune system has recently been proposed based on the discovery of HLA-E-restricted T-cell populations in several individuals with latent or resolved Cytomegalovirus (CMV) infections. It has been proposed that the product of the open reading frame UL40 (a Type 1 membrane protein) of some CMV strains has evolved to contain mimotopes of the MHC-I leader sequences, and that in infected individuals whose MHC-I haplotypes do not match the viral mimotopes, a T-cell response may be generated (*Ulbrecht et al., 2000*).

Based on the haplotypes of individuals, a range of non-self pHLA-E-reactive TcRs may be generated. To date, two groups of HLA-E restricted TcR have been characterised, based on peptide recognition patterns (*Pietra et al., 2003*). The TcRs GF4 (Group 1) and KK50.4 (Group 2) have been isolated as representative of each of these groups. To investigate the mechanism of this TcR:MHC-Ib interaction, the crystal structure of GF4 has been determined in complex with HLA-E presenting the two related peptides VMAPRTLVL and VMAPRTLIL. These structures have enabled comparison with the previously determined KK50.4:HLA-E^{VMAPRTLIL} complex structure (*Hoare et al., 2006*) as well as those of MHC-Ia:TcR complexes.

Collectively, the work presented in this thesis has provided insight into the basis of peptide presentation and subsequent TcR recognition by MHC-Ib molecules in humans.

General Declaration

In accordance with Monash University Doctorate Regulation 17 / Doctor of Philosophy and Master of Philosophy (MPhil) regulations the following declarations are made:

I hereby declare that this thesis contains no material which has been accepted for the award of any other degree or diploma at any university or equivalent institution and that, to the best of my knowledge and belief, this thesis contains no material previously published or written by another person, except where due reference is made in the text of the thesis.

This thesis includes one original paper published in a peer-reviewed journal. The core theme of the thesis is Structural Studies of Class Ib MHC Molecules in Humans. The ideas, development and writing up of all the papers in the thesis were the principal responsibility of myself, the candidate, working within the Protein Crystallography Unit under the supervision of Prof. Jamie Rossjohn and Dr. Craig Clements.

The inclusion of co-authors reflects the fact that the work came from active collaboration between researchers and acknowledges input into team-based research.

In the case of Chapter 3 my contribution to the work involved the following:

Thesis chapter	Publication title	Publication status	Nature and extent of candidate's contribution
3	The Structure and Stability of the Monomorphic HLA-G Are Influenced by the Nature of the Bound Peptide	Published	Experimental design – protein production and purification; Conduct of research – protein crystallisation, data collection, structural determination and refinement studies; Data analysis and revision of manuscript

Signed:

Date:

Declaration for Thesis Chapter 3

Declaration by candidate

In the case of Chapter 3, 'The effect of peptide binding on HLA-G' the nature and extent of my contribution to the work was the following:

Nature of contribution	Extent of contribution (%)
Experimental design – protein production and purification; Conduct of research – protein crystallisation, data collection, structural determination and refinement studies; Data analysis and revision of manuscript	40%

The following co-authors contributed to the work. Co-authors who are students at Monash University must also indicate the extent of their contribution in percentage terms:

Name	Nature of contribution	Extent of contribution (%) for student co-authors only
Lars Kjer-Nielsen ²	Conduct of research – protocol design	N/A
Lyudmila Kostenko ²	Conduct of research – protocol design	N/A
James McCluskey ²	Conception; manuscript revisions	N/A
Andrew Brooks ²	Conception; manuscript revisions	N/A
Jamie Rossjohn ¹	Conception; manuscript revisions	N/A
Craig Clements ¹	Conception; manuscript preparations	N/A

Candidate's
Signature

	Date 22/08/2012
---	--------------------


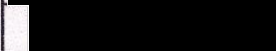
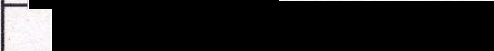
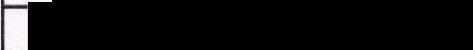
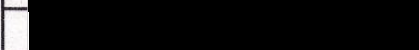
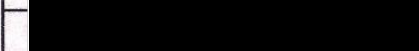
Declaration by co-authors

The undersigned hereby certify that:

1. the above declaration correctly reflects the nature and extent of the candidate's contribution to this work, and the nature of the contribution of each of the co-authors.
2. they meet the criteria for authorship in that they have participated in the conception, execution, or interpretation, of at least that part of the publication in their field of expertise;
3. they take public responsibility for their part of the publication, except for the responsible author who accepts overall responsibility for the publication;
4. there are no other authors of the publication according to these criteria;
5. potential conflicts of interest have been disclosed to (a) granting bodies, (b) the editor or publisher of journals or other publications, and (c) the head of the responsible academic unit; and
6. the original data are stored at the following location(s) and will be held for at least five years from the date indicated below:

Location(s)

1. Department of Biochemistry and Molecular Biology, Monash University, Clayton, Victoria
2. Department of Microbiology and Immunology, University of Melbourne, Parkville, Victoria

	Signature	Date
Lars Kjer-Nielsen ²		18/1/2012
Lyudmila Kostenko ²		18/1/2012
James McCluskey ²		01/02/2012
Andrew Brooks ²		23/1/2012
Jamie Rossjohn ¹		8/2/12
Craig Clements ¹		15/2/12

Copyright Notices

Notice 1

Under the Copyright Act 1968, this thesis must be used only under the normal conditions of scholarly fair dealing. In particular no results or conclusions should be extracted from it, nor should it be copied or closely paraphrased in whole or in part without the written consent of the author. Proper written acknowledgement should be made for any assistance obtained from this thesis.

Notice 2

I certify that I have made all reasonable efforts to secure copyright permissions for third-party content included in this thesis and have not knowingly added copyright content to my work without the owner's permission.

Acknowledgements

It almost goes without saying that the primary inspiration for any student performing any serious research will come from their supervisor, or supervisors, and that has certainly been the case with this body of work. I would like to thank my PhD supervisors Prof Jamie Rossjohn and Dr Craig Clements for providing that inspiration, dating back to my first days in the Rossjohn Lab in 2005, and also for providing the resources and advice that has made the work described in this publication possible.

A number of post-doctoral researchers in the Rossjohn Lab, both 'early career' and senior, have proven invaluable with technical advice and words of wisdom useful both in and out of the laboratory setting. Dr Travis Beddoe, Dr Hugh Reid, Dr Stephanie Gras, Dr Richard Berry and Dr Emma Petrie have all been most generous with wisdom generated from experience, and I have always been glad to benefit from that experience.

The many collaborators of the Rossjohn Lab, and the Class Ib projects in particular, all deserve thanks, with special thanks going to Dr Andrew Brooks, Dr Lucy Sullivan and other members of the Brooks Lab in the Department of Microbiology and Immunology at the University of Melbourne, for taking me under their wing when I ventured out of the Protein Crystallography Unit and into the terrifying, yet exciting, world of immunology.

Technical advice aside, there are many people that deserve recognition. My friends, both in and out of the Department of Biochemistry and Molecular Biology, have been marvellous in providing support and encouragement, and while I will always be guilty of missing many worthy names, the Rossjohn Lab would have been a different place but for the likes of Dr Sophie Broughton, Dr Kwok Wun, Dr Andy Welland, Dr Jerome Le Nours, Dr Julia Archbold, Dr Julian Vivian, Steven Scally, Maya Olshina, Li Zeng, Andy Clarke and Adam Shahine, some of whom have also provided proof that hard work results in grand rewards, and others of whom will no doubt have their well-deserved rewards in the near future.

My family have been a constant source of unconditional love and support, and this has been priceless in ways too numerous to mention. Mum, Dad, Lisa and Amanda all deserve a thousand thanks, as well as my grandparents (thanks to Gran and Grandad, and many more to Nanna who lives on in our hearts) who have always been a source of inspiration in all walks of life. It goes without saying that I would not be the person I am without them, but I am extremely thankful to have such a wonderful family, each of whom, time and again, have gone above and beyond the call.

My final thanks are reserved for someone who has shown me, at every step of our journey together, that she understands everything that I have felt, someone who has provided at various times a carrot, a stick, a pillar of support, a listening ear and words of wisdom. To my partner Natalie, who has shown in herself an inspirational ability to rise above any hardship, I offer my deepest thanks, and an everlasting place in my heart.

List of Abbreviations

°	degrees
Å	Angstrom
Ac	acetate
Ag	antigen
Ala	alanine (single letter code: A)
Arg	arginine (single letter code: R)
Asn	asparagine (single letter code: N)
Asp	aspartate (single letter code: D)
β ₂ -m	β ₂ -microglobulin, the light chain observed in MHC Class I molecules
β-ME	β-mercaptoethanol, a.k.a. 2-mercaptoethanol
BSA	bovine serum albumin
C	carbon
CD	circular dichroism
CD4+	a class of T-cells, based on the receptors expressed
CD8+	a class of T-cells, based on the receptors expressed
CD94/NKG2	a family of receptors found on NK cells
cDNA	cyclic deoxyribonucleic acid
CDR	complimentarity determining region
Cl	chlorine
CMV	Cytomegalovirus, a member of the herpesvirus group
Co	cobalt
CTL	cytotoxic T-lymphocyte
Cys	cysteine (single letter code: C)
Da	Dalton (see also kDa, kilo Dalton)
DEAE	diethylaminoethyl cellulose
DMEM	Dulbecco's modified eagle medium
DNA	deoxyribonucleic acid
DTT	dithiothreitol
EK	enterokinase
EndoH	endoglycosidase H
ER	endoplasmic reticulum
FACS	fluorometry-assisted cell sorting
FCS	fetal calf serum

Gln	glutamine (single letter code: Q)
Glu	glutamate (single letter code: E)
Gly	glycine (single letter code: G)
H	hydrogen
H-2D	a murine MHC Class Ia molecule
H-bond	hydrogen bond
HC	heavy chain of an MHC class I molecule
HEK293	human embryonic kidney 293 (cell line)
HFE	human hemochromatosis protein, a human MHC Class Ib molecule
HIC	hydrophobic interaction chromatography
His	histidine (single letter code: H)
HIV	human immunodeficiency virus
HLA	human leukocyte antigen
hrs	hours
Hsp60	heat shock protein 60
Ig	immunoglobulin
Ile	isoleucine (single letter code: I)
ILT	see LILR
IPTG	isopropyl-1-thio- β -D-galactopyranoside
ITAM	intracellular tyrosine activating motif
ITIM	intracellular tyrosine inhibitory motif
K	potassium
kDa	kilo Dalton
KIR	killer immunoglobulin-like receptor, a family of receptors found on NK cells
LB	Luria-Bertani medium
Leu	leucine (single letter code: L)
LILR	leukocyte immunoglobulin-like receptor, a.k.a. immunoglobulin-like transcript (ILT)
Lys	lysine (single letter code: K)
Met	methionine (single letter code: M)
Mg	magnesium
MHC	major histocompatibility complex
mRNA	messenger ribonucleic acid
MW	molecular weight

MWCO	molecular weight cut-off
N	nitrogen
Na	sodium
NaEDTA	sodium ethylene diamine tetra-acetic acid
NCS	non-crystallographic symmetry
NK	natural killer cell
nm	nanometres
O	oxygen
OD	optical density
ORF	open reading frame
PCR	polymerase chain reaction
PDB	protein data bank
PEG	polyethylene glycol
PEI	polyethylenimine
Phe	phenylalanine (single letter code: F)
pHLA	HLA presenting bound peptide
pMHC	MHC presenting bound peptide
PMSF	phenylmethylsulfonyl fluoride
Pro	proline (single letter code: P)
PTK	phosphatase tyrosine kinase
Qa-1 ^b	a murine MHC Class Ib molecule
Qa-2	a murine MHC Class Ib molecule
Qdm	Qa-1 determinant modifier - a 9 amino-acid peptide (AMAPRTLTL) derived from the leader sequence of murine MHC class I molecules and presented by Qa-1 ^b
R_{cryst}	crystallographic R-factor
R_{free}	free R-factor
R_g	radius of gyration
R_{max}	maximal radius
R_{merge}	a measure of the internal agreement of symmetry-related measurements within crystallographic data
RNA	ribonucleic acid
R_{pim}	as for R_{merge} , but weighted for multiplicity of data
RSA	recurrent spontaneous abortion
RT	room temperature
SAXS	small-angle x-ray scattering

SDS-PAGE	sodium dodecyl sulphate – polyacrylamide gel electrophoresis
Ser	serine (single letter code: S)
SPR	surface plasmon resonance
TAP	transporter associated with antigen processing
TcR	T-cell receptor, composed of one α -chain and one β -chain unless specified
TE	a buffer, composed of 10mM Tris-HCl (pH 8.0) and 1mM NaEDTA
Thr	threonine (single letter code: T)
T _m	thermal stability, the temperature at which a protein sample is 50% denatured
Trp	tryptophan (single letter code: W)
Tyr	tyrosine (single letter code: Y)
UTR	untranslated region – may be either 3' or 5' of a gene
UV	ultraviolet (light)
Val	valine (single letter code: V)
VDW	van der Waals

List of Figures and Tables

Figure 1.1. <i>Structures of MHC Class I and II</i>	3
Figure 1.2. <i>Conformation of bound peptide in pHLA-A2</i>	5
Figure 1.3. <i>Splice variants of HLA-G</i>	7
Table 1.1. <i>Downstream effects of HLA-G signalling</i>	8
Figure 1.4. <i>Accommodation of the peptide within the HLA-G antigen-binding cleft</i>	12
Table 1.2. <i>HLA-G peptide ligands</i>	13
Figure 1.5. <i>Peptide conformation within the HLA-G binding cleft</i>	15
Figure 1.6. <i>Comparison of HLA-G, HLA-E and HLA-A2 peptide binding positions</i>	15
Figure 1.7. <i>Structure of the HLA-G homodimer</i>	16
Figure 1.8. <i>NK responses to HLA-E signalling events</i>	18
Table 1.3. <i>HLA Class I leader sequence peptides</i>	20
Figure 1.9. <i>Comparison of HLA-E peptide binding conformations</i>	21
Figure 1.10. <i>Receptors of MHC-Ib</i>	22
Table 1.4. <i>KIR family receptors</i>	23
Figure 1.11. <i>KIR family domain configurations</i>	24
Figure 1.12. <i>Structures of KIR2DL1 and KIR2DS2</i>	25
Figure 1.13. <i>Structures of HLA-Cw4:KIR2DL1 and HLA-B*5701:KIR3DL1</i>	27
Figure 1.14. <i>Structures of HLA-A2:LILRB1 and HLA-G:LILRB2</i>	29
Table 1.5. <i>LILR family receptors</i>	29
Figure 1.15. <i>CD94/NKG2 receptors</i>	30
Figure 1.16. <i>Structure of CD94/NKG2A:HLA-E^{VMAPRTLFL}</i>	32
Figure 1.17. <i>TcR:pMHC interactions</i>	34
Figure 1.18. <i>A T-cell response to HLA-E signalling events</i>	38
Table 2.1. <i>Peptides used for generation of folded pMHC</i>	47
Table 2.2. <i>Optimised crystallisation conditions of pHLA-G and GF4:pHLA-E complexes</i>	49
Ch.3 Fig. 1. <i>Structure of pHLA-G complexes</i>	57
Ch.3 Fig. 2. <i>Conserved interactions between peptide and HLA-G</i>	58
Ch.3 Table 1. <i>HLA-G^{KGPPAALTL} contacts</i>	59
Ch.3 Fig. 3. <i>Peptide Conformation</i>	60
Ch.3 Fig. 4. <i>Orientation of His70</i>	61
Ch.3 Table 2. <i>HLA-G^{KLPAQFYIL} contacts</i>	62
Ch.3 Fig. 5. <i>Comparison of the three pHLA-G complexes</i>	63
Ch.3 Fig. 6. <i>Conserved peptide contacts</i>	64
Ch.3 Fig. 7. <i>Thermal stability of pHLA-G complexes</i>	64
Ch.3 Table 3. <i>Data collection and refinement statistics</i>	65
Figure 4.1. <i>Purification of baculovirus-expressed recombinant KIR2DL4</i>	72
Figure 4.2. <i>Circular Dichroism spectrum of KIR2DL4</i>	72
Figure 4.3. <i>SDS-PAGE analysis of KIR2DL4</i>	73
Table 4.1. <i>Broad screening conditions yielding KIR2DL4 crystals</i>	74
Figure 4.4. <i>KIR2DL4 crystal morphology</i>	75
Figure 4.5. <i>KIR2DL4 diffraction</i>	75

Figure 4.6. <i>Purification of mammalian-expressed recombinant KIR2DL4</i>	77
Figure 4.7. <i>Anion-exchange purification of mammalian-expressed recombinant KIR2DL4</i>	78
Figure 4.8. <i>Endoglycosidase H treatment of mammalian-expressed KIR2DL4</i>	78
Figure 4.9. <i>β-mercaptoethanol treatment of recombinant KIR2DL4</i>	81
Figure 4.10. <i>Iodoacetamide treatment of baculovirus-expressed KIR2DL4</i>	81
Table 4.2. <i>Molecular weight of KIR2DL4 as determined by SAXS</i>	83
Figure 4.11. <i>Sequence alignment of KIR family D0 domains</i>	83
Figure 4.12. <i>Structures of KIR3DL1 and KIR2DL1</i>	84
Figure 4.13. <i>Native-PAGE assay</i>	85
Table 4.3. <i>Comparison of R_g and D_{max} for KIR2DL4 at 1.25mg/ml and 5.0mg/ml</i>	87
Figure 4.14. <i>Raw SAXS data for recombinant KIR2DL4 samples</i>	88
Figure 4.15. <i>$P(r)$ functions of recombinant KIR2DL4 samples</i>	89
Figure 4.16. <i>Ab initio SAXS models of recombinant KIR2DL4</i>	91
Figure 4.17. <i>KIR2DL1 models within the ab initio KIR2DL4 SAXS shell</i>	92
Figure 5.1. <i>Purification of pHLA-E</i>	97
Figure 5.2. <i>Purification of the GF4 TcR</i>	98
Figure 5.3. <i>Native-PAGE assay</i>	99
Figure 5.4. <i>Purification of the GF4:pHLA-E complexes</i>	100
Table 5.1. <i>Broad screening conditions yielding GF4:HLA-E^{VMAPRTLVL} crystals</i>	102
Figure 5.5. <i>Fine screening to optimise pH and PEG concentration</i>	102
Figure 5.6. <i>GF4:pHLA-E crystal morphology</i>	103
Table 5.2. <i>Data collection and refinement statistics</i>	105
Figure 5.7. <i>Crystal structures of the GF4 TcR:pHLA-E complexes</i>	108
Figure 5.8. <i>Comparison of peptide conformation</i>	109
Figure 5.9. <i>HLA-E antigen-binding cleft</i>	110
Table 5.3. <i>Contribution of CDR loops to GF4 TcR Buried Surface Area</i>	111
Figure 5.10. <i>Complementarity of the GF4 CDR2β loop with the HLA-E α1 helix</i>	111
Table 5.4. <i>GF4 TcR:HLA-E^{VMAPRTLVL} TcR-MHC and TcR-peptide contacts</i>	113
Table 5.5. <i>GF4 TcR:HLA-E^{VMAPRTLIL} TcR-MHC and TcR-peptide contacts</i>	118
Figure 5.11. <i>Energetic footprints of GF4 and KK50.4 on HLA-E^{VMAPRTLIL}</i>	120
Figure 5.12. <i>Docking orientation of GF4 and KK50.4 on HLA-E^{VMAPRTLIL}</i>	121
Figure 5.13. <i>Overlay of GF4 and KK50.4 CDR loops at the HLA-E^{VMAPRTLIL} antigen-binding cleft</i>	121

Publications arising from this PhD

Walpole NG, Kjer-Nielsen L, Kostenko L, McCluskey J, Brooks AG, Rossjohn J, Clements CS. (2010) The Structure and Stability of the Monomorphic HLA-G Are Influenced by the Nature of the Bound Peptide. *J Mol Biol.* Mar 26;397(2):467-80

Chapter 1 - Introduction

Introduction to the Human Innate and Adaptive Immune Responses

The innate and adaptive immune responses in humans form the vast majority of the host defence against pathogens, as well as malignant abnormalities (such as tumours) within the body itself. These defences are based around both humoral and cell mediated responses.

Upon initial invasion by pathogens (or foreign substances in general), the innate immune system response provides the first major defences. These defences are non-specific and include humoral responses such as cytokine release to cause inflammation and recruit macrophages to the site of infection (*Philip and Epstein, 1986*), as well as activation of the complement cascade by injured cells to aid distinction of pathogens (*Carroll, 2004*). Cell-mediated innate immune responses include non-specific removal of foreign substances by leukocytes, lysis of 'non-self' and damaged cells by Natural Killer (NK) cells and also activation of the adaptive immune system through various means.

The adaptive immune response is more specific than the innate response, and is produced by effector cells, including B-lymphocytes which produce antibodies (the humoral response), and T-lymphocytes which may have cytotoxic capabilities (cytotoxic T-lymphocytes, or CTL) or simply direct cytotoxic responses (helper T-cells). Unlike the innate immune system, the adaptive immune response induces immunological memory, enabling a faster and stronger response with each successive invasion by the same pathogen (*Raff, 1973*).

Cell-mediated immunity in both the innate and adaptive immune responses involves interactions between antigen presenting molecules on the surface of cells, and receptors on lymphocytes, including T-cells and NK cells. These receptors, including T-cell receptors (TcRs), Leukocyte Immunoglobulin-like Receptor (LILR) family receptors, Killer Immunoglobulin-like Receptor (KIR) family receptors and CD94/NKG2 family receptors, transduce activating or inhibitory signals in order to promote or hinder cytotoxic responses from the lymphocyte. Once activated, these

responses lead to lysis of the antigen-presenting cell. Both antigen presenting molecules and lymphocyte receptors are highly polymorphic, in order to provide defence against pathogens of all types, while recognising and preventing collateral damage to 'self' tissues.

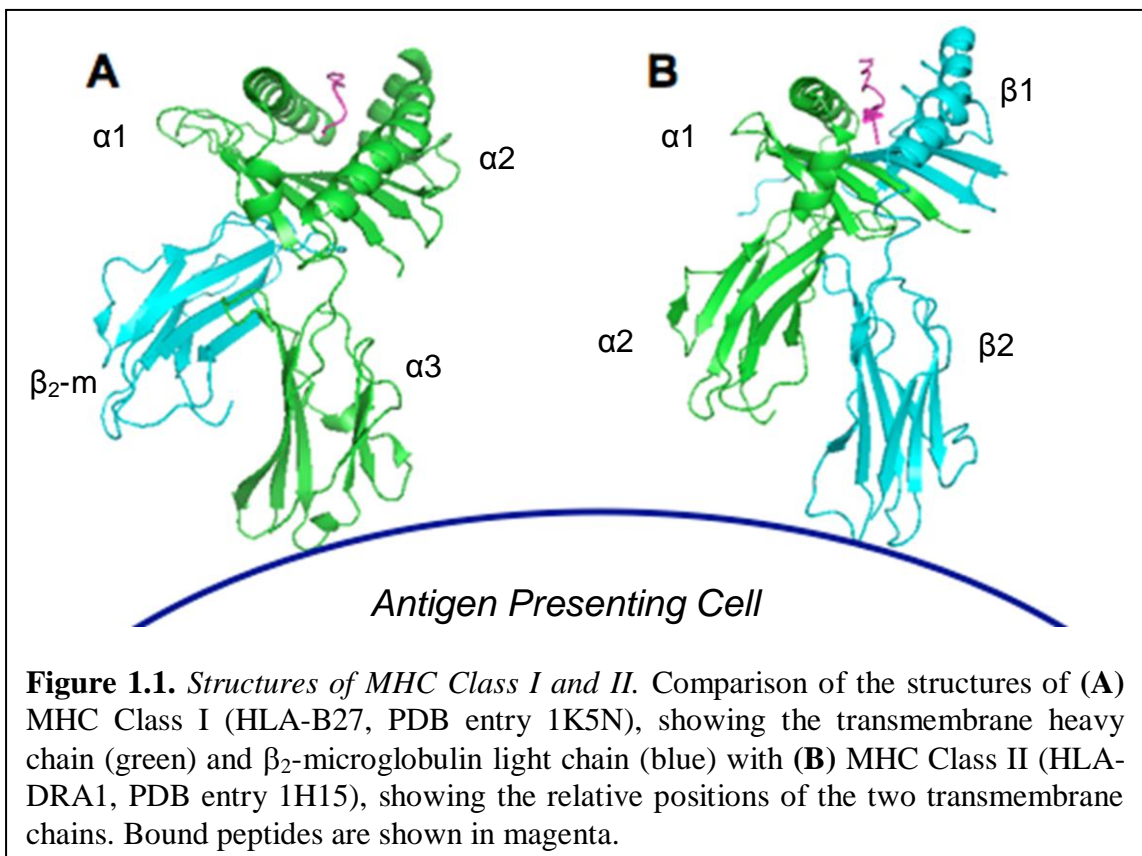
In general, tolerance of 'self' tissue by the innate immune system is maintained by recognition, by inhibitory receptors on NK cells, of 'self' antigen (peptides produced by normal cellular turnover of proteins in the proteasome) presented by 'self' antigen presenter, leading to signals inhibiting the NK cytotoxic response. While the specificity of the interaction is such that self and foreign antigens (which are generally produced by the processing of pathogens) may be distinguished, the polymorphism of antigen presenting molecules also allows the recognition of 'non-self' antigen presenting molecules. These are generally present on foreign tissues and may be introduced to the body through organ transplant mismatching among many other routes (*Munro and Bright, 1976, Miller, 1993*). The innate immune system also mediates the NK-mediated lysis of cells lacking 'self' antigen presenting molecules, or 'missing-self' (*Ljunggren and Karre, 1990*). This is described in more detail below in *Role of HLA-E in Innate Immunity*.

Tolerance of 'self' tissue by the adaptive immune system is achieved by thymic selection of immature T-cells, or thymocytes. Described below in *$\alpha\beta$ T-cell Receptors*, thymic selection is the process by which T-cells producing TcRs that recognise 'self' antigen presenting molecules (called Major Histocompatibility Complex, or MHC molecules) presenting 'self' antigen, or that do not recognise 'self' MHC molecules at all, undergo apoptosis. This process ensures that mature T-cells only produce TcRs which recognise 'self' MHC molecules presenting foreign antigen.

Introduction to Human Leukocyte Antigen (HLA)

The Major Histocompatibility Complex, called the Human Leukocyte Antigen (HLA) system in humans, is a gene cluster comprised of different subsets of antigen presenting molecules, including Class I and Class II MHC molecules. Class I MHC molecules are heterodimers, with each member consisting of a 3-domain heavy chain

and a common β_2 -microglobulin (β_2 -m) chain (Orr *et al.*, 1982), as shown in figure 1.1A. Class I MHC molecules present small peptides, generally between 8 and 14 residues in length and from either exogenous (during infection) or endogenous (from normal cellular turnover) sources, to receptors on lymphocytes (Munro and Bright, 1976). The first Class I MHC structure (that of HLA-A2) was determined in 1987 (Bjorkman *et al.*, 1987), and showed that the antigen-binding cleft of Class I MHC molecules is flanked by two α -helices and constrained by an eight-stranded β -sheet at the floor of the cleft. The α -helices are encoded by the $\alpha 1$ and $\alpha 2$ domains of the MHC heavy chain, and are named $\alpha 1$ and $\alpha 2$ accordingly. The peptide antigen is constrained in a series of specific binding pockets within the antigen-binding cleft. This requirement for constraint limits the peptide-binding repertoire of the MHC molecule to an allele-specific binding motif featuring strong preference for certain residues at specific positions in the peptide antigen (often termed ‘anchor residues’). These binding pockets also force the peptide antigen into an extended conformation that may be recognised by a receptor of the adaptive or innate immune systems (Garrett *et al.*, 1989).



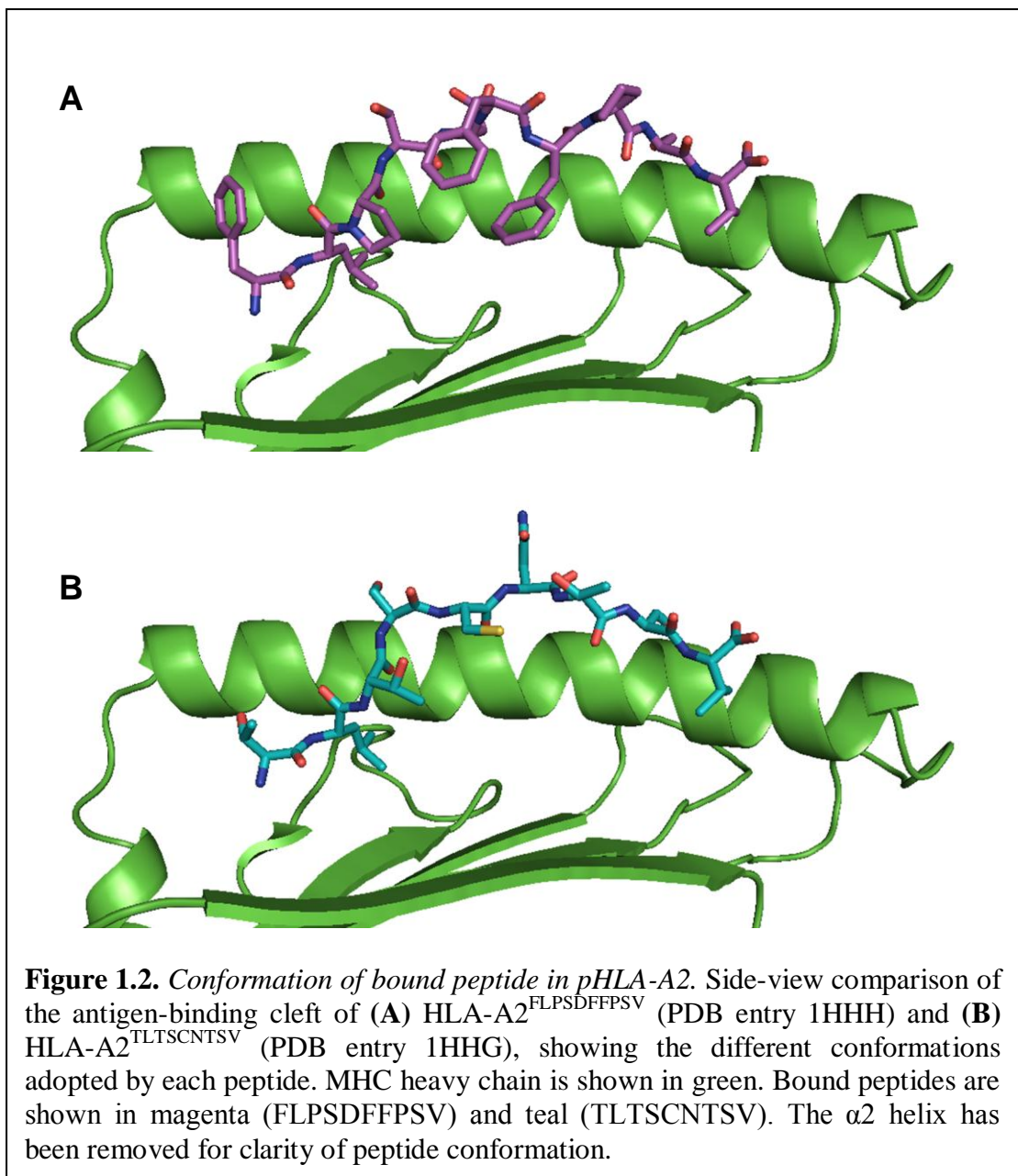
Like Class I MHC molecules, Class II MHC molecules are heterodimers, however they contain two homologous transmembrane chains, each consisting of two extracellular domains (*Kaufman et al., 1984*). The structure of HLA-DR1, determined in 1993 (*Brown et al., 1993*), was the first to show that Class II MHC adopt a similar overall shape as had previously been observed in Class I structures (shown in figure 1.1B). This similarity extends to the antigen-binding cleft, which is constrained by 2 α -helices and an eight-stranded β -sheet, however due to the open-ended nature of the Class II MHC antigen-binding cleft, the peptides presented may be longer than those of Class I (*Chicz et al., 1992*). Class II MHC are primarily expressed by specialised antigen presenting cells including B-lymphocytes, dendritic cells and macrophages. Peptides are sourced from protein degradation in cellular vesicles (*Cresswell et al., 1987*) and may be from exogenous (during infection) or endogenous (during autophagy) sources (*Castellino et al., 1997*).

Class I MHC are further divided into Class Ia and Class Ib, with distinctions generally based on polymorphism, cognate receptors and peptide specificity (*Shawar et al., 1994*). The Class Ia, or 'classical' MHC molecules, including the human HLA-A, HLA-B and HLA-C as well as the murine H-2D, have been well documented in their roles of peptide presentation to T-cells. Class Ia MHC molecules (MHC-Ia) are found on the surface of nearly all mammalian leukocytes (with the notable exception of placental tissues during pregnancy), and can generally bind a wide range of host and pathogen-derived peptides (*Rammensee et al., 1993*). MHC-Ia molecules are highly polymorphic and the resultant allelic diversity forms the basis of organ rejection due to monocyte recognition of foreign cells displaying 'non-self' MHCs (*Miller, 1993*). MHC-Ia are also heavily involved in the immune response to tissue invasion by viruses and bacteria, with the MHC-Ia-mediated presentation of pathogen-derived epitopes to T-cell receptors promoting a cytotoxic immune response from the CTL.

Allelic diversity is a prominent feature of MHC-Ia and helps to ensure that peptide epitopes from a wide variety of pathogenic sources may be presented to T-cell receptors (*Lawlor et al., 1990*). There are around 4000 variants of HLA (*Robinson et al., 2003*), and polymorphisms often map to the antigen-binding cleft, altering either the surface-exposed regions of the $\alpha 1$ and $\alpha 2$ helices, or the binding pockets in which

peptide antigens are constrained. Even small alterations to the binding pockets may cause changes to the peptide repertoire which a MHC molecule may present (Macdonald *et al.*, 2003, Burrows *et al.*, 2007). Micropolymorphisms, differences of only a few amino acids, at the antigen-binding cleft often have a significant effect, directly or indirectly, on receptor recognition and resultant immune responses (Archbold *et al.*, 2009).

In addition to MHC-Ia polymorphism, the bound peptide presented by MHC-Ia often has a dramatic effect on receptor recognition of the pMHC (peptide/MHC) complex, and the large peptide-binding repertoire of MHC-Ia allows recognition of a wide

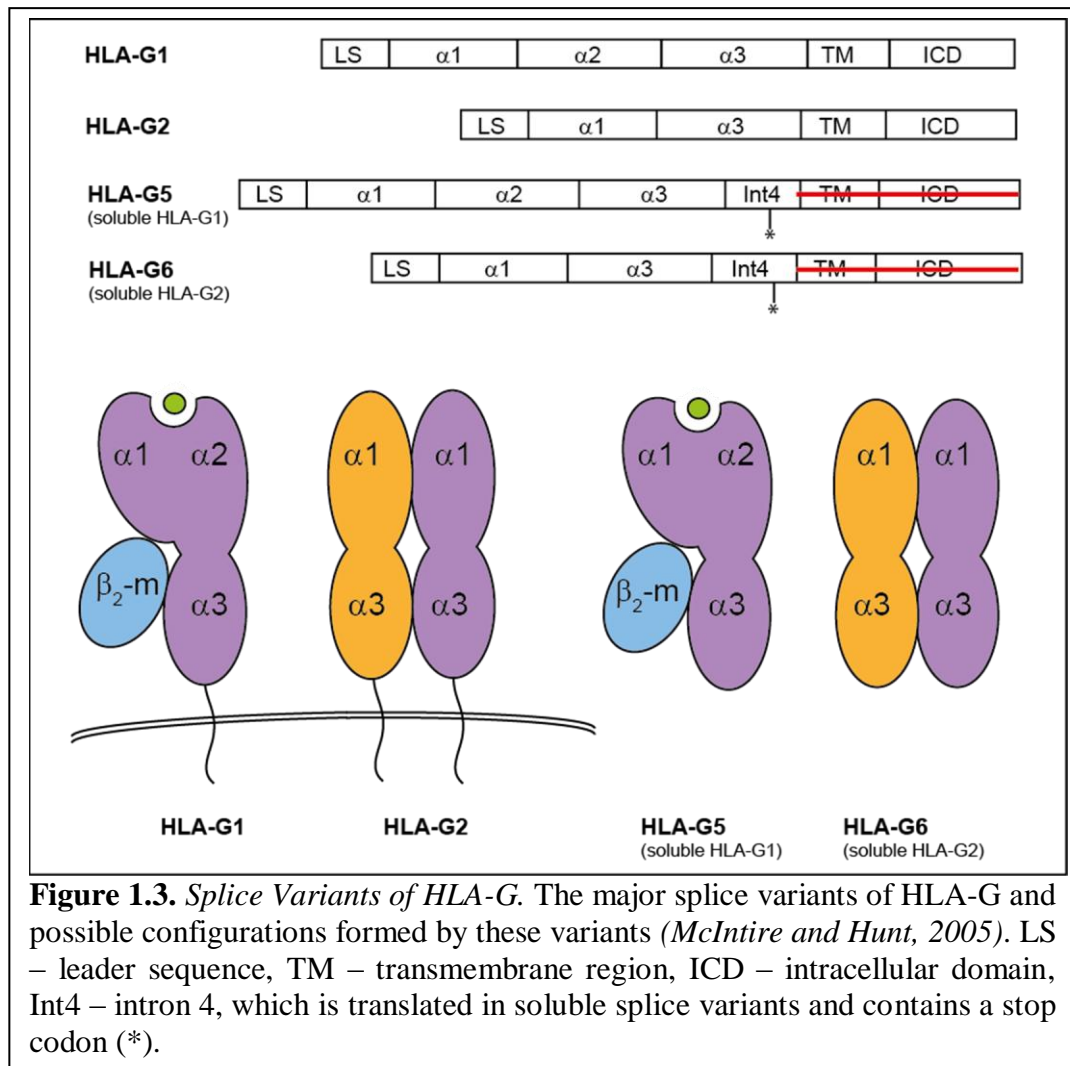


range of pathogens. While the effect of peptide sequence on TcR recognition was already known, structural determination of one MHC molecule (HLA-A2) in complex with five distinct viral peptides (*Madden et al., 1993*) enabled analysis of the different conformations formed by these peptides (two are shown in figure 1.2), giving a structural rationalisation of this effect. More recently, the structures of pMHC:TcR complexes have allowed further structural analysis of the role of the peptide in recognition of pMHC-Ia (*Rudolph et al., 2006, Burrows et al., 2010*).

Despite being structurally similar to MHC-Ia, the Class Ib, or ‘nonclassical’ MHC molecules (MHC-Ib), including HLA-E, HLA-F, HLA-G and HFE as well as the murine Qa-2, Q9, Qa-1b and H2-M3, are largely non-polymorphic and tend to have primary roles in the regulation of innate immunity, though these roles are generally less well-characterised than those of MHC-Ia (*Rodgers and Cook, 2005*). Suggested roles involving self-peptide presentation to various innate immune receptors are supported by the relatively narrow range of peptides capable of binding to MHC-Ib compared with MHC-Ia, and the ‘classical’ mode of antigen presentation used by MHC-Ib at the surface of the cell (*Diehl et al., 1996*). MHC-Ib may have a narrow tissue expression pattern, such as that of HLA-G, which is predominantly expressed at the feto-maternal interface by fetal trophoblast cells (*Le Bouteiller et al., 1999*), or a broad expression pattern, such as that of HLA-E, which is expressed on most tissues, including the placenta (*Koller et al., 1988, Ulbrecht et al., 1992*). The work described in this thesis has been focussed on characterising the MHC-Ib molecules HLA-G and HLA-E, and in particular the interactions that each has with putative receptors KIR2DL4 (HLA-G) and the GF4 $\alpha\beta$ T-cell receptor (HLA-E).

Introduction to HLA-G

HLA-G was first isolated and sequenced by Ellis *et al* (1990). Despite having 23 alleles encoding 7 unique proteins (*Pyo et al., 2006*), its amino acid sequence is highly conserved (*Bainbridge et al., 1999, Ishitani et al., 1999*), however HLA-G is found in various membrane-bound and soluble forms mediated by alternative splicing events (Figure 1.3). Only the full-length splice variant HLA-G1 has been detected on the cell surface (*Mallet et al., 2000*), though HLA-G2 also includes transmembrane domains, and the truncated HLA-G5 (also referred to as soluble



HLA-G1), which contains the same extracellular domains as the full-length splice variant, may be secreted and interact with monocyte receptors in endosomes as well as on the cell surface (*Fournel et al., 2000*). Other truncated isoforms may play a role in stabilising HLA-E surface expression by providing ligands derived from the HLA-G leader sequence (*Ulbrecht et al., 2004*). Comparative studies have found evidence that HLA-G has a functional homologue in the murine class Ib MHC Qa-2 (*Comiskey et al., 2003*).

The peptide-binding properties of HLA-G have been intensively studied (*Diehl et al., 1996, Ishitani et al., 2003, Munz et al., 1999a*), and the generic peptide motif (XI/LPXXXXXL) specific to HLA-G has been defined and documented, as described below under the heading *HLA-G: Peptide Binding and Structural Considerations*.

Initial characterization of HLA-G showed a localisation to a limited subset of trophoblast cells at the materno-fetal interface, though expression has also been demonstrated in small populations of thymic and dendritic cells (*Ellis et al., 1990, Mallet et al., 1999, Pangault et al., 2002*). This, when combined with the general amino acid sequence conservation, has prompted the notion that HLA-G could have a role in maternal tolerance of the semiallogenic fetus during pregnancy (*Rouas-Freiss et al., 1997b, Yokoyama, 1997*). Alternative roles in tumour escape (*Urošević et al., 2001*) and tolerance of organ transplants (*Lila et al., 2000*) have also been put forward, and are discussed below in *HLA-G in Cancer and Organ Transplantation*.

HLA-G in Pregnancy

The capacity of HLA-G to present nonameric endogenous peptides to inhibitory receptors on NK cells and other monocytes is likely to form the basis for a primary role in ‘self’ recognition and selective inhibition of the innate immune system during pregnancy (*Munz et al., 1999b, King et al., 2000*). Selective expression of HLA-G by cytotrophoblasts at the feto-maternal interface has been shown to protect these cells from maternal NK cytotoxicity (*Rouas-Freiss et al., 1997a*), and an association between HLA-G genotype and recurrent spontaneous abortion has also been reported (*Pfeiffer et al., 2001*). Many interactions between surface-expressed and soluble HLA-G and receptors on immune system effector cells have been demonstrated (Table 1.1).

Table 1.1. Downstream effects of HLA-G signalling. The <i>in vitro</i> effects of membrane-bound and soluble HLA-G isoforms on NK, CD4+ & CD8+ T-cells and Dendritic Cells (<i>Rouas-Freiss et al., 2003</i>).				
Cell Type	Effect	Receptors Involved	HLA-G1	HLA-G5
Dendritic Cells	Inhibition of maturation	ILT2, ILT4	Yes	
CD4+ T-cells	Inhibition of allo-proliferation	ILT2	Yes	Yes
CD8+ T-cells (PHA activated)	Apoptosis	KIR2DL4, ILT2		Yes
CD8+ T-cells (all)	Inhibition of lysis of Allogeneic targets	KIR2DL4, ILT2		Yes
	Inhibition of antigen-specific lysis	KIR2DL4, ILT2	Yes	
NK Cells	Inhibition of lysis of MHC-I negative targets	KIR2DL4, ILT2	Yes	Yes
	Inhibition of lysis of Allo- and Xenogeneic targets	KIR2DL4, ILT2	Yes	
	Decreased adhesion and migration	KIR2DL4, ILT2	Yes	

Genotypic analysis by Pfeiffer *et al* (2001) of German couples designated RSA (Recurrent Spontaneous Abortion, having had 3 or more miscarriages) and fertile controls showed that HLA-G allele frequencies differed significantly between the two populations: HLA-G*01013, an allele associated with lower amounts of HLA-G5 in peripheral blood, and HLA-G*0105N were found to be significantly more common in RSA patients. Carriers for *0105N and *01013 were significantly more likely to suffer spontaneous abortion in further pregnancies than both fertile controls and RSA couples homozygous for 'functional' HLA-G alleles (Pfeiffer *et al.*, 2001).

Other groups have also shown statistical analyses of the correlation between HLA-G genotype and recurrent miscarriage. Aldrich *et al* (2001) suggested that variation in the $\alpha 2$ domain of HLA-G may contribute to recurrent miscarriage after detailing pregnancy outcome in American HLA-G*0104 and HLA-G*0105N carriers, while Ober *et al* (2003) described other polymorphisms in the 5' UTR (Untranslated Region) and 3' UTR that could result in reduced expression of functional HLA-G, and elucidated an association between some of these polymorphisms and fetal loss over a 15-year period.

Castro *et al* (2000) reported the genotypic analysis of a family with five healthy siblings all homozygous for HLA-G*0105N. This allele contains a shift in the reading frame in exon 3, and a stop codon at the beginning of exon 4, which corresponds to the $\alpha 3$ domain of the heavy chain. This results in a truncated protein, and only G2, G3 and G6 isoforms (which all lack exon 3) are formed normally. None of these isoforms reach the cell surface *in vivo* (Mallet *et al.*, 2000), and the peptide binding cleft is slightly disrupted in the $\alpha 2$ domain due to the exclusion of exon 3. The health of the homozygous HLA-G*0105N siblings, and even the fact that they were carried to term, casts doubt on the necessity of the HLA-G1 isoform for survival of the fetus in some pregnancies, and raises the previously under-studied concept that the truncated or soluble isoforms of HLA-G may be sufficient to support a pregnancy to full term in some cases. This concept has since sparked considerable debate, being supported by Fournel *et al* (2000), who reported specific HLA-G5-mediated apoptosis of activated CD8+ peripheral blood cells, but refuted by Contini

et al (2003) and Pistoia *et al* (2007), whose evidence show that physiological levels of sHLA-G are too low to induce T cell and NK cell apoptosis. It is possible, however, that physiological levels of sHLA-G are sufficient for inhibition of NK cytotoxicity, and it is clear that further research needs to be completed in this area of study.

HLA-G in Cancer and Organ Transplantation

The immune-inhibitory pathway initiated by HLA-G binding to monocyte receptors has also stimulated considerable discussion regarding whether malignant tumours may use it as a method of immune evasion. This escape from immunosurveillance would involve a high level of transcription of both membrane-bound and soluble HLA-G, thus inhibiting T-cell and NK function as the tumour cells proliferate. Cell lines that exhibit high levels of HLA-G mRNA expression have been isolated from many types and malignancies of human cancer (including ovarian carcinoma, gastric carcinoma, coetaneous melanoma, haematopoietic tumours, endometrial carcinoma, renal cell carcinoma, lung carcinoma, mesothelioma, breast carcinoma and trophoblastic tumours), and HLA-G expression has been shown to protect many of these cell lines from T-cell and NK lysis (*Hansel et al., 2005, Bukur et al., 2003, Urosevic et al., 2005, Paul et al., 1998, Urosevic et al., 2002, Rouas-Freiss et al., 2005, Gros et al., 2006, Leleu et al., 2005, Kleinberg et al., 2006, Rebmann et al., 2003, Urosevic et al., 2001, Singer et al., 2002*). On the basis of this evidence, it has been suggested that HLA-G expression be used as a possible marker for malignant tumours *in vivo*, and even as a diagnostic tool in some cancers (*Singer et al., 2003, Shih, 2007*). However, Davies *et al* (2001) found no evidence that tumour cells express translated HLA-G in order to evade NK cell cytotoxicity, upon examination of 66 tumours of varying type and malignancy. This points to the possibility that HLA-G expression in human tumours may be too infrequent an occurrence to provide a viable diagnostic tool.

In support of a third possible *in vivo* role for HLA-G, soluble HLA-G found in the serum of heart-transplant recipients has been associated with a decrease in acute and chronic rejection episodes (*Lila et al., 2000*). Follow-up studies investigating the same effect in a larger group of patients concluded that HLA-G expression in the

serum was associated with a reduced incidence of acute transplant rejection, and did not find any cases of chronic rejection in HLA-G⁺ patients, while HLA-G⁻ patients showed chronic rejection in 35% of cases (*Lila et al., 2002*). The likelihood that HLA-G expression affects the responsive capacity of the immune system in graft acceptance has since been investigated, with several findings that membrane-bound and soluble HLA-G both have the potential to inhibit allogeneic responses from NK cells, CD4⁺ and CD8⁺ T cells, both *in vitro* and *in vivo*, and that HLA-G may have potential uses in preventing rejection of allograft and even xenograft transplantations (*Sasaki et al., 1999, Rouas-Freiss et al., 2003, Lila et al., 2001, Horuzsko et al., 2001, Forte et al., 2001, Forte et al., 2000*). Studies to date have not focussed on which receptors may be involved in this immune suppression, and more investigation in this area is needed to elucidate the clinical benefits that may arise from research.

HLA-G: Peptide Binding and Structural Considerations

Variations in peptide binding specificity between MHC-I molecules are caused by amino acid polymorphisms in the β -sheet at the floor of the peptide-binding cleft, as well as in the α 1 and α 2 helices, altering the properties of the pockets which harbour specific peptide residues and the potential interactions between residues of the peptide and those that surround it.

As mentioned earlier, the peptide binding properties of HLA-G have been intensively studied (*Diehl et al., 1996, Ishitani et al., 2003, Munz et al., 1999b, Munz et al., 1999a, Clements et al., 2005*), and the basic peptide motif (XI/LPXXXXXL) specific to HLA-G has been defined and documented, including justifications for the preferred residues at positions 2, 3 and 9 (P2, P3 and P9) within their respective binding pockets (*Diehl et al., 1996*). The binding preference of HLA-G overlaps with that of HLA-A2 (notably at the anchors at P2 and P9), however is much more specific in its binding capacity, as would be expected from a molecule evolved to bind a small set of predominantly host peptides. Of the Human Leukocyte Antigen family, only HLA-E shows a more limited peptide-binding capacity than HLA-G.

As a rule, positions 2 (isoleucine or leucine), 3 (proline) and 9 (leucine) of HLA-G-bound antigens are considered anchor residues, however peptide-binding assays have

shown that two of these are sufficient for binding, especially where the conditions at P3 and P9 have been met (*Lee et al., 1995, Diehl et al., 1996, Munz et al., 1999b*). These studies also demonstrated a preference for the positively charged residues Arginine and Lysine at P1. The residues at P4, P5 and P8 were not shown by these studies to require any specific interactions with pockets found in the HLA-G peptide-binding cleft, suggesting that these positions may be occupied by a variety of residues, and that they may function as signal residues. These conclusions were later confirmed by the determination of the crystal structure of the monomeric HLA-G^{RIIPHLQL} to a resolution of 1.9Å (*Clements et al., 2005*). This structure is described in more detail below, and an illustration of the MHC accommodation of the bound peptide is shown in figure 1.4.

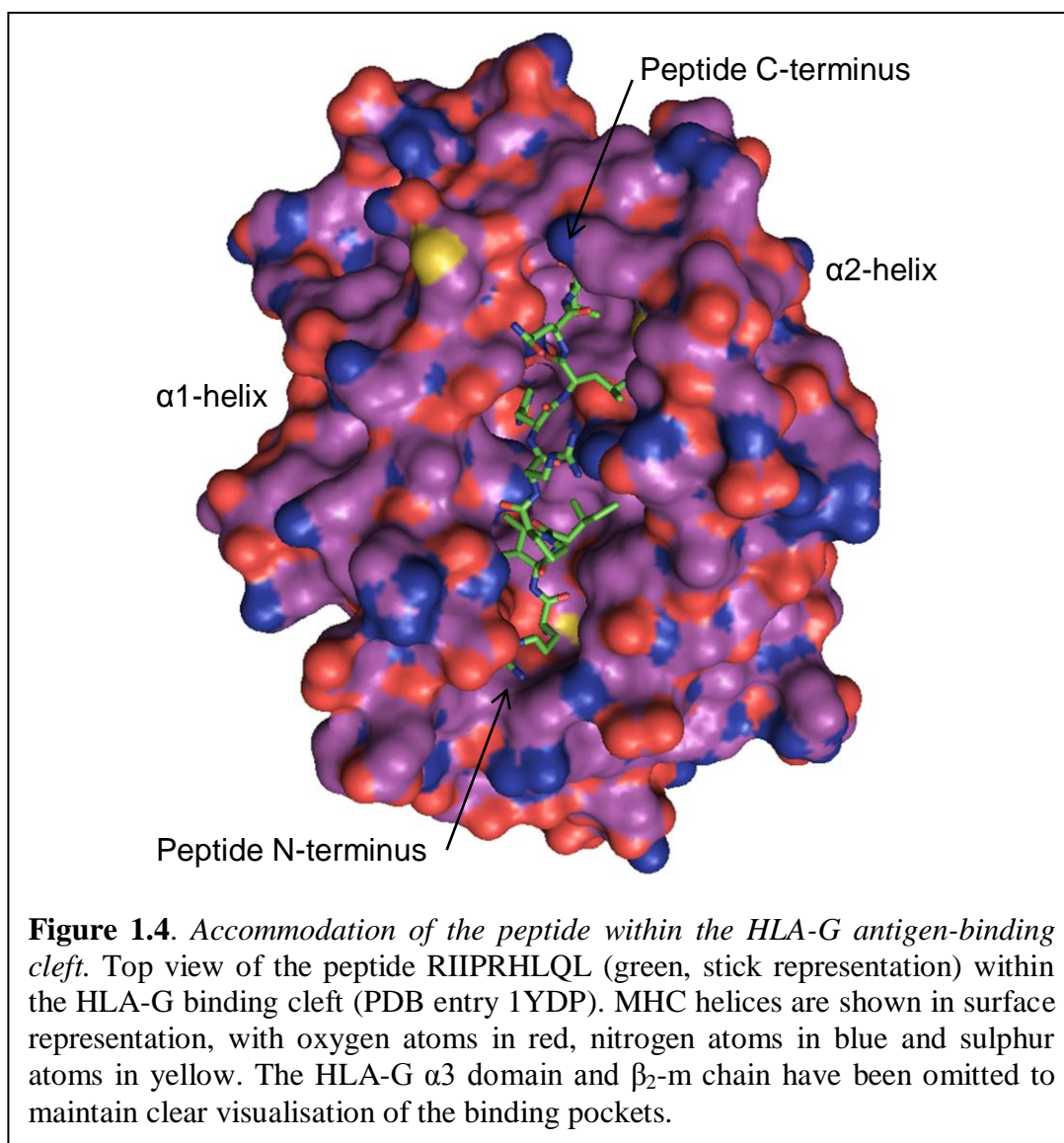


Table 1.2. HLA-G peptide ligands. Comparison between the preferred ligands of HLA-G and peptides identified in published studies (*Clements et al., 2007, Munz et al., 1999b, Ishitani et al., 2003, Diehl et al., 1996, Lee et al., 1995, Lenfant et al., 2003*).

Reference	Position									Source
	1	2	3	4	5	6	7	8	9	
Anchor Residues (<i>Munz et al, 1999b</i>)		I	P						L	
		L								
Preferred Residues (<i>Munz et al, 1999b</i>)	R									
(<i>Munz et al, 1999b</i>)	K									
(<i>Diehl et al, 1996</i>),	R	I	I	P	R	H	L	Q	L	Histone H2A
(<i>Lee et al, 1995</i>)										
(<i>Diehl et al, 1996</i>)	R	L	P	K	D	F	R	I	L	Unknown
(<i>Diehl et al, 1996</i>)	K	L	P	A	Q	F	Y	I	L	Unknown
(<i>Lee et al, 1995</i>),	K	G	P	P	A	A	L	T	L	Cytokine receptor
(<i>Ishitani et al, 2003</i>)										
(<i>Lee et al, 1995</i>)	R	H	P	K	Y	K	T	E	L	Nuclear protein
(<i>Lee et al, 1995</i>)	H	V	P	E	H	A	V	V	L	Rat fatty acid synthase
(<i>Lee et al, 1995</i>)	M	Q	P	T	H	P	I	R	L	HS1 protein
(<i>Lee et al, 1995</i>)	K	I	A	G	Y	V	T	H	L	Ribosomal protein S17
(<i>Lee et al, 1995</i>)	G	V	P	K	T	H	L	E	L	HLA class III gene
(<i>Lee et al, 1995</i>)	S	Y	P	T	R	I	A	S	L	Unknown
(<i>Lee et al, 1995</i>)	R	L	P	D	G	R	V	V	L	Interferon binding protein
(<i>Lee et al, 1995</i>)	M	R	P	R	K	A	F	L	L	ERP 72
(<i>Lee et al, 1995</i>)	R	L	P	K	D	F	V	D	L	Unknown
(<i>Lee et al, 1995</i>)	V	L	P	K	L	Y	V	K	L	Ribosomal protein 40S
(<i>Lenfant et al, 2003</i>)	V	F	P	T	K	D	V	A	L	CMV pp65*
(<i>Lenfant et al, 2003</i>)	L	C	P	K	S	I	P	G	L	CMV pp65*
(<i>Lenfant et al, 2003</i>)	L	G	P	I	S	G	H	V	L	CMV pp65*
(<i>Lenfant et al, 2003</i>)	V	L	P	H	E	T	R	L	L	CMV pp65*
(<i>Lenfant et al, 2003</i>)	H	L	P	V	A	D	A	V	I	CMV pp65*
* – These putative HLA-G ligands from the CMV proteome were elucidated by bioinformatic means, not by peptide elution studies.										

While a range of peptides have been shown to bind to HLA-G (Table 1.2), the 4 major native ligands are RIIPRHLQL (from Histone H2A), RLPKDFRIL and KLPAQFYIL (both from unknown host-derived sources), isolated in 1996 (*Diehl et al., 1996*), along with KGPPAALTL (from a cytokine receptor), isolated in 2003 (*Ishitani et al., 2003*). RLPKDFRIL and KLPAQFYIL contain all three HLA-G anchor residues, however RIIPRHLQL and KGPPAALTL only contain two. The peptide RIIPRHLQL differs from the consensus motif by a non-conservative substitution at position 3, being from the rigid proline to the aliphatic isoleucine.

However, RIIPRHLQL displays a proline at position 4 which may achieve the same overall peptide conformation as having the residue at position 3. The substitution at position 2 in KGPPAALTL is more conservative, with the small, moderately hydrophobic glycine unlikely to interfere detrimentally with any of the surrounding heavy chain residues contacted by the aliphatic isoleucine or leucine.

The determination of the crystal structure of HLA-G (C42S mutant) in complex with the endogenous peptide RIIPRHLQL (*Clements et al., 2005*) showed that HLA-G conforms to the previously described MHC-I fold (shown in figure 1.1A), and allowed comparison of the accommodation of the bound peptide with that of previously solved pMHC structures. Figure 1.5 shows a detailed representation of the position of RIIPRHLQL within the HLA-G antigen binding cleft. Figure 1.6 shows a comparison of the peptide binding positions of HLA-G^{RIIPRHLQL} with those of HLA-A2^{GILGFVFTL} (*Madden et al., 1993*) and HLA-E^{VMAPRALLL} (*Hoare et al., 2008*), demonstrating the greater depth of the bound peptide within the antigen-binding cleft of Class Ib MHC molecules when compared to Class Ia. The depth of the peptide backbone within the MHC-Ib antigen-binding cleft has implications for peptide sidechain availability for receptor interaction, potentially resulting in lower peptide solvent exposure than may be seen for a similar peptide bound to MHC-Ia.

At the start of my PhD studies, the only crystal structures of HLA-G showed the MHC binding the peptide RIIPRHLQL. The idea that structural studies of HLA-G binding a range of peptides might provide a useful opportunity for detailed comparison of the peptide binding specificity and conformational changes inherent in binding alternative peptides led to the work described in Chapter 3 – ‘The Effect of Peptide Binding on HLA-G’. Further understanding of the activities of HLA-G *in vivo* would also be obtained through the determination of the crystal structure of HLA-G in complex with the various receptors with which it associates. To date, only one such complex has been solved, that of pHLA-G:LILRB2 (*Shiroishi et al., 2006b*). This structure showed recognition by LILRB2 of the HLA-G $\alpha 3$ domain, and is described below in *Leukocyte Ig-like Receptors*.

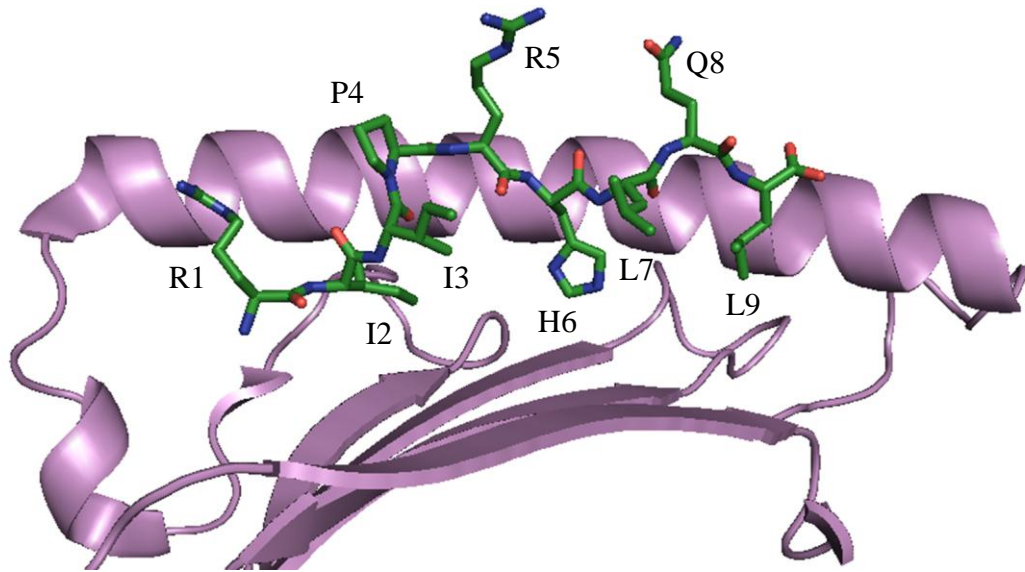


Figure 1.5. *Peptide conformation within the HLA-G binding cleft.* Conformation of the peptide RIIPRHLQL within the HLA-G binding cleft (PDB entry 1YDP). The $\alpha 2$ helix has been removed to allow better clarity of peptide conformation.

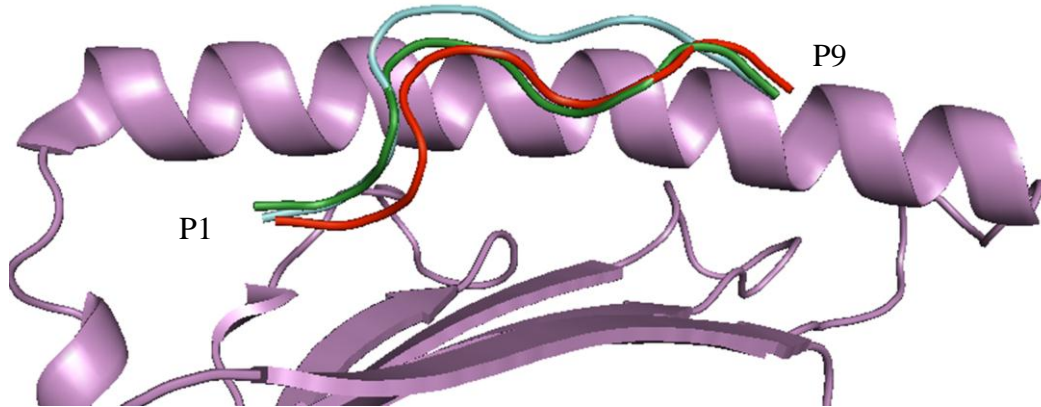
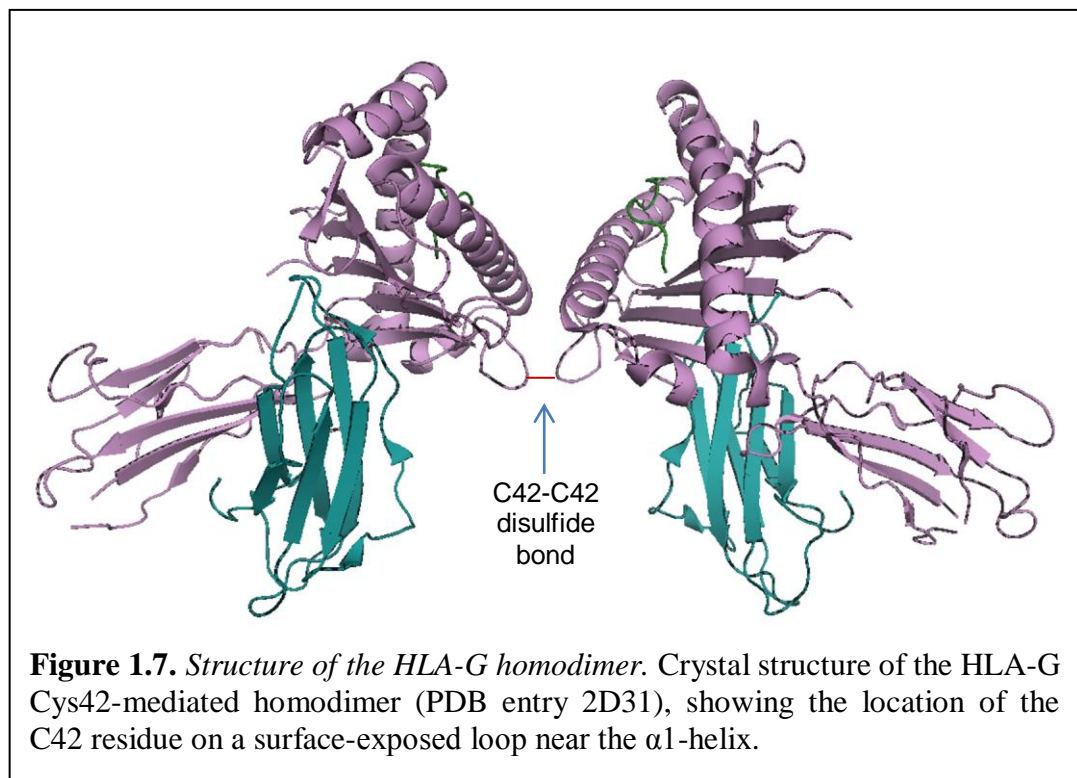


Figure 1.6. *Comparison of HLA-G, HLA-E and HLA-A2 peptide binding positions.* Comparison of the binding positions of peptides in HLA-G (green) (PDB entry 1YDP), HLA-E (red) (PDB entry 3BZF) and HLA-A2 (cyan) (PDB entry 1HHI) (Clements *et al.*, 2005, Madden *et al.*, 1993, Hoare *et al.*, 2008). The $\alpha 2$ helix has been removed to allow better clarity of peptide backbone conformation.

One observation about the function of HLA-G which has stimulated much discussion is that of some level of dimerisation of the molecule by intermolecular disulfide bonds facilitated by the exposed cysteine residue at position 42 not found in other MHC-I molecules (Boyson *et al.*, 2002). It has been proposed that the dimerisation of HLA-G enables better interaction with some ligands of HLA-G, including LILRB1. The crystal structure of the disulfide-linked HLA-G^{RIIPRHLQL} homodimer has been determined (Figure 1.7), leading to identification of interactions between β -strands of the two heavy chains including the Cys42-Cys42 disulfide bridge (Shiroishi *et al.*, 2006a). Further to this, dimerisation of the recombinant HLA-G was shown to allow optimised access of the α 3 domain to LILRB1. Analysis of the homodimer supported the proposal that binding kinetics with LILRB1 was enhanced in the dimer when compared with the monomer due to the avidity effect (Shiroishi *et al.*, 2006c). Importantly, the *in vivo* expression of HLA-G has not been investigated with regard to the relative proportion of dimeric and monomeric protein expressed.



Introduction to HLA-E

HLA-E was identified, isolated, sequenced and initially characterised by Koller *et al* (1988). It was immediately apparent that HLA-E differed from all human Class I MHCs characterised to that point (ie, HLA-A, -B and -C) as it showed very different tissue expression patterns, as well as vastly reduced polymorphism. Two major HLA-E allelic variants have been described, with HLA-E*0103 differing from HLA-E*0101 by the substitution of an arginine residue by glycine at position 107. These alleles are found at nearly equal frequencies (Geraghty *et al.*, 1992).

Like HLA-G, HLA-E is considered to have a primary involvement in ‘self’ recognition, which is achieved by the presentation of nonameric MHC class I leader sequences to CD94/NKG2 receptors on NK cells (Lee *et al.*, 1998b, Lee *et al.*, 1998a, Rodgers and Cook, 2005). This peptide repertoire is highly restricted, with only a couple of residues showing any variability (Lee *et al.*, 1998a), as is discussed below. Unlike HLA-G, HLA-E is expressed in most tissues, and therefore is considered to have a much broader role in innate immune system regulation (Ulbrecht *et al.*, 1992).

HLA-E is considered to have a functional homologue in the murine Qa-1b, which also presents a nonameric MHC-I leader peptide (AMAPRTLTL) termed the Qa-1 determinant modifier, or Qdm peptide, to CD94/NKG2 receptors on NK cells (Vance *et al.*, 1998, DeCloux *et al.*, 1997). In addition to a similar peptide binding motif, HLA-E and Qa-1b share 73% amino acid identity. However, as they each bear higher similarity to MHC-Ia in their respective species, they are thought to have arisen from independent evolutionary events (Yeager *et al.*, 1997).

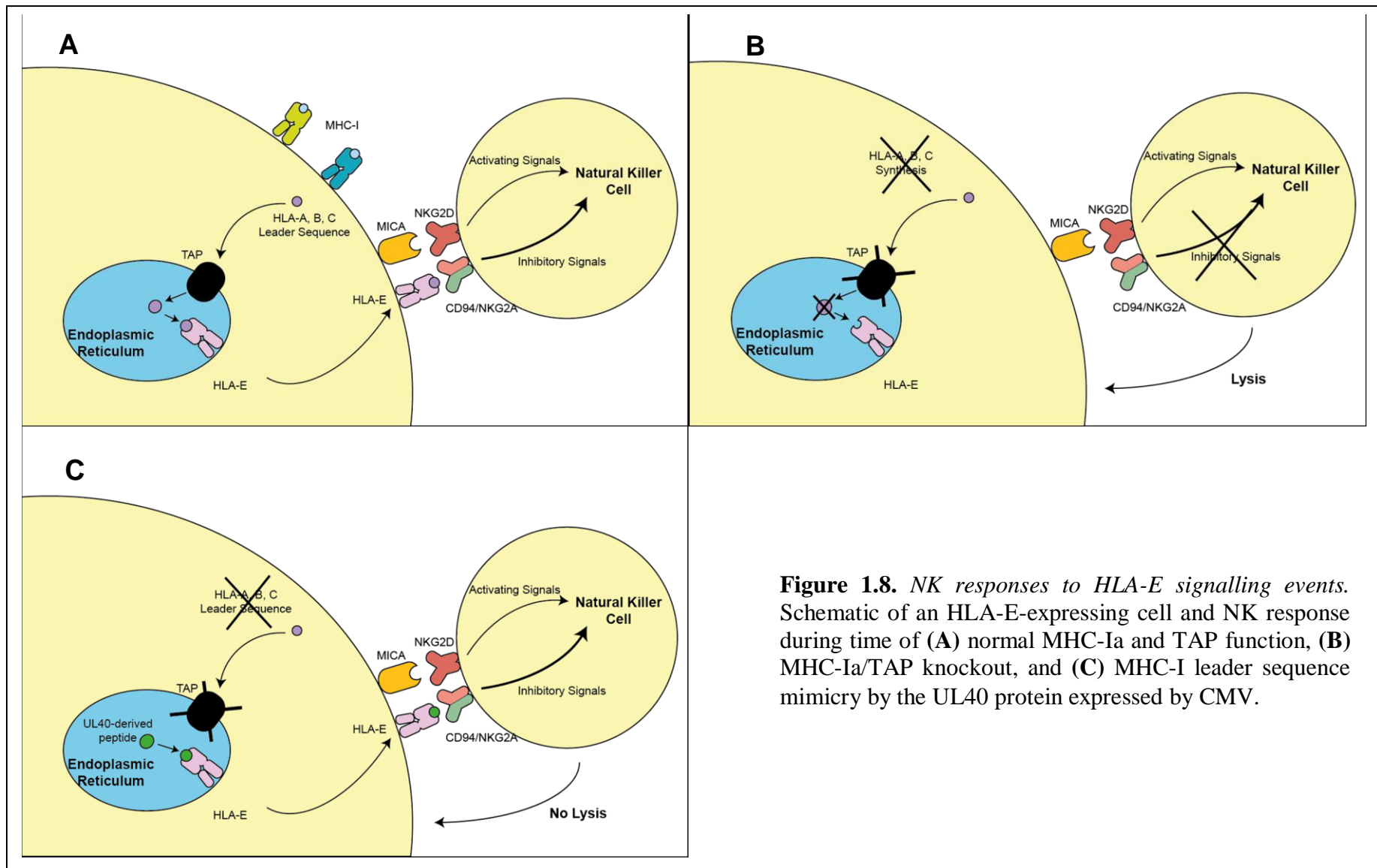


Figure 1.8. *NK responses to HLA-E signalling events.* Schematic of an HLA-E-expressing cell and NK response during time of (A) normal MHC-Ia and TAP function, (B) MHC-Ia/TAP knockout, and (C) MHC-I leader sequence mimicry by the UL40 protein expressed by CMV.

Role of HLA-E in Innate Immunity

Presentation of a nonameric MHC-I leader sequence by HLA-E is considered a checkpoint for correct expression of Class I MHCs and correct function of TAP, an endoplasmic reticulum transporter complex (Figure 1.8A) (*Rodgers and Cook, 2005*). This is an important function as Class Ia MHCs have major roles within the adaptive immune response, while TAP is a vital component of the antigen processing pathway, by which viral epitopes are transported to the ER and taken up by Class Ia MHCs (*Braud et al., 1998b*). If Class I MHC expression or TAP function is downregulated (for example by mutation or viral infection) then the MHC-I leader sequences, normally transported into the ER by TAP after proteasome processing, are unavailable to HLA-E, which is then retained in the ER. As a result, inhibitory CD94/NKG2 receptors on NK cells, which function to recognise HLA-E, have no ligand. In the absence of inhibitory signals from these receptors, a cytotoxicity-activating pathway, mediated by constitutive signals to activating CD94/NKG2 receptors, triggers NK-mediated cell lysis (Figure 1.8B) (*Braud et al., 1998a*).

Interestingly, some viruses with the ability to down-regulate MHC-Ia molecules or knock out TAP function (for example the beta-herpesvirus Cytomegalovirus (CMV)) have evolved to mimic the leader sequences of some Class I MHCs (Figure 1.8C) (*Ulbrecht et al., 2000*). While this is effective as a means of NK lysis prevention, in some cases it may provide a means for HLA-E to invoke an adaptive immune response. This HLA-E-restricted T-cell response is discussed in further detail in *Class Ib MHCs in Adaptive Immunity*.

HLA-E: Peptide Binding and Structural Considerations

Peptide presentation by HLA-E is highly specific, with primary anchor residues at peptide positions 2 (Methionine) and 9 (Leucine), while positions 3, 6 and 7 also function as anchor sites (*O'Callaghan et al., 1998*). The accepted peptide motif for leader sequence peptides is VMAPRT/AXXL, where the last three residues may be LIL, LLL, LVL, LFL or VLL, as shown in Table 1.3. Limited residue variability in endogenous peptides has primarily been demonstrated at positions 7 and 8 (*Lee et al., 1998a*), though HLA-E has also been shown to bind significantly different peptides from both endogenous and exogenous sources. These include the murine

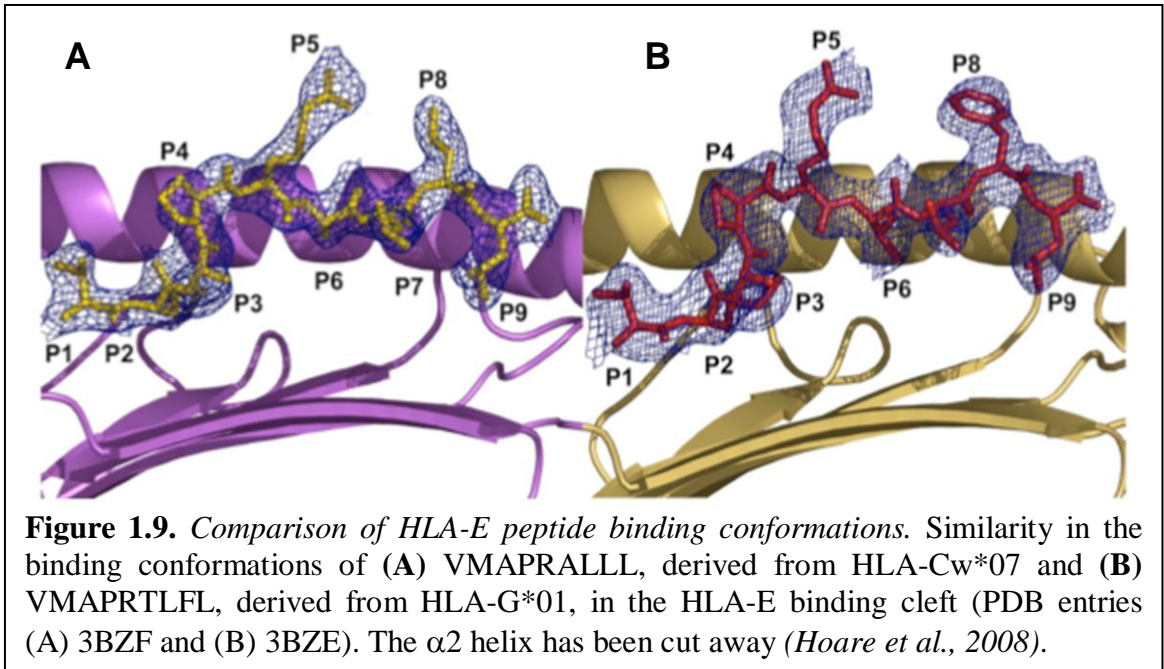
Table 1.3. HLA Class I leader sequence peptides (Pietra et al., 2003).

Leader Sequence	HLA Class I Alleles	HLA-E binding?	CMV Mimic?
VMAPRTLIL	HLA-A*01, -A*03, -A*11, -A*29, -A*30, -A*31, -A*32, -A*33, -A*36 & -A*74	Yes	No
VMAPRTLVL	HLA-A*02, -A*23, -A*24, -A*25, -A*26, -A*3402, -A*43, -A*66 & -A*69	Yes	Yes (Toledo)
IMAPRTLVL	HLA-A*3401	No	No
VMPRTLIL	HLA-A*80	No	No
VMAPRTLVL	HLA-B*07, -B*08, -B*14, -B*38, -B*39, -B*42, -B*67, -B*73 & -B*81	Yes	No
VTAPRTLIL	HLA-B*13, -B*18, -B*27, -B*35, -B*37, -B*40, -B*44, -B*47, -B*54, -B*56, -B*58, -B*59, -B*82 & -B*83	Yes	No
VTAPRTLVL	HLA-B*15, -B*35, -B*40, -B*41, -B*44, -B*45, -B*49, -B*50, -B*51, -B*52, -B*57 & -B*78	No	No
VMAPRTLIL	HLA-Cw*01, -Cw*03, -Cw*04, -Cw*05, -Cw*06, -Cw*0801-03, -Cw*12, -Cw*14, -Cw*16 & -Cw*1702	Yes	Yes (AD169)
VMAPRTLIL	HLA-Cw*2 & -Cw*15	Yes	No
VMAPRTLIL	HLA-Cw*0809	No	No
VMAPRALLL	HLA-Cw*07 & -Cw*18	Yes	No
VMAPQALLL	HLA-Cw*1701 & -Cw*1703	No	No
VMAPRTLFL	HLA-G*01	Yes	No

Qdm peptide AMAPRTLIL as well as peptides derived from Heat Shock Protein 60 (QMRPVSRVL) (Michaelsson et al., 2002), Hepatitis C virus (YLLPRRGPRIL) (Nattermann et al., 2005a), HIV p24 (AISPRTLNA) (Nattermann et al., 2005b) and *Salmonella enterica* serovar Typhi GroEL (KMLRGVNVIL) (Salerno-Goncalves et al., 2004). Despite these findings, HLA-E is considered unlikely to bind a large variety of pathogen-derived peptides *in vivo* due to the restrictive nature of the binding pockets within its antigen-binding cleft.

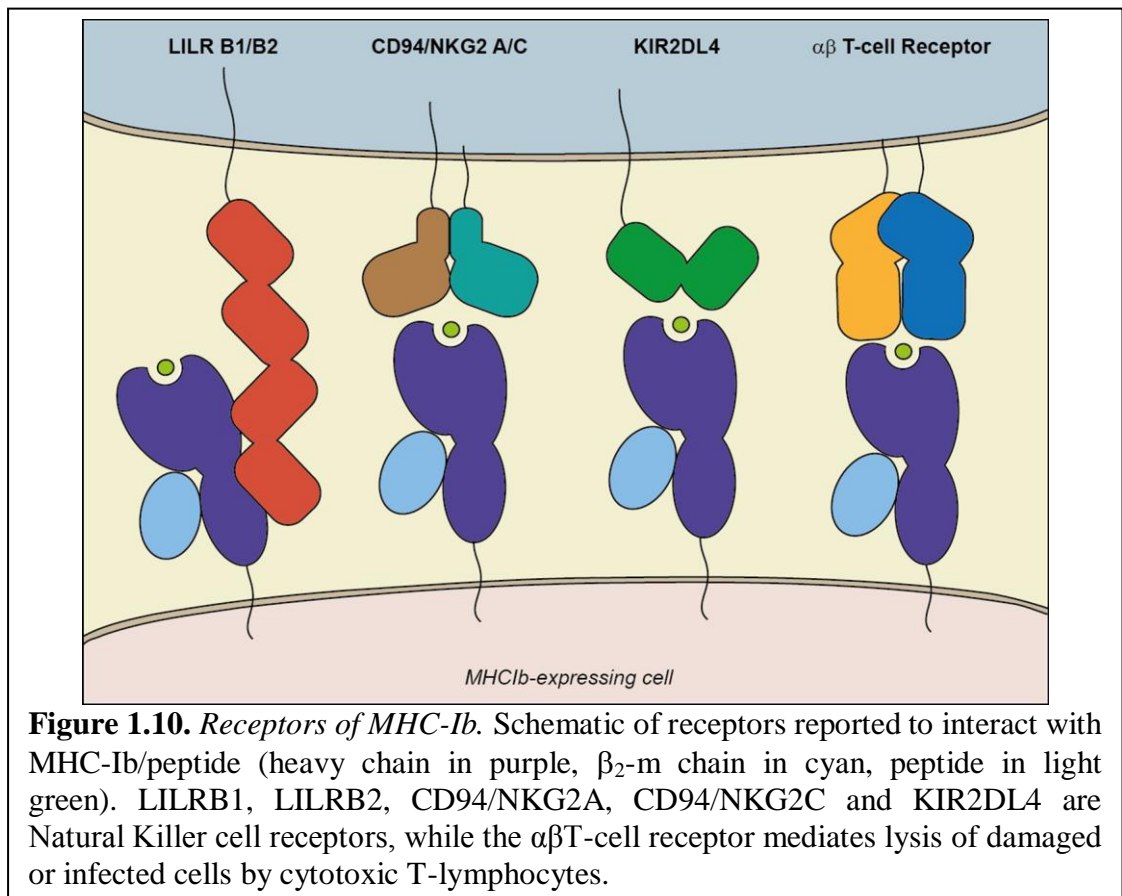
The crystal structure of HLA-E has been solved with various MHC-I leader peptides (O'Callaghan et al., 1998, Strong et al., 2003, Hoare et al., 2008), and the structure of Qa-1b with its native peptide AMAPRTLIL has also been solved recently (Zeng et al., 2012). These structures, along with those of the HLA-E:CD94/NKG2A and HLA-E:TcR complexes, have already given great insight into the mode of peptide binding and receptor recognition, and will continue to do so as more complexes are solved. Figure 1.9 shows the subtlety of the difference between the presentation of the HLA-Cw*07 leader sequence VMAPRALLL, and that of HLA-G,

VMAPRTLFL. Even this slight conformational change causes significant differences in CD94/NKG2 recognition, and may influence the balance of CD94/NKG2-mediated inhibitory and activatory signals to the NK cell nucleus (Hoare *et al.*, 2008, Strong *et al.*, 2003, Miller *et al.*, 2003, Sullivan *et al.*, 2007).



Receptors of Class Ib MHC

While characterisation of MHC molecules may give some understanding of the immune response to invasion and tolerance of self, knowledge of the pathways triggered by antigen presentation is essential to gain an understanding of how the response is generated within monocytes, including NK cells, CD4+ and CD8+ T-cells and antigen-presenting cells. Receptors that have been reported to recognise class Ib MHC molecules generally fall into one of four groups – Killer Immunoglobulin-like Receptors (KIRs), Leukocyte Ig-like Receptors (LILR) receptors (also called Ig-like Transcript, or ILT), CD94/NKG2 receptors and $\alpha\beta$ TcRs. Of these, KIR2DL4 and receptors in the LILR family are reported to bind to HLA-G (Rajagopalan and Long, 1999, Shiroishi *et al.*, 2003), while CD94/NKG2 receptors primarily to HLA-E (Braud *et al.*, 2003). While both HLA-G and HLA-E have been reported to elicit a T-cell response (Ulbrecht *et al.*, 2000, Lenfant *et al.*, 2003), only HLA-E has been demonstrated to interact directly with $\alpha\beta$ TcR (Pietra *et al.*, 2003).



The KIR, LILR, CD94/NKG2 and T-cell receptor families all have distinct characteristics, which are dependent on the immunological roles that they perform. Basic structures of these receptors, as well as their mode of binding to MHC-Ib, are shown in figure 1.10. Most of these receptors, with the exception of LILRs, bind to the peptide-binding region of the MHC (as determined by mutagenesis studies or crystal structures of the complexes), which raises the possibility that a change in peptide sequence or conformation may have a dramatic effect on binding specificity and affinity.

Receptors of HLA-G

KIR2DL4 and the KIR family

The KIR family of NK cell receptors, with 16 members identified to date, plays an important role in innate immunity. While some members have been identified as interacting with allotypic forms of MHC-Ia molecules, the ligands for others have yet to be determined, as shown in Table 1.4 (*Gardiner, 2008*). Interestingly, despite having an orthologous MHC locus, mice do not possess KIRs, instead possessing the Ly49 family of C-type lectin NK receptors.

Table 1.4. KIR family receptors. Summary of signalling potentials and ligand specificities (*Gardiner, 2008*). Extracellular domains are also indicated.

KIR gene	Signalling Potential	Ligand	Domain Configuration
2DL1	Inhibitory	HLA-C2	D1, D2
2DL2, 2DL3	Inhibitory	HLA-C1	D1, D2
2DL4	Activatory + Inhibitory*	HLA-G	D0, D2
2DL5	Inhibitory	Unknown	D0, D2
3DL1	Inhibitory	HLA-Bw4	D0, D1, D2
3DL2	Inhibitory	HLA-A3, A11	D0, D1, D2
2DS1	Activatory	HLA-C2	D1, D2
2DS2	Activatory	HLA-C1	D1, D2
2DS3	Activatory	Unknown	D1, D2
2DS4	Activatory	Unknown	D1, D2
2DS5	Activatory	Unknown	D1, D2
3DS1	Activatory	HLA-Bw4?	D0, D1, D2
3DL3	Unknown	Unknown	D0, D1, D2
2DP1, 3DP1**	Not Expressed		

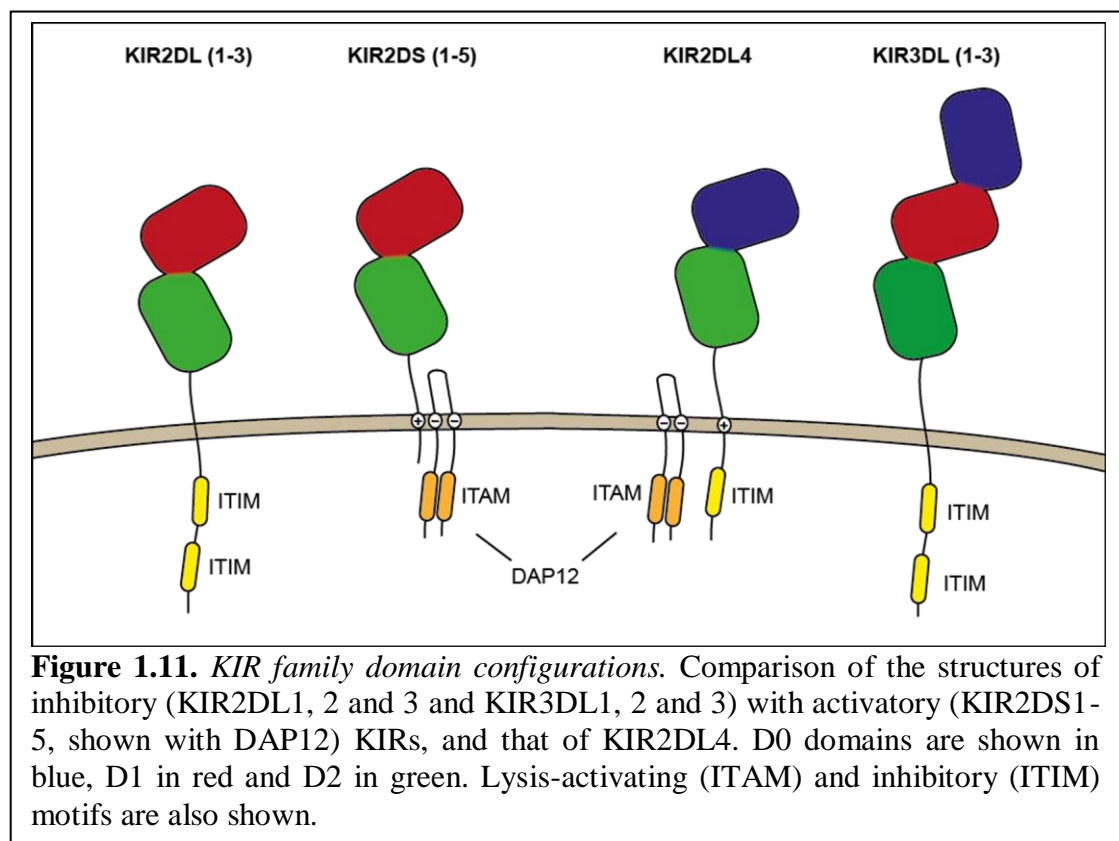
* - KIR2DL4 is designated an activatory signalling potential in the cited review by Gardiner, however is generally considered both activatory and inhibitory due to the presence of a functional ITIM and a demonstrated association with the activating signal-transducing molecule DAP12 (*Faure et al., 2003*).

** - 2DP1 and 3DP1 are pseudogenes.

The names of KIR family members denote the number of E-type Immunoglobulin-like extracellular domains contained (ie 2D or 3D), along with the size of the intracellular tail (Short or Long). As shown in figure 1.11, the extracellular domains are classed as D0, D1 or D2. While each of these domains is highly polymorphic (*Gardiner et al., 2008*), they share around 35-41% amino acid identity and 46-56% similarity, with the D0 domain showing slightly more divergence than the D1 and D2 domains. Compared with the D1 and D2 domains, little is known of the role of the D0 domain. This domain appears to be an essential feature for receptors that interact with HLA-A and HLA-B alleles, and its presence in progenitor KIRs has been demonstrated - deletion events later contributed to the formation of the KIR2D genes (*Guethlein et al., 2007*). KIRs that recognise HLA-C alleles do not contain a D0 domain, instead possessing a single D1 & D2 domain (*Khakoo et al., 2002*). What is also clear is that the length of the cytoplasmic tail has an effect on signalling potential (*Moretta et al., 2000b*). KIRs containing a long tail possess either 1 or 2 Immunoreceptor Tyrosine-based Inhibitory Motifs (ITIMs), which recruit

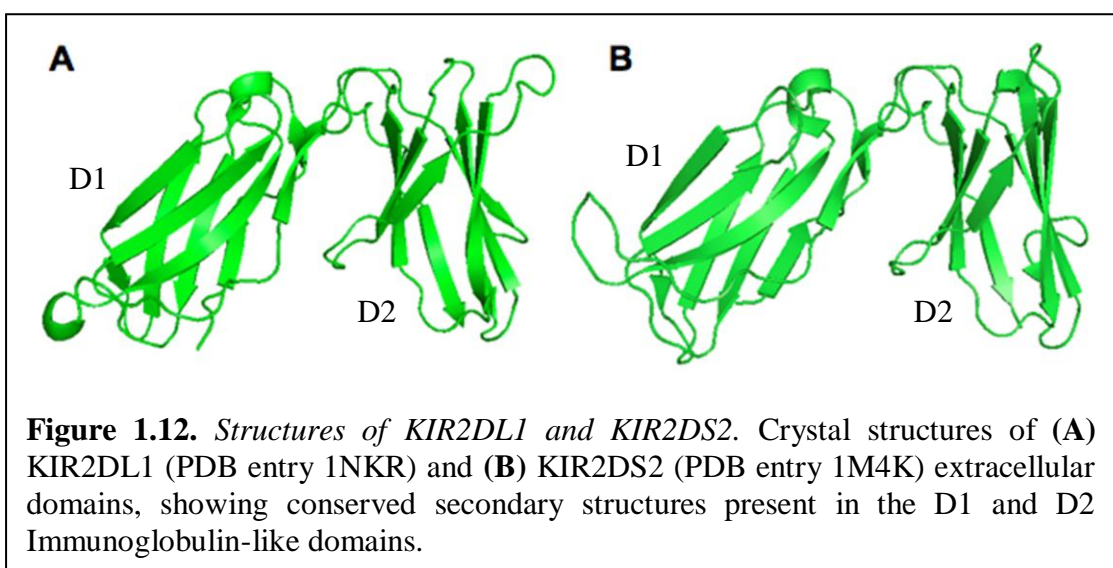
cytoplasmic inhibitory signal-transducing molecules. KIRs that contain a short tail lack ITIMs, however they possess a membrane-embedded positively charged amino acid, which recruits membrane-associated activating signal transducers such as CD3 ζ , Fc ϵ RI γ and DAP-12. These signal transducers possess cytoplasmic Immunoreceptor Tyrosine Activating Motifs (ITAMs). The ITAMS facilitate the transduction of activation signals via p72^{syk} and ZAP70, which are cytoplasmic Phosphatase Tyrosine Kinase (PTK) signalling molecules (*Biassoni et al., 2001, Moretta et al., 2000a, Biassoni et al., 2003*). The exception to this is KIR2DL4, which possesses a long cytoplasmic tail with one ITIM, however has also been shown to recruit DAP-12 (via a charged membrane-embedded amino acid) and transduce activation signals (*Kikuchi-Maki et al., 2003, Kikuchi-Maki et al., 2005, Faure and Long, 2002, Rajagopalan et al., 2001*).

KIR expression is significantly variable, with only 3 of 16 family members expressed in every haplotype – 3DL2, 3DL3 and 2DL4, all of which have inhibitory function (*Gardiner, 2008*). While it is acknowledged that KIR2DL4 has an additional activatory function, it is widely inferred from the ‘minimal’ haplotype, as well as the weak binding of activatory KIRs to Class I MHC (*Rajagopalan and*



Long, 2005), that only inhibitory KIRs are necessary for normal immune function. From this it is considered that their primary role is in immunological tolerance of self, rather than immune activation during invasion.

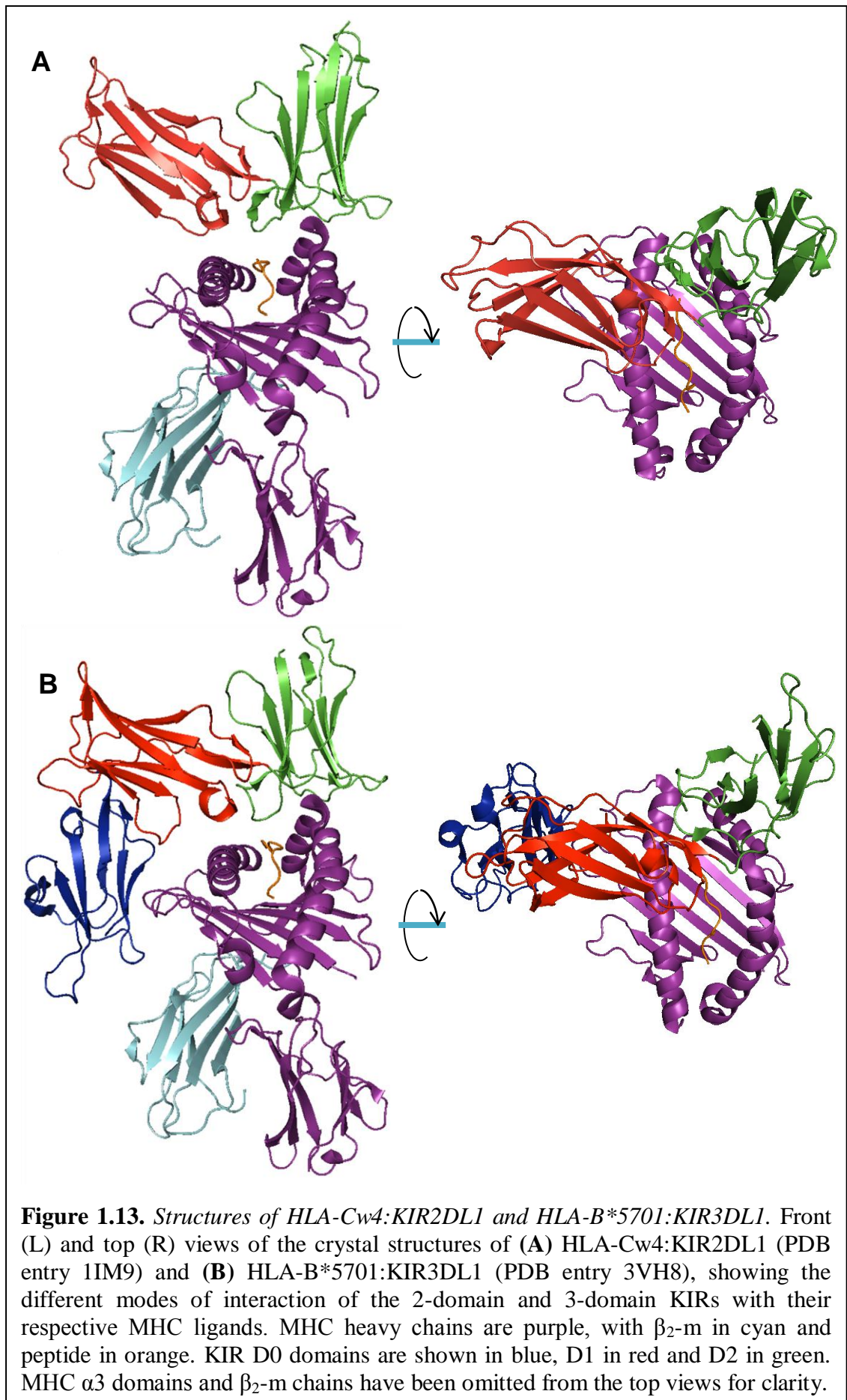
The KIR2DL4 receptor (also called p49), unlike other KIR family members, is largely non-polymorphic, is expressed by the vast majority of NK cells (*Rajagopalan and Long, 1999*), and has the potential to transduce both activating and inhibitory signals (*Faure et al., 2003*) due to its possession of an intracellular ITIM and its ability to recruit DAP-12 for activatory signal transduction. KIR2DL4 contains only the D0 and D2 domains (KIR2DL5 is the only other KIR with this domain configuration), and direct binding analysis has demonstrated an interaction with HLA-G (*Rajagopalan and Long, 1999*), the only known KIR:MHC-Ib interaction. The involvement of HLA-G residues Met76 and Gln79 on the $\alpha 1$ helix (*Yan and Fan, 2005*) suggests that KIR2DL4 interacts with HLA-G via the peptide-binding region of the MHC. However the interaction observed in these cell-based studies, in addition to earlier work (*Cantoni et al., 1999*) could not be reproduced by Boyson *et al.*, who did not detect an interaction between either recombinant or transfected HLA-G^{VLPKLYVKL} and a KIR2DL4-Ig fusion protein by surface plasmon resonance or by a cell-based system (*Boyson et al., 2002*). Though a later study has shown an interaction between recombinant KIR2DL4 and cells expressing HLA-G1 (*Yu et al., 2006*), the nature of the association between KIR2DL4 and HLA-G remains controversial.



Of the KIR2D (2 domain) proteins, the crystal structures of 2DL1 (*Fan et al., 1997*) (Figure 1.12A), 2DL2 (*Snyder et al., 1999*), 2DL3 (*Maenaka et al., 1999*), and 2DS2 (*Saulquin et al., 2003*) (Figure 1.12B) have been determined. All of these KIRs contain a D1-D2 domain configuration. In addition, the complexes KIR2DL1:HLA-Cw4 (Figure 1.13A) (*Fan et al., 2001*) and KIR2DL2:HLA-Cw3 (*Boyington et al., 2000*), have been determined, each showing the KIRs sitting nearly orthogonally across the antigen-binding cleft of the MHC, as seen in figure 1.13A. More recently, the crystal structure of KIR3DL1 in complex with HLA-B*5701 was determined (*Vivian et al., 2011*), enabling analysis of the D0 domain for the first time. This allowed analysis of the location and orientation of this domain, contacting two loops within the $\alpha 1$ domain of the MHC, as is shown in figure 1.13B.

The relatively low polymorphism (among HLA-A and -B allotypes) of the MHC loops contacted by the D0 domain of KIR3DL1 led to the conclusion that the D0 domain functions as an ‘innate pHLA sensor’ (*Vivian et al., 2011*). This correlated with previous studies, one of which demonstrated a role for the D0 domain in enhancing the primary interaction between the KIR D1 & D2 domains and the pMHC (*Khakoo et al., 2002*) and another demonstrating that while KIR3DL1 specifically recognises pMHC of the HLA-Bw4 serogroup (a group containing a number of HLA-A as well as HLA-B alleles), the D0 domain of KIR3DL1 can weakly recognise other MHC-I, including HLA-B*0702 (of the HLA-Bw6 serogroup) and HLA-G (*Fu et al., 2011*).

As the crystal structure of KIR2DL4 has not yet been determined in complex or in isolation, the exact nature of its interaction with pHLA, and the role that the D0 domain plays in this interaction, has not been elucidated. Determination of the crystal structures of KIR2DL4 and the pHLA-G:KIR2DL4 complex would result in clarification of the current understanding of the role of the D0 domain in KIRs, as well as that of HLA-G:KIR2DL4 interactions. Work performed in characterising the recombinant KIR2DL4 as part of this wider aim is described in Chapter 4 – ‘Characterisation of KIR2DL4’.



Leukocyte Ig-like Receptors (LILRs)

Often given the acronym LIR, and also labelled Immunoglobulin-like Transcript or Macrophage Immunoglobulin-like Receptors (ILT/MIRs), LILRs are broadly expressed on NK cells, T cells, B cells and myeloid cells. Like KIRs, LILRs may act as inhibitory receptors through the function of two to four cytoplasmic ITIM motifs (LILRB receptors), or as activatory receptors through association with Fc ϵ RI γ (Borges *et al.*, 1997, Colonna *et al.*, 1999), as shown in Table 1.5. Most LILRA receptors fall into the latter category, however they are named for a lack of cytoplasmic signalling domains, rather than specific signalling potential. While most LILRs are not fully characterised (Garner *et al.*, 2006, Anderson and Allen, 2009), LILRB1 and LILRB2 have been shown to interact with endogenous MHC-I molecules to maintain tolerance of the MHC expressing cells. Both of these molecules bind preferentially to HLA-G, ensuring a strong inhibitory response mediated by that particular interaction (Shiroishi *et al.*, 2003).

Unlike KIR receptors, most LILR receptors show fairly stable expression, with the exception of LILRA3, which is found in only a small percentage of haplotypes (Wilson *et al.*, 2000). LILR receptors contain 4 extracellular domains (2 in the case of LILRB4), designated D1-D4. The D1 and D2 domains of LILRB1 and LILRB2 are known to recognise and bind a motif in the α 3 domain of their MHC-I ligands (Figure 1.14) (McIntire and Hunt, 2005, Willcox *et al.*, 2003, Shiroishi *et al.*, 2006b).

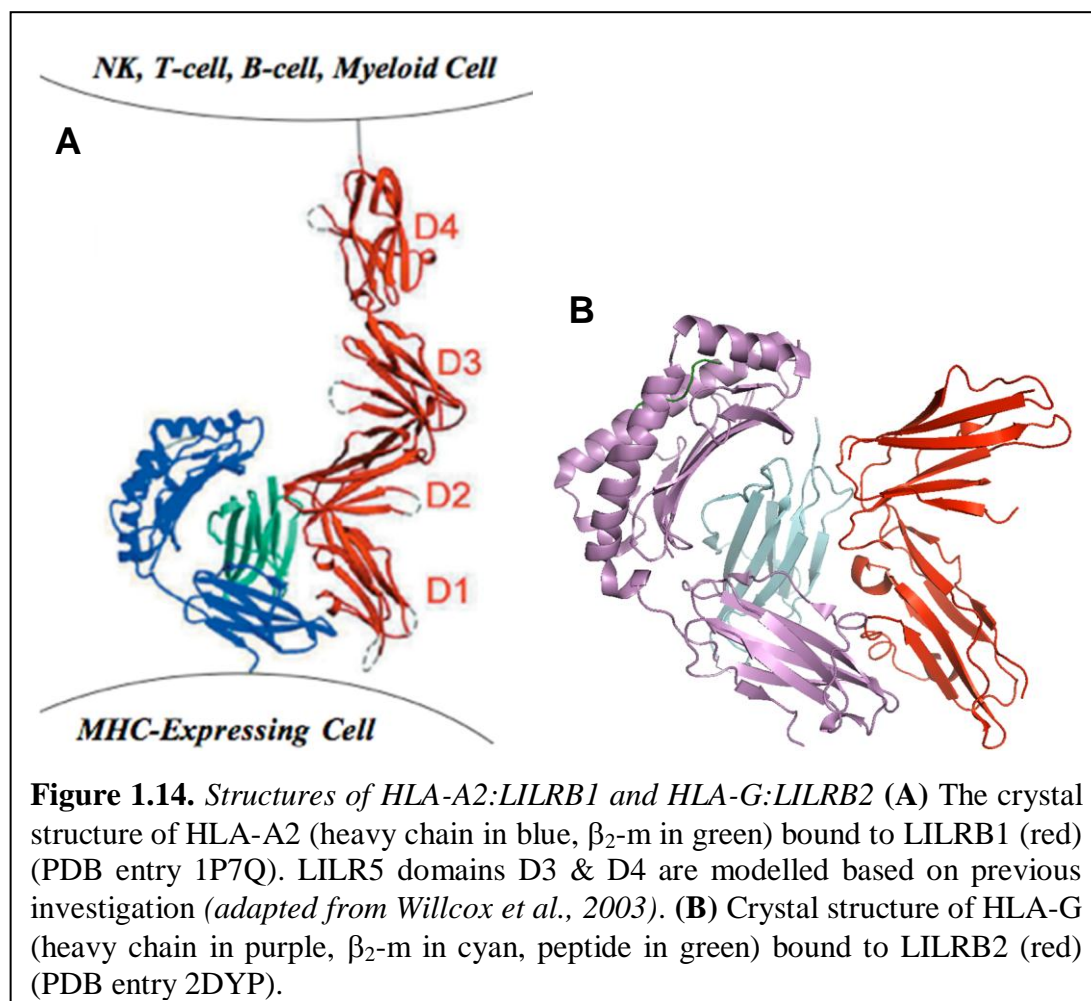


Table 1.5. *LILR family receptors*. Signalling potentials and alternative names for known members of the LILR/LIR/ILT/MIR family (*Colonna et al., 1999, Borges et al., 1997, Anderson and Allen, 2009*).

LILR Designation	Alternate Names	Signalling Potential	Major ligands (if known)
LILRB1	LIR1, ILT2, MIR7	Inhibitory	HLA-A, -B, -G
LILRB2	LIR2, ILT4, MIR10	Inhibitory	
LILRB3	LIR3, ILT5, HL9	Inhibitory	
LILRB4	LIR5, ILT3, HM18	Inhibitory	
LILRB5	LIR8	Inhibitory	
LILRA1	LIR6	Activatory	
LILRA2	LIR7, ILT1	Activatory	MHC-I (including HLA-B27) MHC-I (soluble)
LILRA3	LIR4, ILT6	Neither*	
LILRA4	ILT7	Activatory	
LILRA5	LIR9, ILT11	Activatory	
LILRA6	ILT8	Activatory	
LILRP1**	ILT9		
LILRP2**	ILT10		

* - LILRA3 is secreted, and therefore does not transduce any signal to the expressing cell. It may function to dampen signal strength, binding to MHCs on antigen-presenting cells.

** - LILRP1 and LILRP2 are non-functional pseudogenes.

Receptors of HLA-E

HLA-E is primarily recognised by NK receptors of the CD94/NKG2 family. Interactions with TcRs have also been demonstrated, dependent on the nature of the peptide epitope presented by the MHC.

CD94/NKG2 Receptors

As opposed to the KIR and ILT families, which are immunoglobulin-like receptors, the heterodimeric CD94/NKG2 receptors are part of the C-type lectin protein family. The primary role of CD94/NKG2 receptors involves the regulation of NK cell activity through recognition of HLA-E (*O'Connor et al., 2006, King et al., 2000*). In these receptors the conserved CD94 polypeptide chain is bound to a member of the NKG2 family of receptors via an intermolecular disulfide bond. Seven different NKG2 proteins have been described in humans, not all of which associate with CD94 (*Ding et al., 1999*). Those that do associate with CD94 are NKG2A, -2B, -2C, -2E and -2H, and these display similar modes of NK activation and inhibition as KIRs and ILTs, with activation signals transduced through association with ITAM-containing transmembrane signal transducers, and suppression through inhibitory signals through ITIMs present on the cytoplasmic tail of the NKG2 chain (Figure 1.15).

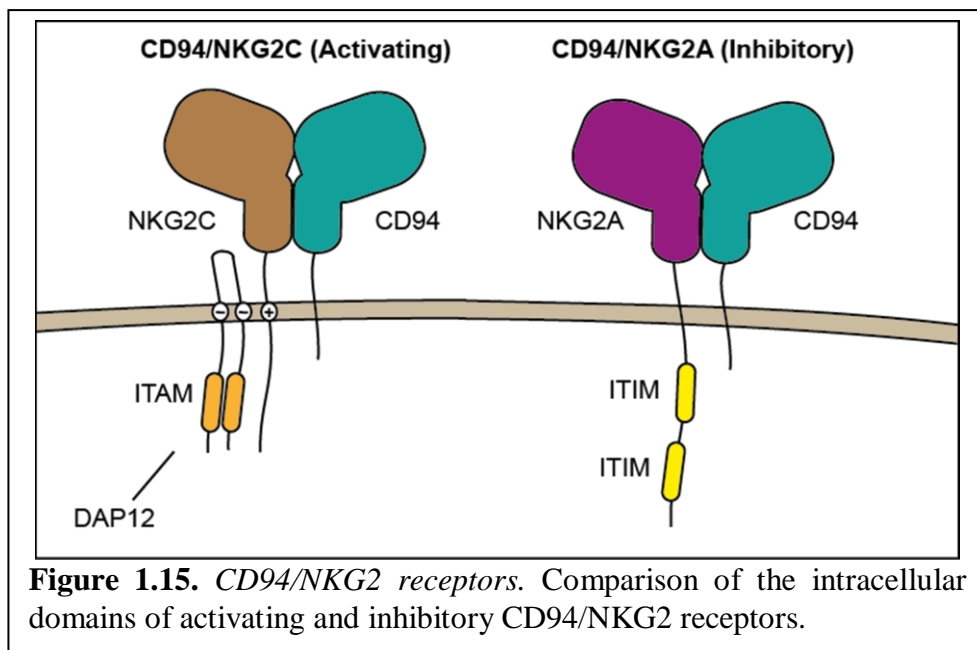
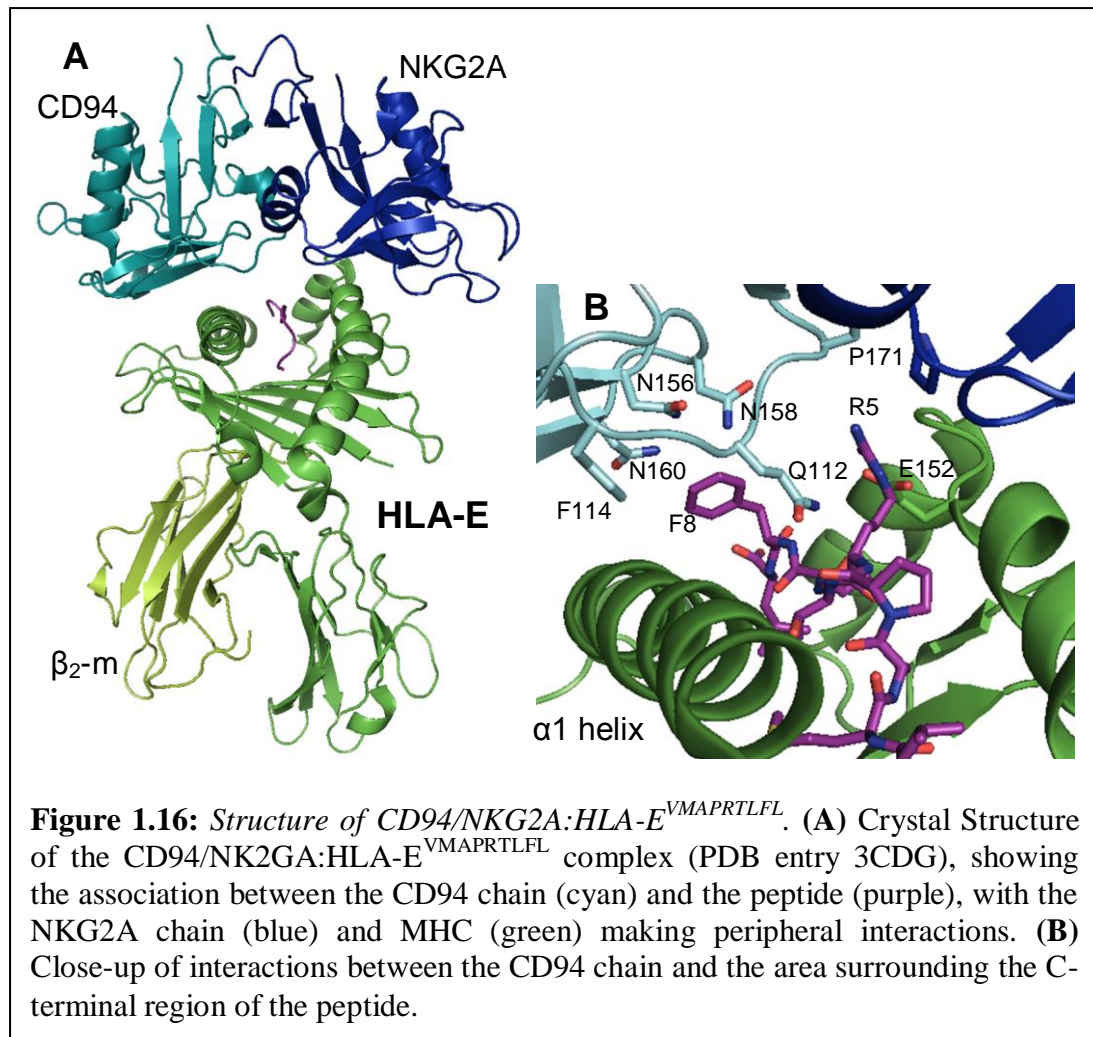


Figure 1.15. *CD94/NKG2 receptors.* Comparison of the intracellular domains of activating and inhibitory CD94/NKG2 receptors.

CD94/NKG2A, -2B, -2C, -2E and -2H are known to interact with pHLA-E (*Braud et al., 1998a, Kaiser et al., 2005*) and the murine pQa-1b (*Vance et al., 1998*) in their respective species. Inhibitory receptors CD94/NKG2A and -2B are near-identical splice variants, which bind HLA-E with a comparable affinity to the activatory splice variants CD94/NKG2E and -2H, and with slightly higher affinity than the activatory receptor CD94/NKG2C (*Kaiser et al., 2005*). The interaction with HLA-E features rapid binding kinetics and is heavily dependent on peptide sequence. Even small changes to the peptide sequence, particularly to the C-terminal region of the peptide, can have a large effect on binding affinity, while HLA-E allelic differences tend to have no effect on affinity (*Miller et al., 2003, Vales-Gomez et al., 1999, Kaiser et al., 2005, Hoare et al., 2008*). Murine CD94/NKG2E recognition of pQa-1b has been implicated in the resistance of C57BL/6 mice to mousepox, and similar mechanisms have been proposed for the human immunological response to the smallpox and monkeypox viruses (*Fang et al., 2011*).

The crystal structure of the CD94/NKG2A heterodimer was solved in 2007 (*Sullivan et al., 2007*) and showed an asymmetric mode of heterodimerisation between the two chains, demonstrating a mode of preferential binding between the invariant CD94 and the different NKG2 chains despite significant structural homology between the CD94 and NKG2 subunits. The same paper from Sullivan *et al* also describes targeted mutagenesis of CD94/NKG2A and pHLA-E based on knowledge of the CD94/NKG2A structure. These experiments suggested that CD94 has a dominant role in the interaction with pHLA-E, and in the recognition of the bound peptide.

The crystal structure of the CD94/NKG2A:HLA-E complex, with the MHC presenting the HLA-G-derived leader peptide VMAPRTLFL, has been solved (Figure 1.16). As illustrated in figure 1.16B, major interactions were seen between the invariant CD94 chain and the area surrounding the C-terminal region of the peptide, verifying the earlier work by Sullivan *et al* and providing a structural basis for the specificity of the interaction between CD94/NKG2A and HLA-E presenting a MHC-I leader sequence peptide. The NKG2A chain was seen to make only minor interactions with the MHC and the peptide (*Petrie et al., 2008, Kaiser et al., 2008*), also correlating with the mutagenesis data of Sullivan *et al*.



$\alpha\beta$ T-cell Receptors (TcRs)

The heterodimeric $\alpha\beta$ T-cell receptor consists of two Ig-like chains, termed the α - and β -chains, each of which contain a V (variable) and a C (constant) domain. Each variable domain contains three complementarity-determining region (CDR) loops, which form the antigen-recognition site of the TcR (*Garcia et al., 1999*). $\alpha\beta$ TcRs exhibit an enormous level of diversity to differentially recognise the large repertoire of MHC-bound peptides. This diversity is achieved through allelic polymorphism at the TcR loci (germline diversity) (*Gras et al., 2010*), rearrangement of the TcR gene segments during T-cell maturation in the thymus (combinatorial joining), imprecise joining of the TcR gene segments (junctional diversity), and random addition or deletion of a variable number of nucleotides at the junctions (termed N regions) of these gene segments (N-region diversity) (*Leiden and Strominger, 1986*).

Combinatorial joining in $\alpha\beta$ TcRs describes the random use of V (variable) and J (junction) genes at the $V\alpha$ locus, as well as the V, D (diversity) and J genes at the $V\beta$ locus, for any individual TcR. As mentioned, this rearrangement is used to increase the diversity of $\alpha\beta$ TcR expression, and is enhanced by the imprecise joining of the gene segments, leading to reading frame shifts at the V-D junction (*Leiden and Strominger, 1986*).

As the CDR1 and 2 loops of both $\alpha\beta$ TcR chains are fully within the V gene segment, these loops are considered to be germline-encoded. However, the sequence and length of the CDR3 loops of either TcR chain may be affected by the V, D and J gene segments used, the reading frame of the D gene segment, and the number of added or deleted residues at the N regions (*Rock et al., 1994*). Thus the CDR3 α and CDR3 β loops in $\alpha\beta$ TcRs are subject to extreme diversity in both sequence and length, and are considered to be nongermline encoded.

Positive selection of CTLs in the thymus is dependent on weak recognition by the $\alpha\beta$ TcR of self-pMHC complexes (*Fink and Bevan, 1978, Zinkernagel et al., 1978*), however the negative selection process causes CTLs expressing $\alpha\beta$ TcRs which recognise self-pMHC too strongly to undergo clonal deletion by apoptosis (*Matzinger et al., 1984, Rammensee and Bevan, 1984*). The outcome of this process is CTLs expressing $\alpha\beta$ TcR which recognise MHC presenting foreign antigen, while recognising self-pMHC too weakly to cause an autoreactive response. In general these $\alpha\beta$ TcR are 'restricted' to a single self-MHC molecule, however cross-reactivity of one TcR with more than one MHC has been demonstrated (*Archbold et al., 2006*).

$\alpha\beta$ TcR interactions with MHC-Ia binding foreign antigen have been well characterised, and it has been shown that the MHC peptide binding region is the site of TcR:MHC interaction (as shown in figure 1.17A). However, only a few residues from the antigenic peptide tend to play any role in interactions, with residues from the MHC-Ia playing a much larger role (*Rudolph et al., 2006, Clements et al., 2006*). To date at least 18 different TcR-pMHC-Ia structures have been determined, and a number of conserved features have been observed from these structures (*Burrows et al., 2010*).

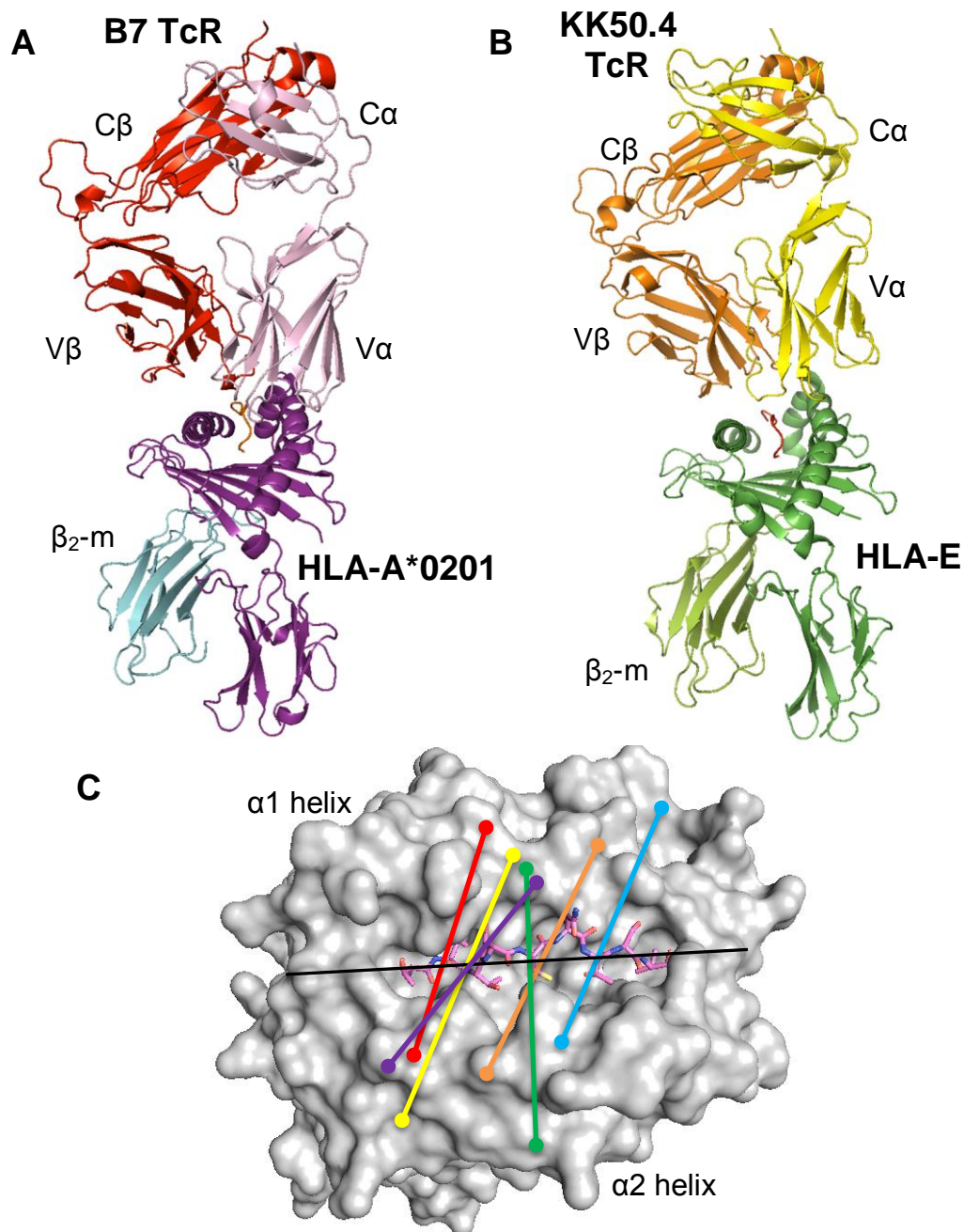


Figure 1.17. *TcR:pMHC interactions.* (A) Crystal structure of the B7 $\alpha\beta$ TcR (pink and red) bound to HLA-A*0201 (heavy chain in purple, β_2 -m in cyan, peptide in orange) (PDB entry 1BD2). (B) Crystal structure of the KK50.4 $\alpha\beta$ TcR (yellow & orange) bound to HLA-E (heavy chain in green, β_2 -m in light green, peptide in red) (PDB entry 2ESV). (C) Analysis of TcR docking at the MHC-I antigen-binding cleft. Superimposed on a surface representation of HLA-A2 (grey, peptide in magenta) (PDB entry 1HHI), docking orientations are shown for the AHIII 12.2 TcR:HLA-A2^{ALWGFFPVLS} (green), KB5-C20 TcR:H-2K^{bKVITFIDL} (purple) (Buslepp *et al.*, 2003), B7 TcR:HLA-A2^{LLFGYPVYV} (red), KK50.4 TcR:HLA-E^{VMAPRTLIL} (beige), LC13 TcR:HLA-B8^{FLRGRAYGL} (blue) (Hoare *et al.*, 2006) and TK3 TcR:HLA-B35^{HPVGEADYFEY} (yellow) (Gras *et al.*, 2010) complexes. Docking orientations were calculated by connecting the centres of mass of the TcR α and β variable domains, and are shown relative to the antigen-binding cleft (black line).

Firstly, the overwhelming majority of TcR-MHC contacts are between the CDR loops of the TcR and the $\alpha 1$ and $\alpha 2$ helices of the MHC. The prevalent dogma is that the germline-encoded CDR1 and 2 loops of each of the α - and β -chains form the primary contacts with the MHC, while the nongerm-line-encoded CDR3 α and CDR3 β loops form primary contacts with the peptide (*Garcia et al., 2009*). This is not exclusively the case, as the CDR3 loops can play a role in interacting with the MHC (*Kjer-Nielsen et al., 2003*), while the CDR1 and 2 loops can make significant interactions with the peptide (*Tynan et al., 2005*).

A second conserved feature of TcR-pMHC structures is a roughly diagonal (though occasionally orthogonal) docking orientation of the TcR across the peptide-binding cleft, as illustrated in figure 1.17C, where docking orientation is determined by calculating the centre of mass of the two TcR variable domains, and connecting these points (*Buslepp et al., 2003*). Such an orientation often results in the TcR V α domain sitting over the MHC $\alpha 2$ -helix and the N-terminal region of the peptide, while the TcR V β domain sits over the MHC $\alpha 1$ -helix and the C-terminal region of the peptide (*Rudolph et al., 2006, Clements et al., 2006, Godfrey et al., 2008*). This docking mode almost invariably results in TcR interactions with the three MHC residues at positions 65, 69 and 155 (*Burrows et al., 2010*). These positions are less polymorphic across MHC-Ia than other α -helix residues, suggesting that this ‘restriction triad’ may play a role in MHC restriction as described earlier.

$\alpha\beta$ TcR interactions with MHC-Ib have not been as well characterised as those with MHC-Ia. However, HLA-E restricted CTL responses specific for the human pathogens *Mycobacterium tuberculosis* (*Heinzel et al., 2002*) and *Salmonella typhi* (*Salerno-Goncalves et al., 2004*) have been isolated, and HLA-E restricted, CMV-peptide specific CTLs form a significant proportion of the CD8⁺ T-cell memory pool in certain CMV-immune individuals (*Ulbrecht et al., 2000, Pietra et al., 2003*). This T-cell response to HLA-E is described in more detail below in *Class Ib MHCs in Adaptive Immunity*.

The structure of the KK50.4 $\alpha\beta$ TcR in complex with HLA-E bound to the CMV UL40-derived peptide VMAPRTLIL (Figure 1.17B) was the first TcR:MHC-Ib complex structure to be determined, and to date is the only published TcR:MHC-Ib

structure. This structure demonstrates a similar mode of recognition to that seen in most $\alpha\beta$ TcR:MHC-Ia interactions, suggesting a direct functional link between Class Ia and Class Ib MHC molecules with regard to adaptive immunity (*Hoare et al., 2006*).

T-cell responses to the Class Ib MHCs HLA-G, HFE, Qa-1b, Q9 and H2M3 have also been reported (*Lenfant et al., 2003, Rohrllich et al., 2005, Soloski and Metcalf, 2001, Lo et al., 2000, Davies et al., 2003, Chiang and Stroynowski, 2004, Chiang and Stroynowski, 2005, Ugrinovic et al., 2005, Chun et al., 2001, Seaman et al., 2000*).

Class Ib MHCs in Adaptive Immunity

Potential roles for HLA-G, HLA-E and other Class Ib molecules in mediating an adaptive immune response have recently been identified as a key area of interest with respect to immunological research, and other roles for these molecules in suppressing the adaptive immune response have also been suggested (*Sullivan et al., 2006*). Further findings in this area will aid our understanding of molecular interactions mediating adaptive immunity, as well as having implications for autoimmune disorders.

HLA-G

While no direct evidence exists for the recognition of HLA-G by $\alpha\beta$ TcRs, a transgenic mouse model has been used to generate HLA-G-restricted T cells that specifically recognise the cytomegalovirus-derived peptide VFPTKDVAL (*Lenfant et al., 2003*). In addition, studies investigating thymus-derived and dendritic-cell populations expressing HLA-G have demonstrated that HLA-G-restricted T-cells could potentially be primed in situations where HLA-G expression is elevated in these tissues (*Mallet et al., 1999, Pangault et al., 2002*). This suggests a possible MHC-Ia-like role recruiting T-cells in adaptive immunity, mediating adaptive immune responses to a restricted subset of viruses, bacteria and tumours, limited by tissue distribution, lack of polymorphism and high peptide specificity. Even taken collectively, these studies provide only a tentative demonstration of a possible adaptive response restricted to HLA-G. However the endogenous peptide repertoire

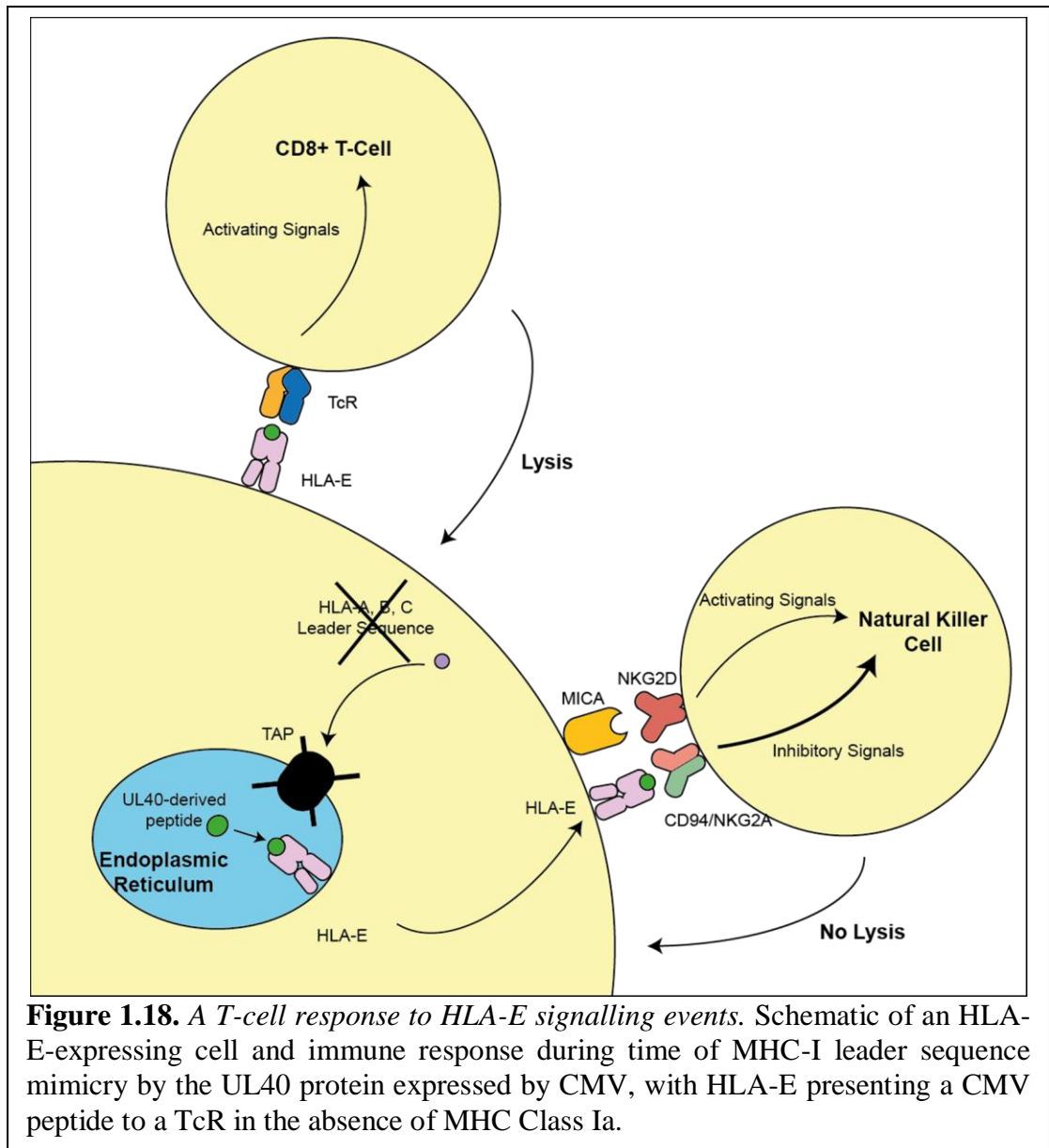
of HLA-G is wider than that of HLA-E, suggesting that HLA-G may also have a wide exogenous peptide repertoire, possibly leading to CTL association in certain circumstances.

HLA-E

As mentioned above, despite restrictive peptide-binding constraints, the ability of HLA-E to bind and present some CMV-derived peptides to cytotoxic T-lymphocytes has been described and discussed in several studies (*Ulbrecht et al., 2000, Pietra et al., 2003, Hoare et al., 2006, Tomasec et al., 2000, Rodgers and Cook, 2005, Sullivan et al., 2006, Sullivan et al., 2008*). These ‘mimotope’ peptides (see Table 1.3) are used by the CMV Toledo and AD169 strains as a means to evade the innate immune system by maintaining HLA-E expression despite TAP knockout, or during MHC-I downregulation (*Ulbrecht et al., 2000*).

Rescue of HLA-E expression is used by these CMV strains to maintain inhibitory signals to NK cells, mediated by CD94/NKG2 receptors. As these receptors are largely unresponsive to changes in peptide sequence, NK-mediated lysis can be evaded even if the mimotope is slightly different to those naturally presented by the host (Figure 1.18).

While the T-cell receptor is more sensitive to changes in peptide sequence than most NK receptors, host genetics plays a key role. Where the CMV-derived mimotope processed in the cell is present in the host’s HLA haplotype, any immature TcR restricted to HLA-E presenting that peptide will be negatively selected during the thymic selection process, and therefore the cell will not be attacked by NK cells (as described above) or by T-cells (because Class I MHC expression has been knocked out and therefore cannot be used to present viral antigen). However, HLA-A and HLA-C haplotypes where these peptides are absent are not infrequent, and in such cases, CTLs recognising HLA-E presenting these peptides would not be negatively selected against, and therefore may mount an adaptive immune response (in the form of cell lysis) to the infected cell. This response is illustrated in figure 1.18.



Pietra *et al* isolated $\alpha\beta$ TcR clones from two distinct groups of donors which recognise, with high avidity, HLA-E presenting the MHC-I leader peptide VMAPRTLIL (with clones from one of these groups also recognising HLA-E^{VMAPRTLVL}) (Pietra *et al.*, 2003). To date, HLA-E-restricted TcRs have been categorised into two groups based on this peptide recognition. Group 2 HLA-E-restricted $\alpha\beta$ TcRs, including the clone KK50.4, recognise HLA-E presenting the peptide VMAPRTLIL (derived from the UL40 ORF of CMV, AD169 strain) with absolute specificity. These TcRs display a highly restricted V β gene usage, while V α gene usage is biased towards specific genes. This gene restriction may be due to the need to avoid cross-recognition of self-pHLA-E, which would stimulate negative

selection during the thymic selection process. Group 1 HLA-E-restricted $\alpha\beta$ TcRs, including the clone GF4, recognise HLA-E presenting either VMAPRTLIL, or VMAPRTLVL, a peptide derived from the UL40 ORF of the CMV Toledo strain. These TcRs show a less restricted V β gene usage pattern, though bias still exists towards the use of certain V α and V β genes.

Other Class Ib MHC

Other MHC-Ib molecules implicated in adaptive immune responses include HFE, as well as the murine Class Ib molecules Qa-1b, Q9 and H2-M3.

Relative to other MHC-I molecules, HFE has a narrowed antigen-binding cleft due to a shift in the α 1-helix, and as a result of buried peptide-binding pockets within this cleft HFE does not bind peptide antigens. Despite this, T-cell responses to HFE have been reported in mice, and HFE-restricted CTLs isolated (*Rohrlich et al., 2005*).

While Qa-1b shows a similar high level of peptide restriction to HLA-E, it has been shown to present the murine Heat Shock Protein 60-derived peptide GMKFDRGYI, as well as pathogen-derived peptides such as the GroEL peptide GMQFDRGYL from *Salmonella typhimurium*, suggesting that there is also some flexibility in the Qa-1b binding repertoire, and T-cells specific for Qa-1b presenting this GroEL peptide have been isolated (*Soloski and Metcalf, 2001, Lo et al., 2000, Davies et al., 2003*).

Q9, a member of the Qa-2 family of murine MHC-Ib molecules, does not have a conventional transmembrane region, and instead is connected to the membrane via a glucosylphosphatidylinositol anchor (*Stroynowski et al., 1987*). Q9 has an unusual shallow, hydrophobic antigen-binding cleft, resulting in a peptide conformation with a large central bulge (*He et al., 2001*). Perhaps because of this, Q9 binds a large peptide repertoire (*Joyce et al., 1994*), resulting in a reported role in anti-tumour responses. Q9-restricted CTL responses have been described in several studies, with Q9-restricted CD8⁺ T-cells possessing a phenotype similar to class-Ia restricted memory cells (*Chiang and Stroynowski, 2004, Chiang and Stroynowski, 2005*).

Like HFE and Q9, H2-M3 has evolved a specialised antigen-binding cleft, and preferentially binds *N*-formylated prokaryotic peptides (Wang *et al.*, 1995, Lindahl *et al.*, 1995). Studies have shown that H2-M3 can present epitopes to CD8⁺ T-cells during *Salmonella enterica*, *Mycobacteria* and *Listeria monocytogenes* infections (Ugrinovic *et al.*, 2005, Chun *et al.*, 2001, Seaman *et al.*, 2000).

Taken collectively, these reports demonstrate that MHC-Ib-mediated adaptive immune responses to certain pathogens may form a significant part of the holistic immune response to these pathogens. There is sufficient evidence that further research in this field is justified, both in the identification of MHC-Ib-mediated adaptive immune responses to further pathogenic challenges, and also in the characterisation of those responses that have already been identified.

Chapter 2 - Materials and Methods

DNA

Plasmid Preparation

Plasmid preparations for use in cloning, transformations and transfections were performed using the Plasmid Miniprep, Midiprep, Megaprep and Gigaprep DNA purification kits (Qiagen, Germany), according to the manufacturer's instructions. Following purification, DNA was dissolved in TE buffer (10mM Tris-HCl pH8.0, 1mM NaEDTA). If sterilisation was necessary, DNA was precipitated for 5 min by the addition of 2 volumes of 100% ethanol and sodium acetate pH 5.2 to 0.1M final concentration. DNA was pelleted by centrifugation at 13,000g for 10 min and the supernatant discarded. The pellet was washed by the addition of 1.5ml 70% ethanol and centrifuged for a further 5 min. The supernatant was removed in a sterile fume hood and the pellet allowed to air dry, before dissolving in sterile TE buffer. Whether sterilisation was performed or not, the concentration of DNA was estimated by comparison to DNA standards by agarose gel electrophoresis or by UV absorption using a NanodropTM (Thermo Fisher Scientific, USA) according to the manufacturer's instructions. DNA was stored at -20°C.

Sequencing

Plasmid DNA template (300-500ng) was used in each 20µl sequencing reaction. Priming was carried out using oligonucleotide primers (3pmol) complementary to a sequence upstream of the multiple cloning site of either the pET-30 or pHLseq vector. Sequencing reactions were performed using Big Dye Terminator Cycle Sequencing. Following the sequencing reaction, reaction products were precipitated for 10 min by the addition of 50µl of 70% ethanol and sodium acetate pH5.2 to 0.1M final concentration. Sequencing reaction products were pelleted by centrifugation at 13,000g for 5 min, and the supernatant discarded. The pellet was washed in 50µl of 70% ethanol and centrifuged for a further 5 min. The supernatant was discarded and the pellet was dried for 2 min at 90°C before being submitted for sequence analysis. Sequence analysis was performed at the Micromon DNA Sequencing Laboratory at Monash University (Clayton, Australia) by dideoxy chain termination sequencing.

Restriction endonuclease digestion and cloning

Commercial restriction endonucleases with accompanying buffers and bovine serum albumin (BSA) (New England Biolabs, USA) were used according to manufacturer's instructions. To sub-clone gene fragments from storage vectors into the pET-30 or pHLseq expression vectors or the pFastBacTM vector, restriction endonuclease digestion of DNA was performed for 2 hrs, following which DNA fragments were separated by electrophoresis on a 1% agarose gel. Gel fragments and empty expression vectors were excised and purified using the PCR Purification kit (Qiagen, Germany) according to the manufacturer's instructions. Ligations were performed using the Quick LigaseTM Kit (New England Biolabs, USA) according to the manufacturer's instructions. Ligation products were purified again using the PCR Purification kit as above in preparation for transformation.

Transformation

Preparation of electrocompetent cells

A single colony of *E. coli* strain BL21 or XL1-Blue was picked from an LB plate, inoculated into 5ml of LB and incubated at 37°C overnight with shaking. 2ml of this culture was used to inoculate 200ml of pre-warmed LB. Bacteria were then grown at 37°C with shaking until growth reached log phase, at which point cells were harvested by centrifugation at 2000g for 10 min at 4°C. Cells were washed 3 times with cold 10% glycerol by centrifugation at 2000g for 10 min at 4°C. Competent cells were then divided into 50µl aliquots and either used fresh or snap frozen in liquid nitrogen and stored at -80°C.

Transformation by electroporation

Competent bacterial cells were thawed on ice for 10 min. 50ng or 5µl of cold plasmid DNA was mixed with 20µl of cells and added to a 0.5cm electroporation cuvette. Cells were then electroporated using a BIO-RAD Gene Pulser at a voltage of 1.8kV, resistance of 200Ω, and capacitance of 25µFD. 1ml of warm LB was then added to the cuvette and the entire suspension was transferred to a sterile culture tube for incubation at 37°C for 1-2 hrs (note: incubation was not performed for electroporation of plasmids containing ampicillin resistance genes). Transformed cells were pelleted and resuspended in 200µl of supernatant, and were spread onto LB plates containing an appropriate selective antibiotic.

Production of KIR2DL4

Insect cell expression system – Preparation and amplification of viral stocks

Production of a baculovirus shuttle vector (bacmid) containing cDNA encoding the KIR2DL4 gene was performed according to the Bac-to-BacTM Baculoviral Expression System (Invitrogen, USA), based on the method of Luckow et al (*Luckow et al., 1993*). The FastBacTM vector containing cDNA encoding the KIR2DL4 extracellular region (residues 24-218), with an N-terminal 6xHis tag, was transformed into DH10Bac Δ CC cells containing bacmid DNA. Colonies containing the recombinant bacmid were identified using blue/white selection on LB Agar plates containing IPTG and Bluo-gal, in addition to selective antibiotics.

Purified recombinant bacmid DNA was transfected into Sf9 insect cells in 2ml Grace's Insect Cell Culture Medium using CellfectinTM Reagent (Invitrogen, USA) to aid transfection. Cells were then incubated for 48 hrs at 27°C to allow the introduced virus to replicate effectively. Following incubation, cells and debris were removed by centrifugation at 4000g for 15 min and the supernatant (P1 viral stock) used to inoculate log phase Sf9 cells in Sf900 media. This was incubated for 72 hrs and the supernatant (P2 viral stock) harvested and stored at 4°C. 5ml of the P2 viral stock was used to inoculate log phase Sf9 cells in 500ml Sf900 media, which was then incubated for 48 hrs and the supernatant (P3 viral stock) harvested and stored at 4°C.

Insect cell expression system – Expression of recombinant KIR2DL4

Insect cell expression of the KIR2DL4 extracellular domains was performed in Hi5 cells in Sf900 media. 25ml of P3 viral stock was used to inoculate 1L of log phase cells. After a 48 hr expression cell media was harvested by centrifugation at 6000g for 15 min and dialysed for 4 hrs in 15 volumes of buffer containing 10mM Tris-HCl pH8.0 and 300mM NaCl. This dialysis step was repeated a further two times. Imidazole was added to a final concentration of 10mM and NaCl to a final concentration of 300mM. The protein was then loaded onto a column containing Nickel resin (GE Healthcare Life Sciences, Uppsala, Sweden), washed with 50ml buffer containing 10mM Tris-HCl pH8.0, 300mM NaCl and 20mM imidazole and eluted with a buffer containing 10mM Tris-HCl pH8.0, 300mM NaCl and 350-400mM imidazole. Protein was further purified by size exclusion on a HiLoad Superdex 200 16/60 gel filtration column (GE Healthcare Life Sciences, Uppsala,

Sweden) in a buffer containing 10mM Tris-HCl pH8.0 and 150mM NaCl. If sufficient purity was not obtained by size exclusion, a further ion exchange purification step was performed on a HiTrap Q column (GE Healthcare Life Sciences, Uppsala, Sweden) using Buffer A containing 10mM Tris-HCl pH8.0 and Buffer B containing 10mM Tris-HCl pH8.0 and 1M NaCl. Protein was eluted over a 0-1M NaCl gradient. Following each purification step, protein was concentrated and buffer exchanged using Amicon 10K MWCO membrane centrifugal concentrators (Millipore, USA). Protein concentration was determined based on comparisons to BSA protein standards on SDS-PAGE or on a NanodropTM (Thermo Fisher Scientific, USA). After purification the pMHC complexes were stored at 4°C in buffer containing 10mM Tris-HCl pH8.0 and 150mM NaCl.

Mammalian cell expression system

Production of the recombinant KIR2DL4 extracellular domains in a transient mammalian cell expression system was performed according to the method of Aricescu et al (Aricescu et al., 2006a, Aricescu et al., 2006b). 700µg of purified and sterilised pHLseq vector containing cDNA encoding the extracellular region (residues 24-218) of the KIR2DL4 gene with an N-terminal 6xHis tag was transfected into HEK293S cells (Sullivan and Satchwell, 2000) in Dulbecco's Modified Eagle Medium (DMEM) supplemented with 2% fetal calf serum (FCS), using 1050µg polyethylenimine (PEI) to aid transfection.

After a 48-72 hr expression cell media was harvested and dialysed for 4 hrs in 15 volumes of buffer containing 10mM Tris-HCl pH8.0 and 300mM NaCl. This dialysis step was repeated a further two times. Imidazole was added to a final concentration of 10mM. The protein was then loaded onto a column containing Nickel resin (GE Healthcare Life Sciences, Uppsala, Sweden), and eluted in a step-wise gradient with a buffer containing 10mM Tris-HCl pH8.0, 300mM NaCl and 100-400mM imidazole. Protein was further purified by size exclusion on a HiLoad Superdex 200 16/60 gel filtration column (GE Healthcare Life Sciences, Uppsala, Sweden) in a buffer containing 10mM Tris-HCl pH8.0 and 150mM NaCl. A further ion exchange purification step was then performed on a HiTrap Q column (GE Healthcare Life Sciences, Uppsala, Sweden) using Buffer A containing 10mM Tris-HCl pH8.0 and Buffer B containing 10mM Tris-HCl pH8.0 and 1M NaCl. Protein was eluted over a

0-1M NaCl gradient. Following each purification step, protein was concentrated and buffer exchanged using Amicon 10K MWCO membrane centrifugal concentrators (Millipore, USA). Protein concentration was determined based on comparisons to BSA protein standards on SDS-PAGE or on a NanodropTM (Thermo Fisher Scientific, USA). After purification the pMHC complexes were stored at 4°C in buffer containing 10mM Tris-HCl pH8.0 and 150mM NaCl.

Production of MHC HC, β_2 -m, TcR α - and β -chains

Protein Expression

The bacterial expression vector pET-30 (Novagen, USA) containing cDNA encoding the heavy chain (HC) extracellular region for HLA-G*0101 (residues 25-299) or HLA-E*0101 (residues 22-297) was used to produce soluble protein for each MHC. These cDNA expression vectors, along with a pET-30 expression vector containing cDNA encoding the β_2 -m light chain (residues 20-119), were transformed into the BL21 strain of *E.coli* as described previously. Expression and purification of MHC and TcR proteins was based on the method of Garboczi et al (*Garboczi et al., 1992*). A single transformed colony was inoculated into 10-50ml of LB media containing kanamycin, and incubated overnight at 37°C with shaking. 8ml of the overnight culture was used to inoculate 800ml of LB media, which was then incubated at 37°C with shaking until an O.D. reading of 0.6 at 600nm was reached. Protein expression was then induced by the addition of 1mM of isopropyl-1-thio- β -galactopyranoside (IPTG), and allowed to proceed for 4 hrs. Bacterial cells were harvested by centrifugation at 6000g for 15 min at 4°C. Cells from 6 x 800ml flasks of LB media were suspended in 30ml of Resuspension Buffer containing 50mM Tris-HCl pH8.0, 25% (w/v) sucrose, 1mM NaEDTA and 10mM dithiothreitol (DTT). 0.2mM phenylmethylsulfonyl fluoride (PMSF) was added to the resuspension which was then stored at -80°C.

Isolation of Inclusion Bodies

Cell suspensions containing expressed protein were thawed to RT and lysed by the addition of 2.5 volumes of Lysis Buffer (containing 50mM Tris-HCl pH8.0, 1% TritonX-100, 1% (w/v) sodium deoxycholate, 100mM NaCl, 10mM DTT and 5mM MgCl₂). 1mg of DnaseI and 5mg lysozyme were added per 50ml of total lysis volume. After 20 min of lysis at RT with agitation, samples were sonicated using a Soniprep sonicator (MSE, United Kingdom). 10mM NaEDTA was added and the lysate was centrifuged at 10,000g for 15 min at 4°C. Insoluble inclusion bodies were purified by resuspension in 150ml Wash Buffer 1 (containing 50mM Tris-HCl pH8.0, 0.5% TritonX-100, 100mM NaCl, 1mM NaEDTA and 1mM DTT) with 0.2mM PMSF, and centrifuged at 10,000g for 15 min at 4°C. This step was repeated 2-4 times. Inclusion bodies were then washed with 100ml Wash Buffer 2 (containing 50mM Tris-HCl pH8.0, 1mM NaEDTA and 1mM DTT) with 0.2mM PMSF and centrifuged at 10,000g for 15 min at 4°C. Inclusion bodies were then solubilised in 10-20ml of Urea Buffer (containing 8M urea, 20mM Tris-HCl pH8.0, 10mM NaEDTA and 1mM DTT) and centrifuged at 30,000g for 30 min at 4°C. The supernatant was then collected and PMSF added to a final concentration of 0.2mM. Inclusion body protein was quantified by comparison to BSA standards using SDS-PAGE. Inclusion bodies were then divided into appropriate aliquots and stored at -80°C.

Generation of correctly folded protein

pMHC Complexes

HLA-E was refolded with two different synthetic peptides (VMAPRTLVL and VMAPRTLIL) and HLA-G with four different synthetic peptides (RIIPRHLQL, KGPPAALTL, KLPAQFYIL and RLPKDFRIL) (Auspep, Australia) to yield six different MHC/peptide complexes, of which four were used for crystallographic studies and the remaining two for biophysical analysis only. These are fully described in Table 2.1. For each of these complexes, 1L refolds were performed in which MHC HC (30mg) and β_2 -m (24mg) were refolded with 30mg peptide over 48-72 hrs, with two additional injections of 30mg MHC HC spread over the length of the refolding step. Refold buffer contained 100mM Tris-HCl pH8.0, 2mM NaEDTA pH8.0, 400mM L-Arginine-HCl, 0.5mM oxidised glutathione and 5mM reduced

glutathione. 1ml of 0.2M PMSF was added directly prior to protein injection. Following refolding, protein was dialysed for 16 hrs against 15 volumes of MilliQ water using 6-8000kDa MWCO dialysis membrane (Livingstone International, Australia). Protein was then purified by ion exchange on a column containing DEAE resin (Sigma-Aldrich, USA) loading with buffer containing 10mM Tris-HCl pH8.0, and eluting in a step-wise gradient with buffer containing 10mM Tris-HCl pH8.0 and 50-200mM NaCl. Protein was further purified by size exclusion on a HiLoad Superdex 75 16/60 gel filtration column (GE Healthcare Life Sciences, Uppsala, Sweden) in a buffer containing 10mM Tris-HCl pH8.0 and 150mM NaCl. A further ion exchange purification step was then performed on a HiTrap Q column (GE Healthcare Life Sciences, Uppsala, Sweden) using Buffer A containing 10mM Tris-HCl pH8.0 and Buffer B containing 10mM Tris-HCl pH8.0 and 1M NaCl. Protein was eluted over a 0-1M NaCl gradient. Following each purification step, protein was concentrated and buffer exchanged using Amicon 10K MWCO membrane centrifugal concentrators (Millipore, USA). Protein concentration was determined based on comparisons to BSA protein standards on SDS-PAGE or on a NanodropTM (Thermo Fisher Scientific, USA). After purification the pMHC complexes were stored at 4°C in buffer containing 10mM Tris-HCl pH8.0 and 150mM NaCl.

Table 2.1. Peptides used for generation of folded pMHC.			
MHC	Peptide	Source	Use
HLA-E	VMAPRTLVL	CMV UL40 or HLA-A leader sequence	Crystallographic studies
HLA-E	VMAPRTLIL	CMV UL40 or HLA-C leader sequence	Crystallographic studies
HLA-G	RIIPRHLQL	Histone H2A	Biophysical analysis
HLA-G	KGPPAALTL	Cytokine receptor	Crystallographic studies
HLA-G	KLPAQFYIL	Unknown (endogenous)	Crystallographic studies
HLA-G	RLPKDFRIL	Unknown (endogenous)	Biophysical analysis

$\alpha\beta$ TcR

The variable domain of the GF4 TcR α -chain consists of the gene segments TRAV35*02 (or Va25) and TRAJ53*01, with the CDR3 α loop sequence AGQPLGGSNYKLT. The corresponding domain of the β -chain consists of gene segments TRBV9*01 (or V β 1), TRBD1*01 and TRBJ1-4*01, with the CDR3 β loop sequence CASSANPGDSSNEKLFF.

The extracellular domains of the GF4 TcR α -chain and β -chain were refolded together over 72 hrs in 1L refold buffer containing 5M Urea, 100mM Tris-HCl pH8.0, 2mM NaEDTA pH8.0, 400mM L-Arginine-HCl, 0.5mM oxidised glutathione and 5mM reduced glutathione. 100mg α -chain and 30mg β -chain was injected every 24 hrs following the addition of 1ml 0.2M PMSF. Following refolding, protein was dialysed for 4 hrs against 15 volumes of a buffer containing 10mM Tris-HCl pH8.0 and 0.1M Urea using 6-8000kDa MWCO dialysis membrane (Livingstone International, Australia), then twice against 15 volumes of 10mM Tris-HCl pH8.0. Protein was then purified by ion exchange on a column containing DEAE resin (Sigma-Aldrich, USA) loading with buffer containing 10mM Tris-HCl pH8.0, and eluting in a step-wise gradient with buffer containing 20mM Tris-HCl pH8.0 and 100-400mM NaCl. Protein was further purified by size exclusion on a HiLoad Superdex 75 16/60 gel filtration column (GE Healthcare Life Sciences, Uppsala, Sweden) in a buffer containing 10mM Tris-HCl pH8.0 and 150mM NaCl. Further purification was achieved by hydrophobic interaction using a Phenyl HP column (GE Healthcare Life Sciences, Uppsala, Sweden) using Buffer A containing 20mM potassium phosphate pH7.9 and 1M $(\text{NH}_4)_2\text{SO}_4$ and Buffer B containing 20mM potassium phosphate pH7.9. Protein was eluted over a 1.0-0.0M $(\text{NH}_4)_2\text{SO}_4$ gradient. Following each purification step, protein was concentrated and buffer exchanged using Amicon 10K MWCO membrane centrifugal concentrators (Millipore, USA). Protein concentration was determined based on comparisons to BSA protein standards on SDS-PAGE or on a NanodropTM (Thermo Fisher Scientific, USA). After purification the GF4 TcR was stored in buffer containing 10mM Tris-HCl pH8.0 and 150mM NaCl.

Pure ternary complex consisting of pHLA-E bound to the GF4 TcR was produced through combining the two purified proteins for 10 min on ice, with pHLA-E in slight molar excess of GF4 (1.2:1 molar ratio). Copurification of complex was achieved by size exclusion on a HiLoad Superdex 200 10/300 gel filtration column (GE Healthcare Life Sciences, Uppsala, Sweden). Purified ternary complex was concentrated to 10mg/ml for crystallographic studies.

Table 2.2. Optimised crystallisation conditions of pHLA-G and GF4:pHLA-E complexes and cryoprotectants used in the crystallisation of those complexes.

Protein	Protein Concentration	Reservoir buffer	Temp	Cryo-protectant
HLA-G ^{KGPPAALT}	8.0mg/ml	14-16% PEG3500 HEPES pH 7.0-7.4 0.2M K(HCOO) 0.1M CoCl	4°C	20% Glycerol
HLA-G ^{KLPAQFYIL}	8.0mg/ml	14-16% PEG3500 HEPES pH 7.0-7.4 0.2M K(HCOO) 0.1M CoCl	4°C	20% Glycerol
GF4:HLA-E ^{VMAPTLIL}	10.0mg/ml	16-20% PEG3350 Bis-Tris Propane pH 8.2 0.2M K ⁺ ,Na ⁺ -(C ₄ H ₄ O ₆)	20°C	5% Glycerol
GF4:HLA-E ^{VMAPTLVIL}	10.0mg/ml	18-20% PEG3350 Bis-Tris Propane pH 8.5-8.6 0.2M K ⁺ ,Na ⁺ -(C ₄ H ₄ O ₆)	20°C	5% Glycerol

Crystallisation

All broad screening crystallisation trials were conducted using the CrystalmationTM system (Rigaku, Japan), using commercial screens from Sigma-Aldrich, Hampton Research and Qiagen. Commercial screen components are described in Appendix 1. Fine screens and optimisation screens were conducted using the hanging drop vapour diffusion technique using 24-well tissue culture Linbro[®] plates with a well size of 1ml. Crystals were grown by mixing 1µl of 6-10mg/ml protein with 1µl reservoir buffer (as shown in Table 2.2) on silicon coated glass cover slips (Hampton Research, USA), which were then sealed over wells containing 1ml reservoir buffer, so that the protein/reservoir mixture was hanging over the reservoir buffer.

Some fine screens were conducted using seeding techniques to enhance crystal nucleation and growth (*Stura et al., 1990*). Streak seeding was performed on 24-well plates that had been set up 24-48 hrs previously. A cat's whisker was dragged in a straight line through a hanging drop from a plate in which crystals of the same protein had already formed, and then dragged once through a hanging drop on the

plate being seeded. The process was repeated using the same crystal-bearing drop, to seed all drops on the new plate.

Macroseeding was also performed on 24-well plates that had been set up 24-48 hrs previously. In this technique, a single whole crystal was transferred from a hanging drop from a plate in which crystals of the same protein had already formed to a drop containing reservoir solution only. After this wash step, the crystal was then transferred to a hanging drop on the plate being seeded. As with streak seeding, the process was repeated so that all drops on the new plate were seeded.

Upon optimal crystal growth, individual crystals were washed in drops containing reservoir buffer solution and sequentially higher concentrations of glycerol, which was used as a cryoprotectant (as shown in table 2.2). Step-wise increases in glycerol concentration were no more than 10% per wash. Following the wash steps, crystals were flash frozen with liquid nitrogen prior to data collection.

Crystallography

All diffraction data was collected using synchrotron radiation on the MX1 or MX2 beamlines at the Australian Synchrotron in Melbourne, Australia. Diffraction data was processed using MOSFLM (version 626) (*Leslie, 1992*) for indexing, refinement of unit cell parameters and integration of the dataset. The CCP4 program SCALA was used to create an internally consistent scaling model for the dataset (*Collaborative Computational Project, 1994*).

Structures were solved by the molecular replacement method using the CCP4 program PHASER. Search models were HLA-G^{RIIPRHLQL} (PDB entry 1YDP) (*Clements et al., 2005*) for HLA-G molecules, HLA-E^{VMAPRTLTL} (PDB entry 3BZF) (*Hoare et al., 2008*) for HLA-E molecules and the LC13 TcR (PDB entry 1KGC) (*Kjer-Nielsen et al., 2002*) for GF4 TcR molecules. These search models were chosen based on the quality of the geometry and the resolution of the structures as well as their similarity to the crystallised proteins. MHC search models included β_2 -m but were otherwise unliganded and the peptide ligands were also omitted. The TcR search model was unliganded and CDR loops were omitted. Refinement of structures

was performed using Coot (*Emsley and Cowtan, 2004*) and programs from the CCP4 suite including REFMAC5 and NCSREF (*Collaborative Computational Project, 1994*). Translation, Libration and Screw parameters were refined using the TLS Motion Determination (TLSMD) server (*Painter and Merritt, 2006*). Structures were validated using MolProbity (*Chen et al., 2010*) and figures were prepared using PyMOL (version 1.3) (*Schrodinger LLC*). More detail regarding the molecular replacement and refinement of the GF4 TcR:pHLA-E structures is given in Chapter 5 under the headings *Structure Solution and Refinement of GF4:HLA-E^{VMAPRTLVL}* and *Structure Solution and Refinement of GF4:HLA-E^{VMAPRTLIL}*.

Biophysical Analysis Techniques

Circular Dichroism (CD) Spectrum Analysis

Circular Dichroism spectrum analysis was performed using a Jasco 810 spectropolarimeter using a temperature controlled cuvette with a 0.1cm path length. The ellipticity (θ) of the recombinant KIR2DL4 at wavelengths between 190nm and 250nm was measured at 25°C. Concentration of the protein sample was 10 μ M.

Small Angle X-ray Scattering (SAXS)

Freshly purified recombinant KIR2DL4 protein samples were prepared in a buffer containing 10mM Tris pH 8.0 and 150mM NaCl. Samples ranged in protein concentration from 1.0mg/ml to 8.0mg/ml for the analysis of KIR2DL4 oligomerisation (described in Chapter 4 under the heading *Biophysical Analysis of Baculovirus-Expressed KIR2DL4* and the sub-heading *Dimerisation and Oligomerisation of Recombinant KIR2DL4*), and from 0.75mg/ml to 5.0mg/ml for the generation of *ab initio* models (described in Chapter 4 under the heading *Small Angle X-ray Scattering (SAXS) of Baculovirus-Expressed KIR2DL4*). SAXS measurements were made using the SAXS/WAXS beamline at the Australian Synchrotron, which is equipped with a Pilatus Detector. Scattering data was collected to provide a range of 0.015-0.5 for the magnitude of the scattering vector (s). Samples and equivalent buffer solutions were analysed in 1.5mm quartz capillaries at room temperature, and were exposed to x-rays for 1 second, 5 seconds and then 1 second as the sample flowed through the capillary. 2D scattering images were normalised for sample transmission and radially averaged. Radiation damage was not

detected for any sample and the 5 second exposure provided the strongest data for each sample. Scattering from the buffer solutions was subtracted after scaling of scattering intensities.

SAXS data analysis was performed using programs in the ATSAS software suite. PRIMUS (Konarev *et al.*, 2003) was used to plot the scattering intensity (I) against the magnitude of the scattering vector (s). The $I(s)$ profiles were extrapolated to zero (s), and comparison with water (using a reference sample) or lysozyme (as a known standard), allowed a molecular mass for the basic unit (and therefore the approximate oligomeric state of the protein) in each sample to be calculated. PRIMUS was also used to generate Guinier plots, wherein $\log_e(I)$ was plotted against the square of the scattering vector (s^2). Close to zero (s), all Guinier plots were approximately linear for a region (the Guinier region). For larger molecules, the Guinier region is small, while for smaller molecules the Guinier region is larger. The gradient of the Guinier region is related to the radius of gyration (R_g) by the equation $\log_e I(s) = \log_e I(0) - \frac{R_g^2}{3} \times s^2$ (Putnam *et al.*, 2007). R_g is defined as the root mean square distance of mass from the centre of gravity of the molecule, and is used to describe the distribution of mass around the centre of gravity.

GNOM (Svergun, 1992) was used to generate a $P(r)$ function via an indirect Fourier transform. The $P(r)$ function provided the relative probabilities of the distances between the scattering atoms and the maximal dimension of the protein in the sample (termed ' R_{\max} ' or ' D_{\max} '), and allowed refinement of the estimated values of R_g and R_{\max} for the protein in the sample. The $P(r)$ function also allowed a preliminary assessment of the basic shape of the protein in solution (Putnam *et al.*, 2007).

DAMMIN (Svergun, 1999) and GASBOR (Svergun *et al.*, 2001) were used to generate 15-20 *ab initio* dummy atom models, which were then aligned, merged and filtered using DAMAVER (Volkov and Svergun, 2003) to give a final dummy atom model adopting the most probable shape of the protein in solution. Final models were viewed and figures prepared using PyMOL (version 1.3) (Schrodinger LLC).

Chapter 3 - The Effect of Peptide Binding on HLA-G

The determination of the crystal structure of monomeric (C42S) (*Clements et al., 2005*) and dimeric HLA-G (*Shiroishi et al., 2006a*) presenting the endogenous peptide RIIPRHLQL provided insight into the mode of peptide binding of HLA-G. Comparison of this structure with previously determined MHC-I structures provided insight into how pHLA-G might be specifically recognised by receptors of the LILR family (via the $\alpha 3$ domain), KIR2DL4 and T-cell receptors (both recognising the peptide-binding cleft). However, the mechanism by which HLA-G could present such a limited yet diverse repertoire of high-affinity peptides, and the effect of the bound peptide on the stability and overall HLA-G structure, remained unclear. It was an aim of my PhD to determine whether unrelated, yet naturally abundant, self-peptides would be presented in a similar conformation by HLA-G in accordance with its role in regulating the immune response, or whether they would cause significant conformational change in either the peptide, the helices flanking the peptide-binding cleft, or other regions of the MHC.

The crystal structures of C42S HLA-G presenting the unrelated peptides KGPPAALTL (the most abundant single peptide derived from placenta) and KLPQAFYIL (the major species eluted from HLA-G-transfected cells) were determined to 2.4Å and 1.7Å resolution respectively. These two HLA-G structures were then compared to the previously solved structure of C42S HLA-G presenting the peptide RIIPRHLQL peptide. While HLA-G^{KGPPAALTL} was observed to be similar to HLA-G^{RIIPRHLQL} in terms of MHC conformation, there were notable differences in the peptide residues P5 and P8, which point out of the antigen binding cleft, and an altered conformation of His70 was observed, possibly to permit a similar mode of binding for the alternative peptide. In contrast, HLA-G^{KLPQAFYIL} was observed to display a number of structural differences in comparison to the two other pMHCs. Conformational flexibility was observed not only in the central region of the peptide, where deviations of up to 2.0Å were observed, but also in the $\alpha 2$ helix, where a deviation of up to 0.9Å was observed, creating a wider peptide-binding cleft in comparison to each of the other HLA-G structures. However, the sites of the peptide anchor residues P1, P2 and P9 remained structurally conserved, and all polar interactions in these areas were conserved across the 3 structures. Thermal stability

of these complexes was found to be similar, with HLA-G^{RIIPRHLQL}, HLA-G^{KGPPAALTL} and HLA-G^{KLPQAFYIL} having T_m values of $73.5 \pm 0.5^\circ\text{C}$, $71.8 \pm 1.8^\circ\text{C}$ and $69.0 \pm 1.7^\circ\text{C}$ respectively. A fourth peptide, RLPKDFRIL, was found to confer the least thermal stability to HLA-G, with a T_m value of $64.3 \pm 1.9^\circ\text{C}$. This is consistent with cell surface expression studies in which the RIIPRHLQL peptide was found to be significantly more effective at stabilising HLA-G on the cell surface than RLPKDFRIL (*Munz et al., 1999b*).

The structural and thermal stability data presented suggest that the peptide presented by HLA-G is likely to influence recognition of HLA-G both directly, through receptor recognition of differing signal residues or conformational flexibility within the peptide-binding cleft, and also indirectly through the regulation of the levels of HLA-G on the cell surface.

The Structure and Stability of the Monomorphic HLA-G Are Influenced by the Nature of the Bound Peptide

Nicholas G. Walpole¹, Lars Kjer-Nielsen², Lyudmila Kostenko², James McCluskey², Andrew G. Brooks², Jamie Rossjohn^{1*†} and Craig S. Clements^{1*†}

¹The Protein Crystallography Unit, Department of Biochemistry and Molecular Biology, School of Biomedical Sciences, Monash University, Clayton, Victoria 3800, Australia

²Department of Microbiology and Immunology, University of Melbourne, Parkville, Victoria 3010, Australia

Received 17 December 2009;
received in revised form
22 January 2010;
accepted 22 January 2010
Available online
1 February 2010

The highly polymorphic major histocompatibility complex class Ia (MHC-Ia) molecules present a broad array of peptides to the clonotypically diverse $\alpha\beta$ T-cell receptors. In contrast, MHC-Ib molecules exhibit limited polymorphism and bind a more restricted peptide repertoire, in keeping with their major role in innate immunity. Nevertheless, some MHC-Ib molecules do play a role in adaptive immunity. While human leukocyte antigen E (HLA-E), the MHC-Ib molecule, binds a very restricted repertoire of peptides, the peptide binding preferences of HLA-G, the class Ib molecule, are less stringent, although the basis by which HLA-G can bind various peptides is unclear. To investigate how HLA-G can accommodate different peptides, we compared the structure of HLA-G bound to three naturally abundant self-peptides (RIIPRHLQL, KGPPAALTL and KLPOAFYL) and their thermal stabilities. The conformation of HLA-G^{KGPPAALTL} was very similar to that of the HLA-G^{RIIPRHLQL} structure. However, the structure of HLA-G^{KLPOAFYL} not only differed in the conformation of the bound peptide but also caused a small shift in the $\alpha 2$ helix of HLA-G. Furthermore, the relative stability of HLA-G was observed to be dependent on the nature of the bound peptide. These peptide-dependent effects on the substructure of the monomorphic HLA-G are likely to impact on its recognition by receptors of both innate and adaptive immune systems.

© 2010 Elsevier Ltd. All rights reserved.

Keywords: human leukocyte antigen G, HLA-G; structural immunology; innate immunity; antigen presentation; adaptive immunity

Edited by I. Wilson

Introduction

Polymorphism is a hallmark of major histocompatibility complex class Ia (MHC-Ia) molecules, enabling them to present a wide spectrum of peptides and providing specificity in recognition by the highly variable $\alpha\beta$ T-cell receptor (TCR) expressed on the surface of cytotoxic T lympho-

cytes. Maintenance of HLA (human leukocyte antigen) polymorphism reflects natural selection for enhanced protective immunity, whereby MHC molecules can differ from one another by many or only a few amino acids. MHC-Ia polymorphism is generally concentrated in the antigen (Ag)-binding cleft, where it can control the size and diversity of the peptide repertoire and the role of tapasin in peptide loading. Moreover, HLA polymorphism can result in altered conformation of the bound peptide or subtly altered juxtapositioning of the α -helices within the Ag-binding cleft, thereby influencing cognate TCR recognition and TCR allorecognition.^{1–3}

In contrast, MHC-Ib molecules are much less polymorphic and often exhibit limited tissue distribution. The MHC-Ib family members include HLA-E, HLA-F, HLA-G and Hfe (HLA-H) in humans and gene products from the H2-M, H2-Q and H2-T regions in mice. The limited polymorphism present

*Corresponding authors. E-mail addresses: jamie.rossjohn@med.monash.edu.au; craig.clements@med.monash.edu.au.

† J.R. and C.S.C. are joint senior authors.

Abbreviations used: MHC, major histocompatibility complex; HLA, human leukocyte antigen; TCR, T-cell receptor; Ag, antigen; NK, natural killer; LILR, leukocyte immunoglobulin-like receptor; KIR, killer cell immunoglobulin-like receptor; vdW, van der Waals; SA, surface area; SC, shape complementarity.

in MHC-Ib genes results in a marked reduction in the diversity of peptides that can be presented by these molecules. For instance, HLA-E has 8 alleles that produce only 3 proteins,⁴ while HLA-G has 36 alleles that make 14 proteins plus additional isoforms from alternate splicing events.⁵ Moreover, class Ib molecules often possess a larger number of primary anchor sites when compared with most class Ia molecules, which further constrains their intrinsic peptide repertoire. For example, the peptide binding groove of HLA-E has evolved to bind peptides derived from the leader sequences of other class I molecules in which residues 2, 3, 6, 7 and 9 of the peptide act as anchor sites.^{6–8} The differences in the repertoire of peptides bound between MHC-Ia and MHC-Ib molecules reflect disparate roles for MHC-Ib in immunity; MHC-Ia molecules are typically involved in adaptive immunity, while MHC-Ib molecules are often considered to act as ligands in innate immunity. For example, HLA-E in humans and Qa-1^b in mice regulate the activation of natural killer (NK) cells by acting as a ligand for the CD94–NKG2 receptors.⁹

The primary site of expression of HLA-G is at the fetal–maternal interface,^{10–13} where it appears to play a role in promoting maternal tolerance of the fetus.¹⁴ The peptide repertoire of HLA-G has been studied both *in vitro*^{15,16} and *in vivo*,¹⁷ leading to the identification of 15 distinct HLA-G-restricted self-peptides.¹⁸ Although HLA-G possesses a large number of anchor sites, the repertoire of peptides that HLA-G can bind appears somewhat less stringent for that observed in HLA-E. HLA-G-restricted peptides display a preference for a basic residue at P1, a proline or small hydrophobic residue at P3 and a leucine at P9.¹⁶ Recently, the high-resolution crystal structure of HLA-G bound to RIIPRHLQL, a peptide derived from histone H2A and one of the most abundant peptides eluted from HLA-G in transfected cells,^{15,16} has been determined.¹⁹ Furthermore, one study reported the low-resolution structure of a disulfide-linked HLA-G^{RIIPRHLQL} dimer,²⁰ consistent with a report that HLA-G exists as a disulfide-linked dimer on the cell surface.²¹ The HLA-G^{RIIPRHLQL} structure revealed an extensive network of bonds between the peptide and HLA-G, providing a molecular basis for the restricted peptide repertoire of HLA-G. The structure also revealed that the mode of peptide binding between HLA-E and HLA-G was remarkably well conserved. Nevertheless, it was unclear how HLA-G could bind disparate self-peptides.

HLA-G has been reported to regulate NK cell activation both directly acting as ligand for the KIR2DL4 receptor and indirectly through the provision of peptides that promote the cell surface expression of HLA-E expression in the trophoblast. HLA-G also binds the receptors LILRB1 (leukocyte immunoglobulin-like receptor B1 or immunoglobulin-like transcript 2) and LILRB2 (leukocyte immunoglobulin-like receptor B2 or immunoglobulin-like transcript 4),^{22–25} where the recognition site is in the $\alpha 3$ domain,²⁶ distal to the Ag-binding

cleft, and therefore unlikely to be affected by the identity of the peptide. The docking mode between HLA-G and KIR2DL4 is unknown; however, HLA-G residues Met76 and Gln79 of the $\alpha 1$ helix are involved,²⁷ suggesting that KIR2DL4 sits atop the Ag-binding cleft—a mode consistent with the binding of other KIRs (killer cell immunoglobulin-like receptors) to MHC-Ia molecules.^{28,29} Thus, the surface formed by the peptide and Ag-binding cleft is likely to influence KIR2DL4 recognition of HLA-G.

To investigate how different peptides are accommodated by HLA-G and how these peptides differentially impact on the conformation on the Ag-binding cleft of HLA-G, we solved the structure of HLA-G presenting two unrelated self-peptides: KGPPAALTL is the most abundant single peptide derived from placenta,¹⁷ whereas KLPQAFYIL is the major species eluted from HLA-G-transfected cells.¹⁵ The observed conformational malleability in the binding modes of these HLA-G-restricted epitopes has implications for the recognition of HLA-G by ligands of adaptive and innate immune systems.

Results

Structure of HLA-G^{KGPPAALTL}

The structure of the HLA-G presenting the peptide KGPPAALTL was determined to 2.4-Å resolution to R_{cryst} and R_{free} values of 21.6% and 29.9%, respectively. The electron density for the peptide, and the contacting residues, was unambiguous and free from crystal contacts. The KGPPAALTL peptide is bound in a linear and extended manner, with a small bulge centered at P4-Pro (Fig. 1a). The peptide is anchored in the Ag-binding cleft at the N- and C-termini via a series of interactions that are conserved throughout MHC-I. Namely, P1-Lys forms H-bonds with Tyr7, Tyr171 and Tyr159 and salt bridges with Glu62 and Glu63 (Fig. 2a). P9-Leu is involved in a network of H-bonds with Asn77, Tyr84, Ser143 (a Thr in MHC-Ia) and Lys146 and a water-mediated H-bond with Thr80 (Fig. 2b).

Collectively, the peptide makes extensive polar and non-polar contacts with HLA-G (Table 1), totaling one salt bridge, 12 H-bonds, eight water-mediated H-bonds and numerous van der Waals (vdW) interactions. Accordingly, the peptide sits lower in the Ag-binding cleft than in MHC-Ia and most closely resembles HLA-E-bound peptides. Indeed, the KGPPAALTL epitope provides a relatively featureless surface in which only the side chain of P8-Thr protrudes from the Ag-binding cleft (Fig. 1a).

The presence of a glycine, two alanines and two prolines within the KGPPAALTL epitope provides little opportunity for side-chain interactions with HLA-G. The two proline residues do not form any

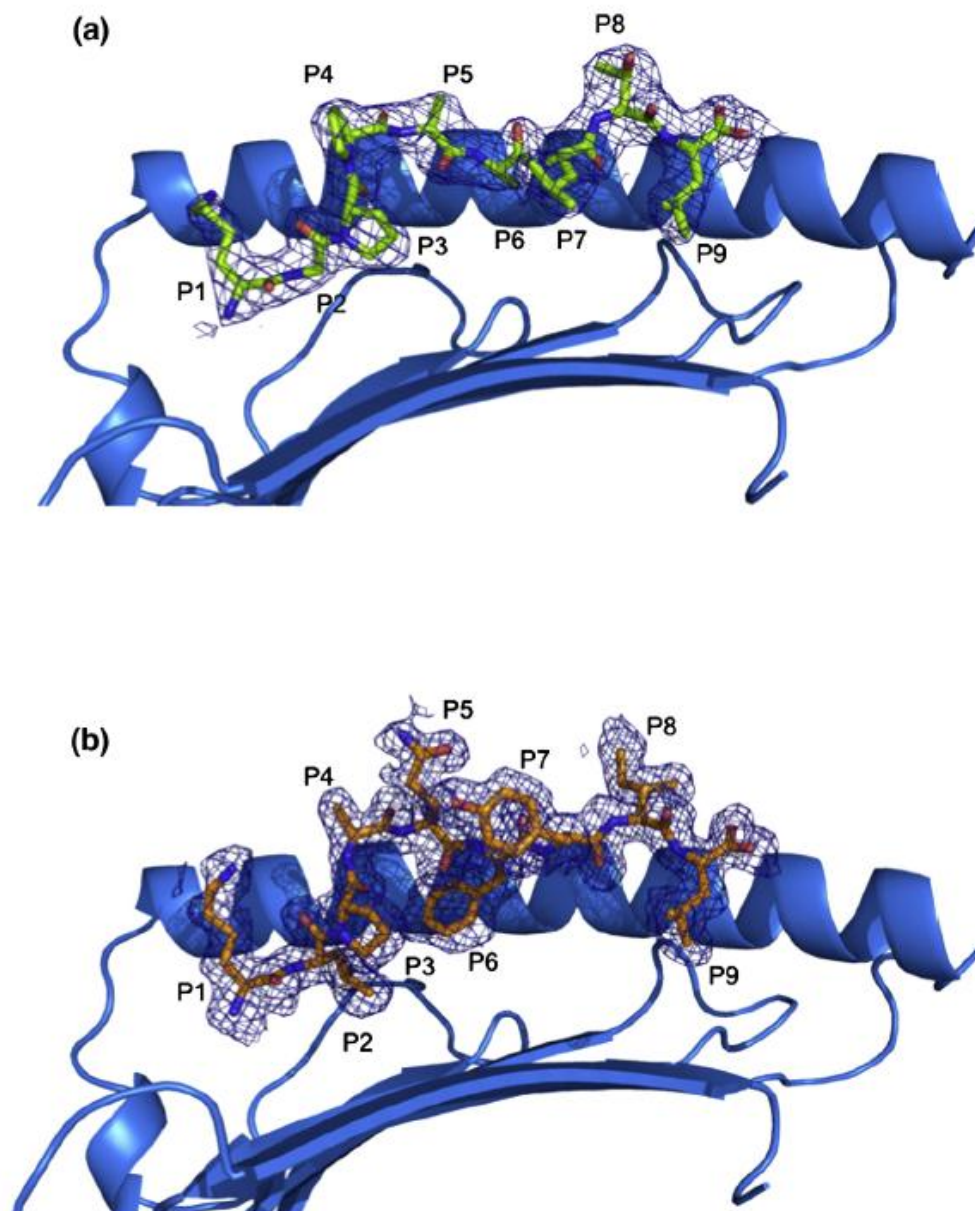


Fig. 1. Structure of pHLA-G complexes. (a and b) Side views of the HLA-G^{KGPPAALTL} complex (a) and the HLA-G^{KLPAQFYIL} complex (b) showing 2.4- and 1.7-Å omit maps, respectively (contoured at 1σ). The $\alpha 2$ helix has been removed for clarity.

polar contacts and only participate in vdW interactions with three residues of HLA-G, suggesting that the prolines are important for maintaining the conformation of the peptide. The main chain of P2-Gly forms H-bonds with Tyr7 and Glu63 and water-mediated H-bonds with Glu63 and Asn66. The O of P5-Ala forms two H-bonds with Arg156, and the N of Ala6 forms water-mediated H-bonds with Ala69 and Thr73. The P7-Leu main chain forms a H-bond

with Asn77 and water-mediated H-bonds with Trp97 and Tyr116 (Table 1).

The overall structure of HLA-G^{KGPPAALTL} is similar to HLA-G^{RIIPRHLQL} with an r.m.s.d. of 0.40 Å over the whole molecule and that of 0.26 Å within the Ag-binding cleft. Furthermore, the KGPPAALTL peptide adopts a conformation remarkably similar to that of the RIIPRHLQL peptide (r.m.s.d. of 0.24 Å between the peptides) despite the

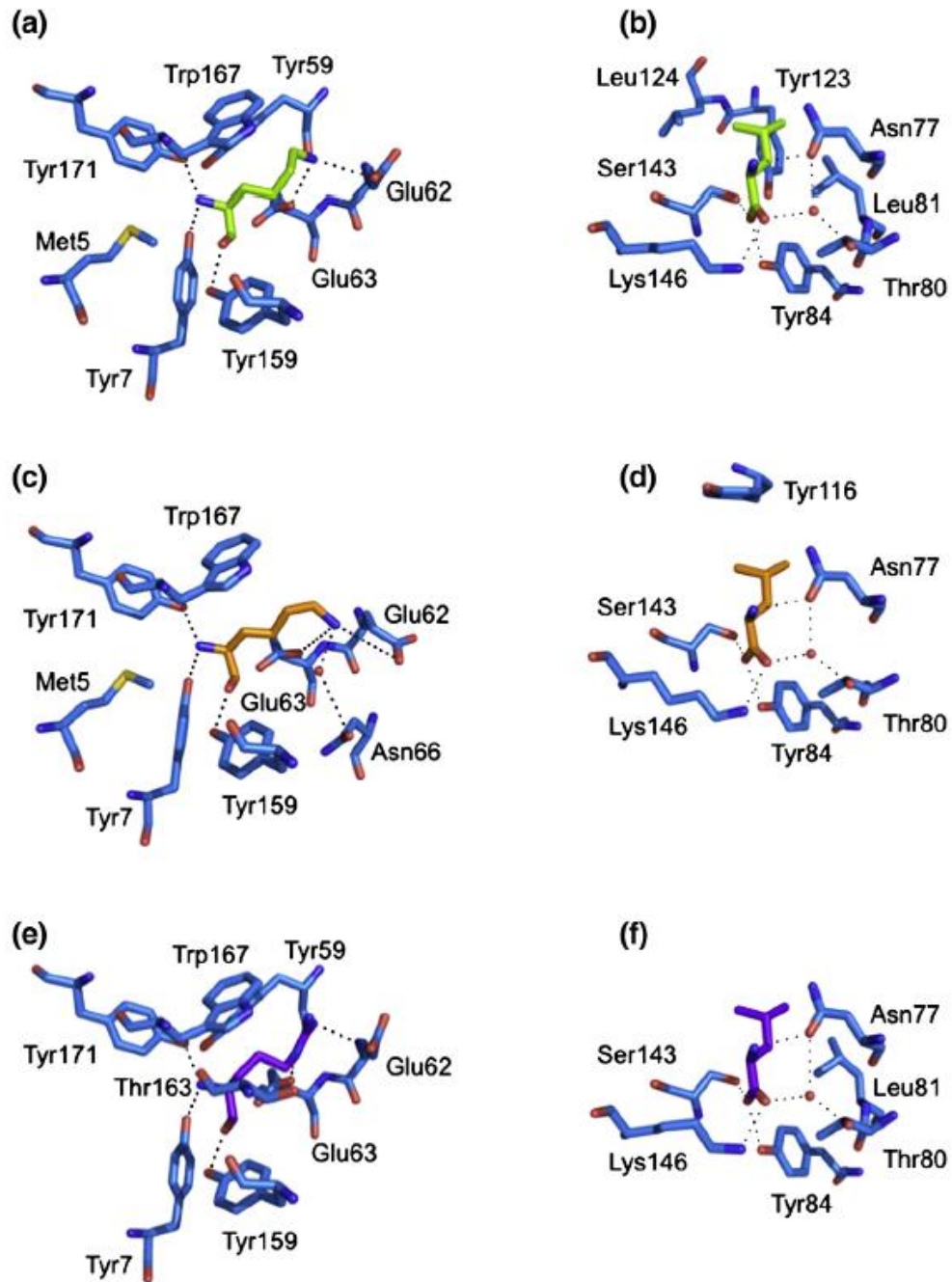


Fig. 2. Conserved interactions between peptide and HLA-G. The polar and non-polar contacts of the P1 residue (a, c, e) and the P9 residue (b, d, f) of each pHLA-G complex are shown. (a and b) HLA-G^{KGPPAALTL}, (c and d) HLA-G^{GKLPAAQFYIL}, (e and f) HLA-G^{RIIPRHLQL}. H-bonds and salt bridges are represented by dashed lines, and water molecules are represented by red spheres.

former not possessing the buried P6-His residue (Fig. 3a). Additional notable differences between the KGPPAALTL and RIIPRHLQL peptides are the

smaller solvent-exposed side chains in the former peptide, specifically Ala and Thr in place of Arg and Gln in P5 and P8, respectively. Accordingly, the

Table 1. HLA-G^{KGPPAALTL} contacts

Peptide residue	HLA-G residue	Interaction
Lys1	Met5, Tyr7, Tyr59, Glu62, Glu63, Tyr159, Trp167, Tyr171	vdW
Lys ^N	Tyr171 ^{OH}	H-bond
Lys ^{Na}	(Glu62 ^{OH}), Glu62 ^{OH}	H-bond
Lys ^O	(Glu63 ^{OH}), Glu63 ^{OH}	Salt bridge
Gly2	Tyr159 ^{OH}	Salt bridge
Gly	Tyr7, Glu63, Tyr159	H-bond
Gly ^N	Tyr7 ^{OH}	vdW
Gly ^O	Glu63 ^{OH}	H-bond
	Glu63 ^{OH}	Water-mediated
	Asn66 ^{N62}	H-bond
Pro3	Asn66, Trp97, Tyr159	Water-mediated
Pro		H-bond
Pro4		vdW
Pro	Asn66	vdW
Ala5		vdW
Ala	Arg156	vdW
Ala ^O	Arg156 ^{NH1}	H-bond
	Arg156 ^{NH2}	H-bond
Ala6		vdW
Ala	His70	vdW
Ala ^N	Ala69 ^O	Water-mediated
	Thr73 ^{Oy1}	H-bond
		Water-mediated
		H-bond
Leu7	Thr73, Asn77, Glu114, Tyr116, Trp133, Arg156	vdW
Leu	Trp97 ^{NH1}	Water-mediated
Leu ^N	Tyr116 ^{OH}	H-bond
		Water-mediated
		H-bond
	Asn77 ^{N62}	H-bond
Leu ^O		H-bond
Thr8	Asn77, Lys146	vdW
Thr		vdW
Leu9	Asn77, Thr80, Leu81, Tyr84, Tyr123, Leu124, Ser143, Lys146	vdW
Leu	Asn77 ^{OH}	H-bond
Leu ^N	Tyr84 ^{OH}	H-bond
Leu ^O	Ser143 ^{Oy}	H-bond
	Lys146 ^{NK}	H-bond
Leu ^{OX}	Asn77 ^{OH}	Water-mediated
		H-bond
	Thr80 ^{Oy1}	Water-mediated
		H-bond

solvent-accessible area of the peptide is only $\sim 300 \text{ \AA}^2$ compared with that of $\sim 400 \text{ \AA}^2$ for the RIIPRHLQL peptide.

The contacts formed between HLA-G and the peptide backbone are well conserved between the two peptides, with only two H-bonds and one water-mediated H-bond absent in the HLA-G^{KGPPAALTL} complex when compared with HLA-G^{RIIPRHLQL}. The two lost H-bonds, from P3 and P4, are due to the different orientation of His70 (Fig. 4), while the lost water-mediated bond between P7-Leu and Arg156 is

due to a slight shift in the water molecule. Furthermore, the conserved side-chain interactions are seen at P1, which is occupied by a conserved basic residue, and at P9-Leu (Fig. 2). The remaining polar contacts that are absent in the HLA-G^{KGPPAALTL} complex (three H-bonds and four water-mediated H-bonds) are due to the substitution of P5-Arg and P6-His for two Ala residues in the KGPPAALTL epitope.

The most significant difference observed between HLA-G^{RIIPRHLQL} and HLA-G^{KGPPAALTL} resides within the altered conformation of the side chain of His70, which moves away from P4-Pro and toward the C^B of P6-Ala in the HLA-G^{KGPPAALTL} complex (Fig. 4a). This reorientation of His70 could not be accommodated in the HLA-G^{RIIPRHLQL} complex as it would result in a steric clash with the side chain of P6-His. In HLA-G^{RIIPRHLQL}, His70 makes contacts with P3-Ile, P4-Pro and P5-Arg of the peptide, whereas in HLA-G^{KGPPAALTL}, His70 of HLA-G sits farther from the N-terminal region of the peptide; the cavity created by the movement of His70 is occupied by a water molecule. Notably, as mentioned above, the shift in the conformation of His70 results in a loss of two H-bonds and several vdW interactions between the KGPPAALTL peptide and HLA-G when compared with the HLA-G^{RIIPRHLQL} complex.

Accordingly, the structures of HLA-G^{RIIPRHLQL} and HLA-G^{KGPPAALTL} are very similar in that malleability of the His70 side chain of HLA-G permits a similar mode of binding.

Structure of HLA-G^{KLPAQFYIL}

The structure of HLA-G^{KLPAQFYIL} was determined to 1.7-Å resolution to R_{cryst} and R_{free} values of 18.2% and 22.6%, respectively. There were two molecules in the asymmetric unit, exhibiting an r.m.s.d. of 0.61 Å—with the difference between the two monomers primarily due to differing juxtapositioning of the $\alpha 3$ domain. The Ag-binding clefts have an r.m.s.d. of 0.34 Å, and the peptides have an r.m.s.d. of 0.30 Å with respect to the binding cleft. Unless stated otherwise, the interactions made with the KLPAQFYIL peptide are confined to one HLA-G molecule. The electron density for the peptide, and the contacting residues, was unambiguous and free from crystal contacts (Fig. 1b).

The peptide termini are anchored through a series of interactions that are conserved throughout MHC-I. These involve H-bonds between P1-Lys and Tyr7, between Tyr171 and Tyr159 (Fig. 2c), between P9-Leu and Asn77 and between Tyr84 and Ser143 (Fig. 2d). The side chain of P1-Lys also forms salt bridges with Glu62 and Glu63 and a water-mediated H-bond with Asn66, while P9-Leu forms an additional water-mediated H-bond with Thr80.

The backbone of the KLPAQFYIL peptide forms a total of 12 H-bonds and seven water-mediated H-bonds with HLA-G. P2-Leu forms both a H-bond and a water-mediated H-bond with Glu65 and a water-mediated H-bond with Asn66. Due to a

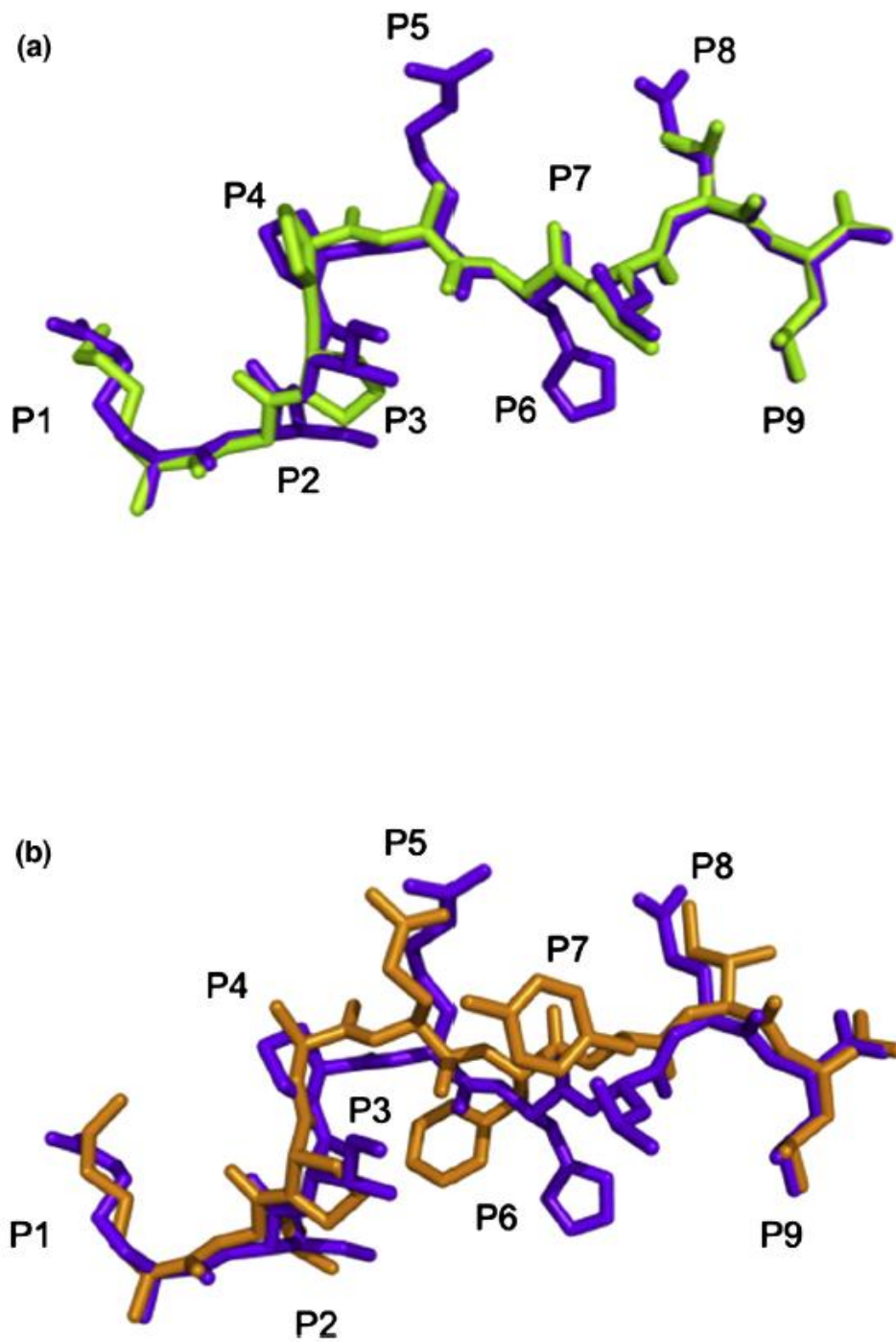


Fig. 3. Peptide conformation. (a) Comparison of the conformations of the KGPPAALTL peptide (green) and the RIIPRHLQL peptide (purple) when presented by HLA-G highlighting the similarity between the two peptides. (b) Comparison of the conformations of the KLPAQFYIL peptide (orange) and the RIIPRHLQL peptide (purple) when presented by HLA-G highlighting the central bulge in KLPAQFYIL.

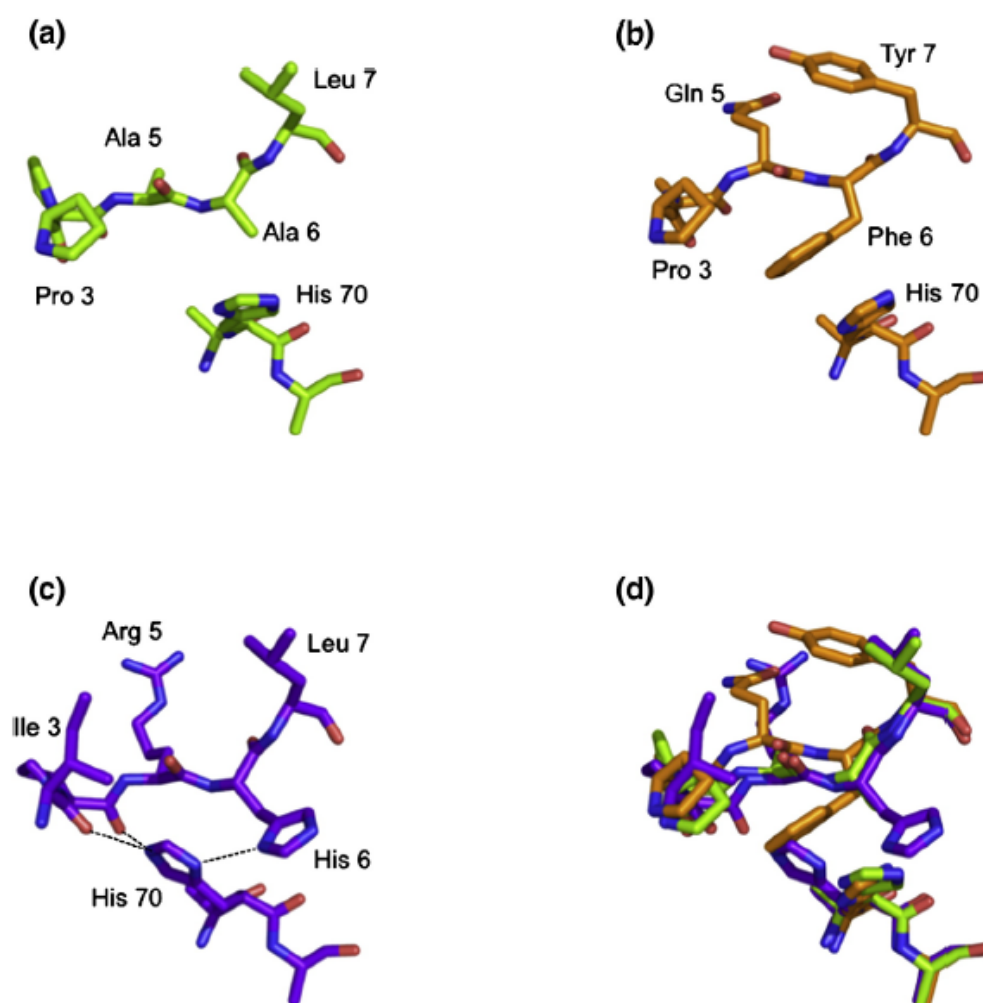


Fig. 4. Orientation of His70. The orientation of His70 side chain is altered by the presence of a His at P6 of RIIPRHLQL (c) compared with that seen in the presence of KGPPAALT (a) and KLPAQFYIL (b). An overlay of the three peptides is shown in (d).

difference in the orientation of the Asn66 side chain, a H-bond between P3-Pro and Asn66 is seen in one molecule in the asymmetric unit, whereas both molecules have H-bonds between P5-Gln and Arg156 and between P7-Tyr and Asn77 and water-mediated H-bonds between P7-Tyr and Tyr116 and between Arg156 and Asp74 (Table 2).

Given the limited side chains available for polar interactions in the KLPAQFYIL peptide, it is not surprising that there are only two salt bridges, two H-bonds and two water-mediated H-bonds between the peptide side chains and HLA-G. Aside from the P1 interactions described above, the only side-chain interactions are with P5-Gln and P7-Tyr. A H-bond is seen in one molecule between P5-Gln and Gln155, and P7-Tyr forms a H-bond with Gln155 and a water-mediated H-bond with Arg156.

The conformation of the termini of the KLPAQFYIL peptide and the nature of the interacting residues with HLA-G are similar to those observed in the HLA-G^{RIIPRHLQL} and HLA-G^{KGPPAALT} complexes (Fig. 2). However, major deviations, up to 2.0 Å, were observed in the central region of the peptide, spanning residues P4-Ala to P8-Ile. As a consequence, the KLPAQFYIL peptide sits slightly higher in the Ag-binding cleft and closer to the α 2 helix than the other two peptides when bound to HLA-G (Fig. 5a and b).

This shift may be due to the presence of a Phe at P6 of the peptide (Fig. 3b). P6-Phe cannot sit as low in the cleft as P6-Ala of KGPPAALT due to its size, whereas P6-His of RIIPRHLQL, although being similarly bulky, forms multiple H-bonds with HLA-G, which anchors the peptide in the cleft.

Table 2. HLA-G^{KLPAQFYIL} contacts

Peptide residue	HLA-G residue	Interaction
Lys1		
Lys	Met5, Tyr7, Glu62, Glu63, Tyr159, Trp167, Tyr171	vdW
Lys ^N	Tyr7 ^{OH}	H-bond
Lys ^{NG}	Tyr171 ^{OH}	H-bond
	Glu62 ^{OG2} , Glu62 ^{OG1a}	Salt bridge
	Glu63 ^{OG2} , Glu63 ^{OG1}	Salt bridge
	Asn66 ^{NE2a}	Water-mediated
		H-bond
	Asn66 ^{OG1b}	Water-mediated
		H-bond
Lys ^O	Tyr159 ^{OH}	H-bond
Leu2		
Leu	Tyr7, Met45, Glu63, Asn66 ^b , Thr67, Tyr159	vdW
Leu ^N	Glu63 ^{OG2}	H-bond
Leu ^O	Glu63 ^{OG1}	Water-mediated
		H-bond
	Asn66 ^{NE2a}	Water-mediated
		H-bond
Pro3		
Pro	Asn66 ^b , Ile99 ^a , Arg156, Tyr159	vdW
Pro ^O	Asn66 ^{OG1b}	H-bond
Ala4		
Ala	Asn66	vdW
Gln5		
Gln	Gln155, Arg156	vdW
Gln ^{NH2}	Gln155 ^{OH1a}	H-bond
Gln ^O	Arg156 ^{NH1}	H-bond
	Arg156 ^{NH2}	H-bond
Phe6		
Phe	Asn66, His70, Trp97, Arg156	vdW
Tyr7		
Tyr	Thr73, Asn77, Val152, Gln155, Arg156	vdW
Tyr ^N	Tyr116 ^{OH}	Water-mediated
		H-bond
	Arg156 ^{NH2}	Water-mediated
		H-bond
Tyr ^{OH}	Gln155 ^{OG1}	H-bond
	Arg156 ^{NH1}	Water-mediated
		H-bond
Tyr ^O	Asp74 ^{OG1}	Water-mediated
		H-bond
	Asn77 ^{NE2}	H-bond
Ile8		
Ile	Asn77, Lys146	vdW
Leu9		
Leu	Asn77, Thr80, Tyr84, Tyr116, Ser143, Lys146	vdW
Leu ^N	Asn77 ^{OG1}	H-bond
Leu ^O	Tyr84 ^{OH}	H-bond
	Ser143 ^{OG1}	H-bond
Leu ^{OXT}	Lys146 ^{NG}	H-bond
	Asn77 ^{OG1}	Water-mediated
		H-bond
	Thr80 ^{OG1}	Water-mediated
		H-bond

^a In molecule 1, not in molecule 2.^b In molecule 2, not in molecule 1.

Between residues P5 and P7, the KLPAQFYIL backbone deviates by 1.5–2.0 Å from that of the RIIPRHLQL and KGPPAALTL peptides.

This movement of the P6 residue alters the H-bonding network of the KLPAQFYIL peptide backbone with respect to RIIPRHLQL. In total, two H-bonds and three water-mediated H-bonds are lost at P3, P4, P6 and P7, with another water-mediated H-bond gained at P7-Tyr. As with the HLA-G^{KGPPAALTL} complex, the absence of P6-His eliminates two H-bonds and four water-mediated H-bonds. The substitution of Gln for Arg at P5 allows the conservation of the H-bond with Gln155 that is lost in the HLA-G^{KGPPAALTL} complex. In the HLA-G^{KLPAQFYIL} complex, His70 adopts the same orientation as observed in the HLA-G^{KGPPAALTL} complex, thereby eliminating the two H-bonds with P3 and P4 seen in HLA-G^{RIIPRHLQL} (Fig. 4).

The Ag-binding cleft of HLA-G^{KLPAQFYIL} has r.m.s.d. values of 0.53 and 0.54 Å when superposed to HLA-G^{RIIPRHLQL} and HLA-G^{KGPPAALTL}, respectively. The greatest deviation was observed in residues 150–154, which are shifted by up to 0.9 Å, creating a slightly wider Ag-binding cleft in HLA-G^{KLPAQFYIL} (Fig. 5c). This region is adjacent to the center of the peptide (residues 4–7), which deviates up to 2.0 Å from the other two peptides toward the α2 helix (Fig. 5a). The side chain of the P7 residue, a Tyr in KLPPAALTL and a Leu in the other two peptides, points toward this region of the α2 helix (Fig. 5c). This suggests that the α2 helix shifts to accommodate the movement in the peptide and the bulky P7-Tyr side chain.

Across all three pHLA-G complexes, one salt bridge, 10 H-bonds and five water-mediated H-bonds are conserved in total (Fig. 6). The major sites of conservation are P1, P2 and P9, where all polar interactions are conserved. The P1 residue forms H-bonds with Tyr7, Tyr171 and Tyr159, a salt bridge with Glu62 and a H-bond (for P1-Arg) or a salt bridge (for P1-Lys) with Glu63. The P2 residue forms a H-bond with Glu63 and water-mediated H-bonds with Glu63 and Asn66. The P9 residues form a H-bond network with Asn77, Tyr84, Ser143 and Lys146, as well as water-mediated H-bonds with Asn77 and Thr80. The other conserved interactions are H-bonds between P5 and Arg156 and a water-mediated H-bond between P7 and Tyr116.

Thermal stability of pHLA-G complexes

In order to evaluate the contribution of the bound peptide to the stability of HLA-G, we assessed the thermal stability of HLA-G in complex with four peptides (RIIPRHLQL, KGPPAALTL, KLPAQFYIL and RLPKDFRIL) using circular dichroism (CD). The ellipticity at 218 nm was measured as temperature was increased from 20 to 90 °C. The relative thermal stability of each pHLA-G complex was determined from the temperature at which the protein was 50% unfolded (T_m) (Fig. 7). The fourth peptide, RLPKDFRIL, was identified after elution of peptides from HLA-G-transfected cells.¹⁵ We found that the yield of HLA-G^{RLPKDFRIL} following *in vitro* refolding was too low for structural studies but of sufficient quantity for thermal denaturation experiments.

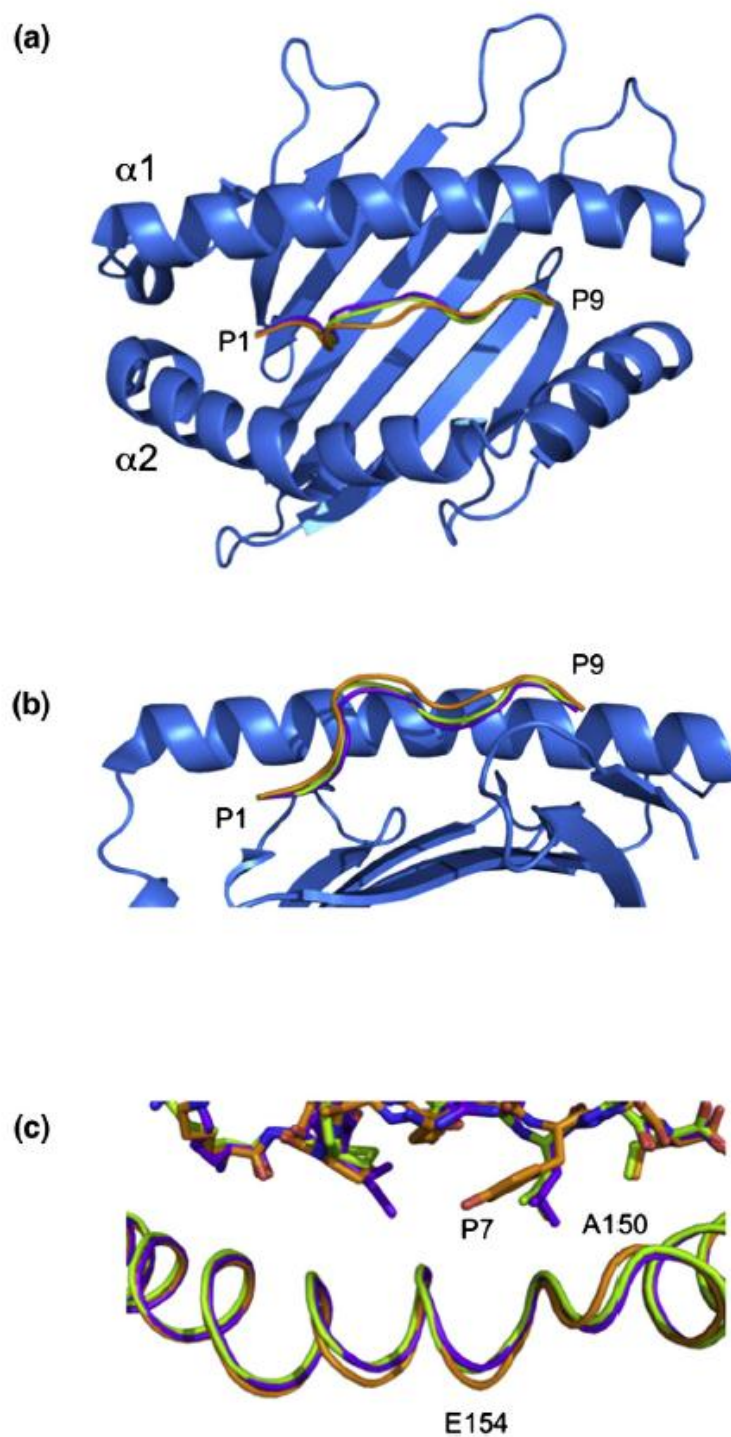


Fig. 5. Comparison of the three pHLA-G complexes. Top view (a) and side view (b) of HLA-G showing the backbones of RIIPRHLQL (purple), KGPPAALT (green) and KLPAQFYIL (orange). The $\alpha2$ helix has been removed from (b) for clarity. (c) A 0.9-Å shift in the $\alpha2$ helix centered at V152 is seen in the HLA-G^{KLPAQFYIL} complex (orange) when compared with HLA-G^{RIIPRHLQL} (purple) and HLA-G^{KGPPAALT} (green).

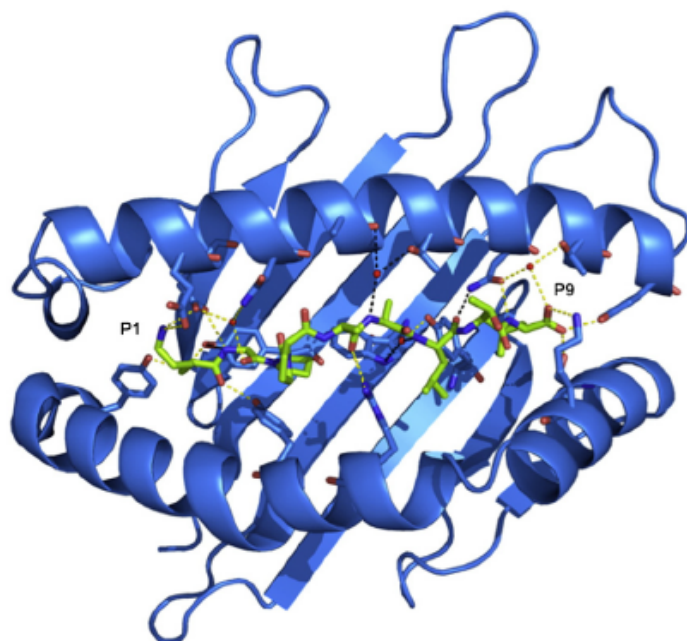


Fig. 6. Conserved peptide contacts. Polar contacts between the KGPPAALTL peptide and HLA-G are represented by dashed lines shown in yellow for conserved contacts and in black for non-conserved contacts. Water molecules are represented by red spheres.

HLA-G^{RLPKDFRIL} was also by far the least thermally stable of the four complexes, with a T_m of 64.3 ± 1.9 °C. The other three peptides stabilised HLA-G to similar degrees, with HLA-G^{RIIPRHLQL} marginally showing the greatest stability with $T_m = 73.5 \pm 0.5$ °C, followed by HLA-G^{KGPPAALTL} and then HLA-G^{KLPAQFYIL} with T_m values of 71.8 ± 1.8 and 69.0 ± 1.7 °C, respectively.

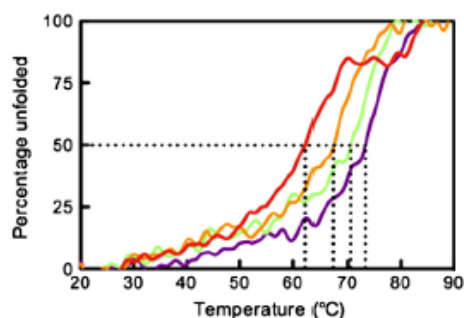


Fig. 7. Thermal stability of pHLA-G complexes. The ellipticity at 218 nm was measured as temperature increased from 20 to 90 °C. The data were normalised to determine the midpoint of thermal denaturation (T_m). Samples were diluted to 5 and 10 μ M in 10 mM Tris, pH 8.0, containing 150 mM NaCl. The complexes were measured twice at both 5 and 10 μ M, and the T_m was averaged over the four experiments. The figure is representative of denaturation at 5 μ M. Data for HLA-G^{RLPKDFRIL}, HLA-G^{KLPAQFYIL}, HLA-G^{KGPPAALTL} and HLA-G^{RIIPRHLQL} are shown in red, orange, green and purple, respectively.

Discussion

Typical of MHC-Ib molecules, and in contrast to MHC-Ia molecules, HLA-G binds a restricted repertoire of peptides. The structure of HLA-G^{RIIPRHLQL} revealed an extensive network of bonds with the epitope along the Ag-binding cleft, thereby providing a snapshot for understanding the peptide binding properties of HLA-G. The mode of HLA-G peptide binding was similar to that of HLA-E, although the peptide repertoire of HLA-G is not as restricted as that of HLA-E.¹⁹ We determined the structure of HLA-G in complex with two unrelated self-peptides, KGPPAALTL and KLPAQFYIL, to simultaneously evaluate the conserved features of peptide binding by HLA-G and provide a basis for the adaptability of HLA-G in being able to accommodate disparate peptide sequences. We demonstrated that an extensive network of contacts along the length of the peptide is present in all pHLA-G complexes. However, superposition of the three pHLA-G complexes showed that while there was little difference at the N- and C-termini, the central region of the peptide demonstrated a greater degree of conformational flexibility. This malleability in the peptide also resulted in a degree of variability in the HLA-G contacting residues, which ultimately impinges on a region of the $\alpha 2$ helix, whereby widening of the Ag-binding cleft in the HLA-G^{KLPAQFYIL} complex was observed.

The nature of the peptide also affected the thermal stability of pHLA-G. The RIIPRHLQL peptide had the greatest stabilising effect, possibly due to the large number of polar interactions it

makes with HLA-G, whereas HLA-G^{RIPKDFRIL} was the least stable. We investigated whether the peptide–HLA-G interface surface area (SA) and shape complementarity (SC) influenced the stability of the complexes. The values were as follows: HLA-G^{RIIPRHLQL}, SA ≈ 750 Å² and SC = 0.76; HLA-G^{KLPAQFYIL}, SA ≈ 750 Å² and SC = 0.76; and HLA-G^{KGPPAALT}, SA ≈ 625 Å² and SC = 0.70. Despite the differences between HLA-G^{KGPPAALT} and HLA-G^{RIIPRHLQL}/HLA-G^{KLPAQFYIL}, the three pHLA-G complexes exhibit similar *T_m* values, suggesting that the SA and the SC of the interface have little bearing on complex stability. The results of the thermal stability studies are consistent with cell surface expression studies on HLA-G, where the RIPKDFRIL peptide was the least effective at stabilising HLA-G on the cell surface, while the RIIPRHLQL and KLPAQFYIL peptides (KLPAQFYIL with a substitution at P2 to improve binding) were more efficient.³⁰ These data suggest that the peptide influences the stability of HLA-G and in turn its cell surface expression. The bound peptide

is therefore likely to affect recognition of HLA-G both directly through interaction with cognate receptors and indirectly through the regulation of the levels of HLA-G on the cell surface.

HLA-G is involved in cancer, inflammation and pregnancy,³¹ all processes involving cells of the innate immune response. HLA-G is recognised by two families of innate immune receptors: LILRB1 and LILRB2 and KIR2DL4, with the latter binding to the Ag-binding cleft of HLA-G.²⁷ The influence of the bound peptide on recognition of MHC-Ia by KIR is well established. The identity of the peptide presented by HLA-B27 affects recognition by KIR3DL1, with the P8 position of primary importance.³² Structural and peptide substitution studies have also demonstrated that the P8 position of the peptide presented by HLA-Cw3 is critical for KIR2DL2 binding.²⁸ Similarly, KIR2DL1 recognition of HLA-Cw4 is influenced by the P7 and P8 residues of the bound peptide.^{29,33} KIR2DL1 and KIR2DL3 both bind HLA-Cw7 but display differing peptide preferences.³⁴ Recognition of MHC-Ib by NK

Table 3. Data collection and refinement statistics

	HLA-G ^{KGPPAALT}	HLA-G ^{KLPAQFYIL}
<i>Data collection statistics</i>		
Peptide	KGPPAALT	KLPAQFYIL
Temperature (K)	100	100
X-ray source	BioCARS, APS	GM/CA-CAT, APS
Detector	Quantum 4 CCD	MARmosaic 300 CCD
Space group	P3 ₂ 21	P2 ₁
Cell dimensions		
<i>a</i> , <i>b</i> , <i>c</i> (Å)	76.9, 76.9, 151.9	58.6, 86.0, 111.6
α , β , γ (°)	90, 90, 120	90, 95.6, 90
Resolution (Å)	37.3–2.4	43.0–1.7
Total no. of observations	65,643	435,436
No. of unique observations	20,503	119,833
Multiplicity	3.20	3.63
Data completeness (%)	97.7 (93.4)	99.4 (98.7)
<i>I</i> / σ _{<i>I</i>}	24.4 (2.8)	33.4 (2.9)
<i>R</i> _{merge} (%) ^a	6.1 (41.6)	8.2 (58.9)
<i>Refinement statistics</i>		
No. of reflections used	19,333	113,595
No. of reflections used for <i>R</i> _{free}	1072	6044
Non-hydrogen atoms		
Protein	3138	6288
Water	113	993
Cobalt	1	2
Chloride	2	—
<i>R</i> _{cryst} (%) ^b	21.6	18.2
<i>R</i> _{free} (%) ^b	29.9	22.6
r.m.s.d from ideality		
Bond lengths (Å)	0.012	0.022
Bond angles (°)	1.7	1.9
Ramachandran plot (%) ^c		
Favoured regions	95.8	98.1
Allowed regions	4.2	1.9
<i>B</i> -factors (Å ²)		
Average main chain	51.1	28.9
Average side chain	53.2	34.1
Average water molecule	48.1	45.6
Cobalt	42.4	84.7
Chloride	66.1	—

Values in parentheses are for the highest-resolution shell.

^a $R_{\text{merge}} = 100 \sum |I_{hk\ell} - \langle I_{hk\ell} \rangle| / \sum I_{hk\ell}$.

^b $R_{\text{cryst}} = 100 \sum |F_o - \langle F_o \rangle| / \sum |F_o|$ for all data except for 5% that was used for the *R*_{free} calculation.

^c MolProbity.³⁵

receptors is also influenced by the bound peptide. Subtle alterations in the HLA-E-bound peptide can have dramatic effects on recognition by CD94–NKG2 receptors.^{35–39} We therefore suggest that variations in the peptide and the Ag-binding cleft of HLA-G are likely to impact on KIR2DL4 binding.

Although MHC-Ib molecules play a primary role in innate immunity, MHC-Ib molecules can play a critical role in adaptive immunity.^{40,41} For example, Qa-1^b-restricted T cells specific for *Salmonella typhimurium*⁴² and HLA-E-restricted T cells for a range of pathogens, including cytomegalovirus,⁴³ *S. typhimurium*⁴⁴ and *Mycobacterium tuberculosis*,⁴⁵ have been described. As yet, a direct role for HLA-G in adaptive immunity has not been described, although HLA-G-specific cytotoxic T lymphocytes have been raised *in vivo* in transgenic mice.⁴⁶ There is currently only one published TCR–pMHC-Ib structure, that of HLA-E presenting a cytomegalovirus-derived peptide to the KK50.4 TCR.⁶ This TCR displays exquisite specificity for a single peptide residue, with substitution of the P8 residue abrogating binding. With only one TCR–pMHC-Ib structure, the influence of the conformational variability of MHC on TCR recognition cannot be assessed. However, TCR–pMHC-Ia structures have demonstrated that small changes in peptide sequence⁴⁷ and subtle alterations in the juxtapositioning of the α -helices can dramatically influence TCR binding and dictate the nature of the MHC-restricted response.^{1–3,48,49} Accordingly, we speculate that that conformational variability observed in the pHLA-G complexes will not only influence innate recognition but also be of sufficient magnitude to allow self-discrimination from non-self-discrimination by receptors of the adaptive immune system.

Materials and Methods

Cloning, expression and crystallization of HLA-G

Details pertaining to the cloning, expression and crystallization of HLA-G have been published previously.⁵⁰ Briefly, the gene encoding HLA-G*0101 was cloned from the human choriocarcinoma cell line JEG-3 using standard protocols. The codon for cysteine at position 42 was changed to encode serine using Quik-Change site-directed mutagenesis (Stratagene, La Jolla, CA). The Cys-to-Ser mutation improved the yield of correctly folded HLA-G and was previously shown not to affect the mode of peptide binding.⁵⁰ The HLA-G1 was expressed in BL21 *Escherichia coli*, and inclusion body protein was prepared, refolded and purified essentially as described previously.^{19,51}

Data collection, structure determination and refinement

Diffracting crystals of HLA-G^{KGPPAALT} were obtained using the vapour diffusion technique at 4 °C with 16% polyethylene glycol, pH 7.2, plus 10 mM CoCl₂ as the precipitant and streak seeding from crystals of HLA-G^{RIPRHLQL}.⁵⁰ The crystals belonged to space

group P3₂21 with unit cell dimensions $a=b=76.9$ Å and $c=151.9$ Å (Table 3). Diffracting crystals of HLA-G^{KLPQAFYIL} were obtained using the vapour diffusion technique at 4 °C with 16% polyethylene glycol, pH 7.2, plus 10 mM CoCl₂ as the precipitant. Although these crystals were grown in similar conditions to HLA-G^{RIPRHLQL} and HLA-G^{KGPPAALT}, they were of a different morphology and belonged to space group P2₁ with unit cell dimensions $a=58.6$ b=86.0 Å, $c=111.6$ Å and $\beta=95.6^\circ$ (Table 3), with two molecules per asymmetric unit.

Data sets for the HLA-G^{KGPPAALT} and HLA-G^{KLPQAFYIL} complexes were collected from flash-frozen crystals at the BioCARS and GM/CA-CAT beamlines using CCD detectors. The data were processed and scaled using the HKL package.⁵³ The crystal structures of the complexes were solved by the molecular replacement method using Phaser,⁵⁴ with the unliganded HLA-G structure (Protein Data Bank ID 1YDP) as the search model. For the search model, all water molecules and the bound peptide were removed. Unbiased features in the initial electron density map confirmed the correctness of the molecular replacement solution. The progress of refinement was monitored by the R_{free} value (5% of the data) with neither a sigma nor a low-resolution cutoff being applied to the data. The structure was manually built in the program Coot interspersed with rounds of refinement using programs from the CCP4 package.⁵⁵ The HLA-G^{KGPPAALT} structure was also subjected to simulated annealing using PHENIX⁵⁶ to eliminate bias from the search model. Tightly restrained individual B-factor refinement was employed, and bulk solvent corrections were applied to the data set. H-bonds were located using programs from the CCP4 package (contacts). Data collection and refinement statistics are shown in Table 3.

Thermostability assay

The thermal stability of HLA-G^{RIPRHLQL}, HLA-G^{KGPPAALT}, HLA-G^{KLPQAFYIL} and HLA-G^{RLPKDFRIL} was investigated using CD. CD spectra were measured on a Jasco 810 spectropolarimeter using a temperature-controlled cuvette with a 0.1-cm path length. Initially, a CD scan of each protein was performed to determine the wavelength minimum, at which unfolding was measured. The ellipticity (θ) of each pHLA-G complex was measured at 218 nm as temperature was increased from 20 to 90 °C over 70 min. The θ_{218} at 80–90 °C was averaged to provide a value for 100% unfolded protein, and the average θ_{218} at 20–30 °C was taken to represent 0% unfolded protein. The midpoint (T_m) of these two values corresponded to the temperature at which the protein was 50% unfolded. Each pHLA-G complex was measured in duplicate at two concentrations, 5 and 10 μ M.

Protein Data Bank accession numbers

Coordinates have been deposited in the Protein Data Bank with codes 3KYN and 3KYO.

Acknowledgements

The National Health and Medical Research Council and the Australian Research Council

(ARC) supported this work. J.R. is supported by an ARC Federation Fellowship, and C.S.C. is supported by an ARC Queen Elizabeth II Fellowship. We thank the staff at the BioCARS and GM/CA-CAT for their assistance with data collection.

References

- Archbold, J. K., Macdonald, W. A., Gras, S., Ely, L. K., Miles, J. J., Bell, M. J. *et al.* (2009). Natural micro-polymorphism in human leukocyte antigens provides a basis for genetic control of antigen recognition. *J. Exp. Med.* **206**, 209–219.
- Macdonald, W. A., Purcell, A. W., Mifsud, N. A., Ely, L. K., Williams, D. S., Chang, L. *et al.* (2003). A naturally selected dimorphism within the HLA-B44 supertype alters class I structure, peptide repertoire, and T cell recognition. *J. Exp. Med.* **198**, 679–691.
- Tynan, F. E., Borg, N. A., Miles, J. J., Beddoe, T., El-Hassen, D., Silins, S. L. *et al.* (2005). High resolution structures of highly bulged viral epitopes bound to major histocompatibility complex class I: implications for T-cell receptor engagement and T-cell immunodominance. *J. Biol. Chem.* **280**, 23900–23909.
- Grimsley, C., Kawasaki, A., Gassner, C., Sageshima, N., Nose, Y., Hatake, K. *et al.* (2002). Definitive high resolution typing of HLA-E allelic polymorphisms: identifying potential errors in existing allele data. *Tissue Antigens*, **60**, 206–212.
- Lajoie, J., Boivin, A.-A., Jeanneau, A., Faucher, M.-C. & Roger, M. (2009). Identification of six new HLA-G alleles with non-coding DNA base changes. *Tissue Antigens*, **73**, 379–380.
- Hoare, H. L., Sullivan, L. C., Pietra, G., Clements, C. S., Lee, E. J., Ely, L. K. *et al.* (2006). Structural basis for a major histocompatibility complex class I α -restricted T cell response. *Nat. Immunol.* **7**, 256.
- O'Callaghan, C. A., Tormo, J., Willcox, B. E., Braud, V. M., Jakobsen, B. K., Stuart, D. I. *et al.* (1998). Structural features impose tight peptide binding specificity in the nonclassical MHC molecule HLA-E. *Mol. Cell*, **1**, 531–541.
- Strong, R. K., Holmes, M. A., Li, P., Braun, L., Lee, N. & Geraghty, D. E. (2003). HLA-E allelic variants. Correlating differential expression, peptide affinities, crystal structures, and thermal stabilities. *J. Biol. Chem.* **278**, 5082–5090.
- Borrego, F., Ulbrecht, M., Weiss, E. H., Coligan, J. E. & Brooks, A. G. (1998). Recognition of human histocompatibility leukocyte antigen (HLA)-E complexed with HLA class I signal sequence-derived peptides by CD94/NKG2 confers protection from natural killer cell-mediated lysis. *J. Exp. Med.* **187**, 813–818.
- Blaschitz, A., Lenfant, F., Mallet, V., Hartmann, M., Bersusian, A., Geraghty, D. *et al.* (1997). Endothelial cells in chorionic fetal vessels of first trimester placenta express HLA-G. *Eur. J. Immunol.* **27**, 3380–3388.
- Chu, W., Fant, M. E., Geraghty, D. E. & Hunt, J. S. (1998). Soluble HLA-G in human placentas: synthesis in trophoblasts and interferon- γ -activated macrophages but not placental fibroblasts. *Hum. Immunol.* **59**, 435–442.
- Kovats, S., Main, E., Librach, C., Stubblebine, M., Fisher, S. & DeMars, R. (1990). A class I antigen, HLA-G, expressed in human trophoblasts. *Science*, **248**, 220–223.
- McMaster, M. T., Librach, C. L., Zhou, Y., Lim, K. H., Janatpour, M. J., DeMars, R. *et al.* (1995). Human placental HLA-G expression is restricted to differentiated cytotrophoblasts. *J. Immunol.* **154**, 3771–3778.
- Le Bouteiller, P., Solier, C., Proll, J., Aguerre-Girr, M., Fournel, S. & Lenfant, F. (1999). Mini symposium. The major histocompatibility complex in pregnancy: Part II. Placental HLA-G protein expression *in vivo*: where and what for? *Hum. Reprod. Update*, **5**, 223–233.
- Diehl, M., Munz, C., Keilholz, W., Stevanovic, S., Holmes, N., Loke, Y. W. & Rammensee, H.-G. (1996). Nonclassical HLA-G molecules are classical peptide presenters. *Curr. Biol.* **6**, 305–314.
- Lee, N., Malacko, A., Ishitani, A., Chen, M., Bajorath, J., Marquardt, H. & Geraghty, D. E. (1995). The membrane-bound and soluble forms of HLA-G bind identical sets of endogenous peptides but differ with respect to TAP association. *Immunity*, **3**, 591–600.
- Ishitani, A., Sageshima, N., Lee, N., Dorofeeva, N., Hatake, K., Marquardt, H. & Geraghty, D. E. (2003). Protein expression and peptide binding suggest unique and interacting functional roles for HLA-E, F, and G in maternal-placental immune recognition. *J. Immunol.* **171**, 1376–1384.
- Clements, C. S., Kjer-Nielsen, L., McCluskey, J. & Rossjohn, J. (2007). Structural studies on HLA-G: implications for ligand and receptor binding. *Hum. Immunol.* **68**, 220–226.
- Clements, C. S., Kjer-Nielsen, L., Kostenko, L., Hoare, H. L., Dunstone, M. A., Moses, E. *et al.* (2005). Crystal structure of HLA-G: a nonclassical MHC class I molecule expressed at the fetal-maternal interface. *Proc. Natl Acad. Sci. USA*, **102**, 3360–3365.
- Shiroishi, M., Kuroki, K., Ose, T., Rasubala, L., Shiratori, I., Arase, H. *et al.* (2006). Efficient leukocyte Ig-like receptor signaling and crystal structure of disulfide-linked HLA-G dimer. *J. Biol. Chem.* **281**, 10439–10447.
- Boyson, J. E., Erskine, R., Whitman, M. C., Chiu, M., Lau, J. M., Koopman, L. A. *et al.* (2002). Disulfide bond-mediated dimerization of HLA-G on the cell surface. *Proc. Natl Acad. Sci. USA*, **99**, 16180–16185.
- Brown, D., Trowsdale, J. & Allen, R. (2004). The LILR family: modulators of innate and adaptive immune pathways in health and disease. *Tissue Antigens*, **64**, 215–225.
- Chapman, T. L., Heikema, A. P. & Bjorkman, P. J. (1999). The inhibitory receptor LIR-1 uses a common binding interaction to recognize class I MHC molecules and the viral homolog UL18. *Immunity*, **11**, 603–613.
- Gonen-Gross, T., Achdout, H., Arnon, T. I., Gazit, R., Stern, N., Horejsi, V. *et al.* (2005). The CD85J/leukocyte inhibitory receptor-1 distinguishes between conformed and β 2-microglobulin-free HLA-G molecules. *J. Immunol.* **175**, 4866–4874.
- Shiroishi, M., Tsumoto, K., Amano, K., Shirakihara, Y., Colonna, M., Braud, V. M. *et al.* (2003). Human inhibitory receptors Ig-like transcript 2 (ILT2) and ILT4 compete with CD8 for MHC class I binding and bind preferentially to HLA-G. *Proc. Natl Acad. Sci. USA*, **100**, 8856–8861.
- Shiroishi, M., Kuroki, K., Rasubala, L., Tsumoto, K., Kumagai, I., Kurimoto, E. *et al.* (2006). Structural basis for recognition of the nonclassical MHC molecule HLA-G by the leukocyte Ig-like receptor B2 (LILRB2/LIR2/ILT4/CD85d). *Proc. Natl Acad. Sci. USA*, **103**, 16412–16417.
- Yan, W. H. & Fan, L. A. (2005). Residues Met76 and Glu79 in HLA-G α 1 domain involved in KIR2DL4 recognition. *Cell Res.* **15**, 176.

28. Boyington, J. C., Motyka, S. A., Schuck, P., Brooks, A. G. & Sun, P. D. (2000). Crystal structure of an NK cell immunoglobulin-like receptor in complex with its class I MHC ligand. *Nature*, **405**, 537–543.
29. Fan, Q. R., Long, E. O. & Wiley, D. C. (2001). Crystal structure of the human natural killer cell inhibitory receptor KIR2DL1–HLA-Cw4 complex. *Nat. Immunol.* **2**, 452–460.
30. Munz, C., Stevanovic, S. & Rammensee, H.-G. (1999). Peptide presentation and NK inhibition by HLA-G. *J. Reprod. Immunol.* **43**, 139.
31. Favier, B., LeMaout, J., Rouas-Freiss, N., Moreau, P., Menier, C. & Carosella, E. D. (2007). Research on HLA-G: an update. *Tissue Antigens*, **69**, 207–211.
32. Stewart-Jones, G. B. E., di Gleria, K., Kollnberger, S., McMichael, A. J., Jones, E. Y. & Bowness, P. (2005). Crystal structures and KIR3DL1 recognition of three immunodominant viral peptides complexed to HLA-B*2705. *Eur. J. Immunol.* **35**, 341–351.
33. Rajagopalan, S. & Long, E. O. (1997). The direct binding of a p58 killer cell inhibitory receptor to human histocompatibility leukocyte antigen (HLA)-Cw4 exhibits peptide selectivity. *J. Exp. Med.* **185**, 1523–1528.
34. Maenaka, K., Juji, T., Nakayama, T., Wyer, J. R., Gao, G. F., Maenaka, T. *et al.* (1999). Killer cell immunoglobulin receptors and T cell receptors bind peptide-major histocompatibility complex class I with distinct thermodynamic and kinetic properties. *J. Biol. Chem.* **274**, 28329–28334.
35. Brooks, A. G., Borrego, F., Posch, P. E., Patamawenu, A., Scorzelli, C. J., Ulbrecht, M. *et al.* (1999). Specific recognition of HLA-E, but not classical, HLA class I molecules by soluble CD94/NKG2A and NK cells. *J. Immunol.* **162**, 305–313.
36. Kaiser, B. K., Barahmand-pour, F., Paulsene, W., Medley, S., Geraghty, D. E. & Strong, R. K. (2005). Interactions between NKG2x immunoreceptors and HLA-E ligands display overlapping affinities and thermodynamics. *J. Immunol.* **174**, 2878–2884.
37. Sullivan, L. C., Clements, C. S., Rossjohn, J. & Brooks, A. G. (2008). The major histocompatibility complex class Ib molecule HLA-E at the interface between innate and adaptive immunity. *Tissue Antigens*, **72**, 415–424.
38. Petrie, E. J., Clements, C. S., Lin, J., Sullivan, L. C., Johnson, D., Huyton, T. *et al.* (2008). CD94–NKG2A recognition of human leukocyte antigen (HLA)-E bound to an HLA class I leader sequence. *J. Exp. Med.* **205**, 725–735.
39. Sullivan, L. C., Clements, C. S., Beddoe, T., Johnson, D., Hoare, H. L., Lin, J. *et al.* (2007). The heterodimeric assembly of the CD94–NKG2 receptor family and implications for human leukocyte antigen-E recognition. *Immunity*, **27**, 900–911.
40. Rodgers, J. R. & Cook, R. G. (2005). MHC class Ib molecules bridge innate and acquired immunity. *Nat. Rev. Immunol.* **5**, 459–471.
41. Sullivan, L. C., Hoare, H. L., McCluskey, J., Rossjohn, J. & Brooks, A. G. (2006). A structural perspective on MHC class Ib molecules in adaptive immunity. *Trends Immunol.* **27**, 413.
42. Lo, W.-F., Ong, H., Metcalf, E. S. & Soloski, M. J. (1999). T cell responses to Gram-negative intracellular bacterial pathogens: a role for CD8⁺ T cells in immunity to *Salmonella* infection and the involvement of MHC class Ib molecules. *J. Immunol.* **162**, 5398–5406.
43. Pietra, G., Romagnani, C., Mazzarino, P., Falco, M., Millo, E., Moretta, A. *et al.* (2003). HLA-E-restricted recognition of cytomegalovirus-derived peptides by human CD8⁺ cytolytic T lymphocytes. *Proc. Natl Acad. Sci. USA*, **100**, 10896–10901.
44. Salemo-Goncalves, R., Fernandez-Vina, M., Lewinsohn, D. M. & Szein, M. B. (2004). Identification of a human HLA-E-restricted CD8⁺ T cell subset in volunteers immunized with *Salmonella enterica* serovar Typhi strain Ty21a typhoid vaccine. *J. Immunol.* **173**, 5852–5862.
45. Heinzel, A. S., Grotzke, J. E., Lines, R. A., Lewinsohn, D. A., McNabb, A. L., Streblow, D. N. *et al.* (2002). HLA-E-dependent presentation of Mtb-derived antigen to human CD8⁺ T cells. *J. Exp. Med.* **196**, 1473–1481.
46. Lenfant, F., Pizzato, N., Liang, S., Davrinche, C., Le Bouteiller, P. & Horuzsko, A. (2003). Induction of HLA-G-restricted human cytomegalovirus pp65 (UL83)-specific cytotoxic T lymphocytes in HLA-G transgenic mice. *J. Gen. Virol.* **84**, 307–317.
47. Degano, M., Garcia, K. C., Apostolopoulos, V., Rudolph, M. G., Teyton, L. & Wilson, I. A. (2000). A functional hot spot for antigen recognition in a superagonist TCR/MHC complex. *Immunity*, **12**, 251–261.
48. Godfrey, D. I., Rossjohn, J. & McCluskey, J. (2008). The fidelity, occasional promiscuity, and versatility of T cell receptor recognition. *Immunity*, **28**, 304–314.
49. Rudolph, M. G., Stanfield, R. L. & Wilson, I. A. (2006). How TCRs bind MHCs, peptides and coreceptors. *Annu. Rev. Immunol.* **24**, 419–466.
50. Clements, C. S., Kjer-Nielsen, L., Kostenko, L., McCluskey, J. & Rossjohn, J. (2006). The production, purification and crystallization of a soluble form of the nonclassical MHC HLA-G: the essential role of cobalt. *Acta Crystallogr., Sect. F, Struct. Biol. Cryst. Commun.* **62**, 70–73.
51. Clements, C. S., Kjer-Nielsen, L., MacDonald, W. A., Brooks, A. G., Purcell, A. W., McCluskey, J. & Rossjohn, J. (2002). The production, purification and crystallization of a soluble heterodimeric form of a highly selected T-cell receptor in its unliganded and liganded state. *Acta Crystallogr., Sect. D: Biol. Crystallogr.* **58**, 2131–2134.
52. Lovell, S. C., Davis, I. W., Arendall, B. W. I., de Bakker, P. I. W., Word, J. M., Prisant, M. G. *et al.* (2003). Structure validation by C^α geometry: ϕ , ψ and C^β deviation. *Proteins: Struct., Funct., Genet.* **50**, 437–450.
53. Otwinowski, Z. & Minor, W. (1997). Processing of X-ray diffraction data collected in oscillation mode. *Methods Enzymol.* **276**, 307–326.
54. McCoy, A. J., Grosse-Kunstleve, R. W., Storoni, L. C. & Read, R. J. (2005). Likelihood-enhanced fast translation functions. *Acta Crystallogr., Sect. D: Biol. Crystallogr.* **61**, 458–464.
55. CCP4. (1994). The CCP4 suite: programs for protein crystallography. *Acta Crystallogr., Sect. D: Biol. Crystallogr.* **50**, 760–763.
56. Adams, P. D., Grosse-Kunstleve, R. W., Hung, L.-W., Ioerger, T. R., McCoy, A. J., Moriarty, N. W. *et al.* (2002). PHENIX: building new software for automated crystallographic structure determination. *Acta Crystallogr., Sect. D: Biol. Crystallogr.* **58**, 1948–1954.

Chapter 4 - Characterisation of KIR2DL4

This chapter details a biophysical and structural study of the extracellular domains of KIR2DL4, targeted towards determination of the crystal structure of these domains. As described in Chapter 1 under the heading *KIR2DL4 and the KIR family*, KIR2DL4 is unique among the KIR family in having both activating and inhibitory potential, however the distinction of KIR2DL4 from other KIRs is also evident in its general lack of polymorphism, its presence in every haplotype (along with KIR3DL2 and KIR3DL3), a wider expression pattern among NK cells, and a D0-D2 domain configuration shared only by KIR2DL5 (*Gardiner, 2008*). A putative receptor of pHLA-G, KIR2DL4 is the only KIR shown to bind to a Class Ib MHC (*Rajagopalan and Long, 1999*). As such, KIR2DL4 is a very attractive target for biophysical and structural study.

As mentioned in Chapter 1 under the heading *KIR2DL4 and the KIR family*, the recognition of pHLA-G by KIR2DL4 has been a point of debate in recent years. While an interaction between KIR2DL4 and HLA-G was shown by direct binding analysis (*Rajagopalan and Long, 1999, Cantoni et al., 1999*), no interaction could be observed by Boyson *et al*, using surface plasmon resonance and a cell based system to determine an interaction between either recombinant or transfected HLA-G^{VLPKLYVKL} and a KIR2DL4 fusion protein expressed on murine BW cells (*Boyson et al, 2002*). Another study showed that soluble HLA-G did not bind to NK cells (*Allan et al., 1999*). Further evidence for the interaction was given by observation of the involvement of two residues on the HLA-G $\alpha 1$ helix (*Yan and Fan, 2005*) suggesting that KIR2DL4 interacts with HLA-G via the peptide-binding region of the MHC, as well as a later study which demonstrated an interaction between recombinant KIR2DL4 and cells expressing HLA-G1 (*Yu et al., 2006*). While there is much evidence to suggest that HLA-G is a ligand for KIR2DL4, the contradiction in the literature indicates that further studies should be carried out with caution.

The recent determination of the structure of KIR3DL1 in complex with HLA-B5701 (*Vivian et al, 2011*) demonstrated that the D0 domain of KIR3DL1 interacts with a largely non-polymorphic region of the MHC distinct from the antigen binding cleft, and therefore may function as an ‘innate HLA sensor’ domain. This was the first

time that the structure of the D0 domain in KIRs had been determined, but it raises further questions regarding the D0 domain in KIR2DL4. Two likely positions exist for KIR2DL4 upon MHC binding. Firstly, the D0 domain may recognise a similar region on the MHC to the KIR3DL1 D0 domain, on the $\alpha 1$ domain but away from the antigen-binding cleft. This positioning would require the KIR2DL4 D2 domain to be positioned over the $\alpha 1$ helix of the MHC, well away from the site that the D2 domain takes up in all KIR:MHC structures to date, over the MHC $\alpha 2$ helix. Secondly, the KIR2DL4 D2 domain may sit over the MHC $\alpha 2$ helix, which would lead the KIR2DL4 D0 domain to take up a position over the $\alpha 1$ helix, a position occupied by KIR D1 domains in all KIR:MHC structures to date.

The work presented in this chapter was aimed at solving the crystal structure of the extracellular domain of KIR2DL4. Significant steps were made with respect to the expression of KIR2DL4 using both a baculovirus-insect cell expression system and a mammalian expression system, the optimisation of these systems for production of KIR2DL4 and the crystallisation of KIR2DL4. This work has also enabled a biophysical analysis of the recombinant KIR2DL4 produced using these expression systems, using techniques such as circular dichroism (CD) and small angle x-ray scattering (SAXS).

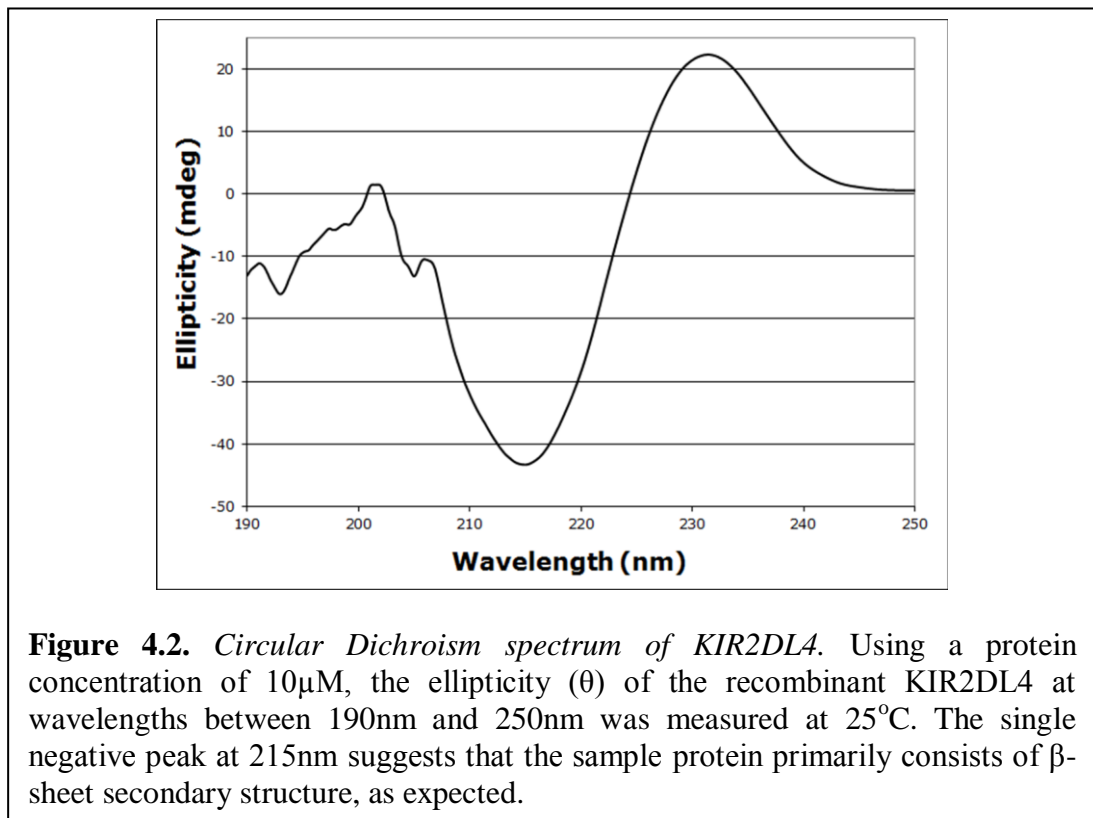
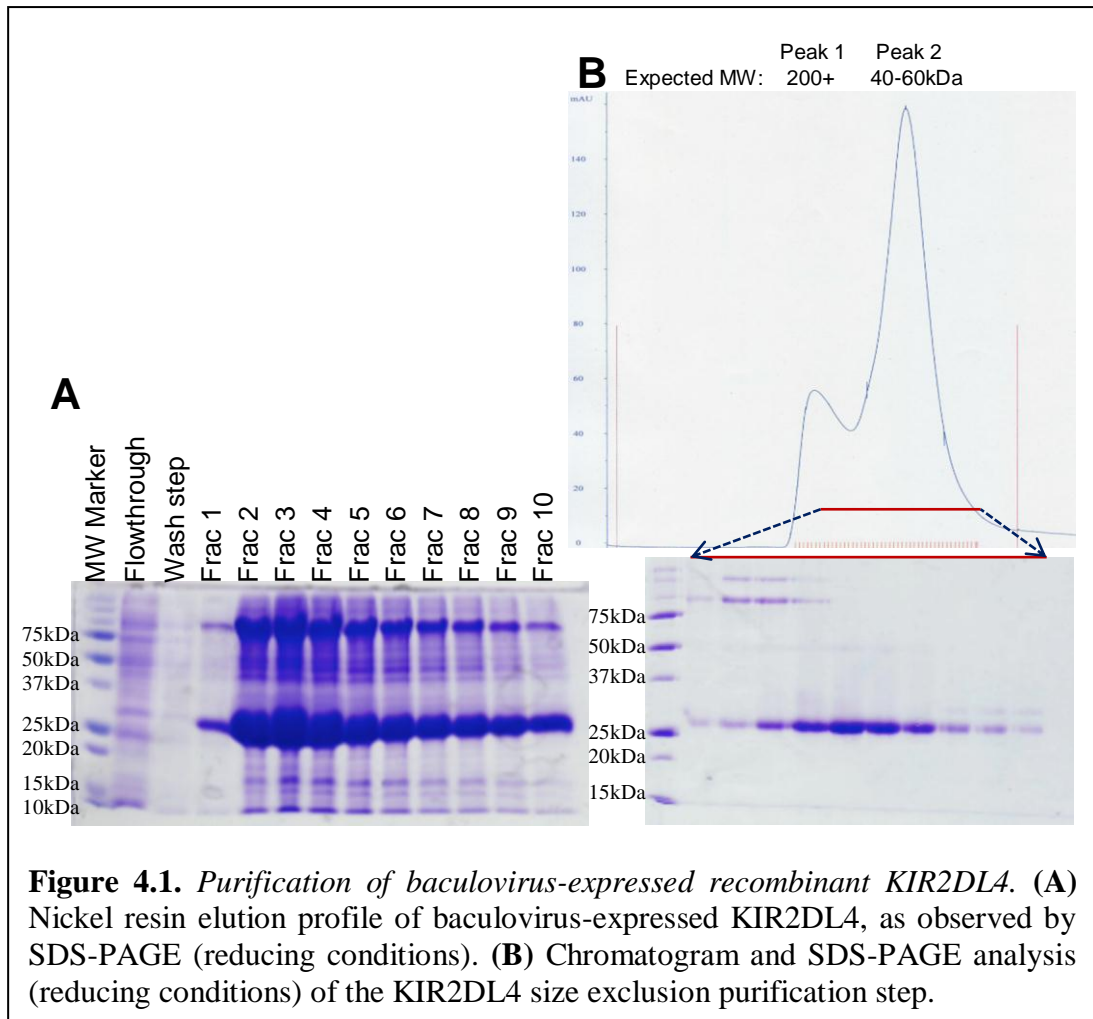
KIR2DL4 Production using a Baculoviral Expression System

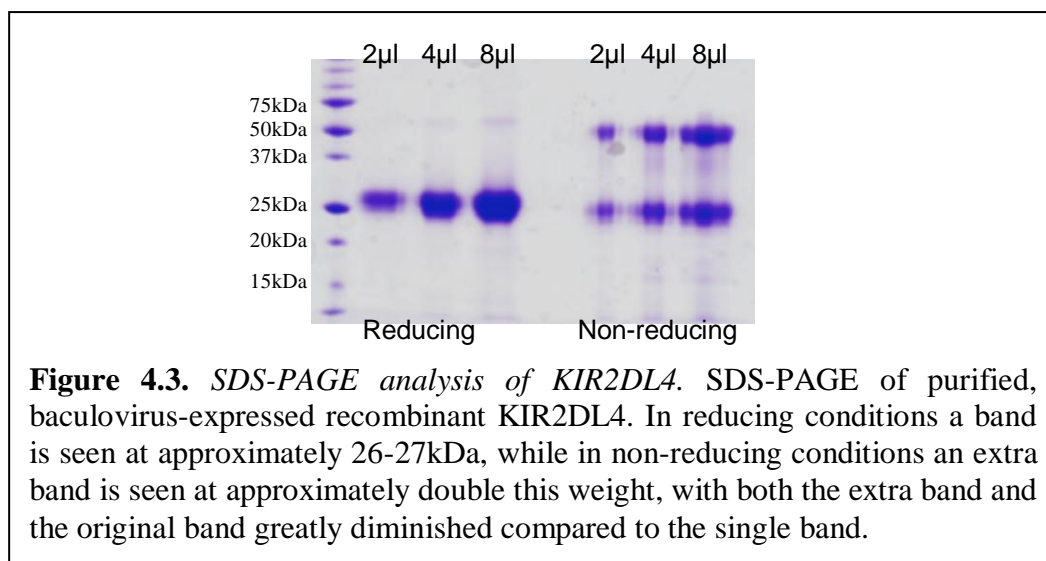
The recombinant KIR2DL4 extracellular region (residues 24-218), with an enterokinase-cleavable N-terminal 6xHis tag, was transiently expressed in Hi5 cells upon inoculation with 25ml of P3 viral stock, as described in Chapter 2. After a 48hr incubation at 27°C, the media containing secreted protein was harvested by centrifugation, followed by dialysis into a buffer containing 10mM Tris-HCl pH8.0 and 300mM NaCl. Initial purification was achieved by nickel affinity, with the elution protocol aimed at maximising yield (while achieving sufficient purity for the subsequent size exclusion chromatography step) rather than ensuring optimal purity. This was achieved using a two-step elution strategy involving a wash step using buffer containing 20-50mM imidazole followed by an elution step using buffer containing 350-400mM imidazole. Following the nickel-affinity purification step, KIR2DL4 was purified further using size exclusion on an S200 16/60 gel-filtration column that allowed separation of KIR2DL4 from aggregated protein. Total yield

was typically 2-4mg KIR2DL4 per 1L of expression medium. A typical SDS-PAGE analysis of a nickel elution and results of the size exclusion purification step are shown in figure 4.1.

The construct used for this work contained the 197-residue extracellular region of KIR2DL4, plus an N-terminal 6xHis tag, for a total construct size of 212 residues, and a predicted theoretical molecular weight of 23.3kDa. However, the molecular weight of the purified recombinant KIR2DL4 was approximately 26-27kDa, as observed by SDS-PAGE analysis. This can be explained by the high level of glycosylation frequently observed in recombinant proteins produced in insect cell expression systems. Consistent with this, the KIR2DL4 extracellular domain contains 2 predicted N-linked glycosylation sites, with motifs NVT at position 118 and NGT at position 152.

Initial quality-control tests and biophysical analysis of the purified KIR2DL4 elucidated a number of features of the recombinant KIR2DL4. CD analysis showed that the recombinant KIR2DL4 was folded with secondary structure consisting predominantly of β -sheet (Figure 4.2), a result consistent with the known structure of other KIRs and with the expected immunoglobulin-like fold of the KIR2DL4 domains. Initial SDS-PAGE analysis of the purified protein under reducing and non-reducing conditions showed that it was disposed to incomplete disulfide-bond-mediated dimerisation (Figure 4.3) Further investigation of this finding is described later in this chapter under the heading *Biophysical Analysis of Baculovirus-Expressed KIR2DL4*. Protein samples were concentrated to 6-8mg/ml for crystallisation trials.





Crystallisation of Baculovirus-Expressed KIR2DL4

Initial crystallisation trials for KIR2DL4 (extracellular domain) were conducted using the CrystallationTM system, using crystallisation screens from Sigma-Aldrich (Basic Crystallisation Kit), Hampton Research (PEG-Ion Screen) and Qiagen (PACT suite and the Joint Centre for Structural Genomics Plus (JCSG+) Suite), and incubated at either 20°C or 4°C. The components of screens used are fully listed in Appendix 1. In these 96-well trays, crystals appeared with similar morphology in a wide range of conditions after several days incubation (Table 4.1). Fine screening was conducted around all conditions that yielded crystals to refine conditions such as protein concentration, pH, precipitate concentration, salt concentration, drop size and drop ratio. This was performed as described in Chapter 2, under the heading *Crystallisation*.

Plate-like crystals were reproducibly grown using the hanging drop vapour-diffusion method at 20°C with a protein/reservoir drop ratio of 1:1. Total drop size was 2µl. Protein concentration was 6mg/ml. The reservoir buffer contained 24-28% PEG4000, 0.1M Tris pH 8.0 and 0.2M Sodium Acetate. Crystal growth was not very sensitive to pH changes between 8.0 and 8.5, or NaAc concentration above 0.1M. Reduction of PEG4000 concentration to below 24% halted crystal growth, while an increase above 28% caused overnucleation and a reduction in crystal size and quality. This is shown in Figure 4.4, with plate-like crystals in 4.4A and B, and overnucleated microcrystals in 4.4C. Crystals took 8 days to 2 weeks to grow to a maximum

dimension of approximately 0.1-0.2 mm, and did not grow beyond this point. To confirm the presence of KIR2DL4 protein, crystals were washed in reservoir solution and analysed using SDS-PAGE (Figure 4.4D).

Despite the successful crystallisation of KIR2DL4, sufficient quality crystals were not achieved. Successive rounds of macro-seeding and optimisation of crystallisation conditions resulted in crystals which diffracted to low levels on the MX2 beamline at the Australian Synchrotron (Figure 4.5), however the plate-like crystals were still very thin and diffracted too weakly to collect data such as crystal space group and unit cell dimension, and a useful dataset was not obtained.

Table 4.1. <i>Broad screening conditions yielding KIR2DL4 crystals.</i> Drop ratios were 0.1µl protein:0.1µl reservoir in all cases.					
Commercial Screen	Protein Concentration	Reservoir buffer	Temp	Time elapsed	Crystal morphology
JCSG+	8.0mg/ml	30% Jeffamine ED-2001 0.1M HEPES pH 7.0	20°C	5 days	Small plates
Sigma Basic Grid	6.0mg/ml	0.2M NaAc 0.1M Tris pH 8.5 30% PEG 4000	20°C	7-10 days	Small plates
Sigma Basic Grid	6.0mg/ml	0.2M Li ₂ SO ₄ 0.1M Tris pH 8.5 30% PEG 4000	20°C	7-10 days	Small plates
PACT suite	8.0mg/ml	25% PEG 1500, 10% Malate-MES-Tris pH 4.0	20°C	7-10 days	Small plates
PACT suite	8.0mg/ml	25% PEG 1500, 10% Malate-MES-Tris pH 4.0	4°C	7-10 days	Small plates

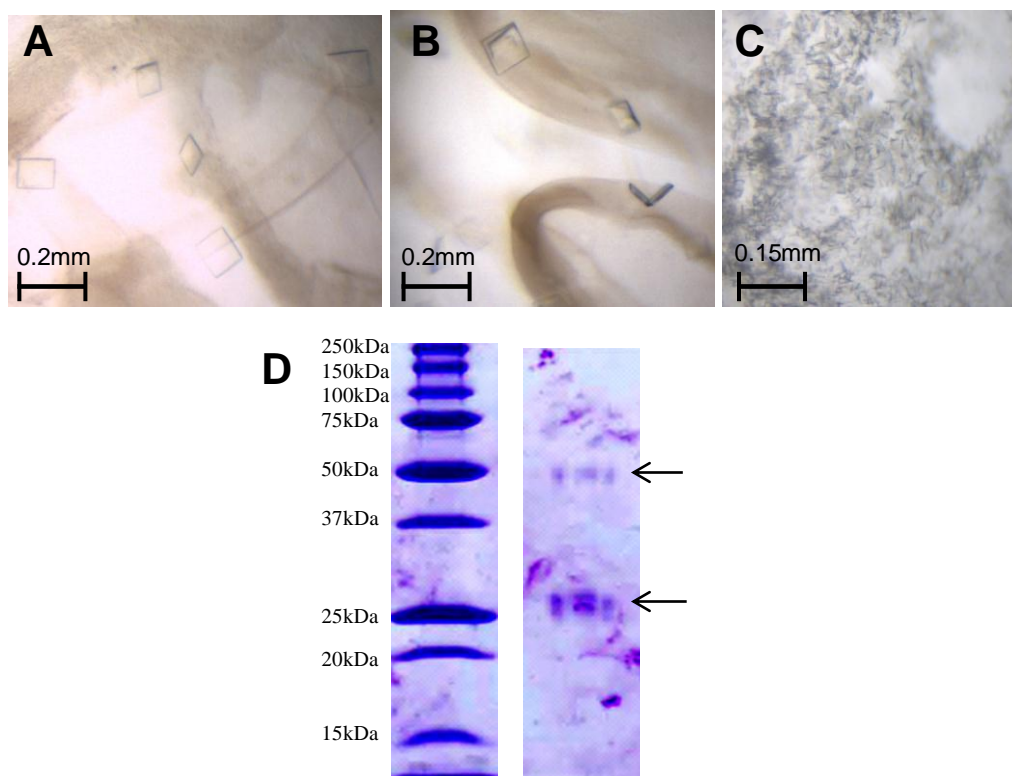


Figure 4.4. *KIR2DL4* crystal morphology. Crystal morphology after 2 weeks in Tris pH 8.0, 0.2M NaAc and (A) 26% PEG4000, (B) 28% PEG4000 and (C) 36% PEG4000. (D) SDS-PAGE analysis (non-reducing) of crystals (washed in reservoir solution) showing faint bands at approximately 26kDa and 52kDa (as shown by arrows).

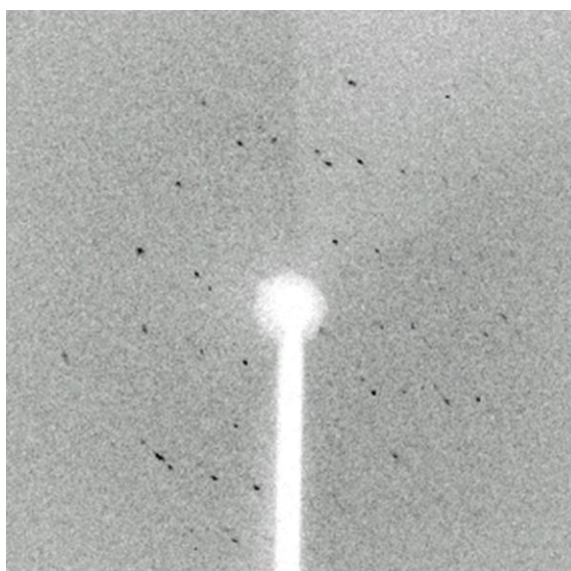


Figure 4.5. *KIR2DL4* diffraction. Example of diffraction achieved by KIR2DL4 crystals on the MX2 beamline at the Australian Synchrotron. Diffraction was not strong enough to gain crystal space group or unit cell information, or to obtain a useful dataset.

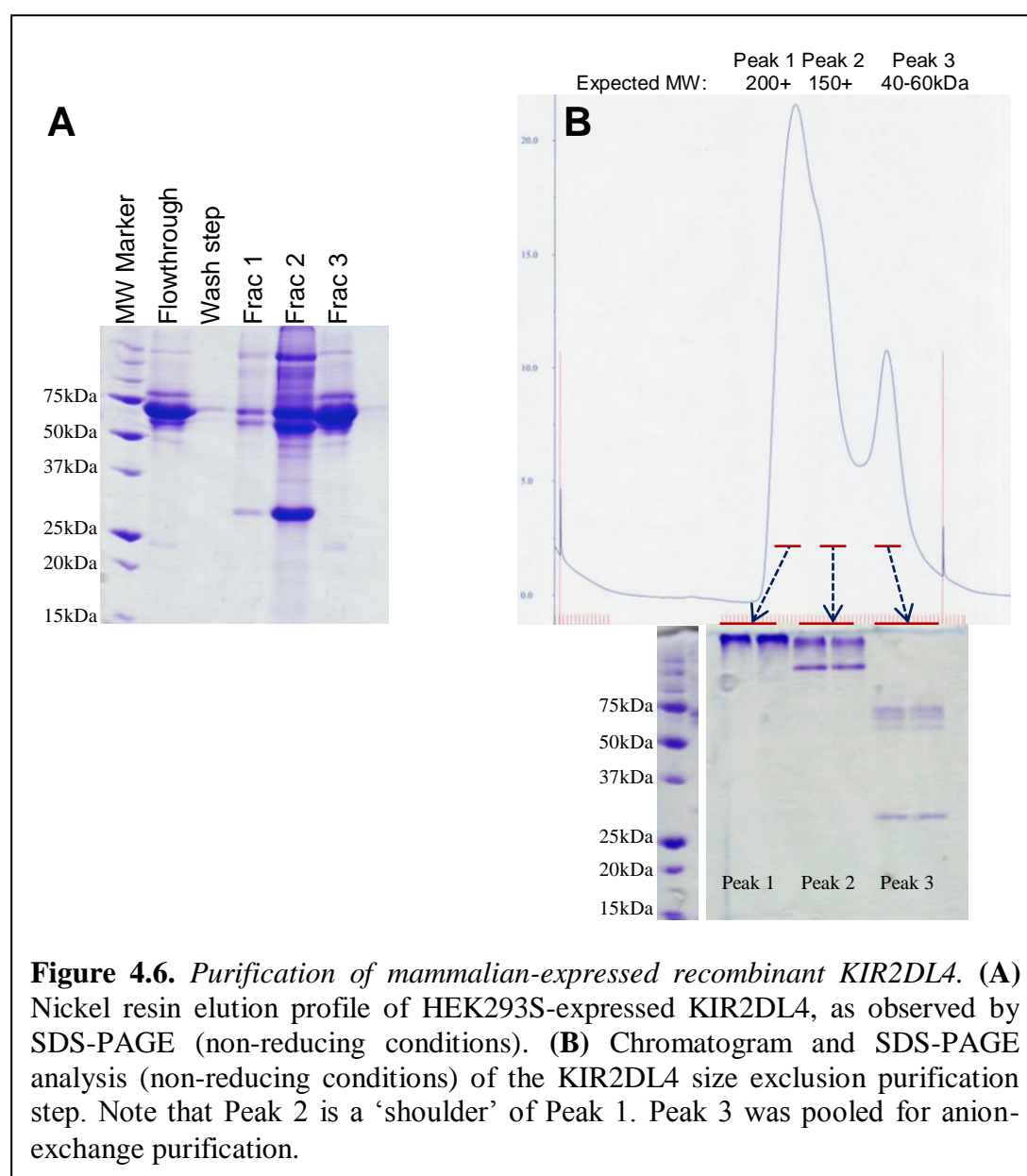
KIR2DL4 Production using a Mammalian Cell Expression System

In an attempt to overcome the issue of poor diffraction of KIR2DL4 crystals, KIR2DL4 was produced in Human Embryonic Kidney (HEK) 293S cells. This cell line was chosen to avoid potential obstruction of better quality crystallisation through the introduction of heterogeneity, a potential side effect of high levels of glycosylation. Glycosylation of protein produced by HEK293S cells is restricted to an invariant sugar group susceptible to cleavage by Endoglycosidase H (Endo-H) (Sullivan and Satchwell, 2000).

The KIR2DL4 construct (containing the KIR2DL4 extracellular domain and the EK cleavable, N-terminal His-tag) was cloned into a pHLseq vector, containing the appropriate signal sequence for secretion by HEK293S cells. This vector was amplified using XL1-Blue cells for transfection into HEK293S cells and 48-72hr expression as described in Chapter 2, under the heading *Production of KIR2DL4*, and subheading *Mammalian Cell Expression System*.

Purification of mammalian-expressed recombinant KIR2DL4 was performed using an adapted, but similar protocol to that produced using the baculovirus system. As described in Chapter 2 and earlier in this chapter, this protocol included Nickel-affinity and size exclusion purification steps. A typical Nickel-affinity elution and size exclusion trace are shown in Figure 4.6. As can be seen, there are significant differences from the equivalent steps for the baculovirus-expressed KIR2DL4 as shown in Figure 4.1. As the protein sample was generally not pure after size exclusion, final purification of mammalian-expressed recombinant KIR2DL4 was achieved with a Q sepharose anion-exchange step (Figure 4.7).

The yield of KIR2DL4 from the mammalian expression system (typically 0.1mg-0.2mg per 500ml of expression medium after size exclusion, and 0.05mg-1mg per 500ml of expression medium after anion-exchange) was far lower than that from the baculovirus expression system, partly due to the smaller expression volume and the absolute number of cells producing protein, but also after these factors were taken into account. The molecular weight of the mammalian-expressed KIR2DL4 monomer (as determined by SDS-PAGE) was just under 30kDa, larger than the baculovirus-expressed protein (26-27kDa), and much larger than the theoretical molecular weight of the KIR2DL4 construct (23.3kDa).



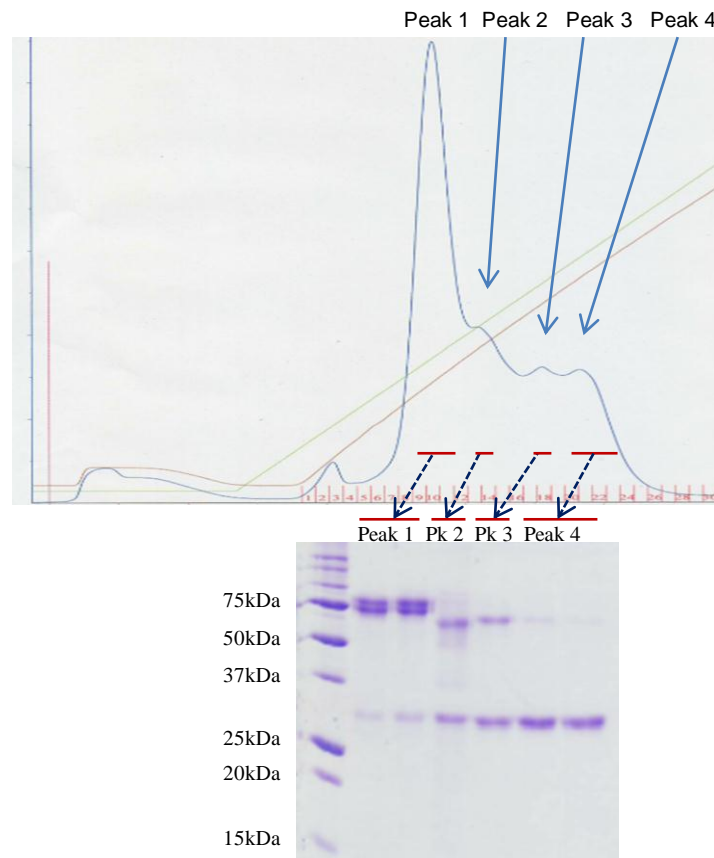


Figure 4.7. Anion-exchange purification of mammalian-expressed recombinant *KIR2DL4*. Chromatogram and SDS-PAGE analysis (reducing conditions) of the mammalian-expressed *KIR2DL4* Q sepharose anion-exchange purification step, performed to ensure optimal purity of the protein sample. Peak 4 was pooled for analysis.

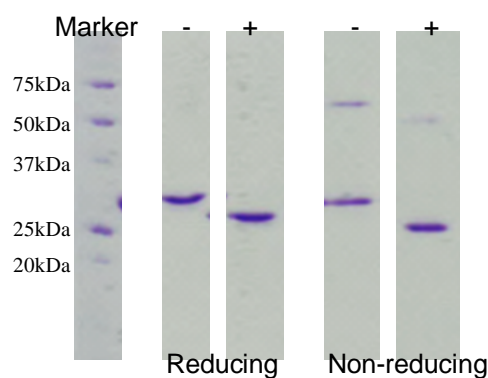


Figure 4.8. Endoglycosidase *H* treatment of mammalian-expressed *KIR2DL4*. SDS-PAGE analysis of mammalian-expressed *KIR2DL4* before (-) and after (+) Endoglycosidase *H* treatment, showing a marked reduction in molecular weight due to cleavage of the invariant sugar group produced by HEK293S cells. The dimeric bands, also visible in the non-reducing lanes, show a corresponding reduction in molecular weight.

Deglycosylation of Mammalian-Expressed KIR2DL4

As described above, the molecular weight of the mammalian-expressed KIR2DL4 monomer was approximately 30kDa, indicating that while glycosylation may have been restricted to the invariant sugar group typical in HEK293S-expressed proteins, it was nonetheless more pronounced in the mammalian-expressed KIR2DL4 than that produced by the baculovirus system. Susceptibility of the mammalian-expressed KIR2DL4 to deglycosylation was tested using commercially available Endo-H. Deglycosylation was performed for 2 hrs at 37°C in a buffer containing 100mM NaAc buffer at pH 5.2, and tested using SDS-PAGE (Figure 4.8). Experiments run over longer time courses showed that the deglycosylation reaction had run to completion after 2 hrs. This analysis showed that deglycosylation reduced the molecular weight of the recombinant KIR2DL4 from approximately 30kDa to approximately 25-26kDa, still above the theoretical molecular weight (23.3kDa). This may have been due to the truncated sugar molecule left by Endo-H treatment.

Despite the successful production and deglycosylation of recombinant, mammalian-expressed KIR2DL4, the yield from this system was considered too low to justify either crystallisation trials or biophysical tests as performed on the baculovirus-expressed protein, and mammalian expression of KIR2DL4 as described was ceased. The following sections describe experiments performed with recombinant KIR2DL4 produced using the baculoviral expression system.

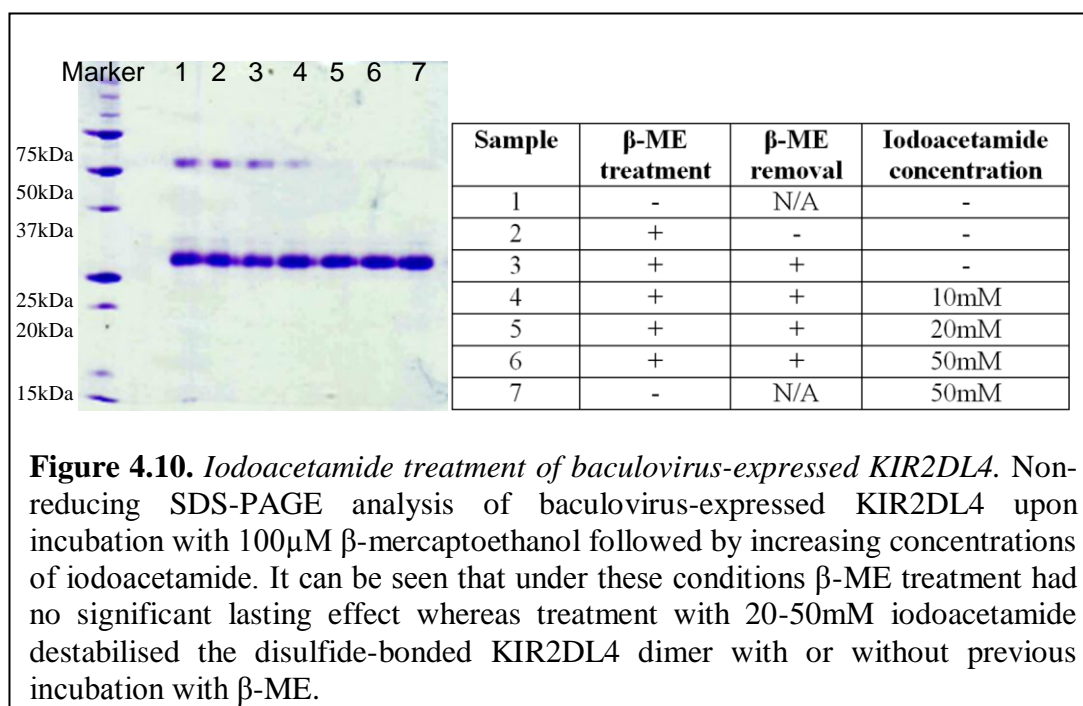
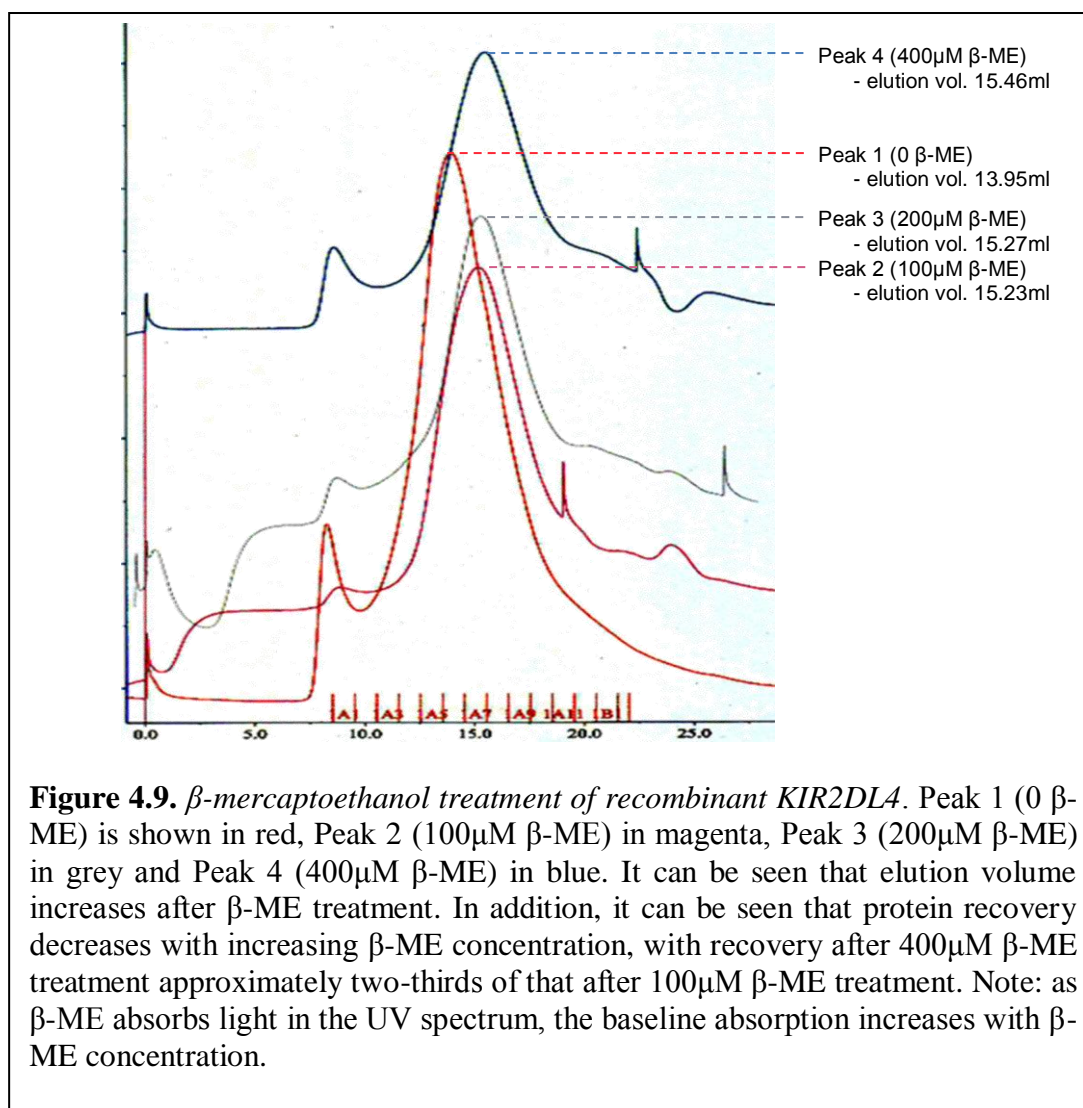
Biophysical Analysis of Baculovirus-Expressed KIR2DL4

Dimerisation and Oligomerisation of Recombinant KIR2DL4

As mentioned earlier in this chapter under the heading *KIR2DL4 Production using a Baculoviral Expression System*, SDS-PAGE comparison of the purified baculovirus-derived KIR2DL4 under reducing and non-reducing conditions showed that it was subject to incomplete disulfide-bond-mediated dimerisation (Figure 4.3). This apparent dimerisation was an interesting and unexpected finding, and was initially investigated by 30 minute incubation on ice with low concentrations of β -mercaptoethanol (β -ME), enough to break surface-exposed intermolecular disulfide bonds while leaving the intramolecular disulfides intact, followed by 30 minute room temperature incubation with iodoacetamide, an alkylating agent which covalently binds with the thiol group of free cysteine residues.

The concentration of β -ME required to break surface-exposed intermolecular disulphide bonds on KIR2DL4 was tested using size-exclusion chromatography to analyse protein samples which had been treated on ice for 30 minutes with a range of β -ME concentrations. This analysis technique was chosen on the premise that if surface-exposed intermolecular disulphide bonds were broken, the protein in the sample would be monomerised, and therefore the elution volume would increase, while if the tertiary structure of the protein was disrupted due to breakage of the intramolecular disulfides, then protein aggregation would occur, decreasing the elution volume and decreasing the amount of correctly folded protein recovered. As shown in figure 4.9, treatment with β -ME concentrations from 100-400 μ M resulted in a significant increase in elution volume, though protein recovery decreased as β -ME concentration increased. 100 μ M β -ME was chosen for the final treatment concentration, as treatment with this concentration resulted in optimal disruption of the intermolecular disulphide bonds along with optimal protein recovery. For the purpose of iodoacetamide treatment, β -ME treated samples were run through a commercial de-salting column to separate the β -ME out of the protein sample.

After β -ME treatment, iodoacetamide was used to ensure that the broken intermolecular disulfide bonds did not re-form. Analysis of this experiment was performed using non-reducing SDS-PAGE, as shown in figure 4.10. This experiment showed that dimerisation of recombinant KIR2DL4 was caused by intermolecular disulfide bonds, and that these bonds could be stably disrupted by treatment with 20-50mM iodoacetamide, with or without prior β -ME treatment.



Dimerisation of baculovirus-expressed recombinant KIR2DL4 was further investigated using SAXS, using the SAXS/WAXS beamline at the Australian Synchrotron as described in Chapter 2, under the heading *Biophysical Analysis Techniques*, and the subheading *Small Angle X-ray Scattering (SAXS)*. A range of concentrations from 1.0mg/ml to 8.0mg/ml were tested along with known standards in order to calculate the molecular weight of KIR2DL4 in solution at these concentrations. Results are listed in Table 4.2. Concentrations lower than 1.0mg/ml (0.1mg/ml & 0.5mg/ml) were also tested, though data from these experiments were not used due to a low signal/background ratio.

The results of this SAXS experiment indicated that the purified KIR2DL4 protein was subject to concentration-dependent, reversible higher-order oligomerisation as indicated by an increase in apparent molecular weight at higher concentrations (up to 8mg/ml), which was completely reversed upon dilution to 1mg/ml. Due to the reversible nature of this oligomerisation, it is unlikely to be due to covalent bonds, and therefore it is probably a distinct process from the dimerisation described above, which is mediated by disulfide bonding. Any biological relevance of KIR2DL4 oligomerisation is difficult to determine. However, it is possible that self-association of large numbers of receptors could aid receptor binding to HLA-G due to the effect of avidity. Further SAXS analysis of baculovirus-expressed recombinant KIR2DL4, including the production of *ab initio* models of recombinant KIR2DL4 in solution, is described below under the heading *Small Angle X-ray Scattering (SAXS) of Baculovirus-Expressed KIR2DL4*.

Disulfide-dependent dimerisation of KIR2DL4 can be explained by sequence analysis of the D0 domain, and alignment of this sequence with D0 domains from other KIRs. As shown in figure 4.11, KIR2DL4 contains the 2 cysteine residues (C28 and C74) which are present in all KIR D0 domains, and are expected to form an intramolecular disulphide bond. However, this domain in KIR2DL4 contains a third cysteine (C10) which is not present in any other D0 domain in the KIR family.

Table 4.2. *Molecular weight of KIR2DL4 as determined by SAXS.* SAXS was used to determine the apparent molecular weight of KIR2DL4 at different concentrations. A reversible, concentration-dependent higher-order oligomerisation is shown by an increase in apparent molecular weight at higher concentrations, which is not seen in the freshly diluted protein. Aggregation was not detected in this experiment.

Protein Concentration (mg/ml)	Apparent molecular weight in solution (kDa)	Average oligomeric state, using 27kDa as monomeric MW
1.0	71	2.64
4.0	100	3.70
8.0	151	5.60
1.0 (freshly diluted from 8.0mg/ml)	72	2.65

KIR2DL4	1	HVGGQDKP F C	SAWPSAVVPQ	GGHVTLR C HY	RRGFNIIFTLY	KKDGVVPVPEL	50
KIR3DL1	1	HMGGQDKPFL	SAWPSAVVPR	GGHVTLR C HY	RHRFNNFMLY	KEDRIHIPIF	50
KIR3DL2	1	LMGGQDKPFL	SARPSTVVPR	GGHVALQ C HY	RRGFNNFMLY	KEDRSHVPIF	50
KIR3DL3	1	HVGGQDKPFL	SAWPGTVVSE	GQHVTLQ C RS	RLGFNEFSLS	KEDGMPVPEL	50
KIR3DS1	1	HMGGQDKPFL	SAWPSAVVPR	GGHVTLR C HY	RHRFNNFMLY	KEDRIHVPIF	50
KIR2DL4	51	YNRIFWNSFL	ISPVTPAHAG	TYR C RGFHPH	S	81	
KIR3DL1	51	HGRIFQESFN	MSPVTTAHAG	NYT C RGSHPH	S	81	
KIR3DL2	51	HGRIFQESFI	MGPVTPAHAG	TYR C RGSRPH	S	81	
KIR3DL3	51	YNRIFRNSFL	MGPVTPAHAG	TYR C SSHPH	S	81	
KIR3DS1	51	HGRIFQEGFN	MSPVTTAHAG	NYT C RGSHPH	S	81	

Figure 4.11. *Sequence alignment of KIR family D0 domains.* Cysteine residues are in bold type and coloured red; KIR2DL4 contains an unpaired cysteine in addition to the two seen in other KIR D0 domain sequences.

As the structure of the KIR2DL4 D0 domain has not been determined, it is difficult to determine exactly where C10 is placed within this domain. The corresponding region in KIR3DL1 is solvent exposed, though the L10 sidechain is not (shown in figure 4.12A). Likewise, the corresponding region in the D1 domain of KIR2DL1 (shown in figure 4.12B) is highly solvent exposed, and if the KIR2DL4 D0 domain displays a similar conformation to these domains, then it is conceivable that the C10 residue may be solvent-exposed and could potentially be involved in self-association. Such an association would potentially give the KIR2DL4 dimer an upturned U shape, with the C-termini and transmembrane domains at each end of the U. This homodimerisation would maintain maximum solvent exposure for the HLA-G interaction sites of both molecules and would have the potential to increase the avidity of any interaction with HLA-G.

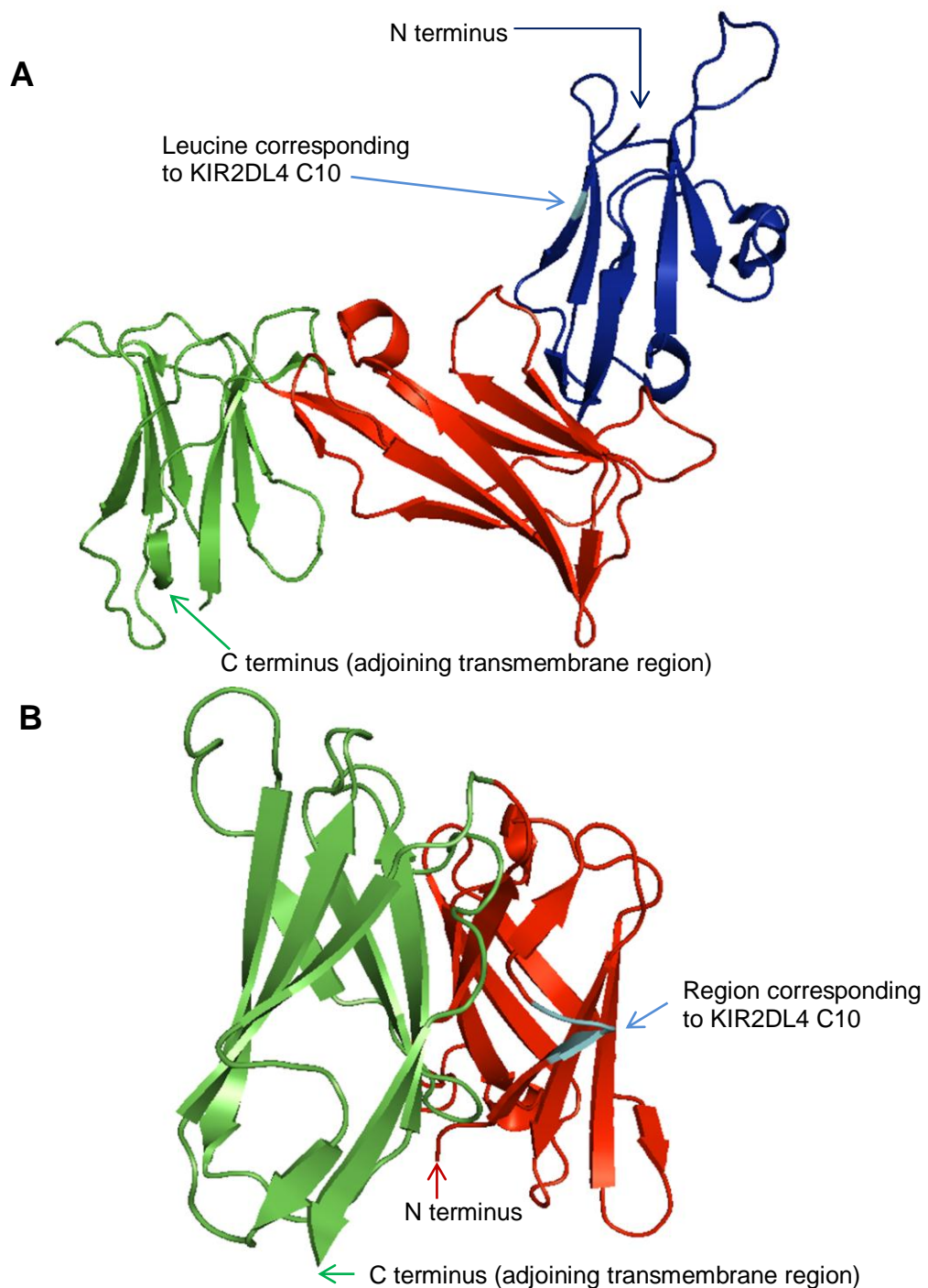
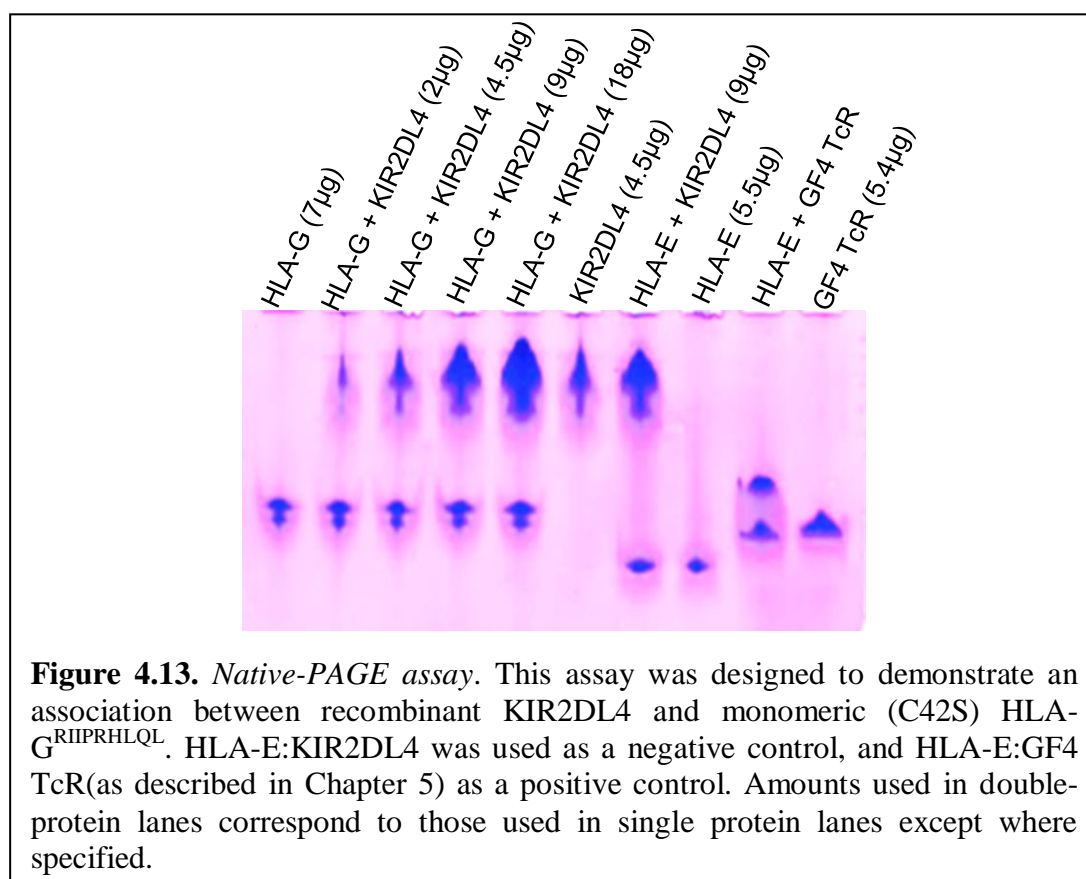


Figure 4.12. Structures of *KIR3DL1* and *KIR2DL1*. Crystal structures of (A) the *KIR3DL1* extracellular region (PDB entry 3VH8) (Vivian *et al.*, 2011) and (B) the *KIR2DL1* extracellular region (PDB entry 1NKR) (Fan *et al.*, 1997). D2 domains are coloured green, D1 domains are coloured red and the *KIR3DL1* D0 domain is coloured royal blue. The leucine residue in the D0 domain of *KIR3DL1*, and the area within the *KIR2DL1* D1 domain, which both correspond to *KIR2DL4* C10, are coloured cyan. It can be seen that this area is solvent exposed in both molecules, and could play a role in *KIR2DL4* self-association.



Association with HLA-G

Preliminary binding studies to test the reported association between KIR2DL4 and HLA-G were performed, with a native-PAGE assay followed by a more sensitive Surface Plasmon Resonance (SPR) study. Native-PAGE analysis showed no detectable association between KIR2DL4 and monomeric (C42S) HLA-G^{RIIPRHLQL} (Figure 4.13); however this technique often fails to detect associations for which the binding affinity is less than approximately 30-40mM. Further analysis by Native-PAGE showed no association between KIR2DL4 and HLA-G presenting the alternative peptides KGPPAALTL and KLPAQFYIL.

An SPR study (conducted by Dr Julian Vivian and Dr Travis Beddoe, Rossjohn Lab, Department of Biochemistry and Molecular Biology, Monash University, Clayton, Australia) also failed to show an association between the purified recombinant KIR2DL4 with either monomeric (C42S) or dimeric (wild-type) HLA-G presenting the peptides RIIPRHLQL, KGPPAALTL and KLPAQFYIL, at either pH 7.4 (to simulate normal cell conditions) or pH 5.5 (to simulate endosomal conditions). The interaction was tested using pHLA-G in solution passed over immobilised KIR2DL4, as well as KIR2DL4 in solution passed over immobilised pHLA-G.

Although no association between KIR2DL4 and HLA-G was shown using the techniques outlined above, it is possible that parameters which would aid such an association were not tested. One such parameter is the peptide presented by HLA-G. As outlined in Chapter 3, HLA-G can present any of several endogenous peptides from various sources, which can show marked differences in conformation at the peptide-binding region and therefore affect recognition by receptors which bind to this region. However, in the experiments outlined above, only four selected peptides were tested.

Small Angle X-ray Scattering (SAXS) of Baculovirus-Expressed KIR2DL4

In addition to the techniques used to test self-association of recombinant KIR2DL4 and the association of recombinant KIR2DL4 with HLA-G, the conformation of the baculovirus-derived KIR2DL4 in solution was investigated using SAXS, performed at the SAXS/WAXS beamline at the Australian Synchrotron as previously described in Chapter 2, under the heading *Biophysical Analysis Techniques*, and the sub-heading *Small Angle X-ray Scattering (SAXS)*. Further to those tests previously described in this chapter under the heading *Biophysical Analysis of Baculovirus-Expressed KIR2DL4* and sub-heading *Dimerisation and Oligomerisation of Recombinant KIR2DL4*, *ab initio* models of recombinant KIR2DL4 were generated from both low and high concentration samples.

After data from all samples were subjected to background subtraction, data processing using PRIMUS and P(r) function generation using GNOM, two recombinant KIR2DL4 samples were selected for the generation of *ab initio* models – one at 1.25mg/ml (low concentration) and the other at 5.0mg/ml (high concentration). For each of these samples, DAMMIN was used to generate 15-20 initial *ab initio* models based on dummy atoms in lattice formation, and DAMAVER used to align, merge and filter these models. Following this, GASBOR was used to generate a further 15-20 *ab initio* models, before alignment, merging and filtering using DAMAVER. DAMMIN and GASBOR use different algorithms for the production of *ab initio* models, and the similarity of the results obtained from the two programs substantiates the validity of those results.

Raw SAXS data for the four concentrations tested is shown in figure 4.14A, with the Guinier plots for the 1.25mg/ml and 5.0mg/ml samples shown in 4.14B. In both of these figures, it can be seen that at low ‘s’ values the scattering intensity values for the two higher concentrations show a slightly increased gradient at low ‘s’ values. This is indicative of a self-association at the higher concentrations not seen as markedly in the lower concentrations. Aggregation, often seen in raw SAXS data as a strong increase in gradient at low ‘s’ values and especially apparent in Guinier plots, was not detected in any of these samples.

The signal/background ratio was higher at higher concentrations of protein, especially at low ‘s’ values. This is evidenced in the I/s plots as a lengthening of the useful data area along the ‘s’ axis. It should be noted that data points identified as outliers due to low signal/background ratio were discarded and not used in further data processing.

The Guinier plots shown in figure 4.14B were used to estimate the length and gradient of the linear Guinier region, which decreases in length as the basic molecular unit in solution increases in size. This region is used to estimate both the radius of gyration (R_g) and the maximal dimension (R_{max}) of the basic molecular unit in solution, though both may be refined upon calculation of the P(r) function using GNOM (these parameters are shown in Table 4.3). Data points at lower ‘s’ values than the Guinier region were discarded.

Table 4.3. Comparison of R_g and D_{max} for KIR2DL4 at 1.25mg/ml and 5.0mg/ml. These parameters were estimated using the Guinier region and refined using the P(r) function.

Protein Concentration (mg/ml)	R_g (Å)	R_{max} (Å)
1.25	39.36 (± 0.72)	100
5.0	55.14 (± 2.06)	160

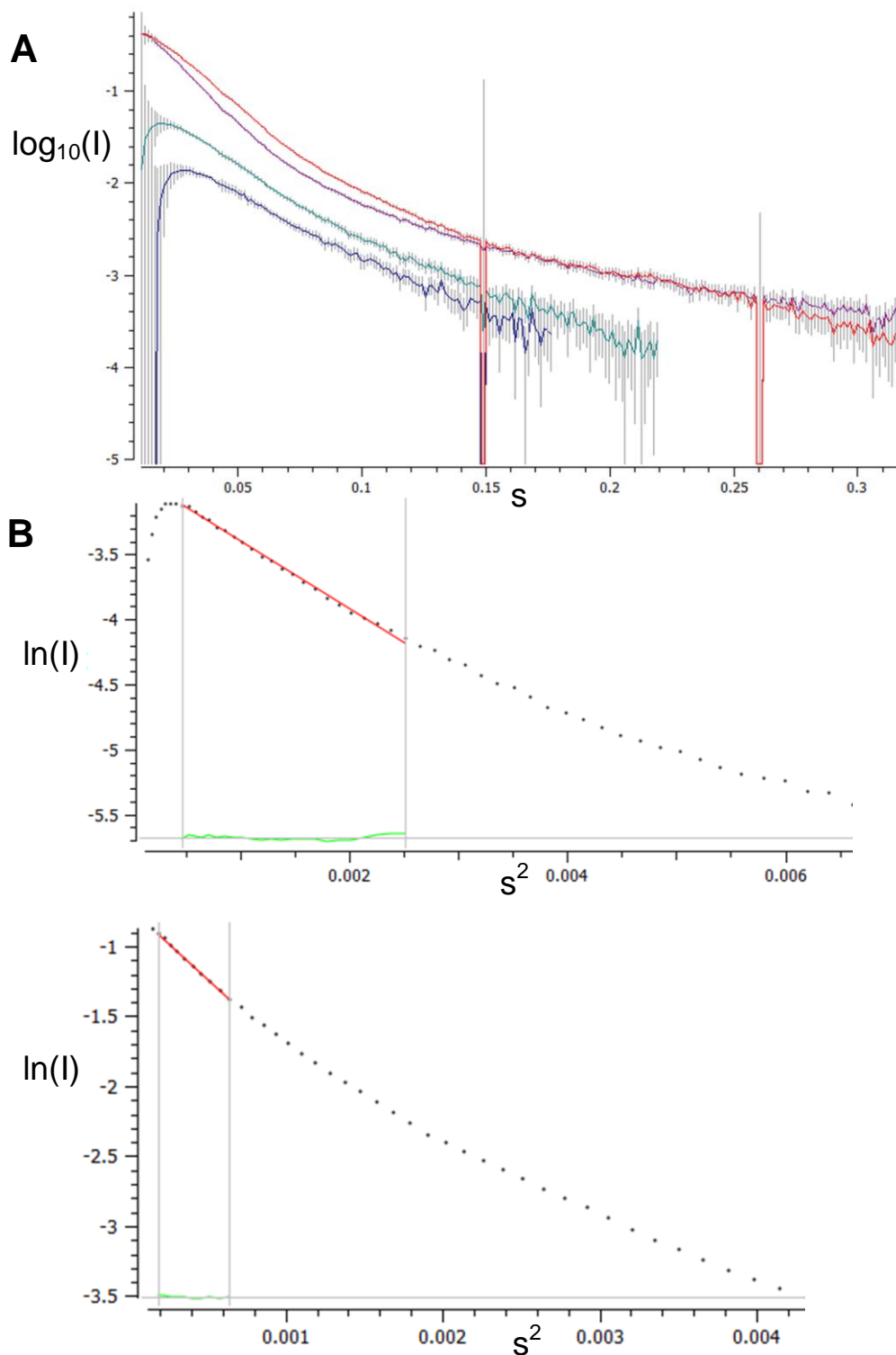
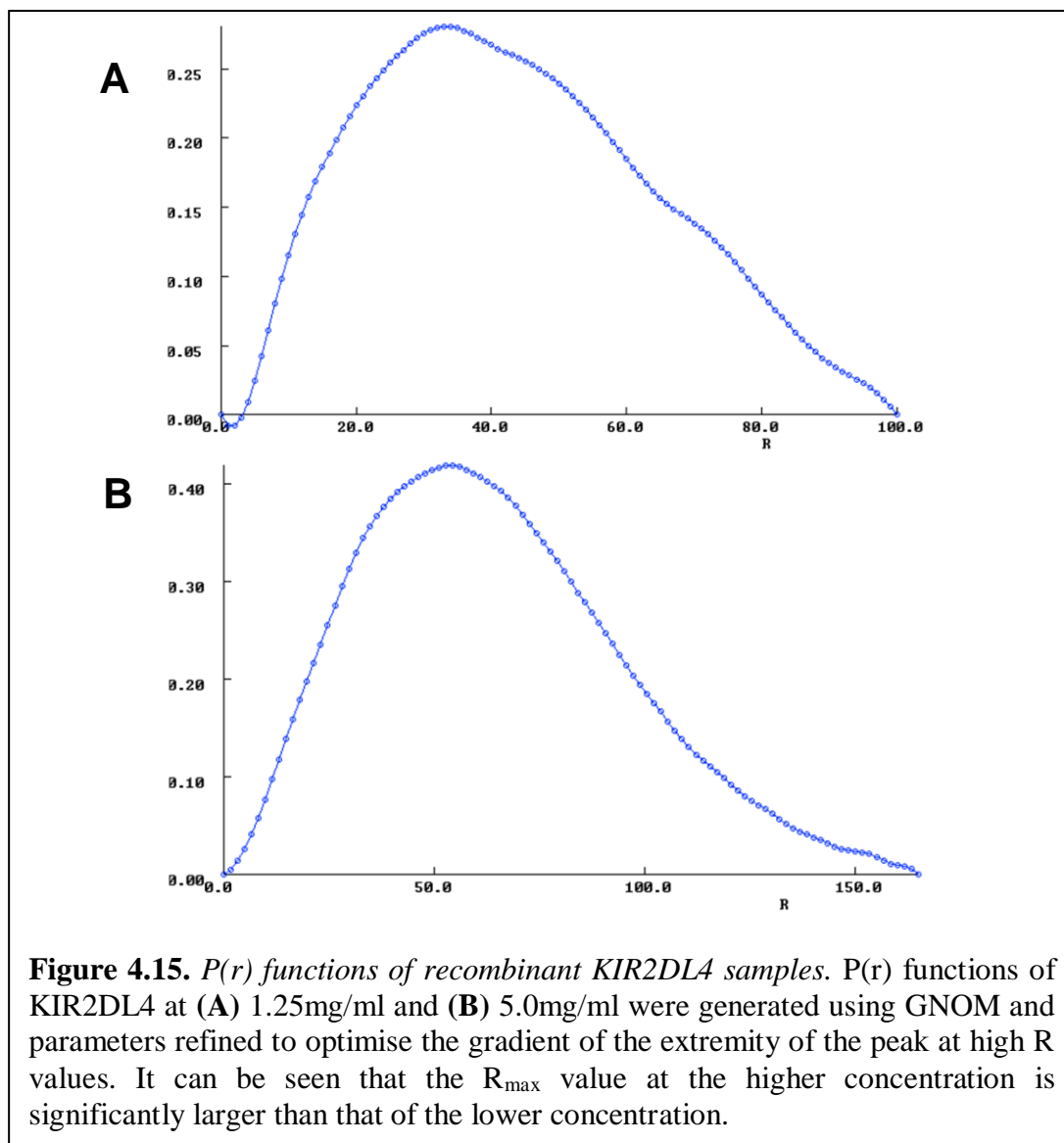


Figure 4.14. Raw SAXS data for recombinant *KIR2DL4* samples. **(A)** Scattering intensity (I) plotted against the magnitude of the scattering vector (s), for *KIR2DL4* samples at 0.75mg/ml (blue), 1.25mg/ml (teal), 2.5mg/ml (purple) and 5.0mg/ml (red). Error bars are shown in grey. **(B)** Guinier plots ($\log_e I$ against s^2) of *KIR2DL4* samples at 1.25mg/ml (higher) and 5.0mg/ml (lower). The estimated Guinier region of these plots is shown within vertical grey lines. In both (A) and (B) it can be seen that scattering intensity of the lower concentration samples falls at low ‘ s ’ values, while that of higher concentrations increases slightly.



$P(r)$ functions used as inputs for *ab initio* model generation in DAMMIN and GASBOR are shown in figure 4.15. These functions show the relative proportion of pairs of atoms which are distance ‘ R ’ (in Angstroms) apart. As can be seen in this figure, the $P(r)$ function at the higher concentration has a higher R_{\max} , indicating that the basic unit of KIR2DL4 in solution at this concentration is larger. R_{\max} estimations at this point were 100Å (for the 1.25mg/ml sample) and 160Å (for the 5.0mg/ml sample). The shape of the $P(r)$ function, a bell-shaped curve whose maximum point is at less than $R_{\max}/2$, suggests that the protein adopts an elongated conformation in solution (Putnam *et al.*, 2007).

Filtered, averaged *ab initio* KIR2DL4 models for both the 1.25mg/ml sample and the 5.0mg/ml sample are shown in figure 4.16. These models are the result of the alignment, merging and filtration (performed using DAMAVER) of 15-20 initial models generated using GASBOR from the P(r) functions shown in figure 4.15. These initial models are generated from random seeds, with ‘dummy atoms’ added or deleted for optimal consistency with the relevant P(r) function. These dummy atoms are arranged in a lattice formation after averaging in DAMAVER, as seen in figure 4.16.

It can be seen that the *ab initio* SAXS models for KIR2DL4 both low (1.25mg/ml) and high (5.0mg/ml) concentrations both form an ‘arch-like’ configuration. These arches are narrow at each end and wide in the middle. Consistent with the quantitative SAXS data presented in this chapter under the heading *Biophysical Analysis of Baculovirus-Expressed KIR2DL4* and sub-heading *Dimerisation and Oligomerisation of Recombinant KIR2DL4*, the *ab initio* model for KIR2DL4 at a high concentration is much larger than the model for the low concentration sample. This may be due to the higher oligomeric state of KIR2DL4 at this concentration.

To test the validity of the KIR2DL4 dimerisation model postulated earlier in this chapter, KIR2DL1 molecules were positioned inside the *ab initio* SAXS model for KIR2DL4 at 1.25mg/ml. KIR2DL1 was chosen as a representation model for KIR2DL4 based on the sequence similarity between the extracellular domains of the two molecules, though small differences would be expected between the KIR2DL1 D1 domain and the KIR2DL4 D0 domain, and the hinge angle between the two domains of KIR2DL4 is unknown. Despite earlier SAXS data showing that the oligomeric state of KIR2DL4 at 1mg/ml was in the dimer/trimer range, four KIR2DL1 molecules were fit inside the SAXS shell, as shown in figure 4.17. This arrangement provided the best fit to the SAXS shell, minimising both vacant areas within the shell, and areas where the models did not fit inside the shell. While eliminating clashes between molecules and providing a reasonable fit to the shell itself, the KIR2DL1 molecules were able to be positioned in such a way that the four molecules were arranged in two pairs. The two regions corresponding to C10 within each pair were in close proximity to each other, providing support for the dimerisation model postulated above.

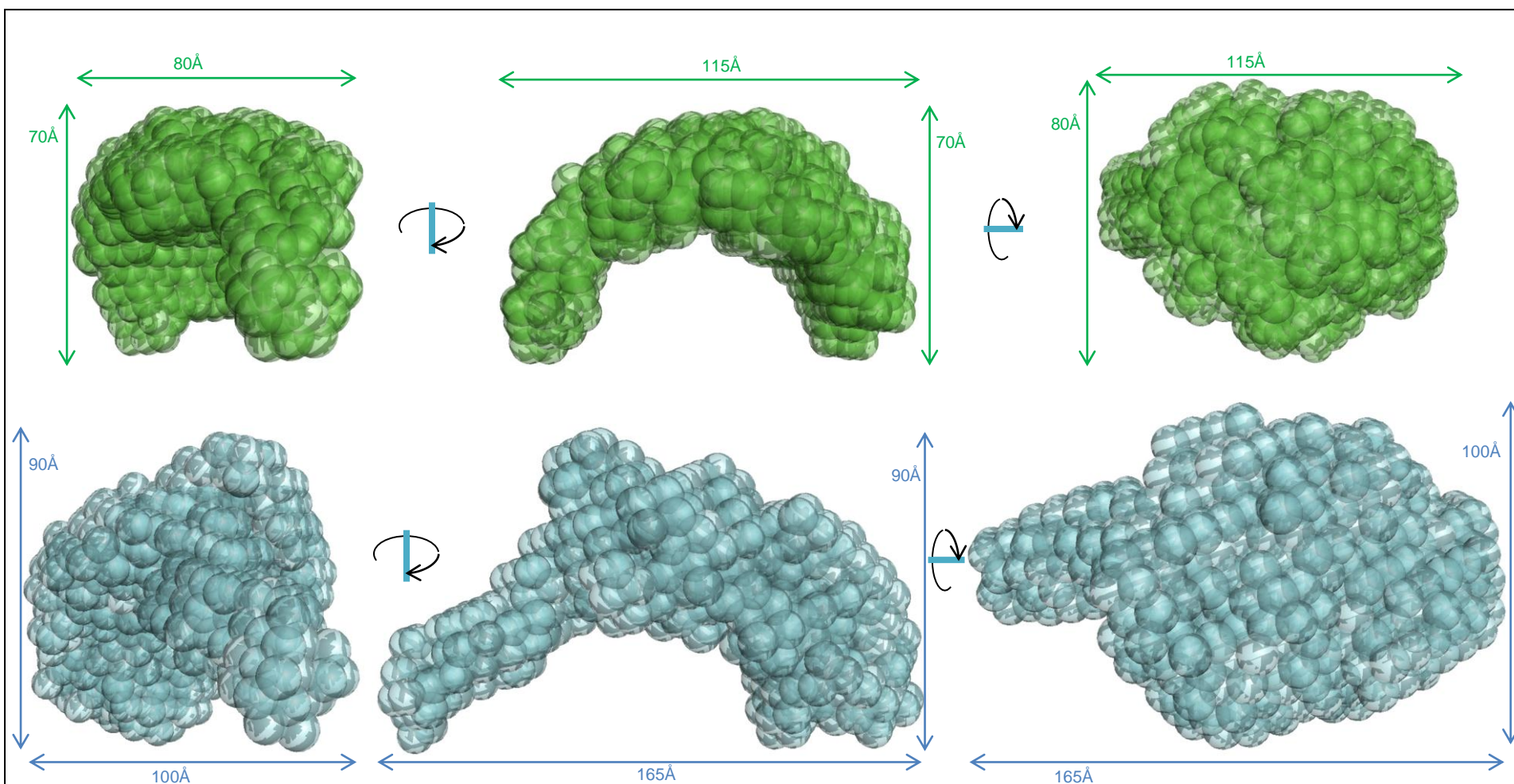


Figure 4.16. Ab initio SAXS models of recombinant KIR2DL4. Front (left), side (middle) and top (right) views of *ab initio* SAXS models of KIR2DL4 at 1.25mg/ml (green, upper) and 5.0mg/ml (blue, lower), with approximate dimensions labelled. 15-20 initial models were generated from the $P(r)$ functions shown above using GASBOR, and these were averaged and filtered using DAMAVER to create the final models shown here. Dummy atoms are shown as spheres.

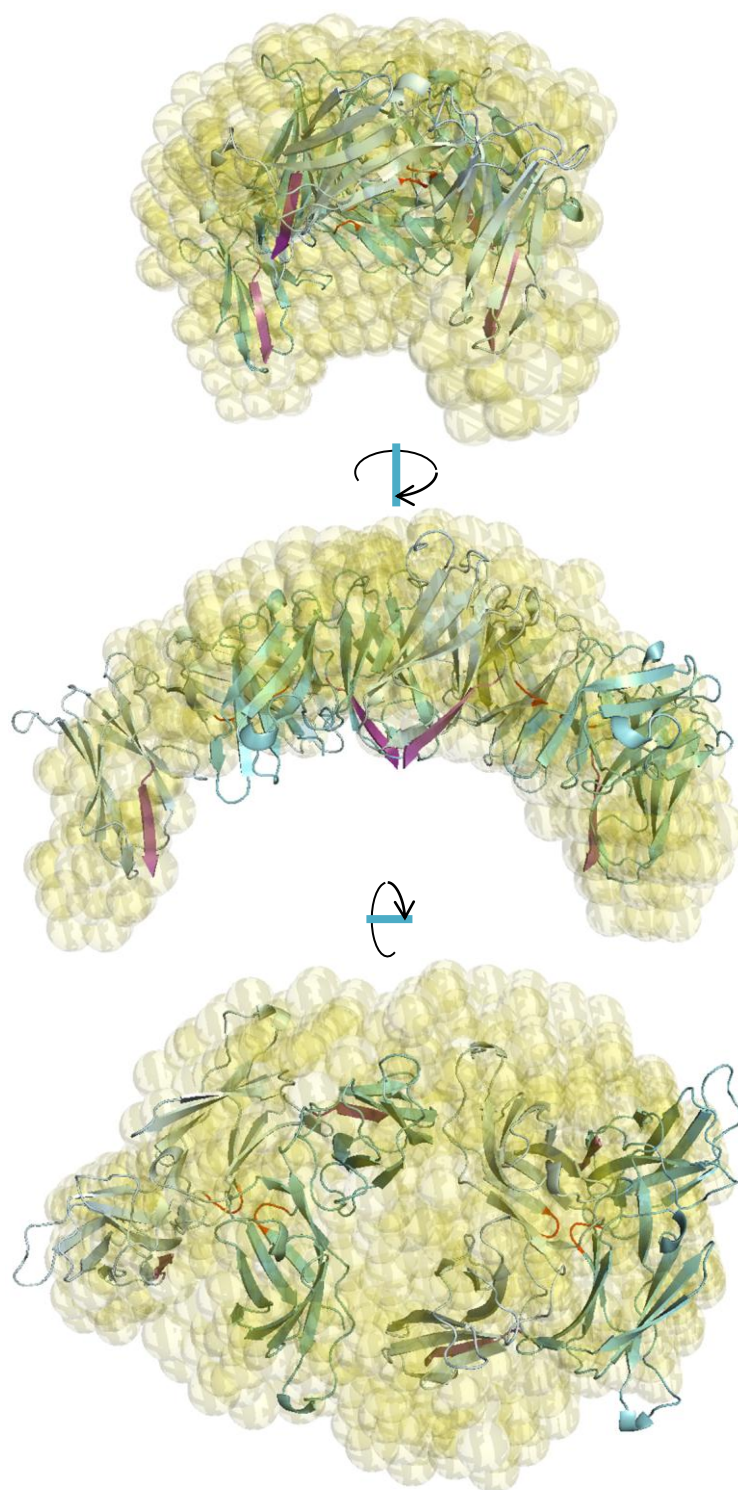


Figure 4.17. *KIR2DL1* models within the *ab initio* *KIR2DL4* SAXS shell. The shell (coloured yellow) corresponds to the *ab initio* SAXS model of *KIR2DL4* at 1.25mg/ml. *KIR2DL1* (coloured cyan) has been used as a model for *KIR2DL4*, due to sequence similarity. It can be seen that four *KIR2DL1* models fit within the SAXS shell at this concentration. These four models may be grouped as two pairs, with the region corresponding to *KIR2DL4* C10 in any model (shown in red) in close proximity to the same region in the molecule it is paired with. The C-termini of all four models (shown in purple) lead in the same direction, potentially allowing *cis* association of receptors on one cell.

In addition, the C-terminus of each molecule, where the extracellular domains meet the transmembrane domain, pointed in the same direction, showing that the molecules may potentially self-associate in a *cis* arrangement on one cell. While not the only model which fits the data, this arrangement of molecules provides a good rationalisation of the link between the dimerisation of KIR2DL4 and the SAXS data achieved.

Discussion

The work described above presents a number of steps towards the biophysical and structural characterisation of KIR2DL4. Primarily, optimisation of recombinant KIR2DL4 expression in both baculoviral and mammalian expression systems will assist future studies which rely on recombinant protein, including those targeted at crystallisation. Such optimisation may be through molecular techniques such as codon optimisation or construct length variation, or through the use of alternative cell lines or plasmids. While the yield of the mammalian-expressed protein was far lower than the corresponding baculovirus-expressed protein, the different oligomeric species were more easily resolvable, and the control over glycosylation is also a valuable tool to decrease heterogeneity of samples. Therefore, if the yield of the mammalian-expressed KIR2DL4 can be increased, this is likely to provide a better system for studies using recombinant KIR2DL4.

Dimerisation of KIR2DL4 as described above is not a unique occurrence among the KIR family. It has been previously suggested that KIR2DL2 also self-associates at the cell surface, based on orderly orientations of molecules within crystals (*Snyder et al., 1999*). The effect that dimerisation has on crystallisation of KIR2DL4 is difficult to determine. Abrogation of KIR2DL4 dimerisation by use of cysteine methylation with iodoacetamide, or mutation of the unpaired cysteine residue, may aid crystallisation. In either case, production of KIR2DL4 monomer, potentially by mutation or by iodoacetamide treatment, may provide a valuable tool for comparison with the dimeric wild-type protein.

The SAXS analysis of recombinant KIR2DL4 and subsequent modelling described above shows a working model of KIR2DL4 self-association at the cell surface. Some issues remain unresolved in this model, which may or may not be resolved with the

determination of the KIR2DL4 crystal structure. One such issue is the compatibility of KIR2DL4 self-association in regions apart from the putative C10-C10 disulfide bond, and the potential clashes in charge or steric hindrance that may occur in these regions.

It should be noted that the work shown in this chapter does not constitute a conclusive demonstration of the dimerisation of KIR2DL4 at the cell surface or the mechanism by which this takes place. The oligomerisation which may be inferred from the quantitative SAXS data and the *ab initio* SAXS models may be a result of a distinct and as yet unknown mechanism. The possibility remains that oligomerisation is an artefact caused by the protein concentrations used. Despite this, the work shown provides the first working model of self-association by this receptor.

In summary, while progress has been made towards determination of the crystal structure and biophysical characterisation of the association between KIR2DL4 and HLA-G as well as the self-association of recombinant KIR2DL4, many obstacles remain to the successful completion of these aims. In view of the unique 'third' D0-domain cysteine residue and dimerisation of the recombinant protein, KIR2DL4 remains a very interesting and attractive target for biophysical and structural analysis.

Chapter 5 - Structural Investigation of an HLA-E-Restricted T-cell Response

The idea that MHC-Ib may play distinct roles in adaptive immunity has provoked much interest in recent years. As described in Chapter 1 under the heading *Class Ib MHCs in Adaptive Immunity*, HLA-E presenting peptides from sources other than host MHC-I leader sequences may be recognised by specific T-cell receptors. HLA-E restricted, CMV-peptide specific CTLs have been identified in CMV-immune individuals (*Ulbrecht et al., 2000, Pietra et al., 2003*). These CMV-derived peptides have been identified as part of the UL40 ORF, and are mimotopes of HLA leader sequence peptides naturally presented by HLA-E in some haplotypes. TcRs which recognise HLA-E presenting CMV UL40-derived mimotope peptides are classed by peptide recognition into the two groups that have been described to date (*Pietra et al., 2003*). Group 1 HLA-E restricted TcRs recognise HLA-E presenting either of the mimotope peptides VMAPRTLIL or VMAPRTLVL, while Group 2 HLA-E restricted TcRs specifically recognise HLA-E presenting the peptide VMAPRTLIL.

The publication of the crystal structure of the Group 2 HLA-E restricted TcR KK50.4 (containing gene segments TRAV26-1, or V α 26, and TRBV14, or V β 16), in complex with HLA-E presenting the CMV UL40-derived peptide VMAPRTLIL (*Hoare et al., 2006*) provided the first detailed look at the basis of this interaction, and indeed was the first crystal structure of a TcR in complex with a Class Ib MHC. Though this was a significant advance in the elucidation of the role of Class Ib MHC in the adaptive immune response, much remained unclear. As no structure of a Group 1 HLA-E restricted TcR in complex with HLA-E was available, comparison with MHC-Ia restricted TcR interactions were hindered, and comparisons between the Group 1 and 2 HLA-E restricted TcRs were limited to those gained using biophysical techniques such as fluorometry-assisted cell sorting (FACS), surface plasmon resonance (SPR) and mutation studies (*Pietra et al., 2003, unpublished data*).

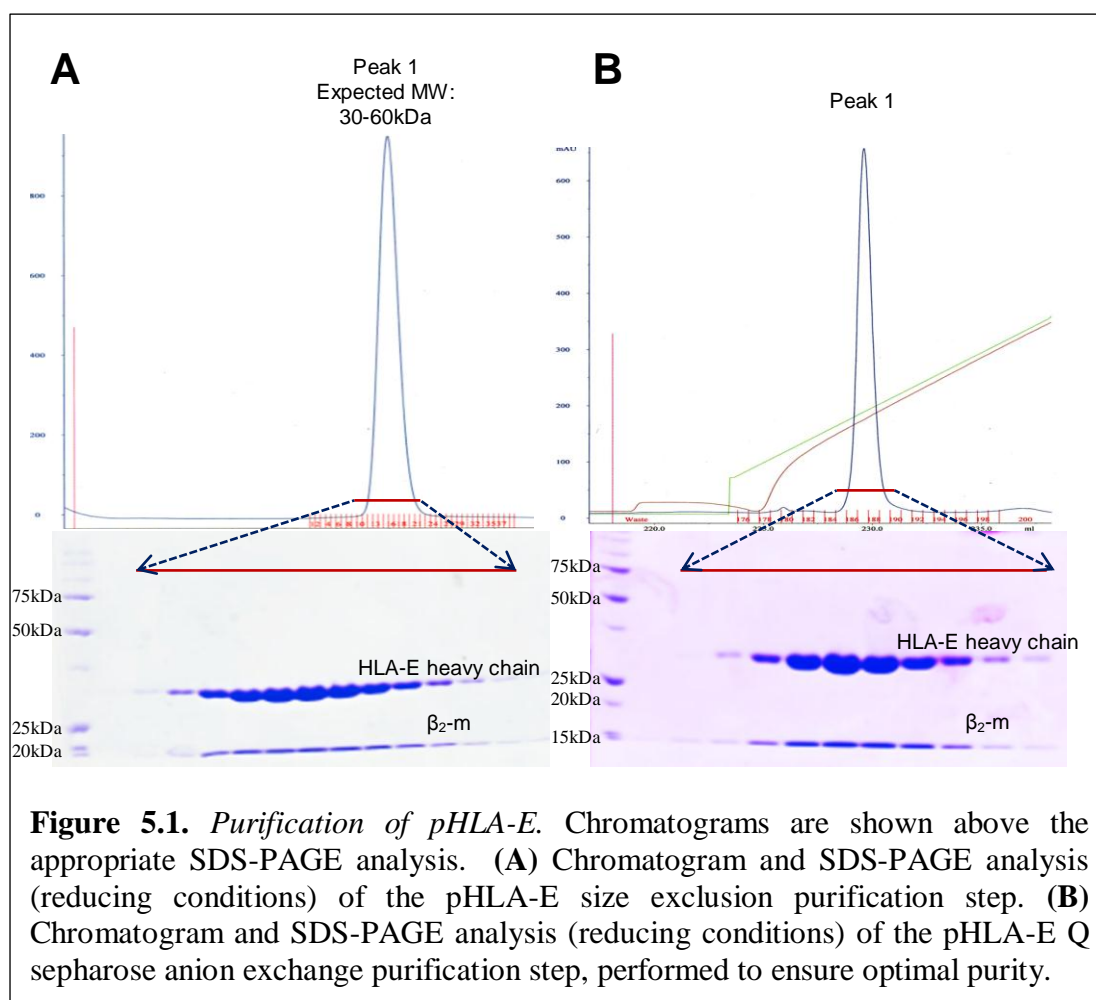
Research to determine the crystal structure of GF4, a Group 1 HLA-E restricted TcR, in complex with pHLA-E was aimed at providing a point of comparison for the KK50.4:HLA-E^{VMAPRTLIL} structure, while adding to the range of MHC-Ib:TcR structures. This chapter describes the crystallisation and structure determination of

the two ternary complexes formed through GF4 TcR recognition of HLA-E^{VMAPRTLVL} and HLA-E^{VMAPRTLIL}.

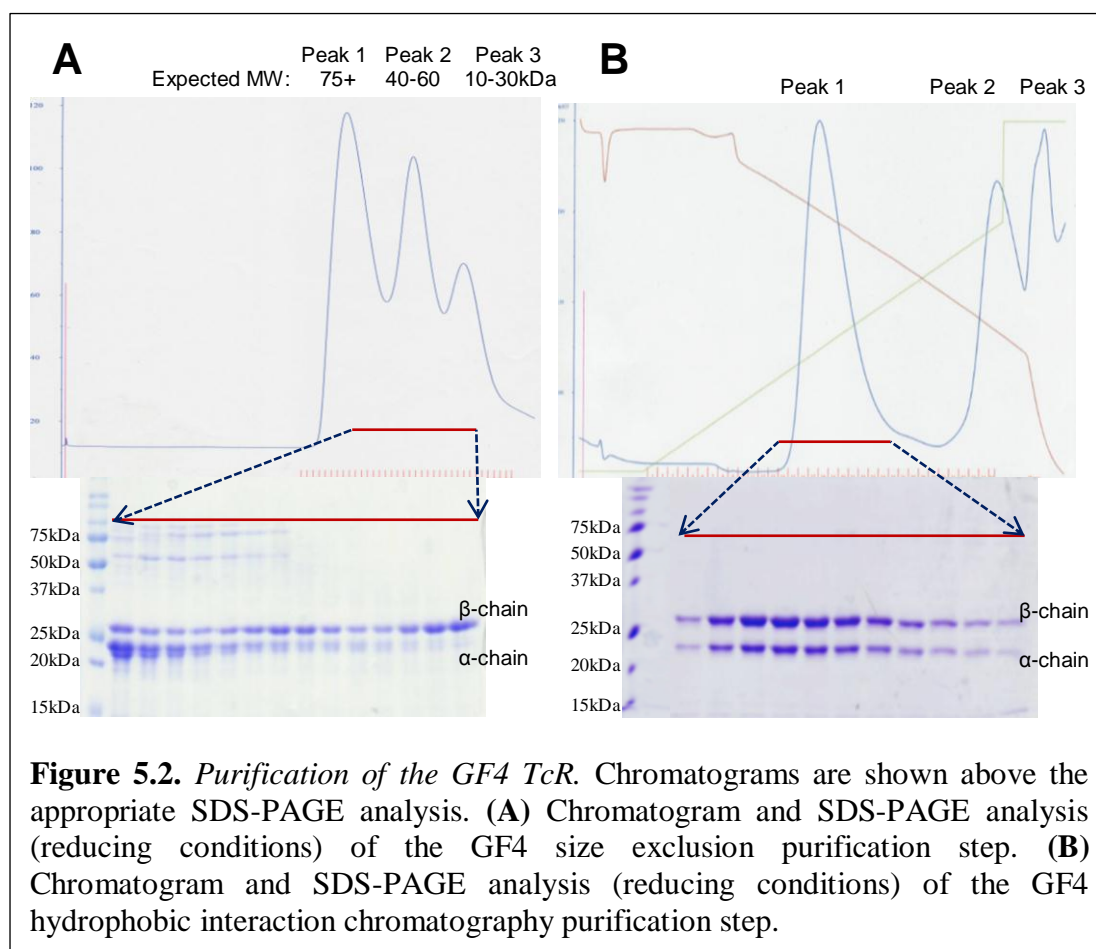
HLA-E and GF4 TcR Production and Copurification of the Ternary Complexes

The extracellular region of HLA-E*0101 (residues 22-297) and β_2 -m (residues 20-119) were expressed separately in *E.coli*, purified from inclusion bodies, and refolded together with synthetic peptide prior to purification, following the method of Garboczi *et al* (1992) described in Chapter 2, under the heading *Production of MHC HC, β_2 -m, TcR α - and β -chains*. Each of the two pHLA-E molecules was treated identically during purification, which involved DEAE anion-exchange and size exclusion chromatography steps. A Q sepharose anion-exchange step was also performed if necessary to obtain optimal purity of the protein for crystallographic purposes. A typical size-exclusion trace and Q sepharose anion exchange trace are shown in figure 5.1. As shown, minimal contaminants were present after the DEAE anion-exchange step. However, significant aggregation was often observed after prolonged storage at 4°C. Following purification, 5-15mg of pHLA-E protein was obtained per 1L refold, depending on a number of factors such as the purity of the HLA-E and β_2 -m inclusion body preparations and the time between purification steps. The molecular weight of the purified protein was approximately 45kDa as determined by SDS-PAGE, which was separated in both reducing and non-reducing conditions to the 33kDa HLA-E heavy chain and the 12kDa β_2 -m chain.

The extracellular domains of the GF4 α - and β -chains were expressed separately in *E.coli*, purified from inclusion bodies, and refolded together prior to purification, as described in Chapter 2, under the heading *Production of MHC HC, β_2 -m, TcR α - and β -chains*. Both the α - and β -chains contained a mutation to cysteine at the interface between the chains to aid heterodimerisation, correct refolding and TcR stability (Boulter *et al.*, 1993). Initial problems involving incorrect β - β homodimer formation were partially resolved by refolding the TcR in 5M urea, with a 10:3 ratio of α -chain to β -chain. The purification protocol as described by Garboczi *et al* (1992), involving DEAE anion-exchange and size exclusion purification steps, was also optimised for GF4 with a hydrophobic interaction chromatography (HIC) step performed after size exclusion to separate β - β homodimer from the correctly folded α - β heterodimer.



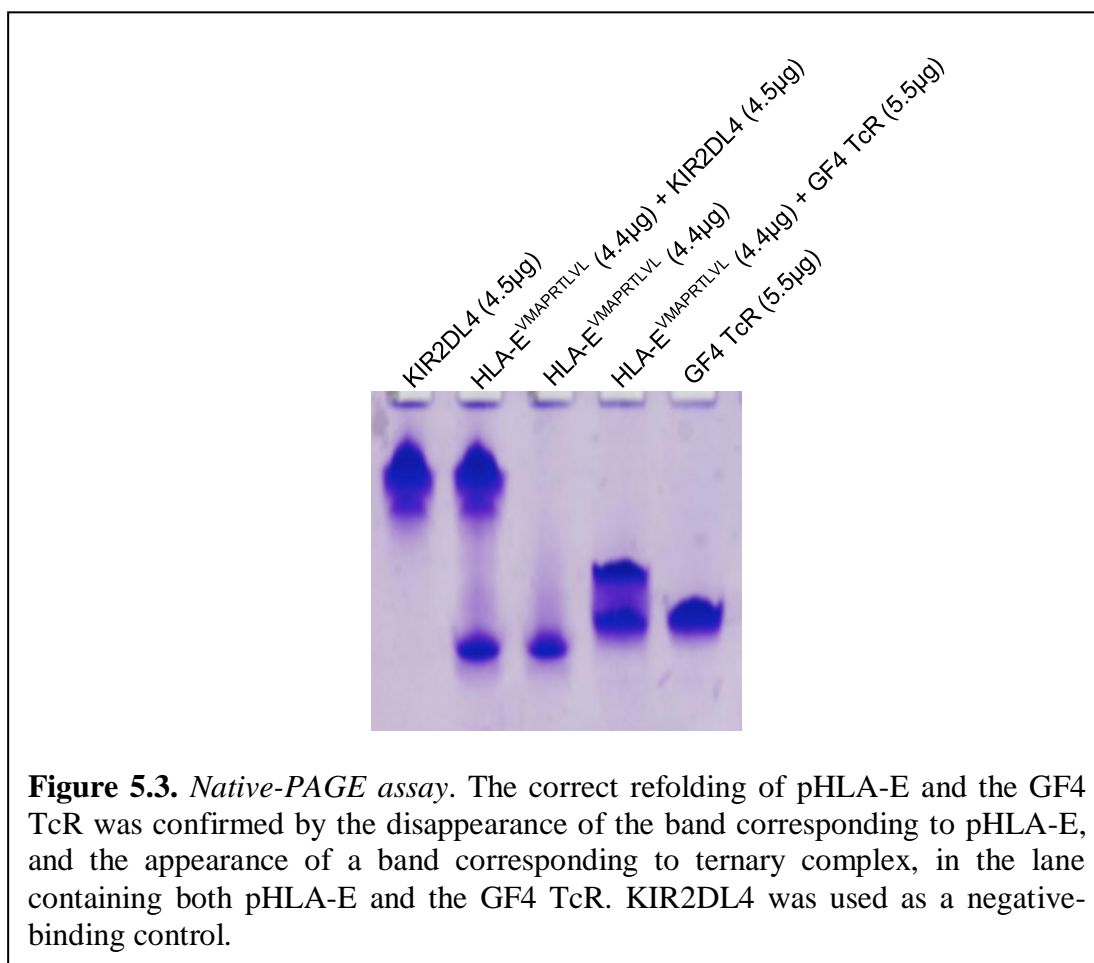
Typical traces from the GF4 size exclusion and HIC purification steps are shown in figure 5.2. It can be seen that size exclusion separated the post-DEAE sample into 3 peaks, which were identified by SDS-PAGE in reducing conditions. The first peak on the size exclusion trace corresponded to aggregate primarily formed of α - α interactions, while the second peak corresponded to a combination of β - β homodimer and the desired α - β heterodimer, as determined by the elution volume and the relative intensity of the bands seen on a reducing SDS-PAGE gel. The third peak corresponded to monomeric chains, primarily β -chain. The second peak was pooled and buffer exchanged for further purification by HIC. As shown in figure 5.2B, the HIC purification step clearly separated correctly folded α - β heterodimer (peak 1) from other contaminants, as determined by the relative intensity of the two bands observed on a reducing SDS-PAGE gel. Typical yields of sufficiently pure GF4 TcR following adoption of the HIC step increased from 0.1-0.25mg per 1L refold, to 0.5-1.0mg per 1L refold. The molecular weight of the purified protein was observed by



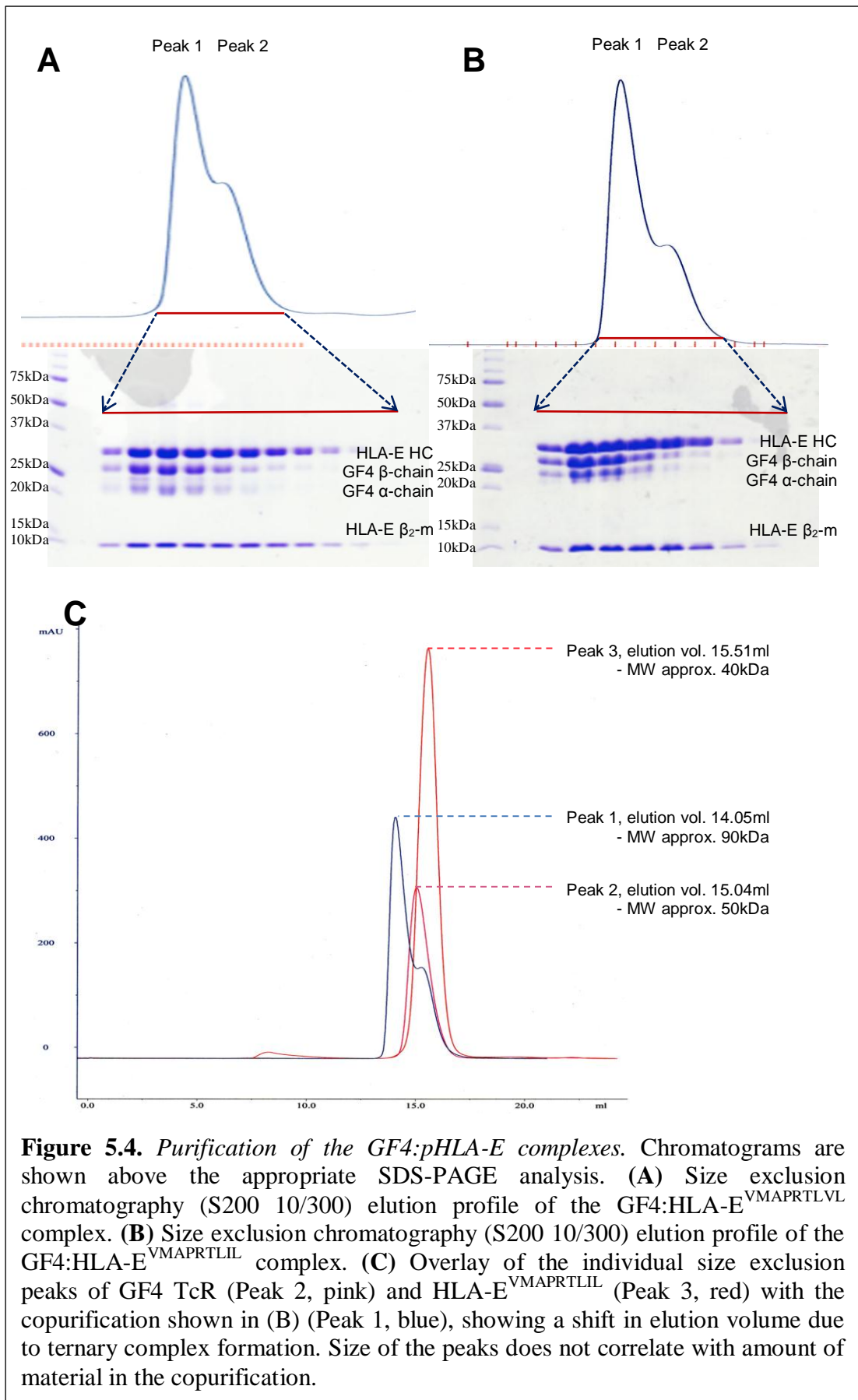
non-reducing SDS-PAGE to be approximately 50kDa, which was separated in reducing conditions to the 27kDa β -chain and the 23kDa α -chain.

Correct folding of the pHLA-E and GF4 constructs was ascertained by a native PAGE assay (Figure 5.3). GF4, pHLA-E and baculovirus-expressed KIR2DL4 (used as a negative control to detect aberrant binding) were analysed in individual lanes, while two mixtures, one containing pHLA-E and GF4, the other containing pHLA-E and KIR2DL4, were also analysed on the same gel, which contained 15% polyacrylamide and no SDS. The amount of each protein in the different lanes was kept constant, with the receptors KIR2DL4 and GF4 kept in molar excess of pHLA-E. As shown in figure 5.3, the band corresponding to pHLA-E shifted in the presence of GF4, indicating the formation of the pHLA-E:GF4 complex. Similar results were achieved for both pHLA-E complexes.

Following concentration of the purified GF4 TcR and pHLA-E to 3-5mg/ml and determination of correct folding, complexation was performed. The affinities of the



GF4 TcR for HLA-E^{VMA^{PRTLVL}} and HLA-E^{VMA^{PRTLIL}} are 35µM and 4.3µM respectively, as determined by surface plasmon resonance studies (work performed by Dr Lucy Sullivan and Dr Andrew Brooks, Dept of Immunology and Microbiology, University of Melbourne, Parkville, Australia). The strength of these affinities enabled purification of both TcR-pMHC complexes by size exclusion chromatography. Copurification, performed with a 1.2:1 molar ratio of MHC to TcR as described in *Chapter 2 – Generation of correctly folded protein*, resulted in separation of the mixture into two species readily distinguished on the chromatogram (Figure 5.4). The elution volume of the first peak (14.0-14.1ml) was consistent with the molecular weight of the GF4:pHLA-E complex, while the elution volume of the second peak (15.1-15.3ml) corresponded to the molecular weight of the unbound pHLA-E. The identity of species eluting at each of these peaks were confirmed by SDS-PAGE. Fractions containing the purified complex were concentrated to 5-10mg/ml for crystallisation trials.



This chapter has to this point described the production and purification of the two complexes GF4:HLA-E^{VMAPRTLVL} and GF4:HLA-E^{VMAPRTLIL}, for which the methods and results were very similar. The remainder of the results sections in this chapter describe work performed on each of the two complexes individually, though some figures have been combined for ease of comparison.

Crystallisation of GF4:HLA-E^{VMAPRTLVL} and Data Collection

Initial crystallisation trials for the GF4:HLA-E^{VMAPRTLVL} complex were conducted using the CrystallisationTM system, using crystallisation screens from Sigma-Aldrich (Basic Crystallisation Kit), Hampton Research (PEG-Ion Screen) and Qiagen (PACT suite and the Joint Centre for Structural Genomics Plus (JCSG+) Suite), and incubated at either 20°C or 4°C. The components of these screens are fully listed in Appendix 1. In these 96-well trays, crystals appeared in several conditions, as shown in Table 5.1. Fine screening was conducted around conditions that yielded crystals, with screens designed to optimise buffer pH and concentration, salt concentration, precipitate type and concentration, drop size and ratio, protein concentration, and to allow for crystallisation techniques such as streak seeding and macro-seeding. Fine screens were performed in 24-well trays as described in Chapter 2, under the heading *Crystallisation*. An example fine screening tray, designed to test pH and PEG concentrations around initial conditions containing 0.2M K-,Na- tartrate, 20% PEG 3350 and 0.1M Bis-Tris Propane pH 8.0, is shown in Figure 5.5.

Diffraction-quality GF4:HLA-E^{VMAPRTLVL} crystals (Figure 5.6A) were reproducibly grown using the hanging drop vapour-diffusion method at 20°C with a protein/reservoir drop ratio of 1:1. Crystals appeared with a needle-like or rod-like morphology and grew up to 1.1mm, however were very fragile, with a tendency to fracture upon handling. Total drop size was 2µl. The reservoir buffer contained 18-20% PEG3350, 0.1M Bis-Tris Propane pH 8.5-8.6 and 0.2M K-,Na- Tartrate. Crystal growth was highly sensitive to pH and PEG concentration, however was not as sensitive to Sodium Potassium Tartrate concentrations above 0.1M. Composition of crystals was tested by SDS-PAGE. Crystals were washed in fresh reservoir buffer, and then analysed using SDS-PAGE under reducing and non-reducing conditions (Figure 5.6C).

Table 5.1. Broad screening conditions yielding GF4:HLA-E^{VMAPRTLVL} crystals. Bold type indicates that the condition was followed up with fine screening trays. Drop ratios were 0.1µl protein:0.1µl reservoir in all cases.

Commercial Screen	Protein Concentration	Reservoir buffer	Temp	Time elapsed	Crystal morphology
JCSG+	5.0mg/ml	20% PEG 8000 0.1M CHES pH 9.5	20°C	3 days	Rods
JCSG+	5.0mg/ml	20% PEG 6000 0.1M BICINE pH 9.0	20°C	4 days	Rods
JCSG+	10.0mg/ml	20% PEG 6000 0.1M BICINE pH 9.0	20°C	10 days	Rods
PACT suite	10.0mg/ml	0.2M K- thiocyanate 20% PEG 3350 Bis-Tris Propane pH8.5	20°C	48hrs	Needles
PACT suite	10.0mg/ml	0.2M K- thiocyanate 20% PEG 3350 Bis-Tris Propane pH8.5	4°C	48hrs	Needles
PACT suite	10.0mg/ml	0.2M K-,Na- tartrate 20% PEG3350 Bis-Tris Propane pH8.5	20°C	48hrs	Rods
PACT suite	10.0mg/ml	0.2M NaCl 20% PEG6000 Tris pH 8.0	20°C	24hrs	Needle clusters

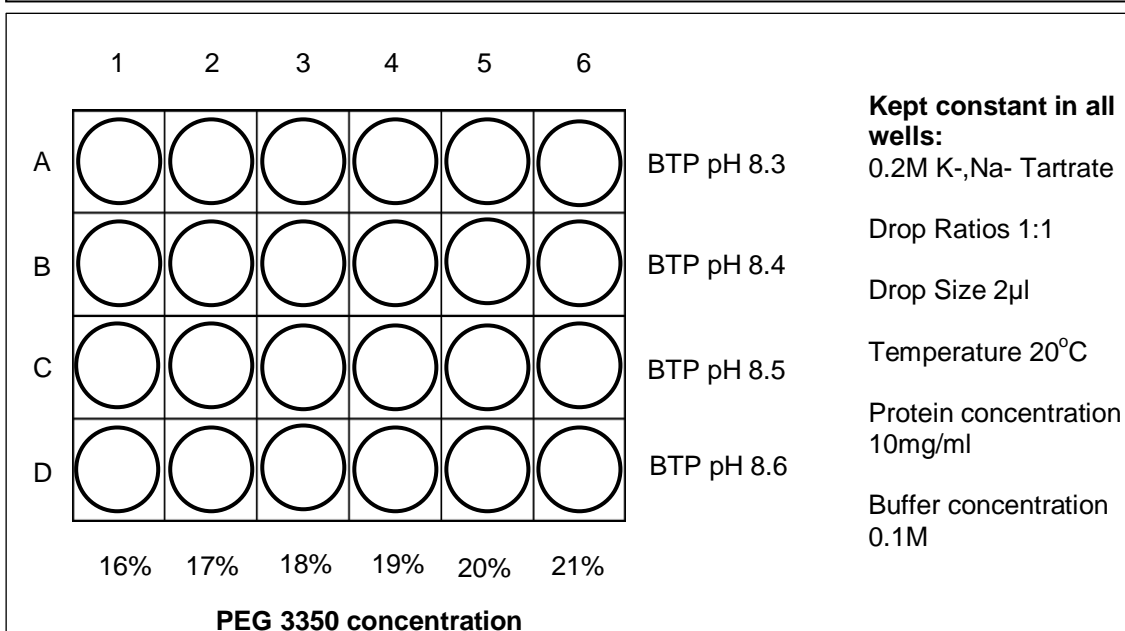


Figure 5.5. Fine screening to optimise pH and PEG concentration. This example fine-screening tray shows how two parameters may be optimised using a 24-well format. The original crystallisation conditions were: 0.2M K-, Na- Tartrate, 0.1M Bis-Tris Propane pH 8.5, 20% PEG 3350. Constants on the right show alternative parameters which may also be varied.

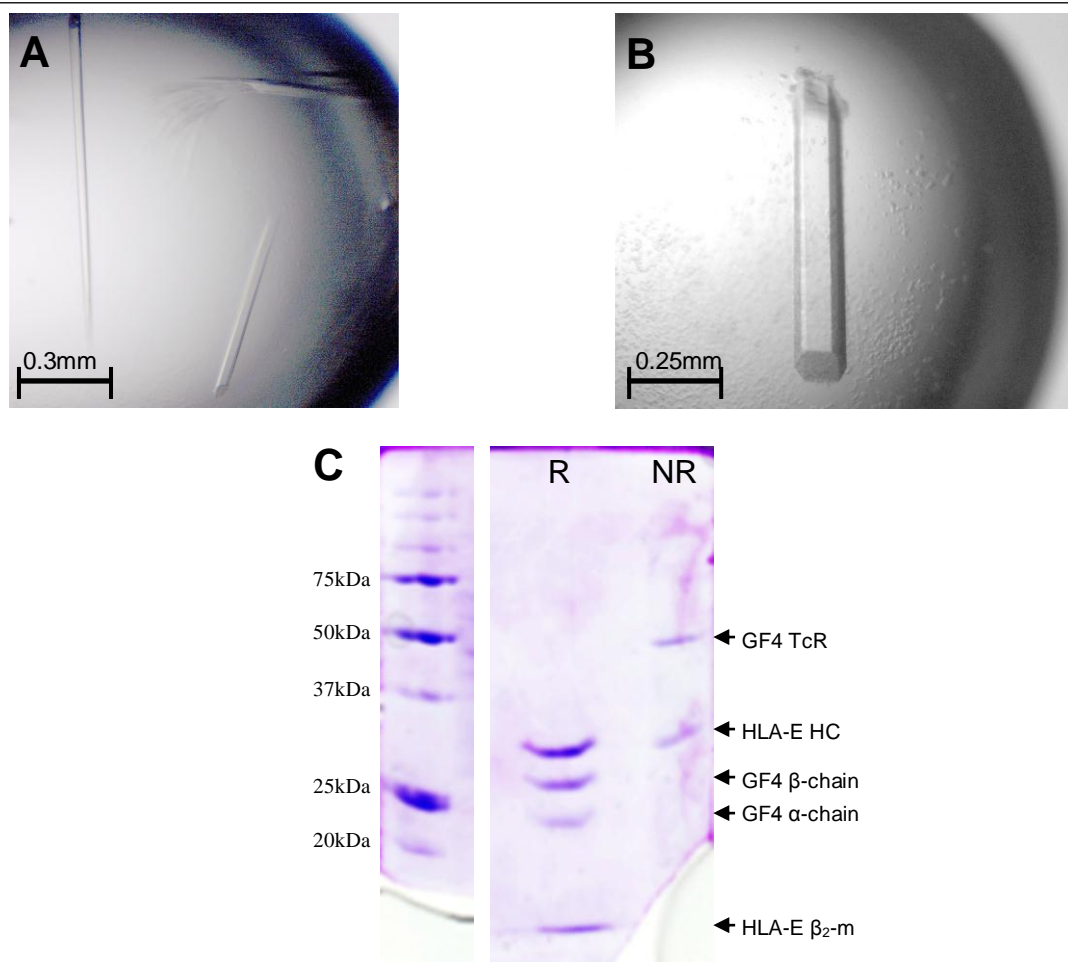


Figure 5.6. *GF4:pHLA-E crystal morphology.* Diffraction-quality crystals of (A) the GF4:HLA-E^{VMAPRTLVL} complex and (B) the GF4:HLA-E^{VMAPRTLIL} complex. (C) SDS-PAGE analysis of GF4:HLA-E^{VMAPRTLVL} crystals under reducing (R) and non-reducing (NR) conditions. All components of the ternary complex are identifiable, including the TcR chains which are separated under reducing conditions.

All datasets were collected on the MX2 beamline at the Australian Synchrotron, with data processing carried out using MOSFLM (Leslie, 1992) and the SCALA program from the CCP4 suite (Collaborative Computational Project, 1994). Matthews coefficients were calculated using the MATTHEWS cell content analysis program from the CCP4 suite (Collaborative Computational Project, 1994). $\Delta\Phi$ (the difference in angle between two consecutive images) was set at 0.5° for all datasets, and the distance (d) between the crystal and the detector was set at 350mm. Some of the initial GF4:HLA-E^{VMAPRTLVL} datasets collected were indexed to the monoclinic space group C121 (typical unit cell dimensions: $a = 259.1\text{\AA}$, $b = 67.1\text{\AA}$, $c = 129.6\text{\AA}$, $\alpha = \gamma = 90^\circ$, $\beta = 104.3^\circ$). These had a Matthews coefficient indicating a high probability of two complexes per asymmetric unit, though three complexes per asymmetric unit was indicated as a possibility. After consideration of R_{merge} (an unweighted measure of the agreement or discrepancy between symmetry-related reflections), R_{pim} (similar to R_{merge} , but weighted according to multiplicity of the data), $I/\sigma I$ (a measure of the ratio of signal to background ‘noise’), completeness (a measure of the number of reflections that are expected according to the unit cell data, but are not observed in the dataset itself) and multiplicity (a measure of the redundancy of the data, where larger multiplicity indicates R_{pim} may be more reliable than R_{merge}) statistics, the resolution of the highest-quality of these datasets was set at 3.5\AA .

Other datasets from crystals in identical conditions, with apparently identical morphology, were indexed to the orthorhombic space group $P2_12_12_1$, related to C121. Distinction between $P2_12_12_1$ and P222 was made by observing systematic absences in the h, k and l axes. Datasets indexed to $P2_12_12_1$ had a Matthews coefficient indicating a high probability of five (solvent content 48.1%, probability = 0.54) or four (solvent content 58.5%, probability = 0.21) complexes per asymmetric unit. Upon consideration of the measurements indicated above, these datasets were generally found to be of better quality than those indexed to C121, and the resolution of the highest-quality dataset was set at 3.1\AA (see Table 5.2 for data collection and refinement statistics). At this resolution, $I/\sigma I$ of the highest-resolution shell was 2.3, significantly above 2.0 (a common threshold for usable data). While the R_{merge} value of the highest-resolution shell was very high at 0.88, the R_{pim} value was 0.39, a reasonable value for this measurement considering multiplicity for this shell was 5.5.

Table 5.2. *Data collection and refinement statistics.* Statistics are shown for the GF4 TcR:HLA-E^{VMAPRTLVL} and GF4 TcR:HLA-E^{VMAPRTLIL} complexes. Values in parentheses are for the highest-resolution shell.

	GF4:HLA-E ^{VMAPRTLVL}	GF4:HLA-E ^{VMAPRTLIL}
Data Collection		
Space group	P2 ₁ 2 ₁ 2 ₁	P2 ₁ 2 ₁ 2 ₁
Cell dimensions		
a,b,c (Å)	73.33, 225.75, 276.16	71.92, 225.88, 275.47
α, β, γ (°)	90, 90, 90	90, 90, 90
Resolution	50.9 - 3.1 Å (3.27-3.1 Å)	55.9 - 3.3 Å (3.48-3.3 Å)
R _{merge}	16.6% (88.0%)	16.5% (68.3%)
R _{pim}	7.5% (39.0%)	5.3% (22.9%)
I/ σ I	10.7 (2.3)	13.3 (2.9)
Completeness	99.9% (100.0%)	99.9% (99.5%)
Multiplicity	5.5 (5.5)	10.4 (9.6)
Refinement		
No. reflections	84487	68876
R _{cryst}	22.77%	24.05%
R _{free}	28.41%	31.63%
No. atoms		
Protein	26531	26507
Ligand/ion	10 (Tartrate)	0
Water	15	61
B-factors		
Protein	46.3	61.9
Ligand/ion	92.5	N/A
Water	24.6	46.3
Ramachandran Plot		
Favoured region	84.69%	78.83%
Allowed region	10.37%	16.11%
R.m.s deviations		
Bond lengths	0.0071 Å	0.0084 Å
Bond angles	1.252°	1.4203°

Overall completeness of the data was 99.9%, and 100% for the highest resolution shell. For this dataset, 135° of data was collected.

Structure Solution and Refinement of GF4:HLA-E^{VMAPRTLVL}

Following data processing, structures were determined by molecular replacement using the PHASER program from the CCP4 suite (*Collaborative Computational Project, 1994*). Search models for GF4:HLA-E^{VMAPRTLVL} were the fully refined LC13 TcR, with CDR loops omitted, and the fully refined, unliganded HLA-

E^{VMAPRTL} structure, including the β_2 -m light chain but with the peptide omitted. These search models were chosen based on the quality of the geometry and the resolution of the structures as well as their similarity to the crystallised proteins. TcR CDR loops and the MHC peptide ligand were omitted to reduce model bias in these regions, while all LC13 sidechains which differed from the corresponding GF4 sidechain were mutated to alanine before molecular replacement.

Electron density maps obtained from datasets indexed to P2₁2₁2₁ showed four complexes in the asymmetric unit, marked as a significant possibility according to the calculated Matthews coefficient, with a high solvent content (58.5%), possibly accounting for the fragility of the crystals. These were present as two ‘pairs’, in apparently identical pairwise arrangements. Model building of GF4:HLA-E^{VMAPRTL} was carried out using the program COOT (*Emsley and Cowtan, 2004*) followed by maximum-likelihood refinement with the REFMAC5 program from the CCP4 suite (*Collaborative Computational Project, 1994*).

A number of techniques were used to aid refinement of the GF4:HLA-E^{VMAPRTL} structure, with a view to improving the stereochemistry of the structure as well as the fit to the electron density map, and accordingly lower the R_{cryst} and R_{free} values in an unbiased approach aimed at keeping those two values to a ratio of approximately 1:1.2-1.4 for R_{cryst}:R_{free} (*Tickle et al., 1998, Tickle et al., 2000*).

Firstly, optimal Torsional, Libration and Screw tensor (TLS) domains for GF4:HLA-E^{VMAPRTL} were determined using the TLS Motion Determination server (*Painter and Merritt, 2006*) and read into REFMAC5. These were used to improve model quality through greater definition of protein domains and likely flexible regions. Secondly, simulated annealing was performed using the program PHENIX (*Adams et al., 2010*). Simulated annealing is a technique involving the use of algorithms to find both global and local best-fit scenarios, and was used to improve the structure with respect to the electron density, and lower the R_{cryst} and R_{free} values (*Brunger, 1988*). Third, medium non-crystallographic symmetry (NCS) restraints were used to improve electron density maps through molecular averaging (*Kleywegt, 1996*). This was not performed as four-fold symmetry involving all four complexes, but instead

as two sets of two-fold symmetry, with each complex from one pair constrained to the corresponding complex in the other pair. In all cases NCS constraints were implemented for individual protein chains, though no NCS constraints were implemented for the nonameric peptides bound by HLA-E.

These techniques were used in conjunction with successive rounds of maximum-likelihood refinement using REFMAC5, focussed on optimising the geometry of the proteins. Each of these rounds of refinement lowered the R_{cryst} and R_{free} values, though if the difference between the two values increased dramatically, the refinement was repeated with alternative parameters. Refinement was ceased when the models could not be improved in COOT and successive rounds of maximum-likelihood refinement did not lower the R_{free} value. The finalised structure was validated using MolProbity (Chen *et al.*, 2010). Refinement statistics are shown in table 5.2. Contacts lists for each complex were created using the CONTACT program from the CCP4 Suite (Collaborative Computational Project, 1994), and PyMOL (version 1.3) (Schrodinger LLC) was used to view and analyse the structures, and to prepare figures. Accessible and buried surface areas were calculated using the CCP4 program AREAIMOL using a 1.4Å probe radius. As the interaction faces of each molecule were very similar in every complex within each asymmetric unit, one representative complex was chosen for analysis.

Major Features of the GF4:HLA-E^{VMAPRTLVL} Structure

As shown in Figure 5.7A, the GF4 TcR binds pHLA-E at the antigen-binding cleft, with contacts between the CDR loops of the TCR and the bound peptide, and also between the TcR CDR loops and the MHC $\alpha 1$ and $\alpha 2$ helices which flank the peptide. These contacts are described below under the heading *Recognition of pHLA-E by the GF4 TcR*. The peptide sits deeply in the cleft, relative to MHC-Ia (Figure 5.8A & C), in a conformation very similar to previously determined pHLA-E structures. Primary anchor residues at P1, P2 and P9 maintain a peptide conformation which forces the residues at P5 and P8 to an ‘upright’ position (Figure 5.8A), protruding from the antigen-binding cleft and enabling receptor recognition of these residues. The exposed surface area of the peptide (in the absence of TcR chains) is 305.2Å², representing 21.7% of the total surface area of the peptide. A further 223Å² of the peptide surface area is buried upon TcR ligation.

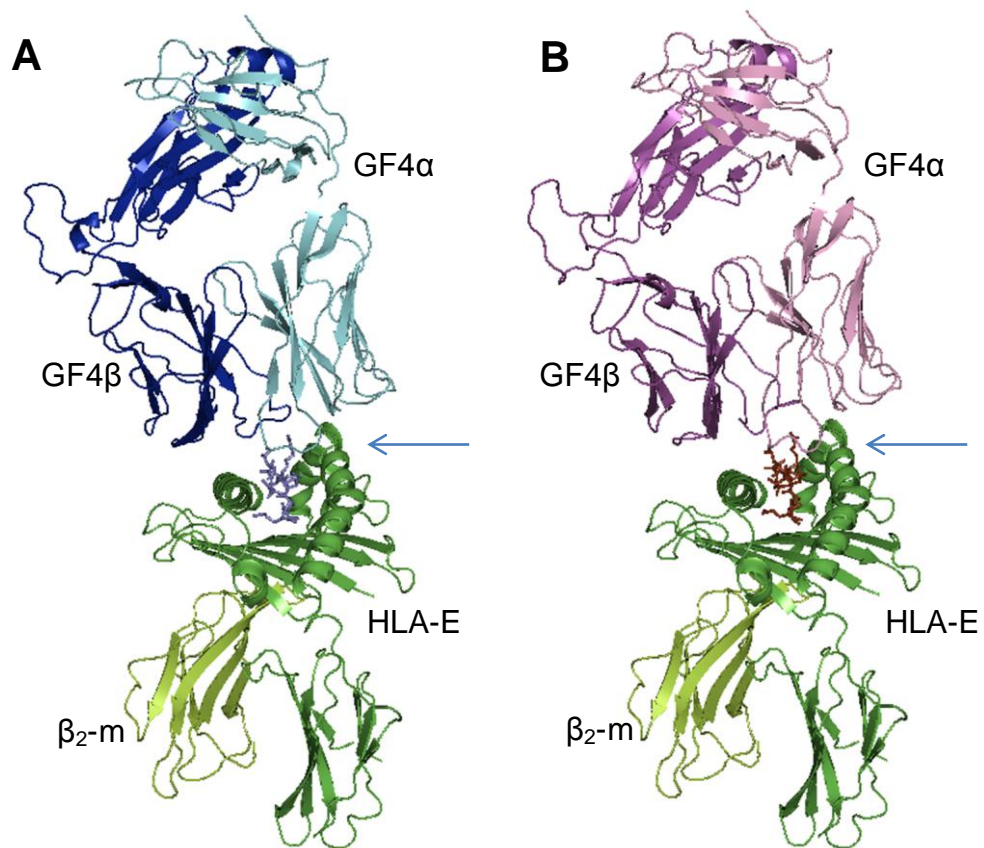


Figure 5.7. *Crystal structures of the GF4 TcR:pHLA-E complexes.* Overview of a single complex of (A) GF4:HLA-E^{VMAPRTLVL} and (B) GF4:HLA-E^{VMAPRTLIL}, showing the TcR docking at the antigen-binding cleft of pHLA-E. HLA-E is shown in green with β₂-m in lemon. Peptides are shown in stick representation, VMAPRTLVL in blue, and VMAPRTLIL in red. GF4 recognising HLA-E^{VMAPRTLVL} is shown with the α-chain in light blue and the β-chain in royal blue. GF4 recognising HLA-E^{VMAPRTLIL} is shown with the α-chain in pink and the β-chain in purple.

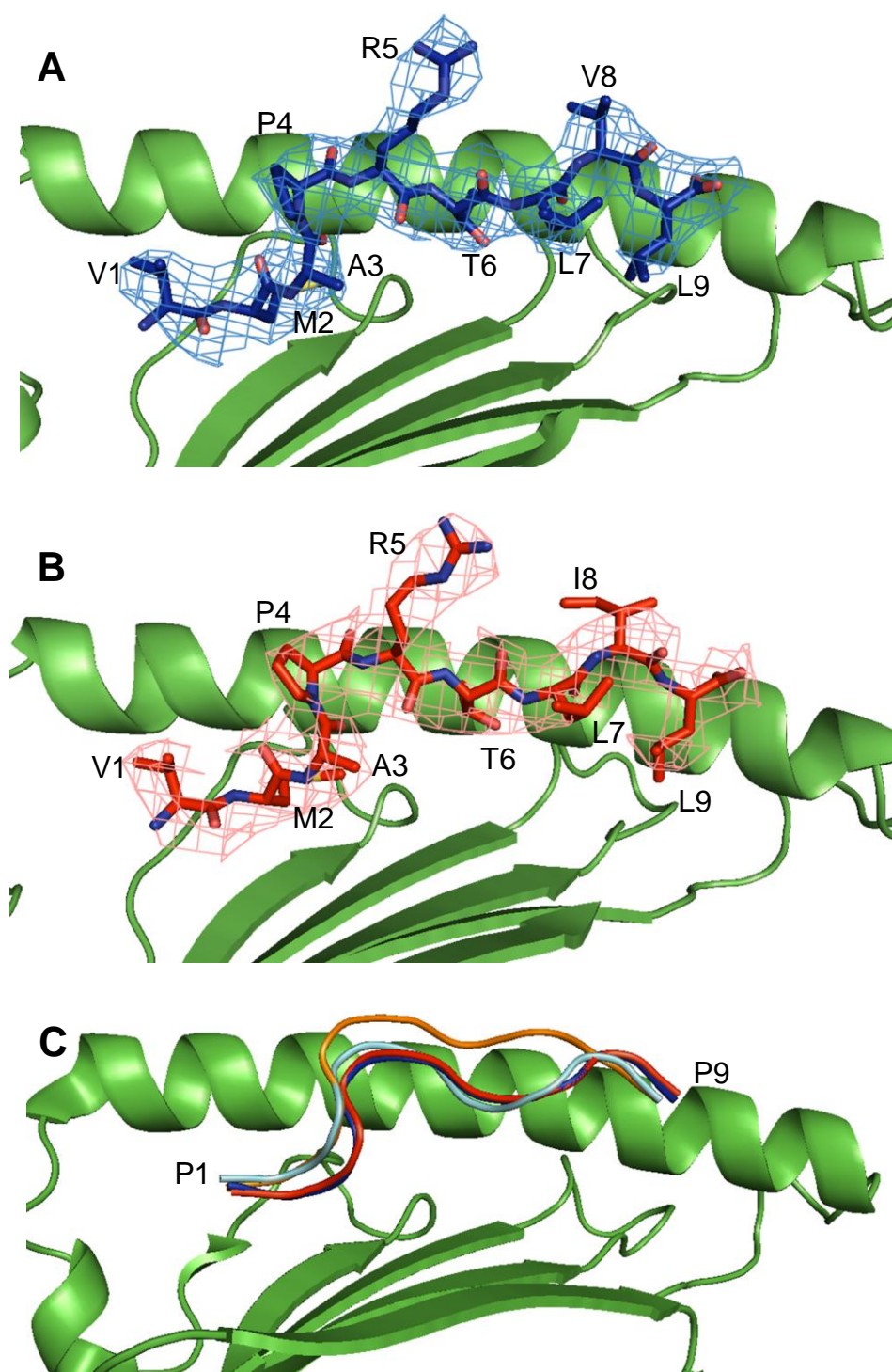


Figure 5.8. *Comparison of peptide conformation.* The peptides (A) VMAPRTLVL (blue) and (B) VMAPRTLIL (red) within the binding cleft of HLA-E, showing corresponding F_o-F_c electron density in mesh format. Electron density shown was produced by a round of maximum-likelihood refinement, omitting the peptide to eliminate model bias. (C) Comparison of peptide backbone conformation in HLA-E^{VMAPRTLVL} (blue), HLA-E^{VMAPRTLIL} (red), HLA-G^{RIIPRHLQL} (cyan) (PDB entry 1YDP) and HLA-A2^{GILGFVFTL} (orange) (PDB entry 1HHI). View is as portrayed by the arrows in Figure 5.5. The α 2 helix has been removed for clarity.

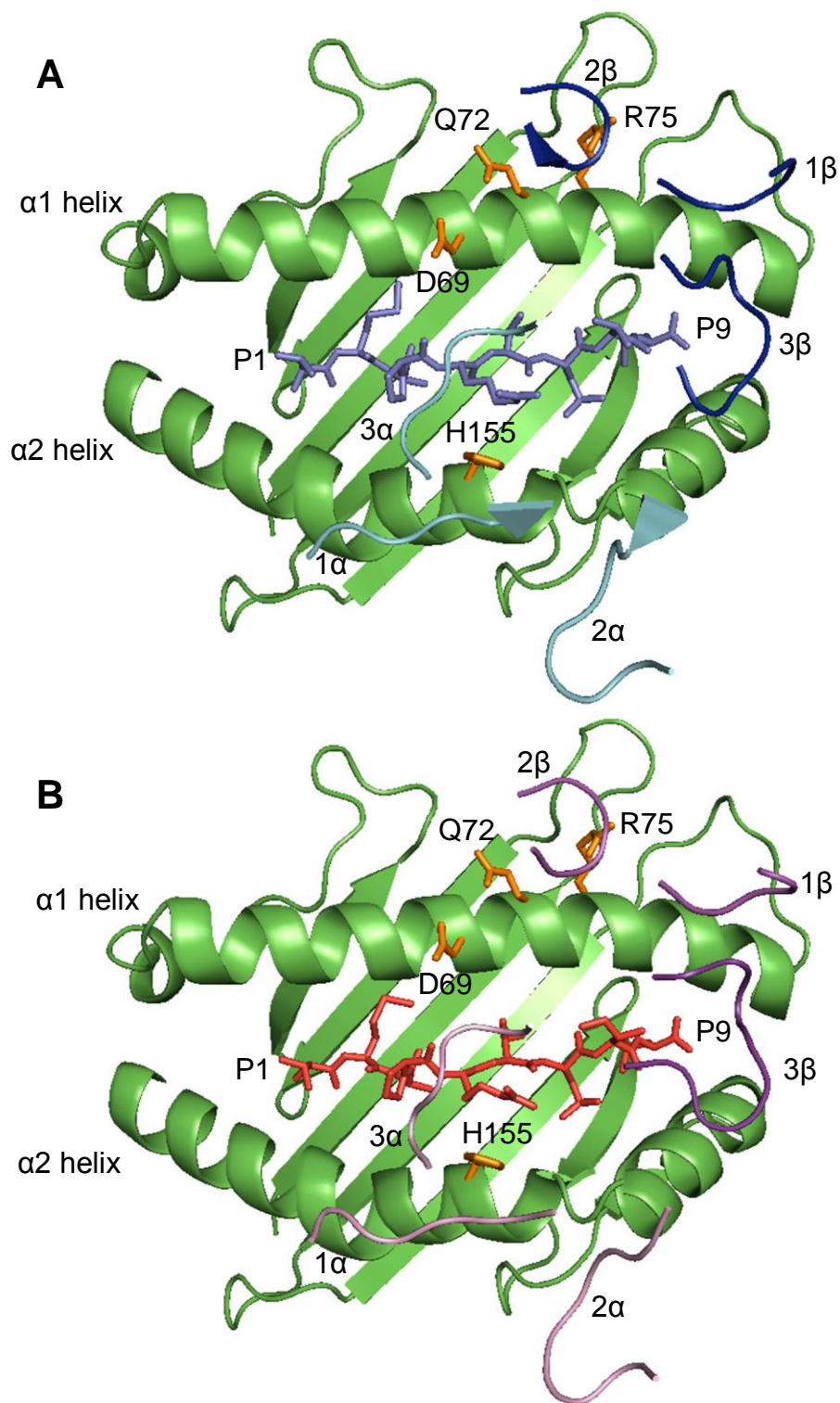


Figure 5.9. *HLA-E* antigen-binding cleft. Top view of the antigen-binding cleft of (A) HLA-E^{VMA^{PRTLVL}} and (B) HLA-E^{VMA^{PRTLIL}} showing GF4 CDR loop positions. HLA-E residues Asp69, Gln72, Arg75 and His155, which make multiple contacts with GF4 CDR loops, are shown in stick format and coloured orange.

Table 5.3. Contribution of CDR loops to GF4 TcR Buried Surface Area. Total buried surface area (BSA, in Å²) of the CDR loops is shown, in addition to the proportion of total TcR buried surface area that is due to each CDR loop (% Total).

CDR Loop	GF4:HLA-E ^{VMAPRTLVL}		GF4:HLA-E ^{VMAPRTLIL}	
	BSA	% Total	BSA	% Total
CDR1 α	54.2Å ²	5.3%	62.9Å ²	6.5%
CDR2 α	99.9Å ²	9.7%	75.5Å ²	7.9%
CDR3 α	331.4Å ²	32.3%	314.9Å ²	32.8%
CDR1 β	28.6Å ²	2.8%	21.8Å ²	2.3%
CDR2 β	208.4Å ²	20.3%	197.8Å ²	20.6%
CDR3 β	160.7Å ²	15.7%	158.9Å ²	16.5%

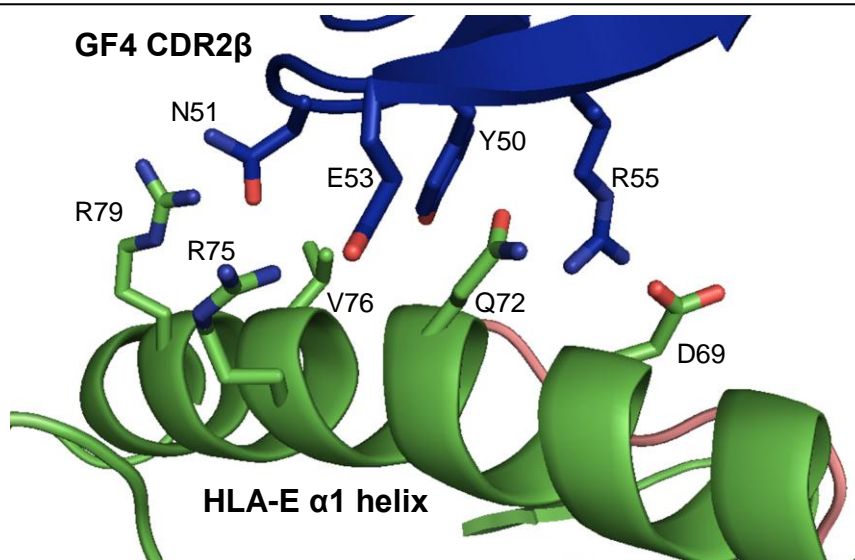


Figure 5.10. Complementarity of the GF4 CDR2 β loop with the HLA-E α 1 helix. HLA-E is shown in green, and the GF4 β -chain in blue. Sidechains involved in contacts are shown in stick representation. It can be seen that large polar residues on both the MHC and the TcR contribute to the high buried surface area of the GF4 CDR2 β loop. The HLA-E α 2 helix and other GF4 CDR loops have been removed for clarity.

GF4 recognition of the peptide is primarily mediated by residues within the CDR3 α loop (in particular Gln91, Ser96 and Asn97), which make multiple contacts with the conserved arginine at P5, and residues within the CDR3 β loop (in particular Glu103), which make contacts with isoleucine or valine at P8. Sidechains of residues in CDR1 α and 2 α are positioned on top of the MHC α 2 helix, while those of CDR1 β and 2 β are positioned on top of the MHC α 1 helix (Figure 5.9A). The CDR1 and CDR2 loops of both TcR chains enhance the affinity of the TcR for the pMHC while maintaining specificity of pHLA-E recognition.

The total surface area on the GF4 TcR that is buried due to the interaction with HLA-E^{VMAPRTLVL} is 1025.1Å², considerably lower than the range previously noted for TcR:MHC-Ia complexes (1360-2220Å²) (*Kjer-Nielsen et al., 2003*), as well as that for the KK50.4 TcR:HLA-E^{VMAPRTLIL} complex (2100Å²) (*Hoare et al., 2006*). The contribution of the Vα (50.67%) and Vβ (49.33%) domains to the total TcR buried surface area is very similar.

The proportion of buried surface area due to each CDR loop is shown in Table 5.3. As shown, CDR3α (32.3%), CDR2β (20.3%) and CDR3β (15.7%) make up a high proportion of the total TcR buried surface area, relative to the other CDR loops. The long CDR3α and CDR3β loops each make interactions with both MHC helices as well as the peptide, forming the basis of the large buried surface area of these CDR loops. The CDR2β loop is short relative to the CDR3 loops, makes no contacts with the peptide and is positioned solely over the MHC α1 helix. The high buried surface area of this loop is primarily due to the interactions of the large residues Tyr50, Asn51, Glu53 and Arg55 with the HLA-E residues Asp69, Gln72, R75 and R79. The GF4 CDR2β loop forms a peptide-independent MHC ‘sensor’, increasing the affinity and specificity of the GF4 TcR:pHLA-E interaction (Figure 5.10).

Recognition of pHLA-E by the GF4 TcR

Determination of the GF4:HLA-E^{VMAPRTLVL} structure enabled the first detailed insight into the mechanism of HLA-E restriction in a group 1 HLA-E-restricted TcR. A consensus contact list for the GF4:HLA-E^{VMAPRTLVL} complexes is shown in Table 5.4. The limitations of resolution led to slight differences between the 4 complexes in each asymmetric unit, a trend previously noted in a range of published crystal structures (*Kleywegt, 1996*). To reduce the introduction of artefactual contacts due to these differences, the contacts list shows van der Waals contacts and salt bridges if they were observed in three complexes, and H-bonds if they were observed in two complexes. This threshold allows unbiased discrimination between potentially artefactual contacts only present in one complex and contacts found in all complexes. The stringency of individual H-bond identification reduced the necessity of this strategy for this type of interaction.

Table 5.4. *GF4 TcR:HLA-E^{VMAPRTLVL} TcR-MHC and TcR-peptide contacts.* Atoms involved in hydrogen bonding and salt bridges are noted in superscript.

TcR α -chain-HLA-E contacts			TcR β -chain-HLA-E contacts		
GF4 α	HLA-E ^{LVL}	Type	GF4 β	HLA-E ^{LVL}	Type
N29	S151, E154, H155	VDW	L30	V76	VDW
N29 ^{Oδ1}	S151 ^O	H-bond	Y50	Q72, I73, V76	VDW
N29 ^{Oδ1}	H155 ^{Nϵ2}	H-bond	N51	R75, V76, R79	VDW
Y49	D149, S151	VDW	N51 ^O	R75 ^{NH1}	H-bond
K50	N148, S151	VDW	N51 ^{Oδ1}	R79 ^{NH1}	Salt Bridge
K50 ^{Nζ}	N148 ^O	H-bond	N51 ^{Oδ1}	R75 ^{NH1}	Salt Bridge
K50 ^{Nζ}	S151 ^{Oγ}	H-bond	E53	Q72, R75	VDW
R68	E154	VDW	E53 ^{Oϵ1}	R75 ^{NH2}	H-bond
R68 ^{NH2}	E154 ^{Oϵ2}	H-bond	E53 ^{Oϵ2}	R75 ^{NH1}	Salt Bridge
R68 ^{NH1}	E154 ^{Oϵ2}	Salt Bridge	E54	R68, Q72	VDW
R68 ^{NH2}	E154 ^{Oϵ1}	Salt Bridge	E54 ^O	Q72 ^{Nϵ2}	H-bond
Q91	H155	VDW	R55	R68, D69, Q72, I73	VDW
Q91 ^{Oϵ1}	H155 ^{Nϵ2}	H-bond	R55 ^O	R68 ^{NH2}	H-bond
P92	H155	VDW	R55 ^{NH1}	Q72 ^{Oϵ1}	H-bond
L93	E154, H155, A158	VDW	R55 ^{NH1}	D69 ^O	H-bond
G94	H155	VDW	R55 ^{NH1}	D69 ^{Oδ1}	Salt Bridge
G94 ^N	H155 ^{Nδ1}	H-bond	R55 ^{NH1}	Q72 ^{Oϵ1}	Salt Bridge
G95	H155	VDW	R55 ^{NH2}	D69 ^{Oδ2}	Salt Bridge
S96	D69	VDW	P97	T80	VDW
S96 ^{Oγ}	D69 ^{Oδ2}	H-bond	G98	K146	VDW
			S100	K146	VDW
TcR α -chain-peptide contacts			TcR β -chain-peptide contacts		
GF4 α	VMAPRTLVL	Type	GF4 β	VMAPRTLVL	Type
Q91	R5	VDW	E103	R5	VDW
Q91 ^{Oϵ1}	R5 ^{NH1}	Salt Bridge	E103 ^{Oϵ2}	R5 ^{NH2}	H-bond
G94	P4	VDW	E103 ^{Oϵ1}	R5 ^{NH1}	Salt Bridge
G95	R5	VDW			
S96	P4, R5	VDW			
S96 ^O	R5 ^{NH1}	H-bond			
N97	R5, T6	VDW			
N97 ^{Nδ2}	T6 ^N	H-bond			
N97 ^{Nδ2}	T6 ^O	H-bond			
N97 ^{Oδ1}	T6 ^O	H-bond			
N97 ^{Oδ1}	R5 ^{NH2}	Salt Bridge			
Y98	V8	VDW			

Multiple contacts between residues in the GF4 CDR1 α (Asn29) and 3 α (Gln91, Pro92, Leu93, Gly94 and Gly95) loops and HLA-E His155, and the GF4 CDR2 β loop (Tyr50, Asn51, Glu53, Glu54 and Arg55) with HLA-E residues Asp69, Gln72 and Arg75, are the most prominent features of the full list of GF4:HLA-E^{VMAPRTLVL} contacts (Table 5.4). Unsurprisingly, given the CDR loop positions shown in Figure 5.9, GF4 CDR α loops predominantly formed contacts with the HLA-E α 2 helix, while GF4 CDR β loops predominantly formed contacts with the HLA-E α 1 helix. All HLA-E residues which formed contacts with the GF4 TcR resided on either the α 1 or α 2 helices, though the proximity of HLA-E Glu19 to GF4 β Glu53, on the CDR2 β loop, suggests that these residues may also make contacts not seen on the consensus contacts list. HLA-E Glu19 sits within a loop connecting anti-parallel strands of the β -sheet which forms the base of the peptide-binding cleft.

As mentioned above, peptide recognition by GF4 is mediated primarily by contacts between the GF4 CDR3 α loop and Arg5 of the peptide. Contacts were also observed between residues Gly94 and Ser 96 on the GF4 CDR3 α loop and Pro4 of the peptide, as well as Asn97 on the GF4 CDR3 α loop and Thr6 of the peptide. The peptide residue Val8, which forms the distinction between host and mimotope presentation by HLA-E is contacted by Tyr98 on the GF4 CDR3 α loop. Despite the position of the GF4 CDR3 β loop over the C-terminal end of the peptide, only one residue (Glu103) from this loop contacted the peptide (residue Arg5) in enough complexes to justify an entry in table 5.4.

Crystallisation of GF4:HLA-E^{VMAPRTLIL} and Data Collection

Initial crystal trials for the GF4:HLA-E^{VMAPRTLIL} complex were conducted as 24-well fine screens around the conditions in which GF4:HLA-E^{VMAPRTLVL} crystals were grown. Modification of the reservoir buffer was necessary for growth of diffraction-quality GF4:HLA-E^{VMAPRTLIL} crystals (Figure 5.6B). Final reservoir buffer composition was 16-18% PEG3350, 0.1M Bis-Tris Propane pH 8.2 and 0.2M Sodium Potassium Tartrate. Crystals appeared as thick needles or rods with hexagonal cross-section, and grew to 1mm in length, however were quite fragile and had a tendency to fracture with handling. As with the GF4:HLA-E^{VMAPRTLVL} crystals, crystal composition was analysed using SDS-PAGE.

As with those datasets collected on GF4:HLA-E^{VMAPRTLVL} crystals, all GF4:HLA-E^{VMAPRTLIL} datasets were collected on the MX2 beamline at the Australian Synchrotron. Processing of GF4:HLA-E^{VMAPRTLIL} datasets was carried out using MOSFLM (Leslie, 1992) and the SCALA program from the CCP4 suite (Collaborative Computational Project, 1994). Matthews coefficients were calculated using the MATTHEWS cell content analysis program from the CCP4 suite (Collaborative Computational Project, 1994). $\Delta\Phi$ was set to 0.5° , while the distance (d) between the crystal and the detector was set at 350mm. While some of the GF4:HLA-E^{VMAPRTLIL} crystals were quite long and thick, the diffraction quality did not increase significantly with size. Diffraction of GF4:HLA-E^{VMAPRTLIL} crystals was found to deteriorate markedly upon data collection, with resolution declining after several 2-second exposures at 50% attenuation. To overcome this issue, up to four or five datasets were collected on the larger crystals. These datasets were then merged during data processing. As with GF4:HLA-E^{VMAPRTLVL}, some datasets collected were indexed to the space group C121, and after consideration of R_{merge} , R_{pim} , $I/\sigma I$, completeness and multiplicity the resolution of the highest-quality of these datasets was set at 3.6\AA . Unit cell dimensions were similar to the corresponding GF4:HLA-E^{VMAPRTLVL} datasets, with the Matthews coefficient predicting a high likelihood of two complexes in the asymmetric unit and the possibility of a third.

Consistent with GF4:HLA-E^{VMAPRTLVL}, higher-quality datasets were indexed to $P2_12_12_1$ after observation of systematic absences in the h, k and l axes. The resolution of the highest-quality dataset indexed to $P2_12_12_1$ was set at 3.3\AA after consideration of $I/\sigma I$ (2.9 in the highest-resolution shell) and R_{pim} (0.229 in the highest-resolution shell). See Table 5.2 for the full list of data collection statistics. This dataset was made up of three merged sets of data obtained from a single crystal, with a combined collection angle of 282° . Unit cell dimensions were similar to the corresponding GF4:HLA-E^{VMAPRTLVL} datasets, with the Matthews coefficient indicating a high likelihood of five (47% solvent content, probability = 0.54) or four (57% solvent content, probability = 0.29) complexes in the asymmetric unit.

Structure Solution and Refinement of GF4:HLA-E^{VMAPRTLIL}

Following data processing, GF4:HLA-E^{VMAPRTLIL} datasets were treated similarly to those of GF4:HLA-E^{VMAPRTLVL}. Structures were determined by molecular replacement using the PHASER program from the CCP4 suite (*Collaborative Computational Project, 1994*). Search models for GF4:HLA-E^{VMAPRTLIL} were unliganded GF4 from the refined GF4:HLA-E^{VMAPRTLVL} dataset (CDR loops omitted) and the fully refined, unliganded HLA-E^{VMAPRTLLL} structure (peptide omitted). The GF4 TcR from the GF4:HLA-E^{VMAPRTLVL} dataset was chosen as a search model in preference to the higher resolution LC13 TcR structure. This choice was due to the introduction of model overlaps between the TcR V α domains when the LC13 TcR was used, which were not present when the GF4 TcR was used.

Electron density maps obtained from datasets indexed to P2₁2₁2₁ showed four complexes in the asymmetric unit, marked as a significant possibility according to the calculated Matthews coefficient, with a high solvent content (57%), possibly accounting for the fragility of the crystals. Model building of GF4:HLA-E^{VMAPRTLIL} was carried out using the program COOT (*Emsley and Cowtan, 2004*) followed by maximum-likelihood refinement with the REFMAC5 program from the CCP4 suite (*Collaborative Computational Project, 1994*).

As with GF4:HLA-E^{VMAPRTLVL}, optimal Torsional, Libration and Screw tensor (TLS) domains for GF4:HLA-E^{VMAPRTLIL} were determined using the TLS Motion Determination server (*Painter and Merritt, 2006*) and read into REFMAC5 in order to define likely domains and flexible regions. Simulated annealing was performed using PHENIX (*Adams et al., 2010*) to improve the structure with respect to the electron density, and accordingly lower the R_{cryst} and R_{free} values. Medium non-crystallographic symmetry (NCS) restraints were used to improve electron density maps through molecular averaging. Consistent with GF4:HLA-E^{VMAPRTLVL}, NCS restraints were implemented as two sets of two-fold symmetry, with each complex from one pair constrained to the corresponding complex in the other pair. NCS constraints were implemented for individual protein chains, though no NCS restraints were implemented for the nonameric peptides bound by HLA-E.

Successive rounds of maximum-likelihood refinement were carried out using the REFMAC5 program in the CCP4 suite (*Collaborative Computational Project, 1994*), with the same parameters as for GF4:HLA-E^{VMAPRTLVL}. These parameters are described above in *Structure Solution and Refinement of GF4:HLA-E^{VMAPRTLVL}*. The finalised GF4:HLA-E^{VMAPRTLIL} structure was analysed using MolProbity (*Chen et al., 2010*), the CONTACT and AREAIMOL programs from the CCP4 suite (*Collaborative Computational Project, 1994*) and PyMOL (version 1.3) (*Schrodinger LLC*). The parameters within which these programs were used are also described above in *Structure Solution and Refinement of GF4:HLA-E^{VMAPRTLVL}*. As the interaction faces of each molecule were very similar in every complex within each asymmetric unit, one representative complex was chosen for analysis.

Major Features of the GF4:HLA-E^{VMAPRTLIL} Structure & Comparison with GF4:HLA-E^{VMAPRTLVL}

The determination of the GF4:HLA-E^{VMAPRTLIL} structure allowed comparison of the two complexes, which differ only in the amino acid residue at P8 of the peptide. Comparison of the general TcR docking conformation (Figure 5.7) and peptide conformation (Figure 5.8) shows that the MHC and peptide backbone overlay with striking similarity, which may be due to the tight binding of the peptide by the MHC which is a feature of MHC-Ib. The exposed surface area (330.6Å²) of the peptide (in the absence of TcR), and the amount of this surface area that is buried by the TcR upon ligation (226.5Å²) are similar to those values obtained for the GF4:HLA-E^{VMAPRTLVL} structure. Neither the total TcR surface area buried due to ligation with HLA-E^{VMAPRTLIL}, nor the proportion of that area buried due to each CDR loop, varies significantly with respect to values obtained for the GF4:HLA-E^{VMAPRTLVL} structure.

One noticeable difference between the two ternary structures is a shift of up to 2.6Å (measured Cα to Cα) in the backbone of the CDR3β loop (Figure 5.9), which is unusually long (17 residues) and potentially flexible. This shift could potentially be a result of isoleucine at P8 displacing the CDR3β loop away from the MHC relative to its position with a valine at P8, and may provide some explanation of the difference in affinity of GF4 for HLA-E presenting VMAPRTLVL (2.4μM) and VMAPRTLIL (40μM). It should be noted, however, that the precise reason for the preference of

Table 5.5. *GF4 TcR:HLA-E^{VMAPRTLIL} TcR-MHC and TcR-peptide contacts.* Atoms involved in hydrogen bonding and salt bridges are noted in superscript.

TcR α -chain-HLA-E contacts			TcR β -chain-HLA-E contacts		
GF4 α	HLA-E	Type	GF4 β	HLA-E	Type
N29	S151, E154, H155	VDW	Y50	Q72, E73, V76	VDW
Y49	D149, S151	VDW	Y50 ^{OH}	Q72 ^O	Salt Bridge
R68	E154	VDW	N51	R75, V76, R79	VDW
R68 ^{NH2}	E154 ^{Oϵ1}	H-bond	N51 ^{Nδ2}	R75 ^{NH1}	H-bond
R68 ^{NH1}	E154 ^{Oϵ1}	Salt Bridge	N51 ^{Oδ1}	R75 ^{NH1}	Salt Bridge
R68 ^{NH1/2}	E154 ^{Oϵ2}	Salt Bridge	N51 ^{Oδ1}	R79 ^{NH2}	Salt Bridge
P92	H155	VDW	E53	E19, Q72, R75	VDW
L93	H155	VDW	E53 ^{Oϵ1}	Q72 ^{Nϵ2}	H-bond
G94	H155	VDW	E54	Q72	VDW
S96	D69	VDW	R55	R65, D69, Q72, I73	VDW
S96 ^{Oγ}	D69 ^{Oδ2}	H-bond	R55 ^{NH1}	D69 ^O	H-bond
			R55 ^{NH1}	D68 ^{Oδ1}	Salt Bridge
			R55 ^{NH1}	Q72 ^{Oϵ1}	Salt Bridge
			R55 ^{NH2}	D68 ^{Oδ2}	Salt Bridge
			P97	K146, T80	VDW
			S100	K146	VDW
TcR α -chain-peptide contacts			TcR β -chain-peptide contacts		
GF4 α	VMAPRTLIL	Type	GF4 β	VMAPRTLIL	Type
Q91	R5	VDW	N102	I8	VDW
Q91 ^{Oϵ1}	R5 ^{NH1}	H-bond	E103	R5	VDW
Q91 ^{Oϵ1}	R5 ^{NH2}	Salt Bridge	E103 ^{Oϵ1}	R5 ^{NH2}	H-bond
G94	P4, R5	VDW	E103 ^{Oϵ1}	R5 ^{NH1}	Salt Bridge
G95	R5	VDW	E103 ^{Oϵ2}	R5 ^{NH2}	Salt Bridge
S96	P4, R5	VDW			
N97	R5, T6	VDW			
N97 ^{Nδ2}	T6 ^O	H-bond			
Y98	I8	VDW			

GF4 for HLA-E^{VMAPRTLVL} over HLA-E^{VMAPRTLIL} could not be clearly determined by these structures due to the limitations of resolution.

A consensus contact list for the GF4:HLA-E^{VMAPRTLIL} complex is shown in Table 5.5. As with the GF4:HLA-E^{VMAPRTLVL} contact list, this consensus list shows van der Waals contacts and salt bridges if they were observed in three complexes, and H-bonds if they were observed in two complexes. The consensus contacts list for the GF4:HLA-E^{VMAPRTLIL} complex is diminished relative to that of the GF4:HLA-E^{VMAPRTLVL} complex. This may be due to the reduced resolution amplifying the subtle differences between complexes in the asymmetric unit (as mentioned above), and reducing the number of contacts present in multiple complexes. The absence of

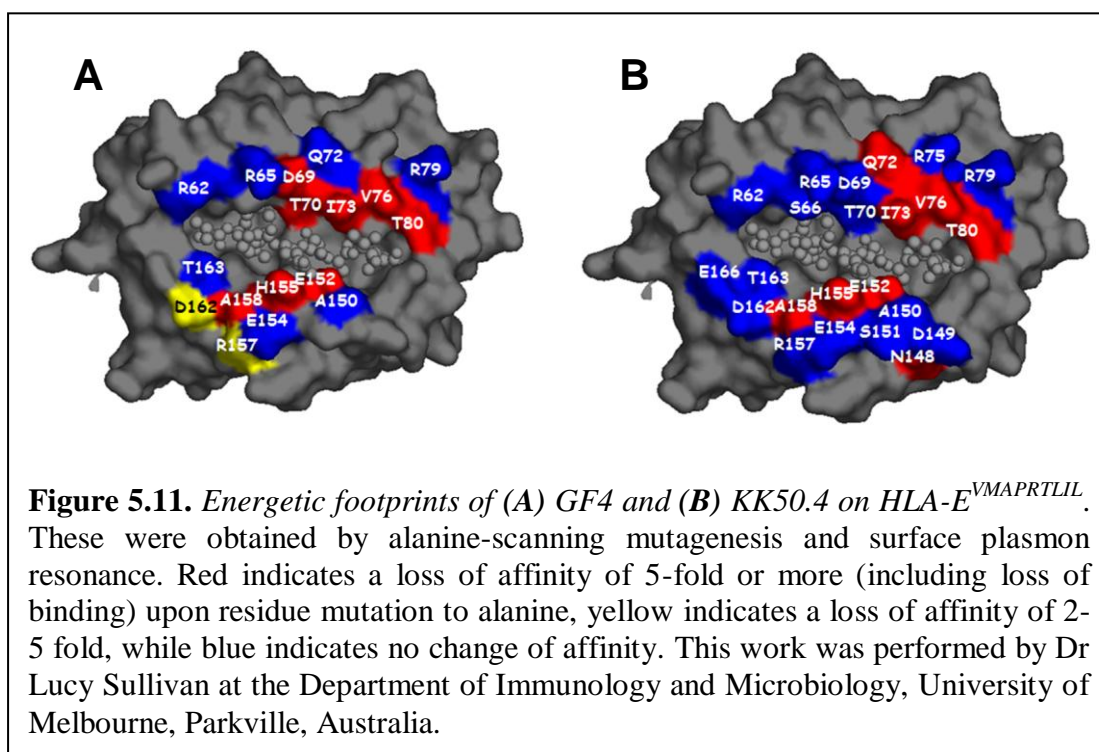
contacts between the MHC and GF4 α Lys50 in this complex is a noticeable example of this, as one complex in the asymmetric unit showed multiple contacts between the MHC (residues Asn148, Asp149 and Ser151 on the α 2 helix) and GF4 α Lys50, including a hydrogen bond. However, the major features of the GF4:HLA-E^{VMAPRTLVL} consensus contacts list are also visible in that of GF4:HLA-E^{VMAPRTLIL}, including similar GF4 CDR1 α (Asn29) and 3 α (Pro92, Leu93 and Gly94) loop contacts with HLA-E His155, and GF4 CDR2 β loop (residues Tyr50, Asn51, Glu53 and Arg55) contacts with HLA-E α 1 helix residues Asp69, Gln72 and Arg75. Contacts between GF4 β Glu50 and HLA-E Glu19 were also observed.

One observation of the GF4:HLA-E^{VMAPRTLIL} consensus contacts list not noted in that of GF4:HLA-E^{VMAPRTLVL} is van der Waals contacts between Asn102 of the GF4 β -chain (in the CDR3 β loop) and Ile8 of the peptide. This may be due to the movement in the GF4 CDR3 β loop which was described above, or to the slight increase in P8 residue size. It is possible that the proximity of Asn102 and neighbouring residues on the GF4 CDR3 β loop to the P8 residue prevents GF4 interaction with HLA-E presenting other host peptides, such as those which contain either Leucine or Phenylalanine at this position.

Discussion

Comparison with KK50.4 TcR:HLA-E^{VMAPRTLIL}

While the two structures described give a good insight as to the mode of peptide recognition of Group 1 HLA-E restricted TcRs, they also present an opportunity to compare the structures shown with that of KK50.4:HLA-E^{VMAPRTLIL} (Hoare *et al.*, 2006), the first MHC-Ib:TcR ternary structure to be solved and the only structure of a Group 2 HLA-E restricted TcR to date. Contrasts seen in this comparison allow insight as to the mechanisms behind the absolute specificity of KK50.4 and other Group 2 HLA-E restricted TcRs, as compared to the limited specificity of GF4 and Group 1 HLA-E restricted TcRs. On the other hand, similarities between the modes of recognition of GF4 and KK50.4 may give some clues as to how pHLA-E, and perhaps Class Ib MHCs in general, are recognised with such specificity despite restricted peptide-binding repertoires and low peptide solvent exposure.



A look at the energetic ‘footprints’ of GF4 and KK50.4 on HLA-E^{VMAPRTLIL}, as determined by alanine-scanning mutagenesis and surface plasmon resonance (work performed by Dr Lucy Sullivan and Dr Andrew Brooks, Dept of Immunology and Microbiology, University of Melbourne, Parkville, Australia) gives a good overview of the focus of both GF4 and KK50.4 binding (Figure 5.11). Mutations on the $\alpha 1$ and $\alpha 2$ helices of HLA-E near the P5 and P8 signal residues completely abrogate binding, showing the extent to which both TcRs focus on and around these residues to increase affinity and maintain specificity of the interaction.

The conserved focal areas of GF4 and KK50.4 on HLA-E are also seen in the crystal structures of each, however GF4 and KK50.4 have very different modes of preserving this focus. Docking orientation (calculated by connecting the centres of mass of the two TcR variable domains) relative to the helices of the peptide-binding cleft (shown in Figure 5.12) is markedly altered, with KK50.4 displaying a diagonal docking orientation and GF4 displaying an orthogonal docking orientation, almost perpendicular to the peptide-binding cleft. However, it can be seen that both TcRs dock at a position on the pMHC where both the arginine at P5 and the isoleucine/valine at P8 may be contacted and thus recognised with high specificity.

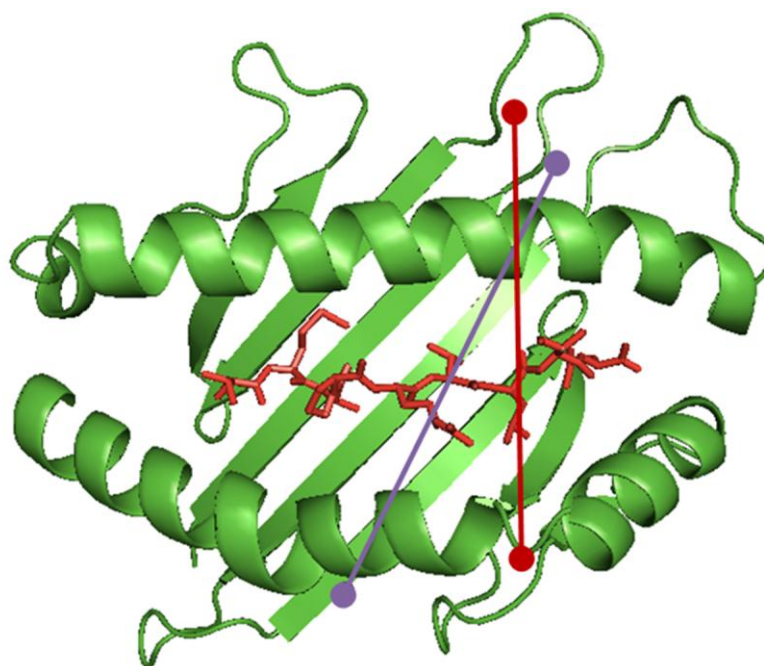


Figure 5.12. Docking orientation of GF4 (red) and KK50.4 (purple) on HLA- $E^{VMAPRTLIL}$. These were calculated by connecting the centres of mass of the TcR variable domains. Docking of GF4 on HLA- $E^{VMAPRTLVL}$ was almost identical to that seen on HLA- $E^{VMAPRTLIL}$.

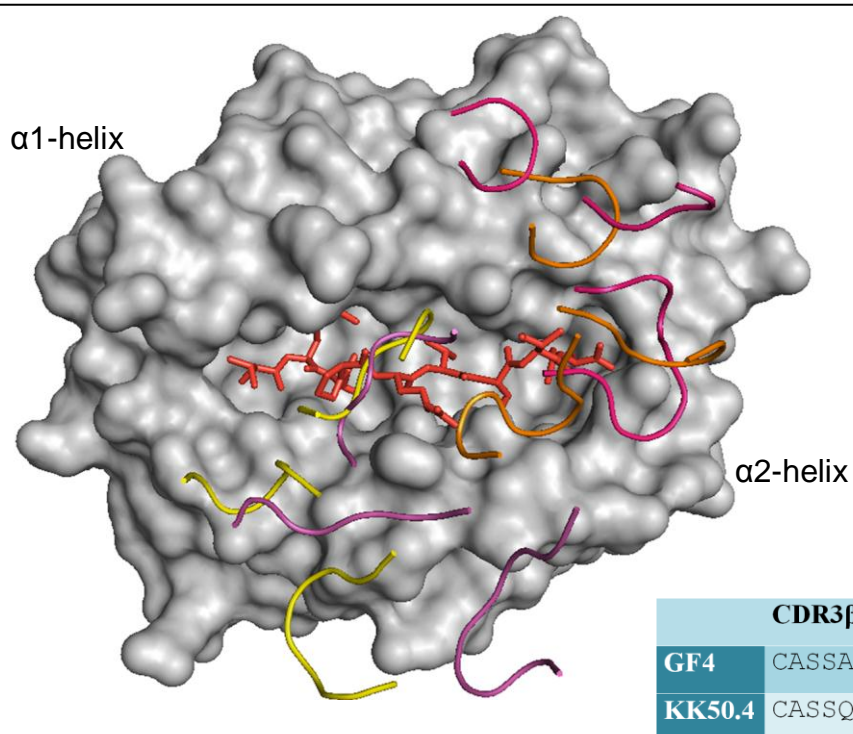


Figure 5.13. Overlay of GF4 and KK50.4 CDR loops at the HLA- $E^{VMAPRTLIL}$ antigen binding cleft. Top view of the antigen-binding cleft of HLA- $E^{VMAPRTLIL}$ (surface view, peptide in red), showing the CDR loops of GF4 (α -chain in purple, β -chain in pink) and KK50.4 (α -chain in yellow, β -chain in orange). Significant shifts in both CDR α and CDR β loops are visible. A sequence comparison of the non-germline encoded CDR3 β loops of GF4 and KK50.4 is also shown (lower right).

The distinction between the two modes of focal preservation is also observed by looking at the area surrounding P8 of the bound peptide, the single amino acid that differs between self and non-self. Whereas residues on the long CDR3 β loop of GF4 are involved in P8 recognition as well as contacts with the α 1 and α 2 helices, residues from all 3 CDR β loops of KK50.4 are involved in contacts with the isoleucine at P8. This is illustrated in Figure 5.13. In a stark contrast to the binding by KK50.4, in which the CDR2 β loop makes up 30% of the buried surface area at the binding interface (*Hoare et al., 2006*), the positions of the GF4 CDR1 β (2.3-2.8% of total buried surface area) and CDR2 β (20.3-20.6% of total buried surface area) loops are shifted across (relative to those of KK50.4) by the CDR3 β loop, and only make contacts with the α 1 helix of HLA-E, peripheral to the main peptide recognition sites. It is likely that the different modes of P8 recognition are the underlying cause of the difference in specificity between GF4 and KK50.4.

Clues to the differences between Group 1 and 2 HLA-E restricted TcRs are also seen in gene usage. All known CTL clones expressing Group 2 HLA-E-restricted TcRs use V β 16 (or TRBV14*01 using IMGT nomenclature) or V β 9 (TRBV3) (*unpublished data*). These may be the only V β genes which have the potential to recognise pHLA-E, while allowing specific recognition of the peptide sidechain at P8 even from chemically similar amino acids. Though less information has been gathered on the α -chains of many HLA-E-restricted TcRs, it appears that Group 2 V α usage shows more variability (TRAV26-1, TRAV4, TRAV13, TRAV8-2 and TRAV35 have been identified in various clones isolated by Pietra *et al*) (*unpublished data*). Group 1 HLA-E-restricted TcRs show some variability in V β gene usage. CTL clones expressing the GF4 TcR use V β 1 (TRBV9*01), while other known CTL clones use V β 22 (TRBV2*01), V β 5 (TRBV5-1*01) and V β 16 (TRBV14*02) (*unpublished data*). Little data exists about the identity of the α -chain gene segments used in these CTL clones, though GF4 is known to use V α 25 (TRAV35*02). It is unknown whether the Group 1 HLA-E-restricted TcRs using V β 16 bear more similarity in their mechanism of P8 recognition to KK50.4, which displays a related V β sequence, or GF4, which displays a similar peptide recognition pattern. Immunological and genetic studies in this field are invaluable, and work in these areas will continue to yield valuable insight into these TcRs, and the variability that exists between HLA-E-restricted TcRs of both Group 1 and Group 2.

Comparison with TcR Recognition of MHC-Ia

Determination of the structure of KK50.4:HLA-E^{VMAPRTLIL} enabled a number of comparisons and contrasts to be made with several TcR:MHC-Ia complex structures that had been previously determined (*Hoare et al., 2006, Sullivan et al., 2006, Sullivan et al., 2008*). These included many general similarities, such as binding of the TcR to the peptide binding cleft (*Garcia et al., 1999*), docking orientation allowing recognition of the peptide by the CDR3 α and CDR3 β loops (*Rudolph and Wilson, 2002, Rudolph et al., 2006, Garcia et al., 2009*), multiple contacts with the MHC α 1 and α 2 helices, and conformational changes in some residues of the MHC heavy chain upon TcR ligation (*Kjer-Nielsen et al., 2003*). In all of these features both KK50.4 and GF4 show a mode of recognition of HLA-E that is similar to TcR recognition of MHC-Ia. However, some features of the KK50.4:HLA-E^{VMAPRTLIL} structure were distinctive among known TcR:MHC structures.

Among these were two features mentioned above – an unusually high (30%) proportion of KK50.4 TcR buried surface area at the interaction interface that was due to the CDR2 β loop, and also an unusual convergence of all 3 KK50.4 CDR β loops onto the isoleucine residue at P8 of the bound peptide. In terms of both of these features, the GF4:pHLA-E structures described in this chapter were more typical of TcR:MHC structures solved to date.

Firstly, the proportion of the GF4 TcR buried surface area due to the CDR2 β loop (20.3-20.6%) falls more closely into the observed range than that of KK50.4. The predominance of the CDR3 α and 3 β loops as seen at the GF4 TcR:pHLA-E interface (48.0-49.3% of total TcR buried surface area) is also a common feature of MHC-Ia:TcR interactions (*Burrows et al., 2010*).

Secondly, the GF4 CDR3 α and 3 β loops completely dominate peptide interactions, leaving the CDR1 and 2 loops of either chain to make interactions only with residues on the MHC. This configuration is more accordant with the prevalent model described by Garcia *et al* (*Garcia et al., 2009*) than the peptide recognition of KK50.4, though as mentioned in Chapter 1, under the heading *Receptors of HLA-E* and sub-heading *$\alpha\beta$ T-cell receptors (TcR)*, some examples of TcR:MHC-Ia structures

in which CDR1 and CDR2 loops of either TcR chain play a major role in peptide recognition are present in the literature (*Stewart-Jones et al., 2003, Tynan et al., 2005, Gras et al., 2009a, Gras et al., 2009b*).

A third feature of HLA-E^{VMAPRTLIL} recognition by KK50.4 was contacts made by the TcR to four amino acids (Asp69, Thr70, His155 and Asp162) either unique to HLA-E, or rare in other MHCs. This suggested a basis for the HLA-E restriction of KK50.4 (*Sullivan et al., 2006*). In both ternary complexes described above, GF4 makes multiple contacts with 2 of these MHC residues, Asp69 and His155 (see Tables 5.4 and 5.5). Asp69 is contacted by residues on the GF4 CDR3 α loop (Ser96) and the CDR2 β loop (Arg55), and is seen to form a H-bond with Arg55 of the GF4 β -chain in the GF4:HLA-E^{VMAPRTLIL} structure. Likewise, His155 is contacted by residues on the CDR1 α (Asn29) and CDR3 α loops (Gln91, Pro92, Leu93, Gly94 and Gly95). His155 forms a H-bond with Gln91 of the GF4 α -chain in the GF4:HLA-E^{VMAPRTLVL} structure. However, the CDR1 α loop of GF4 is positioned further away from the N-terminus of the peptide than that of KK50.4. Because of this, GF4 does not form any contacts with Asp162. In addition, though contacts are seen in some complexes between the GF4 CDR2 β and the MHC protein backbone at HLA-E Thr70, the Thr70 sidechain is not exposed enough to the TcR for contacts to exist between the TcR and the Thr70 sidechain, as are seen in the KK50.4:HLA-E^{VMAPRTLIL} structure. Overall, the contacts made with Asp69 and His155 may be enough to form a basis for GF4 restriction to HLA-E.

Lastly, surface plasmon resonance studies showed that the interaction between KK50.4 and HLA-E^{VMAPRTLIL} was of low affinity (26 μ M) compared to those previously measured between TcRs and MHC-Ia presenting agonist peptides (typically 1-10 μ M) (*Burrows et al., 2010*). As mentioned previously, the affinity of GF4 for HLA-E^{VMAPRTLIL} (35 μ M) is also lower than this range, however GF4 recognises HLA-E^{VMAPRTLVL} with considerably higher affinity (4.3 μ M). This refutes any general concept of low affinity amongst TcR:MHC-Ib interactions, however provides further evidence that TcRs recognising HLA-E^{VMAPRTLIL} may be forced to bind that ligand with lower affinity, given the need for absolute specificity of interaction.

In a host whose HLA haplotype lacks the leader sequence VMAPRTLIL but contains other common leader sequences, any significant affinity of an immature CTL for HLA-E presenting the host ligands VMAPRTLLL (derived from the leader sequence of some HLA-A and HLA-C alleles), VMAPRTLVL (other HLA-A alleles), VMAPRALLL (HLA-Cw*07 and -Cw*18) or VMAPRTLFL (HLA-G) will cause that CTL to undergo clonal deletion by apoptosis (*Rammensee and Bevan, 1984, Matzinger et al., 1984*). For this reason, Group 2 HLA-E restricted TcRs which specifically recognise HLA-E presenting the peptide VMAPRTLIL must be able to distinguish the isoleucine at P8 from both leucine and valine – amino acids with similar size and chemical properties to isoleucine.

It is likely that any receptor able to bind to HLA-E^{VMAPRTLIL} with high affinity would at least partially tolerate a conservative, single amino acid substitution at P8 such as isoleucine to leucine, except in the case that TcR contacts made with isoleucine were tight enough to cause steric hindrance with a leucine sidechain. For that case, it would be almost certain that the high affinity receptor would tolerate the conservative substitution at P8 of isoleucine to valine. However, where the affinity of the receptor for HLA-E^{VMAPRTLIL} is relatively low, it is conceivable that even conservative substitutions at P8 provide enough hindrance to binding to prevent receptor recognition HLA-E presenting alternative peptides. This reasoning goes some way to explaining the low affinities observed in Group 2 TcR:HLA-E^{VMAPRTLIL} interactions.

In contrast, Group 1 HLA-E-restricted TcRs are not bound by such tight restraints when binding to HLA-E^{VMAPRTLVL}. While distinction between isoleucine and leucine is still imperative (leading to lower affinity of the TcR for HLA-E^{VMAPRTLIL}), these TcRs are able to recognise valine at P8 with a similar affinity to TcR:MHC-Ia interactions, without causing any significant affinity for HLA-E presenting other host peptides.

Concluding Remarks

Structural characterisations such as those presented above can give great insight into the similarities and differences of different immune receptors, ligands and their interactions, especially in conjunction with biophysical, immunological, genetic and clinical data. In this chapter, it has been shown that the long CDR3 β loop of GF4 may lead to flexibility of that loop, leading to recognition of two different amino acids at a pivotal position in the HLA-E bound peptide sequence, and also leading to significantly different affinities for those interactions. It has been shown that GF4 and KK50.4, examples of the Group 1 and Group 2 HLA-E-restricted TcRs respectively, achieve a similar energetic focus on the MHC, while displaying different docking orientations, and different modes of P8 recognition leading to different peptide specificities. Following this, it has been shown that TcR:MHC-Ib responses could potentially show similar levels of variability as those of MHC-Ia, as well as showing similar general structural features.

In summary, recent studies have shown that the Class Ib MHC HLA-E can act as an activating ligand for adaptive immune system effector cells, as well as playing a major role in mediating the innate immune response. Despite having a highly restricted peptide-binding repertoire, HLA-E has been shown to present viral peptides to CTLs. Three of these interactions, involving two separate TcRs and two separate CMV-derived peptides, have now been structurally characterised using X-ray crystallography, allowing many comparisons to be made to each other, as well as to previously solved TcR:MHC-Ia structures. Further HLA-E-restricted CTLs specific for other human pathogens have also been isolated, attaching further importance to the potential roles of HLA-E and other Class Ib MHCs in the adaptive immune response. With many questions still left unanswered by the recent work done in this field, it is imperative to establish the importance of the MHC-Ib response in the wider context of the adaptive immune system.

Chapter 6 – Discussion and Future Directions

Peptide Presentation by Class Ib MHC

The work presented in Chapter 3 described the distinct conformations adopted by the HLA-G peptide-binding region upon binding of different peptide ligands. This is particularly relevant in the context of association with receptors which bind to the MHC peptide-binding region, including T-cell receptors, which have been seen to exclusively recognise the peptide-binding region (*Rudolph and Wilson, 2002*), and KIR2DL4, which has been shown to recognise residues unique to the HLA-G α 1-helix (*Yan and Fan, 2005*). Indeed, it is possible that the lack of association between HLA-G and KIR2DL4 reported in Chapter 4 was entirely due to suboptimal peptide selection, despite the range of peptides chosen for Native-PAGE and SPR analysis. However, this would be in direct contrast with crystal structures of the complexes between KIR2DL1 and HLA-Cw4 (*Fan et al., 2001*) and KIR2DL2 and HLA-Cw3 (*Boyington et al., 2000*), both of which displayed minimal contacts between receptor and peptide. These interactions were also shown to tolerate peptide substitutions that did not introduce electrostatic repulsion.

Despite the minimal effect of HLA-C peptide substitutions on KIR interactions, MHC-Ib peptide-dependent differences have been demonstrated in the affinity of CD94/NKG2 receptors for HLA-E (*Kaiser et al., 2005, Sullivan et al., 2007, Vales-Gomez et al., 1999*), as well as the specificity of interaction demonstrated by HLA-E-restricted T-cell receptors (*Pietra et al., 2003*). Notably, these differences were observed upon substitutions which were restricted to P6 and P8 of the HLA-E-bound peptide, whereas the range of host-derived HLA-G-associated peptides shows significantly more variability (*Diehl et al., 1996, Lee et al., 1995*).

Roles of Class Ib MHC in Adaptive Immunity

The variability of the antigen-binding cleft conformation within Class Ib MHC raises further issues with regard to their putative roles in the adaptive immune response. Though all have primary roles mediating the innate immune system, each of HLA-G, Qa-1b and HLA-E have also been shown to bind a range of pathogen-derived peptides, and it is possible that in each case the number of pathogen-derived peptides

may exceed the number of endogenous peptides naturally bound by the MHC-Ib. Of these three MHC-Ib molecules, HLA-G has been implicated the least in presentation of pathogen-derived antigens, however this may be due primarily to limited tissue distribution, as the peptide binding cleft of HLA-G is able to bind a much wider range of peptide antigens than those of Qa-1b and HLA-E. HLA-G expression in the thymus may facilitate the positive selection of an HLA-G-specific T-cell repertoire (*Mallet et al., 1999*), and in addition to expression in tumors as described in Chapter 1, ectopic expression of HLA-G may also be caused by a number of factors including stress (*Carosella et al., 2003*), hypoxia (*Mouillot et al., 2007*), hormones (*Yie et al., 2006b, Yie et al., 2006a*) and cytokines (*Carosella et al., 2003*), increasing the potential for exposure of HLA-G-expressing cells to pathogenic invasion. Though not observed in humans, specific T-cell recognition of HLA-G presenting the CMV-derived antigen VFPTKDVAL has been shown in a transgenic mouse model (*Lenfant et al., 2003*). This study raised two interesting points. Firstly, HLA-G is capable of binding and presenting a number of peptides potentially formed as a result of pathogenic invasion, and secondly, that these peptides cause enough conformational change at the peptide-binding region of HLA-G that a CTL response restricted to HLA-G presenting viral antigen may be generated.

The narrow binding repertoire of Qa-1b, considered in its primary role to be restricted to the MHC-I leader sequence AMAPRTLII (*Vance et al., 1998, DeCloux et al., 1997*), has been shown to bind unrelated host peptides derived from the preproinsulin leader sequence (*Chun et al., 1998*) and Heat shock protein 60 (Hsp60) (*Lo et al., 2000*), each of which is associated with a CTL response. While CTL recognition of Qa-1b presenting the preproinsulin sequence has been linked to pancreas islet inflammation, no association with pathogen-derived antigens has been described. However, CTL reactivity to Qa-1b presenting Hsp60 protein has been associated with crossreactivity from CTL responses to Qa-1b presenting a *Salmonella enterica* serovar Typhimurium GroEL peptide. These CTLs were not shown to be crossreactive with Qa-1b presenting the canonical Qdm peptide. As well as the *S.typhimurium* response, Qa-1b has also been implicated as a restricting element in the CTL response to *Listeria monocytogenes* infection (*Bouwer et al., 1997*). As with HLA-G, it is becoming clear that the bound peptide has an effect on immune signalling by Qa-1b.

Peptide-dependent conformational changes in HLA-E presentation have been demonstrated at a structural level both in Chapter 5 and in other studies (*Hoare et al., 2008, Hoare et al., 2006*), generally focussing on the presentation of related peptides derived from MHC-I leader sequences. However, as described in Chapter 1, HLA-E has also been shown to bind to markedly variable peptides derived from the host Heat Shock Protein 60 (*Michaelsson et al., 2002*), Hepatitis C virus (*Nattermann et al., 2005a*), HIV p24 (*Nattermann et al., 2005b*) and other sources. Further evidence of TcR recognition of peptide-dependent HLA-E conformational changes is evident in the isolation of HLA-E-restricted CTL responses in individuals infected with *Salmonella enterica* (*Salerno-Goncalves et al., 2004*) and *Mycobacterium tuberculosis* (*Heinzel et al., 2002*), which are not crossreactive with HLA-E presenting host MHC-I leader peptides. The HLA-E-restricted *M.tuberculosis* response was found to comprise the dominant CD8 T-cell response in latently infected individuals.

Though still mediated by a MHC-Ia-like interaction, the CTL response to HLA-E presenting ‘mimotope’ peptides derived from the UL40 ORF from CMV is a markedly different example to those listed above. This response is haplotype dependent, and is based on detection of a peptide which, while foreign to the individual, is still relatively common in MHC-I leader sequences among the general population. As such, introduction of foreign MHC-I leader sequences may occur by other means, including solid organ transplantation.

In contrast to HLA-G’s status as a marker for good patient outcomes after organ transplant events (*Lila et al., 2002*), a CTL response to HLA-E could potentially be a cause of acute organ rejection in transplantation cases where HLA-A and -C alleles are mismatched in such a way that a MHC-I leader sequence foreign to the recipient is transplanted. To date, there have been no formal studies evaluating this risk factor in transplantation, or assessing whether any CTL response generated this way would bear any similarities to a virus-specific response. This may be due to difficulties in the identification of alloreactive T-cells directly *ex vivo* in human systems. Sullivan *et al* hypothesised that such a response would behave in an analogous manner to MHC-Ia-restricted T-cells (*Sullivan et al., 2008*), and noted that a detailed analysis of

such a response is feasible. Regardless of the outcome of such studies, solid organ transplantation is becoming increasingly common in modern medicine, and potential risk factors cannot be ignored.

Future Directions

pHLA-G Structural Studies

The paper presented in Chapter 3 describes the determination and analysis of two pHLA-G structures. These, in addition to the monomeric and dimeric HLA-G^{RIIPRHLQL} structures which have previously been determined (*Clements et al., 2005, Shiroishi et al., 2006a*), provide an opportunity for comparison of the nature of HLA-G when presenting each of the peptides RIIPRHLQL, KGPPAALTL and KLPQAFYIL. Out of the 11 further endogenous peptides determined by peptide elution studies to bind to HLA-G (*Ishitani et al., 2003, Diehl et al., 1996, Lee et al., 1995*), it may be suggested that those which show significant sequence variation, or those that do not conform fully to the HLA-G binding motif described in Chapter 1 under the heading *HLA-G Peptide Binding and Structural Considerations*, could gainfully be crystallised to provide further structures for analysis.

In addition, it would be advantageous to test the possibility that the conformational variability, observed in the pHLA-G complexes described, may be of sufficient magnitude to influence recognition by receptors from both the innate and adaptive immune systems. While the effect on HLA-G of binding viral peptides should only be analysed after it has been shown that those peptides are available *in vivo* for HLA-G presentation, it has been shown that a number of peptides isolated from the CMV proteome conform to the HLA-G binding motif (*Lenfant et al., 2003*). The isolation of a viral peptide that can be presented by HLA-G and specifically recognised by a TcR would be a significant advance in the analysis of a potential role for HLA-G in the adaptive immune response.

KIR2DL4

Despite successful crystallisation of baculovirus-expressed recombinant KIR2DL4, future work towards determination of the KIR2DL4 crystal structure would need to take into account the issues presented above, regardless of protein expression system. Crystallisation is highly dependent on tight ‘packing’ of molecules and it is possible

that oligomerisation of KIR2DL4 at high concentrations may hinder crystal nucleation and growth. From this standpoint, it would be highly beneficial to determine the mechanism of oligomerisation and deal with this mechanism appropriately, to improve both yield and crystal quality. Likewise, high levels of glycosylation may hinder crystal growth, and deglycosylation using Endoglycosidase H treatment of mammalian-expressed KIR2DL4 as shown in Chapter 4 under the heading *Deglycosylation of Mammalian-Expressed KIR2DL4*, would be likely to aid crystallisation. Alternatively, mutation of the glycosylation motifs within baculovirus-expressed KIR2DL4 may counter glycosylation, if consequential problems maintaining the native fold can be avoided.

A second option that may result in improved crystal nucleation and growth is monomerisation of KIR2DL4. This may be achieved by method described in Chapter 4 under the heading *Biophysical Analysis of Baculovirus-Expressed KIR2DL4*, using iodoacetamide to permanently cap the unpaired cysteine residue, or alternatively by mutation of the unpaired cysteine residue to an alternative amino acid. Likely choices for mutation of the C10 residue would be serine, a similar residue to cysteine in terms of size, or leucine, which is present at that location in every other KIR D0 domain, as shown in Chapter 4 under the heading *Biophysical Analysis of Baculovirus-Expressed KIR2DL4*.

Alternative expression systems for production of recombinant KIR2DL4 remain possible options with respect to crystallographic studies. One such system is that described by Yu *et al*, who used a prokaryotic system to produce a KIR2DL4 fusion protein, which was then refolded in alkaline buffer (Yu *et al*, 2006).

With respect to the analysis of the self-association of KIR2DL4, it will be useful to determine whether dimerisation and oligomerisation occur at the cell surface as well as in solution. However, if KIR2DL4 self-association at the cell surface is demonstrated, further research using analytical ultracentrifugation (AUC) or SAXS could focus on the determination of the concentration at which KIR2DL4 forms a dimer (rather than higher oligomers), with the aim of using SAXS to determine the conformation that KIR2DL4 adopts at this concentration.

TcR Recognition of pHLA-E

Following the conclusions of the structural work presented in Chapter 5, it remains to be seen whether TcR binding mechanisms to HLA-E show greater similarity to CD94/NKG2A recognition of HLA-E, with a rigid ‘lock and key’ mechanism, or to the adaptive binding shown by TcR recognition of MHC-Ia, where the CDR loops may flex in such a way as to optimally bind the pMHC. Crystal structures of the unliganded KK50.4 and GF4 TcRs should provide an answer to this question, in addition to providing evidence as to the natural position (if any) of the long CDR3 β loop in the GF4 TcR.

To expand the current understanding of HLA-E restricted TcRs and the different mechanisms of peptide recognition employed by those TcRs, it would be useful to pursue structural investigations of more of these TcRs, including those with different gene segment usages to the GF4 and KK50.4 TcRs. These include an identified Group 1 HLA-E restricted TcR which contains the V β 16 (TRBV14*02) gene segment, and an identified Group 2 HLA-E restricted TcR which uses the V β 9 (TRBV3) gene segment. Immunological, genetic and biophysical techniques also provide good means by which to study HLA-E restricted TcRs, and the variability that exists within and between the different groups. It is also possible that as-yet unidentified HLA-E restricted TcRs may feature different peptide specificities, necessitating the recognition of further ‘groups’ of HLA-E restricted TcRs.

On a wider scale, it is important to understand the clinical relevance of HLA-E-mediated responses in suppressing severe CMV infections, and in certain individuals, in providing immunity from this endemic pathogen. It is widely understood that both humoral and cell-mediated immune responses are utilised in the human defence against CMV, which is present as a chronic infection in 50-90% of healthy adults globally and can cause serious medical complications in immunocompromised individuals, newborns and organ recipients. The proportion of individuals able to mount a HLA-E-mediated T-cell response to CMV infection is very low, and the response itself is restricted to the CMV strains Toledo and AD169. However, given the success of the immunomodulatory mechanisms utilised by CMV to escape clearance by the immune system, and the effectiveness of the HLA-E-mediated T-cell response in circumventing these mechanisms, it may be possible (and beneficial)

to reach a level of understanding of the HLA-E-mediated T-cell response whereby more wide-ranging therapies become available.

Concluding Remarks

The data presented in this thesis provide detailed insight into the roles that MHC-Ib perform in the human adaptive and innate immune systems, and the implications of peptide-dependent conformational changes at a region recognised by multiple receptor types. General conservation of MHC-Ib structure may allow unprecedented novel vaccination strategies for those pathogens which elicit a Class Ib-mediated CTL response, though any immunotherapy aimed at modulating Class Ib MHC will need to take into account the range of roles played by those molecules. The data presented in Chapter 3 provides new insight into the ways that HLA-G, a generally non-polymorphic molecule, might play roles in areas as diverse as pregnancy, organ transplantation and cancer. In addition, while the data presented in Chapter 5 adds to the knowledge of the role of HLA-E in the adaptive immune response, further understanding of the CTL response to HLA-E presenting foreign MHC-I leader sequences is critical for the therapeutic developments that may lead to new possibilities including greater control over CMV infection and organ transplantation.

Bibliography

- ADAMS, P. D., AFONINE, P. V., BUNKOCZI, G., CHEN, V. B., DAVIS, I. W., ECHOLS, N., HEADD, J. J., HUNG, L. W., KAPRAL, G. J., GROSSE-KUNSTLEVE, R. W., MCCOY, A. J., MORIARTY, N. W., OEFFNER, R., READ, R. J., RICHARDSON, D. C., RICHARDSON, J. S., TERWILLIGER, T. C. & ZWART, P. H. 2010. PHENIX: a comprehensive Python-based system for macromolecular structure solution. *Acta Crystallogr D Biol Crystallogr*, 66, 213-21.
- ALDRICH, C., STEPHENSON, M., KARRISON, T., ODEM, R., BRANCH, D., SCOTT, J., SCHREIBER, J. & OBER, C. 2001. HLA-G Genotypes and pregnancy outcome in couples with unexplained recurrent miscarriage. *Molecular Human Reproduction*, 7, 1167-1172.
- ALLAN, D. S., COLONNA, M., LANIER, L. L., CHURAKOVA, T. D., ABRAMS, J. S., ELLIS, S. A., MCMICHAEL, A. J. & BRAUD, V. M. 1999. Tetrameric complexes of human histocompatibility leukocyte antigen (HLA)-G bind to peripheral blood myelomonocytic cells. *J Exp Med*, 189, 1149-56.
- ANDERSON, K. J. & ALLEN, R. L. 2009. Regulation of T-cell immunity by leucocyte immunoglobulin-like receptors: innate immune receptors for self on antigen-presenting cells. *Immunology*, 127, 8-17.
- ARCHBOLD, J., MACDONALD, W., MILES, J., BRENNAN, R., KJERNIELSEN, L., MCCLUSKEY, J., BURROWS, S. & ROSSJOHN, J. 2006. Alloreactivity between disparate cognate and allogeneic pMHC-I complexes is resultant of highly focused, peptide-dependent structural mimicry. *Journal of Biological Chemistry*, Epub September 8, 2006.
- ARCHBOLD, J. K., MACDONALD, W. A., GRAS, S., ELY, L. K., MILES, J. J., BELL, M. J., BRENNAN, R. M., BEDDOE, T., WILCE, M. C., CLEMENTS, C. S., PURCELL, A. W., MCCLUSKEY, J., BURROWS, S. R. & ROSSJOHN, J. 2009. Natural micropolymorphism in human leukocyte antigens provides a basis for genetic control of antigen recognition. *J Exp Med*, 206, 209-19.
- ARICESCU, A. R., ASSENBERG, R., BILL, R. M., BUSO, D., CHANG, V. T., DAVIS, S. J., DUBROVSKY, A., GUSTAFSSON, L., HEDFALK, K., HEINEMANN, U., JONES, I. M., KSIAZEK, D., LANG, C., MASKOS, K., MESSERSCHMIDT, A., MACIEIRA, S., PELEG, Y., PERRAKIS, A., POTERSZMAN, A., SCHNEIDER, G., SIXMA, T. K., SUSSMAN, J. L., SUTTON, G., TARBOUREICH, N., ZEEV-BEN-MORDEHAI, T. & JONES, E. Y. 2006a. Eukaryotic expression: developments for structural proteomics. *Acta Crystallogr D Biol Crystallogr*, 62, 1114-24.
- ARICESCU, A. R., LU, W. & JONES, E. Y. 2006b. A time- and cost-efficient system for high-level protein production in mammalian cells. *Acta Crystallogr D Biol Crystallogr*, 62, 1243-50.
- BAINBRIDGE, D., ELLIS, S. & SARGENT, I. 1999. Little evidence of HLA-G mRNA polymorphism in Caucasian or Afro-Caribbean populations. *Journal of Immunology*, 163, 2023-2027.
- BIASSONI, R., CANTONI, C., MARRAS, D., GIRON-MICHEL, J., FALCO, M., MORETTA, L. & DIMASI, N. 2003. Human Natural Killer cell receptors: insights into their molecular function and structure. *Journal of Cellular and Molecular Medicine*, 7, 376-87.

- BIASSONI, R., CANTONI, C., PENDE, D., SIVORI, S., PAROLINI, S., VITALE, M., BOTTINO, C. & MORETTA, A. 2001. Human natural killer cell receptors and co-receptors. *Immunological Reviews*, 181, 203-214.
- BJORKMAN, P., SAPER, M., SAMRAOUI, B., BENNETT, W., STROMINGER, J. & WILEY, D. 1987. Structure of the human class I histocompatibility antigen, HLA-A2. *Nature*, 329, 506-512.
- BORGES, L., HSU, M.-L., FANGER, N., KUBIN, M. & COSMAN, D. 1997. A Family of Human Lymphoid and Myeloid Ig-like Receptors, Some of Which Bind to MHC Class I Molecules. *Journal of Immunology*, 159, 5192-5196.
- BORREGO, F., KABAT, J., KIMA, D.-K., LIETO, L., MAASHOA, K., PEÑA, J., SOLANA, R. & COLIGAN, J. 2001. Structure and function of major histocompatibility complex (MHC) class I specific receptors expressed on human natural killer (NK) cells. *Molecular Immunology*, 38, 637-660.
- BOULTER, J. M., GLICK, M., TODOROV, P. T., BASTON, E., SAMI, M., RIZKALLAH, P. & JAKOBSEN, B. K. 2003. Stable, soluble T-cell receptor molecules for crystallization and therapeutics. *Protein Eng*, 16, 707-11.
- BOUWER, H. G., SEAMAN, M. S., FORMAN, J. & HINRICHS, D. J. 1997. MHC class Ib-restricted cells contribute to antilisterial immunity: evidence for Qa-1b as a key restricting element for Listeria-specific CTLs. *J Immunol*, 159, 2795-801.
- BOYINGTON, J., MOTYKA, S., SCHUCK, P., BROOKS, A. G. & SUN, P. 2000. Crystal structure of an NK cell immunoglobulin-like receptor in complex with its class I MHC ligand. *Nature*, 405, 537-543.
- BOYSON, J., ERSKINE, R., WHITMAN, M., CHIU, M., LAU, J., KOOPMAN, L., VALTER, M., ANGELISOVA, P., HOREJSI, V. & STROMINGER, J. 2002. Disulfide bond-mediated dimerisation of HLA-G on the cell surface. *Proceedings of the National Academy of Sciences of the United States of America*, 99, 16180-16185.
- BRAUD, V., ALLAN, D., O'CALLAGHAN, C., SODERSTROM, K., D'ANDREA, A., OGG, G., LAZETIC, S., YOUNG, N., BELL, J., PHILLIPS, J., LANIER, L. & MCMICHAEL, A. 1998a. HLA-E binds to natural killer cell receptors CD94/NKG2A, B and C. *Nature*, 391, 795-799.
- BRAUD, V., ALLAN, D., WILSON, D. & MCMICHAEL, A. 1998b. TAP- and tapasin-dependent HLA-E surface expression correlates with the binding of an MHC class I leader peptide. *Current Biology*, 8, 1-10.
- BROWN, J. H., JARDETZKY, T. S., GORGA, J. C., STERN, L. J., URBAN, R. G., STROMINGER, J. L. & WILEY, D. C. 1993. Three-dimensional structure of the human class II histocompatibility antigen HLA-DR1. *Nature*, 364, 33-9.
- BRUNGER, A. T. 1988. Crystallographic refinement by simulated annealing. Application to a 2.8 Å resolution structure of aspartate aminotransferase. *J Mol Biol*, 203, 803-16.
- BUKUR, J., REBMANN, V., GROSSE-WILDE, H., LUBOLDT, H., RUEBBEN, H., DREXLER, I., SUTTER, G., HUBER, C. & SELIGER, B. 2003. Functional Role of Human Leukocyte Antigen-G Up-Regulation in Renal Cell Carcinoma. *Cancer Research*, 63, 4107-4111.
- BURROWS, J. M., WYNN, K. K., TYNAN, F. E., ARCHBOLD, J., MILES, J. J., BELL, M. J., BRENNAN, R. M., WALKER, S., MCCLUSKEY, J., ROSSJOHN, J., KHANNA, R. & BURROWS, S. R. 2007. The impact of HLA-B micropolymorphism outside primary peptide anchor pockets on the CTL response to CMV. *Eur J Immunol*, 37, 946-53.

- BURROWS, S. R., CHEN, Z., ARCHBOLD, J. K., TYNAN, F. E., BEDDOE, T., KJER-NIELSEN, L., MILES, J. J., KHANNA, R., MOSS, D. J., LIU, Y. C., GRAS, S., KOSTENKO, L., BRENNAN, R. M., CLEMENTS, C. S., BROOKS, A. G., PURCELL, A. W., MCCLUSKEY, J. & ROSSJOHN, J. 2010. Hard wiring of T cell receptor specificity for the major histocompatibility complex is underpinned by TCR adaptability. *Proc Natl Acad Sci U S A*, 107, 10608-13.
- BUSLEPP, J., WANG, H., BIDDISON, W. E., APPELLA, E. & COLLINS, E. J. 2003. A correlation between TCR Valpha docking on MHC and CD8 dependence: implications for T cell selection. *Immunity*, 19, 595-606.
- CANTONI, C., FALCO, M., PESSINO, A., MORETTA, A., MORETTA, L. & BIASSONI, R. 1999. P49, a putative HLA-G1 specific inhibitory NK receptor belonging to the immunoglobulin Superfamily. *J Reprod Immunol*, 43, 157-65.
- CAROSELLA, E. D., MOREAU, P., LE MAOULT, J., LE DISCORDE, M., DAUSSET, J. & ROUAS-FREISS, N. 2003. HLA-G molecules: from maternal-fetal tolerance to tissue acceptance. *Adv Immunol*, 81, 199-252.
- CARROLL, M. 2004. The complement system in regulation of adaptive immunity. *Nature Immunology*, 5, 981-6.
- CASTELLINO, F., ZHONG, G. & GERMAIN, R. 1997. Antigen presentation by MHC Class II molecules: invariant chain function, protein trafficking, and the molecular basis of diverse determinant capture. *Human Immunology*, 54, 159-69.
- CASTRO, M. 2000. Homozygous HLA-G*0105N healthy individuals indicate that membrane-anchored HLA-G1 molecule is not necessary for survival. *Tissue Antigens*, 56, 232-239.
- CHEN, V. B., ARENDALL, W. B., 3RD, HEADD, J. J., KEEDY, D. A., IMMORMINO, R. M., KAPRAL, G. J., MURRAY, L. W., RICHARDSON, J. S. & RICHARDSON, D. C. 2010. MolProbity: all-atom structure validation for macromolecular crystallography. *Acta Crystallogr D Biol Crystallogr*, 66, 12-21.
- CHIANG, E. Y. & STROYNOWSKI, I. 2004. A nonclassical MHC class I molecule restricts CTL-mediated rejection of a syngeneic melanoma tumor. *J Immunol*, 173, 4394-401.
- CHIANG, E. Y. & STROYNOWSKI, I. 2005. Protective immunity against disparate tumors is mediated by a nonpolymorphic MHC class I molecule. *J Immunol*, 174, 5367-74.
- CHICZ, R. M., URBAN, R. G., LANE, W. S., GORGA, J. C., STERN, L. J., VIGNALI, D. A. & STROMINGER, J. L. 1992. Predominant naturally processed peptides bound to HLA-DR1 are derived from MHC-related molecules and are heterogeneous in size. *Nature*, 358, 764-8.
- CHUN, T., ALDRICH, C. J., BALDEON, M. E., KAWCZYNSKI, L. V., SOLOSKI, M. J. & GASKINS, H. R. 1998. Constitutive and regulated expression of the class IB molecule Qa-1 in pancreatic beta cells. *Immunology*, 94, 64-71.
- CHUN, T., SERBINA, N. V., NOLT, D., WANG, B., CHIU, N. M., FLYNN, J. L. & WANG, C. R. 2001. Induction of M3-restricted cytotoxic T lymphocyte responses by N-formylated peptides derived from Mycobacterium tuberculosis. *J Exp Med*, 193, 1213-20.

- CLEMENTS, C., KJER-NIELSEN, L., MCCLUSKEY, J. & ROSSJOHN, J. 2007. Structural Studies on HLA-G: Implications for Ligand and Receptor Binding. *Human Immunology*, 68, 220-226.
- CLEMENTS, C. S., DUNSTONE, M. A., MACDONALD, W., MCCLUSKEY, J. & ROSSJOHN, J. 2006. Specificity on a knife-edge: the alphabeta T cell receptor. *Current Opinion in Structural Biology*, 16, 1-9.
- CLEMENTS, C. S., KJER-NIELSEN, L., KOSTENKO, L., HOARE, H. L., DUNSTONE, M. A., MOSES, E., FREED, K., BROOKS, A. G., ROSSJOHN, J. & MCCLUSKEY, J. 2005. Crystal structure of HLA-G: a nonclassical MHC class I molecule expressed at the fetal-maternal interface. *Proceedings of the National Academy of Sciences of the United States of America*, 102, 3360-5.
- COLLABORATIVE COMPUTATIONAL PROJECT, N. 1994. The CCP4 suite: programs for protein crystallography. *Acta Crystallographica Sect D Biological Crystallography*, 50, 760-763.
- COLONNA, M., NAKAJIMA, H. & CELLA, M. 1999. Inhibitory and activating receptors involved in immune surveillance by human NK and myeloid cells. *Journal of Leukocyte Biology*, 66, 718-22.
- COMISKEY, M., GOLDSTEIN, C., DE FAZIO, S., MAMMOLENTI, M., NEWMARK, J. & WARNER, C. 2003. Evidence that HLA-G is the functional homolog of mouse Qa-2, the Ped gene product. *Human Immunology*, 64, 999-1004.
- CONTINI, P., GHIO, M., POGGI, A., FILACI, G., INDIVERI, F., FERRONE, S. & PUPPO, F. 2003. Soluble HLA-A, -B, -C and -G molecules induce apoptosis in T and NK CD8+ cells and inhibit cytotoxic T cell activity through CD8 ligation. *European Journal of Immunology*, 33, 125-134.
- CRESSWELL, P., BLUM, J. S., KELNER, D. N. & MARKS, M. S. 1987. Biosynthesis and processing of class II histocompatibility antigens. *Crit Rev Immunol*, 7, 31-53.
- DAVIES, A., KALB, S., LIANG, B., ALDRICH, C., LEMONNIER, F., JIANG, H., COTTER, R. & SOLOSKI, M. 2003. A Peptide from Heat Shock Protein 60 is the Dominant Peptide Bound to Qa-1 in the Absence of the MHC Class Ia Leader Sequence Peptide Qdm. *Journal of Immunology*, 170, 5027-5033.
- DAVIES, B., HIBY, S., GARDNER, L., LOKE, Y. & KING, A. 2001. HLA-G Expression by Tumors. *American Journal of Reproductive Immunology*, 45, 103-107.
- DECLoux, A., WOODS, A., COTTER, R., SOLOSKI, M. & FORMAN, J. 1997. Dominance of a Single Peptide Bound to the Class Ib Molecule, Qa-1b. *Journal of Immunology*, 158, 2183-2191.
- DIEHL, M., MUNZ, C., KEILHOLZ, W., STEVANOVIC, S., HOLMES, N., LOKE, Y. & RAMMENSEE, H.-G. 1996. Nonclassical HLA-G molecules are classical peptide presenters. *Current Biology*, 6, 305-314.
- DING, Y., SUMITRAN, S. & HOLGERSSON, J. 1999. Direct binding of purified HLA class I antigens by soluble NKG2/CD94 C-type lectins from natural killer cells. *Scandinavian Journal of Immunology*, 49, 459-465.
- ELLIS, S., PALMER, M. & AJ, M. 1990. Human trophoblast and the choriocarcinoma cell line BeWo express a truncated HLA Class I molecule. *Journal of Immunology*, 144, 731-735.
- EMSLEY, P. & COWTAN, K. 2004. Coot: model-building tools for molecular graphics. *Acta Crystallogr D Biol Crystallogr*, 60, 2126-32.

- FAN, Q., MOSYAK, L., WINTER, C., WAGTMANN, N., LONG, E. & WILEY, D. 1997. Structure of the inhibitory receptor for human natural killer cells resembles haematopoietic receptors. *Nature*, 389, 96-100.
- FAN, Q. R., LONG, E. O. & WILEY, D. C. 2001. Crystal structure of the human natural killer cell inhibitory receptor KIR2DL1-HLA-Cw4 complex. *Nat Immunol*, 2, 452-60.
- FANG, M., ORR, M. T., SPEE, P., EGEBJERG, T., LANIER, L. L. & SIGAL, L. J. 2011. CD94 is essential for NK cell-mediated resistance to a lethal viral disease. *Immunity*, 34, 579-89.
- FAURE, M., BARBER, D., TAKAHASHI, S., JIN, T. & LONG, E. 2003. Spontaneous Clustering and Tyrosine Phosphorylation of NK Cell Inhibitory Receptor Induced by Ligand Binding. *Journal of Immunology*, 170, 6107-6114.
- FAURE, M. & LONG, E. 2002. KIR2DL4 (CD158d), and NK Cell-Activating Receptor with Inhibitory Potential. *Journal of Immunology*, 168, 6208-14.
- FINK, P. J. & BEVAN, M. J. 1978. H-2 antigens of the thymus determine lymphocyte specificity. *J Exp Med*, 148, 766-75.
- FORTE, P., MATTER-REISSMANN, U., STRASSER, M., SCHNEIDER, M. & SEEBACH, J. 2000. Porcine aortic endothelial cells transfected with HLA-G are partially protected from xenogeneic human NK cytotoxicity. *Human Immunology*, 61, 1066-73.
- FORTE, P., PAZMANY, L., MATTER-REISSMANN, U., STUSSI, G., SCHNEIDER, M. & SEEBACH, J. 2001. HLA-G inhibits rolling adhesion of activated human NK cells on porcine endothelial cells. *Journal of Immunology*, 167, 6002-6008.
- FOURNEL, S., AGUERRE-GIRR, M., HUC, X., LENFANT, F., ALAM, A., TOUBERT, A., BENSUSSAN, A. & LE BOUTEILLER, P. 2000. Cutting edge: soluble HLA-G1 triggers CD95/CD95 ligand-mediated apoptosis in activated CD8+ cells by interacting with CD8. *Journal of Immunology*, 164, 6100-6104.
- FU, L., HAZES, B. & BURSHTYN, D. N. 2011. The first Ig domain of KIR3DL1 contacts MHC class I at a secondary site. *J Immunol*, 187, 1816-25.
- GARBOCZI, D. N., HUNG, D. T. & WILEY, D. C. 1992. HLA-A2-peptide complexes: refolding and crystallization of molecules expressed in *Escherichia coli* and complexed with single antigenic peptides. *Proc Natl Acad Sci U S A*, 89, 3429-33.
- GARCIA, K., TEYTON, L. & WILSON, I. 1999. Structural Basis of T Cell Recognition. *Annual Review of Immunology*, 17, 369-397.
- GARCIA, K. C., ADAMS, J. J., FENG, D. & ELY, L. K. 2009. The molecular basis of TCR germline bias for MHC is surprisingly simple. *Nat Immunol*, 10, 143-7.
- GARDINER, C. 2008. Killer cell immunoglobulin-like receptors on NK cells: the how, where and why. *International Journal of Immunogenetics*, 35, 1-8.
- GARNER, L., SALIM, M., MOHAMMED, F. & WILLCOX, B. 2006. Expression, purification and refolding of the myeloid inhibitory receptor leukocyte immunoglobulin-like receptor-5 for structural and ligand identification studies. *Protein Expression and Purification*, 47, 490-7.
- GARRETT, T. P., SAPER, M. A., BJORKMAN, P. J., STROMINGER, J. L. & WILEY, D. C. 1989. Specificity pockets for the side chains of peptide antigens in HLA-Aw68. *Nature*, 342, 692-6.

- GERAGHTY, D. E., STOCKSCHLEADER, M., ISHITANI, A. & HANSEN, J. A. 1992. Polymorphism at the HLA-E locus predates most HLA-A and -B polymorphism. *Hum Immunol*, 33, 174-84.
- GODFREY, D. I., ROSSJOHN, J. & MCCLUSKEY, J. 2008. The fidelity, occasional promiscuity, and versatility of T cell receptor recognition. *Immunity*, 28, 304-14.
- GRAS, S., BURROWS, S. R., KJER-NIELSEN, L., CLEMENTS, C. S., LIU, Y. C., SULLIVAN, L. C., BELL, M. J., BROOKS, A. G., PURCELL, A. W., MCCLUSKEY, J. & ROSSJOHN, J. 2009a. The shaping of T cell receptor recognition by self-tolerance. *Immunity*, 30, 193-203.
- GRAS, S., SAULQUIN, X., REISER, J. B., DEBEAUPUIS, E., ECHASSERIEAU, K., KISSENPFENNIG, A., LEGOUX, F., CHOUQUET, A., LE GORREC, M., MACHILLOT, P., NEVEU, B., THIELENS, N., MALISSEN, B., BONNEVILLE, M. & HOUSSET, D. 2009b. Structural bases for the affinity-driven selection of a public TCR against a dominant human cytomegalovirus epitope. *J Immunol*, 183, 430-7.
- GRAS, S., CHEN, Z., MILES, J. J., LIU, Y. C., BELL, M. J., SULLIVAN, L. C., KJER-NIELSEN, L., BRENNAN, R. M., BURROWS, J. M., NELLER, M. A., KHANNA, R., PURCELL, A. W., BROOKS, A. G., MCCLUSKEY, J., ROSSJOHN, J. & BURROWS, S. R. 2010. Allelic polymorphism in the T cell receptor and its impact on immune responses. *J Exp Med*, 207, 1555-67.
- GROS, F., SEBTI, Y., DE GUIBERT, S., BRANGER, B., BERNARD, M., FAUCHET, R. & AMIOT, L. 2006. Soluble HLA-G Molecules Are Increased during Acute Leukemia, Especially in Subtypes Affecting Monocytic and Lymphoid Lineages. *Neoplasia*, 8, 223-230.
- GUETHLEIN, L. A., OLDER AGUILAR, A. M., ABI-RACHED, L. & PARHAM, P. 2007. Evolution of killer cell Ig-like receptor (KIR) genes: definition of an orangutan KIR haplotype reveals expansion of lineage III KIR associated with the emergence of MHC-C. *J Immunol*, 179, 491-504.
- HANSEL, D., RAHMAN, A., WILENTZ, R., SHIH, I., MCMASTER, M., YEO, C. & MAITRA, A. 2005. HLA-G upregulation in pre-malignant and malignant lesions of the gastrointestinal tract. *International Journal of Gastrointestinal Cancer*, 35, 15-23.
- HE, X., TABACZEWSKI, P., HO, J., STROYNOWSKI, I. & GARCIA, K. 2001. Promiscuous antigen presentation by the nonclassical MHC Ib Qa-2 is enabled by a shallow, hydrophobic groove and self-stabilized peptide conformation. *Structure*, 9, 1213-1224.
- HEINZEL, A., GROTZKE, J., LINES, R., LEWINSOHN, D., MCNABB, A., STREBLOW, D., BRAUD, V., GRIESER, H., BELISLE, J. & LEWINSOHN, D. 2002. HLA-E-dependent Presentation of Mtb-derived Antigen to Human CD8+ T Cells. *Journal of Experimental Medicine*, 196, 1473-1481.
- HOARE, H. L., SULLIVAN, L. C., CLEMENTS, C. S., ELY, L. K., BEDDOE, T., HENDERSON, K. N., LIN, J., REID, H. H., BROOKS, A. G. & ROSSJOHN, J. 2008. Subtle changes in peptide conformation profoundly affect recognition of the non-classical MHC class I molecule HLA-E by the CD94-NKG2 natural killer cell receptors. *J Mol Biol*, 377, 1297-303.
- HOARE, H. L., SULLIVAN, L. C., PIETRA, G., CLEMENTS, C. S., LEE, E. J., ELY, L. K., BEDDOE, T., FALCO, M., KJER-NIELSEN, L., REID, H. H., MCCLUSKEY, J., MORETTA, L., ROSSJOHN, J. & BROOKS, A. G. 2006.

- Structural basis for a major histocompatibility complex class Ib-restricted T cell response. *Nat Immunol*, 7, 256-64.
- HORUZSKO, A., LENFANT, F., MUNN, D. & MELLOR, A. 2001. Maturation of antigen-presenting cells is compromised in HLA-G transgenic mice. *International Immunology*, 13, 385-94.
- ISHITANI, A., KISHIDA, M., SAGESHIMA, N., YASHIKI, S., SONODA, S., HAYAMI, M., SMITH, A. & HATAKE, K. 1999. Re-examination of HLA-G polymorphism in African Americans. *Immunogenetics*, 49, 808-811.
- ISHITANI, A., SAGESHIMA, N., LEE, N., DOROFEEVA, N., HATAKE, K., MARQUADT, H. & GERAGHTY, D. 2003. Protein Expression and Peptide Binding Suggest Unique and Interacting Functional Roles for HLA-E, F, and G in Maternal-Placental Immune Recognition. *Journal of Immunology*, 171, 1376-1384.
- JOYCE, S., TABACZEWSKI, P., ANGELETTI, R. H., NATHENSON, S. G. & STROYNOWSKI, I. 1994. A nonpolymorphic major histocompatibility complex class Ib molecule binds a large array of diverse self-peptides. *J Exp Med*, 179, 579-88.
- KAISER, B., BARAHMAND-POUR, F., PAULSENE, W., MEDLEY, S., GERAGHTY, D. & STRONG, R. 2005. Interactions between NKG2x immunoreceptors and HLA-E ligands display overlapping affinities and thermodynamics. *Journal of Immunology*, 174, 2878-84.
- KAISER, B. K., PIZARRO, J. C., KERNS, J. & STRONG, R. K. 2008. Structural basis for NKG2A/CD94 recognition of HLA-E. *Proc Natl Acad Sci U S A*, 105, 6696-701.
- KAUFMAN, J., AUFFRAY, C., KORMAN, A., SHACKELFORD, D. & STROMINGER, J. 1984. The Class II Molecules of the Human and Murine Major Histocompatibility Complex. *Cell*, 36, 1-13.
- KHAKOO, S., GELLER, R., SHIN, S., JENKINS, J. & PARHAM, P. 2002. The D0 domain of KIR3D acts as a major histocompatibility complex class I binding enhancer. *Journal of Experimental Medicine*, 196, 911-921.
- KIKUCHI-MAKI, A., CATINA, T. & CAMPBELL, K. 2005. Cutting Edge: KIR2DL4 Transduces Signals into Human NK Cells through Association with the Fc Receptor gamma Protein. *Journal of Immunology*, 174, 3859-63.
- KIKUCHI-MAKI, A., YUSA, S.-I., CATINA, T. & CAMPBELL, K. 2003. KIR2DL4 is an IL-2-Regulated NK Cell Receptor That Exhibits Limited Expression in Humans but Triggers Strong IFN-gamma Production. *Journal of Immunology*, 171, 3415-25.
- KING, A., HIBY, S., GARDNER, L., JOSEPH, S., BOWEN, J., VERMA, S., BURROWS, T. & LOKE, Y. 2000. Recognition of Trophoblast HLA Class I Molecules by Decidual NK Cell Receptors - A Review. *Placenta*, 21, Supplement A, S81-S85.
- KJER-NIELSEN, L., CLEMENTS, C. S., PURCELL, A., BROOKS, A. G., WHISSTOCK, J., BURROWS, S., MCCLUSKEY, J. & ROSSJOHN, J. 2003. Structural Basis for the Selection of Dominant alphabeta T Cell Receptors in Antiviral Immunity. *Immunity*, 18, 53-64.
- KJER-NIELSEN, L., CLEMENTS, C. S., BROOKS, A. G., PURCELL, A. W., MCCLUSKEY, J. & ROSSJOHN, J. 2002. The 1.5 Å crystal structure of a highly selected antiviral T cell receptor provides evidence for a structural basis of immunodominance. *Structure*, 10, 1521-32.

- KLEINBERG, L., FLORENES, V., SKREDE, M., DONG, H., NIELSEN, S., MCMASTER, M., NESLAND, J., SHIH, I. & DAVIDSON, B. 2006. Expression of HLA-G in malignant mesothelioma and clinically aggressive breast carcinoma. *Virchows Archiv*, 449, 31-9.
- KLEYWEGT, G. J. 1996. Use of non-crystallographic symmetry in protein structure refinement. *Acta Crystallogr D Biol Crystallogr*, 52, 842-57.
- KOLLER, B., GERAGHTY, D., SHIMIZU, Y., DEMARS, R. & ORR, H. 1988. HLA-E: A Novel HLA Class I Gene Expressed in Resting T Lymphocytes. *Journal of Immunology*, 141, 897-904.
- KONAREV, P. V., VOLKOV, V. V., SOKOLOVA, A. V., KOCH, M. H. & SVERGUN, D. 2003. PRIMUS: a Windows PC-based system for small-angle scattering data analysis. *Journal of Applied Crystallography*, 36, 1277-1282.
- LAWLOR, D. A., ZEMMOUR, J., ENNIS, P. D. & PARHAM, P. 1990. Evolution of class-I MHC genes and proteins: from natural selection to thymic selection. *Annu Rev Immunol*, 8, 23-63.
- LE BOUTEILLER, P., SOLIER, C., PROLL, J., AGUERRE-GIRR, M., FOURNEL, S. & LENFANT, F. 1999. Placental HLA-G protein expression in vivo: where and what for? *Human Reproduction Update*, 5, 223-33.
- LEE, N., GOODLETT, D., ISHITANI, A., MARQUARDT, H. & GERAGHTY, D. 1998a. HLA-E Surface Expression Depends on Binding of TAP-Dependent Peptides Derived from Certain HLA Class I Signal Sequences. *Journal of Immunology*, 160, 4951-4960.
- LEE, N., LLANO, M., CARRETERO, M., ISHITANI, A., NAVARRO, F., LOPEZ-BOTET, M. & GERAGHTY, D. 1998b. HLA-E is a major ligand for the natural killer inhibitory receptor CD94/NKG2A. *Proceedings of the National Academy of Sciences of the United States of America*, 95, 5199-5204.
- LEE, N., MALACKO, A., ISHITANI, A., CHEN, M.-C., BAJORATH, J., MARQUADT, H. & GERAGHTY, D. 1995. The Membrane-Bound and Soluble Forms of HLA-G Bind Identical Sets of Endogenous Peptides but Differ with Respect to TAP Association. *Immunity*, 3, 591-600.
- LEIDEN, J. M. & STROMINGER, J. L. 1986. Generation of diversity of the beta chain of the human T-lymphocyte receptor for antigen. *Proc Natl Acad Sci U S A*, 83, 4456-60.
- LELEU, X., LE FRIEC, G., FACON, T., AMIOT, L., FAUCHET, R., HENNACHE, B., COITEUX, V., YAKOUB-AGHA, I., DUBUCQUOI, S., AVET-LOISEAU, H., MATHIOT, C., BATAILLE, R. & MARY, J. 2005. Total soluble HLA class I and soluble HLA-G in multiple myeloma and monoclonal gammopathy of undetermined significance. *Clinical Cancer Research*, 11, 7297-303.
- LENFANT, F., PIZZATO, N., LIANG, S., DAVRINCHE, C., LE BOUTEILLER, P. & HORUZSKO, A. 2003. Induction of HLA-G-restricted human cytomegalovirus pp65 (UL83)-specific cytotoxic T lymphocytes in HLA-G transgenic mice. *Journal of General Virology*, 84, 307-317.
- LESLIE, A. 1992. MOSFLM. *Joint CCP4 & ESF-EAMCB Newsletter on Protein Crystallography*, No. 26. Recent changes to the MOSFLM package for processing film and image plate data.
- LILA, N., AMREIN, C., GUILLEMAIN, R., CHEVALIER, P., LATREMOUILLE, C., FABIANI, J., DAUSSET, J., CAROSELLA, E. D. & CARPENTIER, A. 2002. Human leukocyte antigen-G expression after heart transplantation is

- associated with a reduced incidence of rejection. *Circulation*, 105, 1949-1954.
- LILA, N., CARPENTIER, A., AMREIN, C., KHALIL-DAHER, I., DAUSSET, J. & CAROSELLA, E. D. 2000. Implication of HLA-G molecule in heart-graft acceptance. *Lancet*, 355, 2138.
- LILA, N., ROUAS-FREISS, N., DAUSSET, J., CARPENTIER, A. & CAROSELLA, E. 2001. Soluble HLA-G protein secreted by allo-specific CD4⁺ T cells suppresses the allo-proliferative response: a CD4⁺ T cell regulatory mechanism. *Proceedings of the National Academy of Sciences of the United States of America*, 98, 12150-5.
- LINDAHL, K. F., DABHI, V. M., HOVIK, R., SMITH, G. P. & WANG, C. R. 1995. Presentation of N-formylated peptides by H2-M3. *Biochem Soc Trans*, 23, 669-74.
- LJUNGGREN, H. G. & KARRE, K. 1990. In search of the 'missing self': MHC molecules and NK cell recognition. *Immunol Today*, 11, 237-44.
- LO, W.-F., WOODS, A., DECLOUX, A., COTTER, R., METCALF, E. & SOLOSKI, M. 2000. Molecular mimicry mediated by MHC class Ib molecules after infection with Gram-negative pathogens. *Nature Medicine*, 6, 215-218.
- LUCKOW, V. A., LEE, S. C., BARRY, G. F. & OLINS, P. O. 1993. Efficient generation of infectious recombinant baculoviruses by site-specific transposon-mediated insertion of foreign genes into a baculovirus genome propagated in *Escherichia coli*. *J Virol*, 67, 4566-79.
- MACDONALD, W. A., PURCELL, A. W., MIFSUD, N. A., ELY, L. K., WILLIAMS, D. S., CHANG, L., GORMAN, J. J., CLEMENTS, C. S., KJER-NIELSEN, L., KOELLE, D. M., BURROWS, S. R., TAIT, B. D., HOLDSWORTH, R., BROOKS, A. G., LOVRECZ, G. O., LU, L., ROSSJOHN, J. & MCCLUSKEY, J. 2003. A naturally selected dimorphism within the HLA-B44 supertype alters class I structure, peptide repertoire, and T cell recognition. *J Exp Med*, 198, 679-91.
- MADDEN, D. R., GARBOCZI, D. N. & WILEY, D. C. 1993. The antigenic identity of peptide-MHC complexes: a comparison of the conformations of five viral peptides presented by HLA-A2. *Cell*, 75, 693-708.
- MAENAKA, K., JUJI, T., STUART, D. & JONES, E. 1999. Crystal structure of the human p58 killer cell inhibitory receptor (KIR2DL3) specific for HLA-Cw3-related MHC class I. *Structure*, 7, 391-8.
- MALLET, V., BLASCHITZ, A., CRISA, L., SCHMITT, C., FOURNEL, S., KING, A., LOKE, Y., DOHR, G. & LE BOUTEILLER, P. 1999. HLA-G in the human thymus: a subpopulation of medullary epithelial but not CD83⁺. *International Immunology*, 11, 889-898.
- MALLET, V., PROLL, J., SOLIER, C., AGUERRE-GIRR, M., DEROSI, M., LOKE, Y., LENFANT, F. & LE BOUTEILLER, P. 2000. The full length HLA-G1 and no other alternative form of HLA-G is expressed at the cell surface of transfected cells. *Human Immunology*, 61, 212-214.
- MATZINGER, P., ZAMOYSKA, R. & WALDMANN, H. 1984. Self tolerance is H-2-restricted. *Nature*, 308, 738-41.
- MCINTIRE, R. H. & HUNT, J. S. 2005. Antigen presenting cells and HLA-G--a review. *Placenta*, 26 Suppl A, S104-9.
- MICHAELSSON, J., TEIXEIRA DE MATOS, C., ACHOUR, A., LANIER, L., KARRE, K. & SODERSTROM, K. 2002. A signal peptide derived from

- hsp60 binds HLA-E and interferes with CD94/NKG2A recognition. *Journal of Experimental Medicine*, 196, 1403-14.
- MILLER, J. 1993. Self-nonsel self discrimination and tolerance in T and B lymphocytes. *Immunologic Research*, 12, 115-30.
- MILLER, J., WEBER, D., IBEGBU, C., POHL, J., ALTMAN, J. & JENSEN, P. 2003. Analysis of HLA-E Peptide-Binding Specificity and Contact Residues in Bound Peptide Required for Recognition by CD94/NKG2. *Journal of Immunology*, 171, 1369-1375.
- MORETTA, A., BIASSONI, R., BOTTINO, C., MINGARI, M. & MORETTA, L. 2000a. Natural cytotoxicity receptors that trigger human NK-cell-mediated cytotoxicity. *Immunology Today*, 21, 228-34.
- MORETTA, A., BIASSONI, R., BOTTINO, C. & MORETTA, L. 2000b. Surface receptors delivering opposite signals regulate the function of human NK cells. *Seminars in Immunology*, 12, 129-138.
- MOUILLOT, G., MARCOU, C., ZIDI, I., GUILLARD, C., SANGROUBER, D., CAROSELLA, E. D. & MOREAU, P. 2007. Hypoxia modulates HLA-G gene expression in tumor cells. *Hum Immunol*, 68, 277-85.
- MUNRO, A. & BRIGHT, S. 1976. Products of the Major Histocompatibility Complex and their Relationship to the Immune Response. *Nature*, 264, 145-52.
- MUNZ, C., NICKOLAUS, P., LAMMERT, E., PASCOLO, S., STEVANOVIC, S. & RAMMENSEE, H.-G. 1999a. The role of peptide presentation in the physiological function of HLA-G. *Seminars in Cancer Biology*, 9, 47-54.
- MUNZ, C., STEVANOVIC, S. & RAMMENSEE, H.-G. 1999b. Peptide presentation and NK inhibition by HLA-G. *Journal of Reproductive Immunology*, 43, 139-155.
- NATTERMANN, J., NISCHALKE, H. D., HOFMEISTER, V., AHLENSTIEL, G., ZIMMERMANN, H., LEIFELD, L., WEISS, E. H., SAUERBRUCH, T. & SPENGLER, U. 2005a. The HLA-A2 restricted T cell epitope HCV core 35-44 stabilizes HLA-E expression and inhibits cytotoxicity mediated by natural killer cells. *Am J Pathol*, 166, 443-53.
- NATTERMANN, J., NISCHALKE, H. D., HOFMEISTER, V., KUPFER, B., AHLENSTIEL, G., FELDMANN, G., ROCKSTROH, J., WEISS, E. H., SAUERBRUCH, T. & SPENGLER, U. 2005b. HIV-1 infection leads to increased HLA-E expression resulting in impaired function of natural killer cells. *Antivir Ther*, 10, 95-107.
- OBER, C., ALDRICH, C., CHERVONEVA, I., BILLSTRAND, C., RAHIMOV, F., GRAY, H. & HYSLOP, T. 2003. Variation in the HLA-G Promoter Region Influences Miscarriage Rates. *American Journal of Human Genetics*, 72, 1425-1435.
- O'CALLAGHAN, C., TORMO, J., WILLCOX, B., BRAUD, V., JAKOBSEN, B., STUART, D., MCMICHAEL, A., BELL, J. & JONES, E. 1998. Structural features impose tight peptide binding specificity in the nonclassical MHC molecule HLA-E. *Molecular Cell*, 1, 531-541.
- O'CONNOR, G., HART, O. & GARDINER, C. 2006. Putting the Natural Killer Cell in its Place. *Immunology*, 117, 1-10.
- ORR, H., BACH, F., PLOEGH, H., STROMINGER, J., KAVATHAS, P. & DEMARS, R. 1982. Use of HLA loss mutants to analyse the structure of the human major histocompatibility complex. *Nature*, 296, 454-6.

- PAINTER, J. & MERRITT, E. A. 2006. Optimal description of a protein structure in terms of multiple groups undergoing TLS motion. *Acta Crystallogr D Biol Crystallogr*, 62, 439-50.
- PANGAULT, C., LE FRIEC, G., CAULET-MAUGENDRE, S., LENA, H., AMIOT, L., GUILLOUX, V., ONNO, M. & FAUCHET, R. 2002. Lung Macrophages and Dendritic Cells Express HLA-G Molecules in Pulmonary Diseases. *Human Immunology*, 63, 83-90.
- PAUL, P., ROUAS-FREISS, N., KHALIL-DAHER, I., MOREAU, P., RITEAU, B., ANNE LE GAL, F., FRANCOISE AVRIL, M., DAUSSET, J., GUILLET, J. G. & CAROSELLA, E. D. 1998. HLA-G expression in melanoma: A way for tumor cells to escape from immunosurveillance. *Proceedings of the National Academy of Sciences of the United States of America*, 95, 4510-4515.
- PETRIE, E. J., CLEMENTS, C. S., LIN, J., SULLIVAN, L. C., JOHNSON, D., HUYTON, T., HEROUX, A., HOARE, H. L., BEDDOE, T., REID, H. H., WILCE, M. C., BROOKS, A. G. & ROSSJOHN, J. 2008. CD94-NKG2A recognition of human leukocyte antigen (HLA)-E bound to an HLA class I leader sequence. *J Exp Med*, 205, 725-35.
- PFEIFFER, K., FIMMERS, R., ENGELS, G., VAN DER VEN, H. & VAN DER VEN, K. 2001. The HLA-G genotype is potentially associated with idiopathic spontaneous abortion. *Molecular Human Reproduction*, 7, 373-378.
- PHILIP, R. & EPSTEIN, L. 1986. Tumour necrosis factor as immunomodulator and mediator of monocyte cytotoxicity induced by itself, gamma-interferon and interleukin-1. *Nature*, 323, 86-89.
- PIETRA, G., ROMAGNANI, C., MAZZARINO, P., FALCO, M., MILLO, E., MORETTA, A., MORETTA, L. & MINGARI, M. 2003. HLA-E-restricted recognition of cytomegalovirus-derived peptides by human CD8+ cytolytic T lymphocytes. *Proceedings of the National Academy of Sciences of the United States of America*, 100, 10896-10901.
- PISTOIA, V., MORANDI, F., WANG, X. & FERRONE, S. 2007. Soluble HLA-G: Are they clinically relevant? *Seminars in Cancer Biology*, 17, 469-79.
- PUTNAM, C. D., HAMMEL, M., HURA, G. L. & TAINER, J. A. 2007. X-ray solution scattering (SAXS) combined with crystallography and computation: defining accurate macromolecular structures, conformations and assemblies in solution. *Q Rev Biophys*, 40, 191-285.
- PYO, C. W., WILLIAMS, L. M., MOORE, Y., HYODO, H., LI, S. S., ZHAO, L. P., SAGESHIMA, N., ISHITANI, A. & GERAGHTY, D. E. 2006. HLA-E, HLA-F, and HLA-G polymorphism: genomic sequence defines haplotype structure and variation spanning the nonclassical class I genes. *Immunogenetics*, 58, 241-51.
- RAFF, M. 1973. T and B lymphocytes and immune responses. *Nature*, 242, 19-23.
- RAJAGOPALAN, S., FU, J. & LONG, E. 2001. Cutting Edge: Induction of IFN-gamma Production but Not Cytotoxicity by the Killer Cell Ig-Like Receptor KIR2DL4 (CD158d) in Resting NK Cells. *Journal of Immunology*, 167, 1877-81.
- RAJAGOPALAN, S. & LONG, E. 1999. A Human Histocompatibility Leukocyte Antigen (HLA)-G-specific Receptor Expressed on All Natural Killer Cells. *Journal of Experimental Medicine*, 189, 1093-1099.
- RAJAGOPALAN, S. & LONG, E. O. 2005. Understanding how combinations of HLA and KIR genes influence disease. *J Exp Med*, 201, 1025-9.

- RAMMENSEE, H. G. & BEVAN, M. J. 1984. Evidence from in vitro studies that tolerance to self antigens is MHC-restricted. *Nature*, 308, 741-4.
- RAMMENSEE, H., FALK, K. & ROTZSCHKE, O. 1993. Peptides naturally presented by MHC class I molecules. *Annual Review of Immunology*, 11, 213-44.
- REBMANN, V., REGEL, J., STOLKE, D. & GROSSE-WILDE, H. 2003. Secretion of sHLA-G molecules in malignancies. *Seminars in Cancer Biology*, 13, 371-7.
- ROBINSON, J., WALLER, M. J., PARHAM, P., DE GROOT, N., BONTROP, R., KENNEDY, L. J., STOEHR, P. & MARSH, S. G. 2003. IMGT/HLA and IMGT/MHC: sequence databases for the study of the major histocompatibility complex. *Nucleic Acids Res*, 31, 311-4.
- ROCK, E. P., SIBBALD, P. R., DAVIS, M. M. & CHIEN, Y. H. 1994. CDR3 length in antigen-specific immune receptors. *J Exp Med*, 179, 323-8.
- RODGERS, J. & COOK, R. 2005. MHC Class Ib Molecules Bridge Innate and Acquired Immunity. *Nature Reviews Immunology*, 5, 459-71.
- ROHRLICH, P. S., FAZILLEAU, N., GINHOUX, F., FIRAT, H., MICHEL, F., COCHET, M., LAHAM, N., ROTH, M. P., PASCOLO, S., NATO, F., COPPIN, H., CHARNEAU, P., DANOS, O., ACUTO, O., EHRLICH, R., KANELLOPOULOS, J. & LEMONNIER, F. A. 2005. Direct recognition by alphabeta cytolytic T cells of Hfe, a MHC class Ib molecule without antigen-presenting function. *Proc Natl Acad Sci U S A*, 102, 12855-60.
- ROUAS-FREISS, N., LEMAOULT, J., MOREAU, P., DAUSSET, J. & CAROSELLA, E. D. 2003. HLA-G in Transplantation: A Relevant Molecule for Inhibition of Graft Rejection? *American Journal of Transplantation*, 3, 11-16.
- ROUAS-FREISS, N., MARCHAL, R., KIRSZENBAUM, M., DAUSSET, J. & CAROSELLA, E. D. 1997a. The alpha-1 domain of HLA-G1 and HLA-G2 inhibits cytotoxicity induced by natural killer cells: Is HLA-G the public ligand for natural killer cell inhibitory receptors? *Proceedings of the National Academy of Sciences of the United States of America*, 94, 5249-5254.
- ROUAS-FREISS, N., MARCHAL, R., MENIER, C., DAUSSET, J. & CAROSELLA, E. D. 1997b. Direct evidence to support the role of HLA-G in protecting the fetus from maternal uterine natural killer cytotoxicity. *Proceedings of the National Academy of Sciences of the United States of America*, 94, 11520-11525.
- ROUAS-FREISS, N., MOREAU, P., FERRONE, S. & CAROSELLA, E. D. 2005. HLA-G proteins in cancer: do they provide tumor cells with an escape mechanism? *Cancer Research*, 65, 10139-44.
- RUDOLPH, M., STANFIELD, R. & WILSON, I. 2006. How TcRS bind MHCs, peptides and coreceptors. *Annual Review of Immunology*, 24, 419-466.
- RUDOLPH, M. G. & WILSON, I. A. 2002. The specificity of TCR/pMHC interaction. *Curr Opin Immunol*, 14, 52-65.
- SALERNO-GONCALVES, R., FERNANDEZ-VINA, M., LEWINSOHN, D. & SZTEIN, M. 2004. Identification of a Human HLA-E-Restricted CD8+ T Cell Subset in Volunteers Immunized with Salmonella enterica Serovar Typhi Strain Ty21a Typhoid Vaccine. *Journal of Immunology*, 173, 5852-62.
- SASAKI, H., XU, X. & MOHANAKUMAR, T. 1999. HLA-E and HLA-G expression on porcine endothelial cells inhibit xenoreactive human NK cells

- through CD94/NKG2-dependent and -independent pathways. *Journal of Immunology*, 163, 6301-5.
- SAULQUIN, X., GASTINEL, L. & VIVIER, E. 2003. Crystal structure of the human natural killer cell activating receptor KIR2DS2 (CD158j). *Journal of Experimental Medicine*, 197, 933-8.
- SCHRODINGER LLC. The PyMOL Molecular Graphics System. Version 1.3.
- SEAMAN, M. S., WANG, C. R. & FORMAN, J. 2000. MHC class Ib-restricted CTL provide protection against primary and secondary *Listeria monocytogenes* infection. *J Immunol*, 165, 5192-201.
- SHAWAR, S., VYAS, J., RODGERS, J. & RICH, R. 1994. Antigen Presentation by Major Histocompatibility Complex Class I-b Molecules. *Annual Review of Immunology*, 12, 839-880.
- SHIH, I. 2007. Application of Human Leukocyte Antigen-G Expression in the Diagnosis of Human Cancer. *Human Immunology*, 68, 272-6.
- SHIROISHI, M., KUROKI, K., OSE, T., RASUBALA, L., SIRATORI, I., ARASE, H., TSUMOTO, K., KUMAGAI, I., KOHDA, D. & MAENAKA, K. 2006a. Efficient Leukocyte Ig-Like Receptor Signalling and Crystal Structure of Disulfide-Linked HLA-G Dimer. *Journal of Biological Chemistry*, 281, 10439-10447.
- SHIROISHI, M., KUROKI, K., RASUBALA, L., TSUMOTO, K., KUMAGAI, I., KURIMOTO, E., KATO, K., KOHDA, D. & MAENAKA, K. 2006b. Structural basis for recognition of the nonclassical MHC molecule HLA-G by the leukocyte Ig-like receptor B2 (LILRB2/LIR2/ILT4/CD85d). *Proceedings of the National Academy of Sciences of the United States of America*, 103, 16412-7.
- SHIROISHI, M., KUROKI, K., TSUMOTO, K., YOKOTA, A., SASAKI, T., AMANO, K., SHIMOJIMA, T., SHIRAKIHARA, Y., RASUBALA, L., VAN DER MERWE, P., KUMAGAI, I., KOHDA, D. & MAENAKA, K. 2006c. Entropically Driven MHC Class I Recognition by Human Inhibitory Receptor Leukocyte Ig-like Receptor B1 (LILRB1/ILT2/CD85j). *Journal of Molecular Biology*, 355, 237-248.
- SHIROISHI, M., TSUMOTO, K., AMANO, K., SHIRAKIHARA, Y., COLONNA, M., BRAUD, V., ALLAN, D., MAKADZANGE, A., ROWLAND-JONES, S., WILLCOX, B., JONES, E., VAN DER MERWE, P., KUMAGAI, I. & MAENAKA, K. 2003. Human inhibitory receptors Ig-like transcript 2 (ILT2) and ILT4 compete with CD8 for MHC class I binding and bind preferentially to HLA-G. *Proceedings of the National Academy of Sciences of the United States of America*, 100, 8856-8861.
- SINGER, G., KURMAN, R., MCMASTER, M. & SHIH, I. 2002. HLA-G immunoreactivity is specific for intermediate trophoblast in gestational trophoblastic disease and can serve as a useful marker in differential diagnosis. *American Journal of Surgical Pathology*, 26, 914-20.
- SINGER, G., REBMANN, V., CHEN, Y., LIU, H., ALI, S., REINSBERG, J., MCMASTER, M., PFEIFFER, K., CHAN, D., WARDELMANN, E., GROSSE-WILDE, H., CHENG, C., KURMAN, R. & SHIH, I. 2003. HLA-G is a potential tumor marker in malignant ascites. 2003, 9, 4460-4.
- SNYDER, G., BROOKS, A. & SUN, P. 1999. Crystal structure of the HLA-Cw3 allotype-specific killer cell inhibitory receptor KIR2DL2. *Proceedings of the National Academy of Sciences of the United States of America*, 96, 3864-9.

- SOLOSKI, M. & METCALF, E. 2001. The involvement of class Ib molecules in the host response to infection with Salmonella and its relevance to autoimmunity. *Microbes and Infection*, 3, 1249-1259.
- STEWART-JONES, G. B., MCMICHAEL, A. J., BELL, J. I., STUART, D. I. & JONES, E. Y. 2003. A structural basis for immunodominant human T cell receptor recognition. *Nat Immunol*, 4, 657-663.
- STRONG, R., HOLMES, M., LI, P., BRAUN, L., LEE, N. & GERAGHTY, D. 2003. HLA-E Allelic Variants: Correlating differential expression, peptide affinities, crystal structures, and thermal stabilities. *Journal of Biological Chemistry*, 278, 5082-5090.
- STROYNOWSKI, I., SOLOSKI, M., LOW, M. G. & HOOD, L. 1987. A single gene encodes soluble and membrane-bound forms of the major histocompatibility Qa-2 antigen: anchoring of the product by a phospholipid tail. *Cell*, 50, 759-68.
- STURA, E. & WILSON, I. 1990. Analytical and Production Seeding Techniques. *Methods (Orlando)*, 1, 38-49.
- SULLIVAN, J. M. & SATCHWELL, M. F. 2000. Development of stable cell lines expressing high levels of point mutants of human opsin for biochemical and biophysical studies. *Methods Enzymol*, 315, 30-58.
- SULLIVAN, L. C., CLEMENTS, C. S., ROSSJOHN, J. & BROOKS, A. G. 2008. The major histocompatibility complex class Ib molecule HLA-E at the interface between innate and adaptive immunity. *Tissue Antigens*, 72, 415-24.
- SULLIVAN, L., CLEMENTS, C., BEDDOE, T., JOHNSON, D., HOARE, H., LIN, J., HUYTON, T., HOPKINS, E., REID, H., WILCE, M., KABAT, J., BORREGO, F., COLIGAN, J., ROSSJOHN, J. & BROOKS, A. 2007. The heterodimeric assembly of the CD94-NKG2 receptor family and implications for human leukocyte antigen-E recognition. *Immunity*, 27, 900-11.
- SULLIVAN, L. C., HOARE, H. L., MCCLUSKEY, J., ROSSJOHN, J. & BROOKS, A. G. 2006. A structural perspective on MHC class Ib molecules in adaptive immunity. *Trends Immunol*, 27, 413-20.
- SVERGUN, D. 1992. Determination of the regularization parameter in indirect-transform methods using perceptual criteria. *Journal of Applied Crystallography*, 25, 495-503.
- SVERGUN, D. I. 1999. Restoring low resolution structure of biological macromolecules from solution scattering using simulated annealing. *Biophys J*, 76, 2879-86.
- SVERGUN, D. I., PETOUKHOV, M. V. & KOCH, M. H. 2001. Determination of domain structure of proteins from X-ray solution scattering. *Biophys J*, 80, 2946-53.
- TICKLE, I. J., LASKOWSKI, R. A. & MOSS, D. S. 1998. Rfree and the rfree ratio. I. Derivation of expected values of cross-validation residuals used in macromolecular least-squares refinement. *Acta Crystallogr D Biol Crystallogr*, 54, 547-57.
- TICKLE, I. J., LASKOWSKI, R. A. & MOSS, D. S. 2000. Rfree and the rfree ratio. II. Calculation Of the expected values and variances of cross-validation statistics in macromolecular least-squares refinement. *Acta Crystallogr D Biol Crystallogr*, 56, 442-50.
- TOMASEC, P., BRAUD, V., RICKARDS, C., POWELL, M., MCSHARRY, B., GADOLA, S., CERUNDOLO, V., BORYSIEWICZ, L., MCMICHAEL, A. & WILKINSON, G. 2000. Surface expression of HLA-E, an inhibitor of

- natural killer cells, enhanced by human cytomegalovirus gpUL40. *Science*, 287, 1031.
- TYNAN, F. E., BURROWS, S. R., BUCKLE, A. M., CLEMENTS, C. S., BORG, N. A., MILES, J. J., BEDDOE, T., WHISSTOCK, J. C., WILCE, M. C., SILINS, S. L., BURROWS, J. M., KJER-NIELSEN, L., KOSTENKO, L., PURCELL, A. W., MCCLUSKEY, J. & ROSSJOHN, J. 2005. T cell receptor recognition of a 'super-bulged' major histocompatibility complex class I-bound peptide. *Nat Immunol*, 6, 1114-22.
- UGRINOVIC, S., BROOKS, C. G., ROBSON, J., BLACKLAWS, B. A., HORMAECHE, C. E. & ROBINSON, J. H. 2005. H2-M3 major histocompatibility complex class Ib-restricted CD8 T cells induced by *Salmonella enterica* serovar Typhimurium infection recognize proteins released by *Salmonella* serovar Typhimurium. *Infect Immun*, 73, 8002-8.
- ULBRECHT, M., MAIER, S., HOFMEISTER, V., FALK, C., BROOKS, A. G., MCMASTER, M. & WEISS, E. 2004. Truncated HLA-G Isoforms are Retained in the Endoplasmic Reticulum and Insufficiently Provide HLA-E Ligands. *Human Immunology*, 65, 200-208.
- ULBRECHT, M., MARTINOZZI, S., GRZESCHIK, M., HENGEL, H., ELLWART, J., PLA, M. & WEISS, E. 2000. Cutting Edge: The Human Cytomegalovirus UL40 Gene Product Contains a Ligand for HLA-E and Prevents NK Cell-Mediated Lysis. *Journal of Immunology*, 164, 5019-22.
- ULBRECHT, M., HONKA, T., PERSON, S., JOHNSON, J. P. & WEISS, E. H. 1992. The HLA-E Gene Encodes Two Differentially Regulated Transcripts and a Cell Surface Protein. *Journal of Immunology*, 149, 2945-2953.
- UROSEVIC, M., KEMPF, W., ZAGRODNIK, B., PANIZZON, R., BURG, G. & DUMMER, R. 2005. HLA-G expression in basal cell carcinomas of the skin recurring after radiotherapy. *Clinical & Experimental Dermatology*, 30, 422-5.
- UROSEVIC, M., KURRER, M., KAMARASHEV, J., MUELLER, B., WEDER, W., BURG, G., STAHEL, R., DUMMER, R. & TROJAN, A. 2001. Human leukocyte antigen G up-regulation in lung cancer associates with high-grade histology, human leukocyte antigen class I loss and interleukin-10 production. *American Journal of Pathology*, 159, 817-24.
- UROSEVIC, M., TROJAN, A. & DUMMER, R. 2002. HLA-G and its KIR ligands in cancer - another enigma yet to be solved? *Journal of Pathology*, 196, 252-253.
- VALES-GOMEZ, M., REYBURN, H., ERSKINE, R., LOPEZ-BOTET, M. & STROMINGER, J. 1999. Kinetics and peptide dependency of the binding of the inhibitory NK receptor CD94/NKG2-A and the activating receptor CD94/NKG2-C to HLA-E. *EMBO Journal*, 18, 4250-60.
- VANCE, R., KRAFT, J., ALTMAN, J., JENSEN, P. & RAULET, D. 1998. Mouse CD94/NKG2A Is a Natural Killer Cell Receptor for the Nonclassical Major Histocompatibility Complex (MHC) Class I Molecule Qa-1b. *Journal of Experimental Medicine*, 188, 1841-1848.
- VIVIAN, J. P., DUNCAN, R. C., BERRY, R., O'CONNOR, G. M., REID, H. H., BEDDOE, T., GRAS, S., SAUNDERS, P. M., OLSHINA, M. A., WIDJAJA, J. M., HARPUR, C. M., LIN, J., MALOVESTE, S. M., PRICE, D. A., LAFONT, B. A., MCVICAR, D. W., CLEMENTS, C. S., BROOKS, A. G. & ROSSJOHN, J. 2011. Killer cell immunoglobulin-like receptor 3DL1-mediated recognition of human leukocyte antigen B. *Nature*, 479, 401-5.

- VOLKOV, V. V. & SVERGUN, D. 2003. Uniqueness of ab initio shape determination in small-angle scattering. *Journal of Applied Crystallography*, 36, 860-864.
- WANG, C. R., CASTANO, A. R., PETERSON, P. A., SLAUGHTER, C., LINDAHL, K. F. & DEISENHOFER, J. 1995. Nonclassical binding of formylated peptide in crystal structure of the MHC class Ib molecule H2-M3. *Cell*, 82, 655-64.
- WILLCOX, B., THOMAS, L. & BJORKMAN, P. 2003. Crystal Structure of HLA-A2 bound to LIR-1, a host and viral major histocompatibility complex receptor. *Nature Immunology*, 4, 913-919.
- WILSON, M., TORKAR, M., HAUDE, A., MILNE, S., JONES, T., SHEER, D., BECK, S. & TROWSDALE, J. 2000. Plasticity in the organisation and sequences of human KIR/ILT gene families. *Proceedings of the National Academy of Sciences of the United States of America*, 97, 4778-83.
- YAN, W. H. & FAN, L. A. 2005. Residues Met76 and Gln79 in HLA-G alpha1 domain involve in KIR2DL4 recognition. *Cell Research*, 15, 176-82.
- YEAGER, M., KUMAR, S. & HUGHES, A. 1997. Sequence convergence in the peptide-binding region of primate and rodent MHC class Ib molecules. *Molecular Biology and Evolution*, 14, 1035-41.
- YIE, S. M., LI, L. H., LI, G. M., XIAO, R. & LIBRACH, C. L. 2006a. Progesterone enhances HLA-G gene expression in JEG-3 choriocarcinoma cells and human cytotrophoblasts in vitro. *Hum Reprod*, 21, 46-51.
- YIE, S. M., XIAO, R. & LIBRACH, C. L. 2006b. Progesterone regulates HLA-G gene expression through a novel progesterone response element. *Hum Reprod*, 21, 2538-44.
- YOKOYAMA, W. 1997. The mother-child union: The case of missing-self and protection of the fetus. *Proceedings of the National Academy of Sciences of the United States of America*, 94, 5998-6000.
- YU, Y. R., TIAN, X. H., WANG, Y. & FENG, M. F. 2006. Rapid production of human KIR2DL4 extracellular domain and verification of its interaction with HLA-G. *Biochemistry (Mosc)*, 71 Suppl 1, S60-4, 4-5.
- ZENG, L., SULLIVAN, L. C., VIVIAN, J. P., WALPOLE, N. G., HARPUR, C. M., ROSSJOHN, J., CLEMENTS, C. S. & BROOKS, A. G. 2012. A structural basis for antigen presentation by the MHC class Ib molecule, Qa-1. *J Immunol*, 188, 302-10.
- ZINKERNAGEL, R. M., CALLAHAN, G. N., KLEIN, J. & DENNERT, G. 1978. Cytotoxic T cells learn specificity for self H-2 during differentiation in the thymus. *Nature*, 271, 251-3.

Appendix 1 – Commercial 48- & 96-well Crystallographic Screens

The Sigma-Aldrich Basic Grid for Proteins (Sigma-Aldrich) (48-well)

1. Ca-chloride 0.02M, Na-acetate (pH 4.6) 0.1M, 2-Methyl-2,4-pentanediol 30%
2. K-,Na-tartrate 0.4M
3. NH₄-dihydrogenphosphate 0.4M
4. Tris-HCl (pH 8.5) 0.1M, NH₄-sulfate 2.0M
5. Na-citrate 0.2M, HEPES Na-salt (pH 7.5) 0.1M, 2-Methyl-2,4-pentanediol 30%
6. Mg-chloride 0.2M, Tris-HCl (pH 8.5) 0.1M, PEG 4000 30%
7. Na-cacodylate (pH 6.5) 0.1M, Na-acetate 1.4M
8. Na-citrate 0.2M, Na-cacodylate (pH 6.5) 0.1M, 2-Propanol 30%
9. NH₄-acetate 0.2M, Na-citrate (pH 5.6) 0.1M, PEG 4000 30%
10. NH₄-acetate 0.2M, Na-acetate (pH 4.6) 0.1M, PEG 4000 30%
11. Na-citrate (pH 5.6) 0.1M, NH₄-dihydrogenphosphate 1.0M
12. Mg-chloride 0.2M, HEPES Na-salt (pH 7.5) 0.1M, 2-Propanol 30%
13. Na-citrate 0.2M, Tris-HCl (pH 8.5) 0.1M, PEG 400 30%
14. Ca-chloride 0.2M, HEPES Na-salt (pH 7.5) 0.1M, PEG 400 28%
15. NH₄-sulfate 0.2M, Na-cacodylate (pH 6.5) 0.1M, PEG 8000 30%
16. HEPES Na-salt (pH 7.5) 0.1M, Li-sulfate 1.5M
17. Li-sulfate 0.2M, Tris-HCl (pH 8.5) 0.1M, PEG 4000 30%
18. Mg-acetate 0.2M, Na-cacodylate pH (6.5) 0.1M, PEG 8000 20%
19. NH₄-acetate 0.2M, Tris-HCl (pH 8.5) 0.1M, 2-Propanol 30%
20. NH₄-sulfate 0.2M, Na-acetate (pH 4.6) 0.1M, PEG 4000 25%
21. Mg-acetate 0.2M, Na-cacodylate (pH 6.5) 0.1M, 2-Methyl-2,4-pentanediol 30%
22. Na-acetate 0.2M, Tris-HCl (pH 8.5) 0.1M, PEG 4000 30%
23. Mg-chloride 0.2M, HEPES Na-salt (pH 7.5) 0.1M, PEG 400 30%
24. Ca-chloride 0.2M, Na-acetate (pH 4.6) 0.1M, 2-Propanol 20%
25. Imidazole (pH 6.5) 0.1M, Na-acetate 1M
26. NH₄-acetate 0.2M, Na-citrate (pH 5.6) 0.1M, 2-Methyl-2,4-pentanediol 30%
27. Na-citrate 0.2M, HEPES Na-salt (pH 7.5) 0.1M, 2-Propanol 20%
28. Na-acetate 0.2M, Na-cacodylate pH (6.5) 0.1M, PEG 8000 30%
29. HEPES Na-salt (pH 7.5) 0.1M, K-,Na-tartrate 0.8M
30. NH₄-sulfate 0.2M, PEG 8000 30%
31. NH₄-sulfate 0.2M, PEG 4000 30%

32. NH_4 -sulfate 2M
33. Na-formiate 4M
34. Na-acetate (pH 4.6) 0.1M, Na-formiate 2M
35. HEPES Na-salt (pH 7.5) 0.1M, K-dihydrogenphosphate 0.8M, Na-dihydrogenphosphate 0.8M
36. Tris-HCl (pH 8.5) 0.1M, PEG 8000 8%
37. Na-acetate (pH 4.6) 0.1M, PEG 4000 8%
38. HEPES Na-salt (pH 7.5) 0.1M, Na-citrate 1.4M
39. HEPES Na-salt (pH 7.5) 0.1M, PEG 400 2%, NH_4 -sulfate 2.0M
40. Na-citrate (pH 5.6) 0.1M, 2-Propanol 20%, PEG 4000 20%
41. HEPES Na-salt (pH 7.5) 0.1M, 2-Propanol 10%, PEG 4000 20%
42. K-dihydrogenphosphate 0.05M, PEG 8000 20%
43. PEG 1500 30%
44. Mg-formiate 0.2M
45. Zn-acetate 0.2M, Na-cacodylate (pH 6.5) 0.1M, PEG 8000 18%
46. Ca-acetate 0.2M, Na-cacodylate (pH 6.5) 0.1M, PEG 8000 18%
47. Na-acetate (pH 4.6) 0.1M, NH_4 -sulfate 2.0M
48. Tris-HCl (pH 8.5) 0.1M, NH_4 -dihydrogenphosphate 2.0M

The PEG/Ion Screen (Hampton Research) (48-well)

1. Na-fluoride 0.2M, PEG 3350 20%
2. K-fluoride 0.2M, PEG 3350 20%
3. NH_4 -fluoride 0.2M, PEG 3350 20%
4. Li-chloride 0.2M, PEG 3350 20%
5. Mg-chloride hexahydrate 0.2M, PEG 3350 20%
6. Na-chloride 0.2M, PEG 3350 20%
7. Ca-chloride dihydrate 0.2M, PEG 3350 20%
8. K-chloride 0.2M, PEG 3350 20%
9. NH_4 -chloride 0.2M, PEG 3350 20%
10. Na-iodide 0.2M, PEG 3350 20%
11. K-iodide 0.2M, PEG 3350 20%
12. NH_4 -iodide 0.2M, PEG 3350 20%
13. Na-thiocyanate 0.2M, PEG 3350 20%

14. K-thiocyanate 0.2M, PEG 3350 20%
15. Li-nitrate 0.2M, PEG 3350 20%
16. Mg-nitrate hexahydrate 0.2M, PEG 3350 20%
17. Na-nitrate 0.2M, PEG 3350 20%
18. K-nitrate 0.2M, PEG 3350 20%
19. NH₄-nitrate 0.2M, PEG 3350 20%
20. Mg-formate dihydrate 0.2M, PEG 3350 20%
21. Na-formate 0.2M, PEG 3350 20%
22. K-formate 0.2M, PEG 3350 20%
23. NH₄-formate 0.2M, PEG 3350 20%
24. Li-acetate dihydrate 0.2M, PEG 3350 20%
25. Mg-acetate tetrahydrate 0.2M, PEG 3350 20%
26. Zn-acetate dihydrate 0.2M, PEG 3350 20%
27. Na-acetate trihydrate 0.2M, PEG 3350 20%
28. Ca-acetate hydrate 0.2M, PEG 3350 20%
29. K-acetate 0.2M, PEG 3350 20%
30. NH₄-acetate 0.2M, PEG 3350 20%
31. Li-sulfate monohydrate 0.2M, PEG 3350 20%
32. Mg-sulfate heptahydrate 0.2M, PEG 3350 20%
33. Na-sulfate decahydrate 0.2M, PEG 3350 20%
34. K-sulfate 0.2M, PEG 3350 20%
35. NH₄-sulfate 0.2M, PEG 3350 20%
36. Na-tartrate dibasic dihydrate 0.2M, PEG 3350 20%
37. K-,Na-tartrate tetrahydrate 0.2M, PEG 3350 20%
38. NH₄-tartrate dibasic 0.2M, PEG 3350 20%
39. Na-phosphate monobasic monohydrate 0.2M, PEG 3350 20%
40. Na-phosphate dibasic dihydrate 0.2M, PEG 3350 20%
41. K-phosphate monobasic 0.2M, PEG 3350 20%
42. K-phosphate dibasic 0.2M, PEG 3350 20%
43. NH₄-phosphate monobasic 0.2M, PEG 3350 20%
44. NH₄-phosphate dibasic 0.2M, PEG 3350 20%
45. Li-citrate tribasic tetrahydrate 0.2M, PEG 3350 20%
46. Na-citrate tribasic dihydrate 0.2M, PEG 3350 20%
47. K-citrate tribasic monohydrate 0.2M, PEG 3350 20%

48. NH₄-citrate dibasic 0.2M, PEG 3350 20%

The PACT Suite (Qiagen) (96-well)

1. SPG buffer (pH 4) 0.1M, PEG 1500 25%
2. SPG buffer (pH 5) 0.1M, PEG 1500 25%
3. SPG buffer (pH 6) 0.1M, PEG 1500 25%
4. SPG buffer (pH 7) 0.1M, PEG 1500 25%
5. SPG buffer (pH 8) 0.1M, PEG 1500 25%
6. SPG buffer (pH 9) 0.1M, PEG 1500 25%
7. Na-chloride 0.2M, Na-acetate (pH 5) 0.1M, PEG 6000 20%
8. NH₄-chloride 0.2M, Na-acetate (pH 5) 0.1M, PEG 6000 20%
9. Li-chloride 0.2M, Na-acetate (pH 5) 0.1M, PEG 6000 20%
10. Mg-chloride 0.2M, Na-acetate (pH 5) 0.1M, PEG 6000 20%
11. Ca-chloride 0.2M, Na-acetate (pH 5) 0.1M, PEG 6000 20%
12. Zn-chloride 0.01M, Na-acetate (pH 5) 0.1M, PEG 6000 20%
13. MIB buffer (pH 4) 0.1M, PEG 1500 25%
14. MIB buffer (pH 5) 0.1M, PEG 1500 25%
15. MIB buffer (pH 6) 0.1M, PEG 1500 25%
16. MIB buffer (pH 7) 0.1M, PEG 1500 25%
17. MIB buffer (pH 8) 0.1M, PEG 1500 25%
18. MIB buffer (pH 9) 0.1M, PEG 1500 25%
19. Na-chloride 0.2M, MES (pH 6) 0.1M, PEG 6000 20%
20. NH₄-chloride 0.2M, MES (pH 6) 0.1M, PEG 6000 20%
21. Li-chloride 0.2M, MES (pH 6) 0.1M, PEG 6000 20%
22. Mg-chloride 0.2M, MES (pH 6) 0.1M, PEG 6000 20%
23. Ca-chloride 0.2M, MES (pH 6) 0.1M, PEG 6000 20%
24. Zn-chloride 0.01M, MES (pH 6) 0.1M, PEG 6000 20%
25. PCB buffer (pH 4) 0.1M, PEG 1500 25%
26. PCB buffer (pH 5) 0.1M, PEG 1500 25%
27. PCB buffer (pH 6) 0.1M, PEG 1500 25%
28. PCB buffer (pH 7) 0.1M, PEG 1500 25%
29. PCB buffer (pH 8) 0.1M, PEG 1500 25%
30. PCB buffer (pH 9) 0.1M, PEG 1500 25%
31. Na-chloride 0.2M, Hepes (pH 7) 0.1M, PEG 6000 20%

32. NH₄-chloride 0.2M, Hepes (pH 7) 0.1M, PEG 6000 20%
33. Li-chloride 0.2M, Hepes (pH 7) 0.1M, PEG 6000 20%
34. Mg-chloride 0.2M, Hepes (pH 7) 0.1M, PEG 6000 20%
35. Ca-chloride 0.2M, Hepes (pH 7) 0.1M, PEG 6000 20%
36. Zn-chloride 0.01M, Hepes (pH 7) 0.1M, PEG 6000 20%
37. MMT buffer (pH 4) 0.1M, PEG 1500 25%
38. MMT buffer (pH 5) 0.1M, PEG 1500 25%
39. MMT buffer (pH 6) 0.1M, PEG 1500 25%
40. MMT buffer (pH 7) 0.1M, PEG 1500 25%
41. MMT buffer (pH 8) 0.1M, PEG 1500 25%
42. MMT buffer (pH 9) 0.1M, PEG 1500 25%
43. Na-chloride 0.2M, Tris (pH 8) 0.1M, PEG 6000 20%
44. NH₄-chloride 0.2M, Tris (pH 8) 0.1M, PEG 6000 20%
45. Li-chloride 0.2M, Tris (pH 8) 0.1M, PEG 6000 20%
46. Mg-chloride 0.2M, Tris (pH 8) 0.1M, PEG 6000 20%
47. Ca-chloride 0.2M, Tris (pH 8) 0.1M, PEG 6000 20%
48. Tris (pH 8) 0.1M, PEG 6000 20%
49. Na-fluoride 0.2M, PEG 3350 20%
50. Na-bromide 0.2M, PEG 3350 20%
51. Na-iodide 0.2M, PEG 3350 20%
52. K-thiocyanate 0.2M, PEG 3350 20%
53. Na-nitrate 0.2M, PEG 3350 20%
54. Na-formate 0.2M, PEG 3350 20%
55. Na-acetate 0.2M, PEG 3350 20%
56. Na-sulphate 0.2M, PEG 3350 20%
57. K-,Na-tartrate 0.2M, PEG 3350 20%
58. Na-,K-phosphate 0.2M, PEG 3350 20%
59. Na-citrate 0.2M, PEG 3350 20%
60. Na-malonate 0.2M, PEG 3350 20%
61. Na-fluoride 0.2M, Bis Tris propane (pH 6.5) 0.1M, PEG 3350 20%
62. Na-bromide 0.2M, Bis Tris propane (pH 6.5) 0.1M, PEG 3350 20%
63. Na-iodide 0.2M, Bis Tris propane (pH 6.5) 0.1M, PEG 3350 20%
64. K-thiocyanate 0.2M, Bis Tris propane (pH 6.5) 0.1M, PEG 3350 20%
65. Na-nitrate 0.2M, Bis Tris propane (pH 6.5) 0.1M, PEG 3350 20%

66. Na-formate 0.2M, Bis Tris propane (pH 6.5) 0.1M, PEG 3350 20%
67. Na-acetate 0.2M, Bis Tris propane (pH 6.5) 0.1M, PEG 3350 20%
68. Na-sulphate 0.2M, Bis Tris propane (pH 6.5) 0.1M, PEG 3350 20%
69. K-,Na-tartrate 0.2M, Bis Tris propane (pH 6.5) 0.1M, PEG 3350 20%
70. Na-,K-phosphate 0.2M, Bis Tris propane (pH 6.5) 0.1M, PEG 3350 20%
71. Na-citrate 0.2M, Bis Tris propane (pH 6.5) 0.1M, PEG 3350 20%
72. Na-malonate 0.2M, Bis Tris propane (pH 6.5) 0.1M, PEG 3350 20%
73. Na-fluoride 0.2M, Bis Tris propane (pH 7.5) 0.1M, PEG 3350 20%
74. Na-bromide 0.2M, Bis Tris propane (pH 7.5) 0.1M, PEG 3350 20%
75. Na-iodide 0.2M, Bis Tris propane (pH 7.5) 0.1M, PEG 3350 20%
76. K-thiocyanate 0.2M, Bis Tris propane (pH 7.5) 0.1M, PEG 3350 20%
77. Na-nitrate 0.2M, Bis Tris propane (pH 7.5) 0.1M, PEG 3350 20%
78. Na-formate 0.2M, Bis Tris propane (pH 7.5) 0.1M, PEG 3350 20%
79. Na-acetate 0.2M, Bis Tris propane (pH 7.5) 0.1M, PEG 3350 20%
80. Na-sulphate 0.2M, Bis Tris propane (pH 7.5) 0.1M, PEG 3350 20%
81. K-,Na-tartarte 0.2M, Bis Tris propane (pH 7.5) 0.1M, PEG 3350 20%
82. Na-,K-phosphate 0.2M, Bis Tris propane (pH 7.5) 0.1M, PEG 3350 20%
83. Na-citrate 0.2M, Bis Tris propane (pH 7.5) 0.1M, PEG 3350 20%
84. Na-malonate 0.2M, Bis Tris propane (pH 7.5) 0.1M, PEG 3350 20%
85. Na-fluoride 0.2M, Bis Tris propane (pH 8.5) 0.1M, PEG 3350 20%
86. Na-bromide 0.2M, Bis Tris propane (pH 8.5) 0.1M, PEG 3350 20%
87. Na-iodide 0.2M, Bis Tris propane (pH 8.5) 0.1M, PEG 3350 20%
88. K-thiocyanate 0.2M, Bis Tris propane (pH 8.5) 0.1M, PEG 3350 20%
89. Na-nitrate 0.2M, Bis Tris propane (pH 8.5) 0.1M, PEG 3350 20%
90. Na-formate 0.2M, Bis Tris propane (pH 8.5) 0.1M, PEG 3350 20%
91. Na-acetate 0.2M, Bis Tris propane (pH 8.5) 0.1M, PEG 3350 20%
92. Na-sulphate 0.2M, Bis Tris propane (pH 8.5) 0.1M, PEG 3350 20%
93. K-,Na-tartrate 0.2M, Bis Tris propane (pH 8.5) 0.1M, PEG 3350 20%
94. Na-,K-phosphate 0.2M, Bis Tris propane (pH 8.5) 0.1M, PEG 3350 20%
95. Na-citrate 0.2M, Bis Tris propane (pH 8.5) 0.1M, PEG 3350 20%
96. Na-malonate 0.2M, Bis Tris propane (pH 8.5) 0.1M, PEG 3350 20%

JCSG+ (Qiagen) (96-well)

1. Li-sulphate 0.2M, Na-acetate (pH 4.5) 0.1M, PEG 400 50%
2. tri-Na-citrate (pH 5.5) 0.1M, PEG 3000 20%
3. tri-NH₄-citrate 0.18M, PEG 3350 20%
4. Ca-chloride 0.02M, Na-acetate (pH 4.6) 0.1M, MPD 30%
5. Mg-formate 0.2M, PEG 3350 20%
6. Li-sulphate 0.2M, Phosphate-citrate (pH 4.2) 0.1M, PEG 1000 20%
7. CHES (pH 9.5) 0.1M, PEG 8000 20%
8. NH₄-formate 0.2M, PEG 3350 20%
9. NH₄-chloride 0.2M, PEG 3350 20%
10. K-formate 0.2M, PEG 3350 20%
11. NH₄-phosphate 0.2M, Tris (pH 8.5) 0.1M, MPD 50%
12. K-nitrate 0.2M, PEG 3350 20%
13. NH₄-sulphate 0.8M, Citric acid (pH 3.5) 0.1M
14. Na-thiocyanate 0.2M, PEG 3350 20%
15. BICINE (pH 9.0) 0.1M, PEG 6000 20%
16. HEPES (pH 7.5) 0.1M, PEG 8000 10%, Ethylene glycol 8%
17. Na-cacodylate (pH 6.5) 0.1M, MPD 40%, PEG 8000 5%
18. Phosphate-citrate (pH 4.2) 0.1M, Ethanol 40%, PEG 1000 5%
19. Na-acetate (pH 4.6) 0.1M, PEG 4000 8%
20. Mg-chloride 0.2M, Tris (pH 7.0) 0.1M, PEG 8000 10%
21. Citric acid (pH 4.0) 0.1M, PEG 6000 20%
22. Mg-chloride 0.2M, Na-cacodylate (pH 6.5) 0.1M, PEG 200 50%
23. tri-Na-citrate (pH 6.5) 1.6M
24. tri-K-citrate 0.2M, PEG 3350 20%
25. Na-chloride 0.2M, Phosphate-citrate (pH 4.2) 0.1M, PEG 8000 20%
26. Li-chloride 1M, Citric acid (pH 4.0) 0.1M, PEG 6000 20%
27. NH₄-nitrate 0.2M, PEG 3350 20%
28. HEPES (pH 6.5) 0.1M, PEG 6000 10%
29. Na-phosphate 0.8M, K-phosphate 0.8M, HEPES (pH 7.5) 0.1M
30. Phosphate-citrate (pH 4.2) 0.1M, PEG 300 40%
31. Zn-acetate 0.2M, Na-acetate (pH 4.5) 0.1M, PEG 3000 10%
32. Tris (pH 8.5) 0.1M, Ethanol 20%
33. Na-,K-phosphate (pH 6.2) 0.1M, 1,2 propanediol 25%, Glycerol 10%

34. BICINE (pH 9.0) 0.1M, PEG 20000 10%, 1,4-Dioxane 2%
35. NH₄-sulphate 2M, Na-acetate (pH 4.6) 0.1M
36. PEG 1000 10%, PEG 8000 10%
37. PEG 1500 24%, Glycerol 20%
38. Mg-chloride 0.2M, HEPES (pH 7.5) 0.1M, PEG 400 30%
39. Na-chloride 0.2M, Na-,K-phosphate (pH 6.2) 0.1M, PEG 200 50%
40. Li-sulphate 0.2M, Na-acetate (pH 4.5) 0.1M, PEG 8000 30%
41. HEPES (pH 7.5) 0.1M, MPD 70%
42. Mg-chloride 0.2M, Tris (pH 8.5) 0.1M, PEG 8000 20%
43. Li-sulphate 0.2M, Tris (pH 8.5) 0.1M, PEG 400 40%
44. Tris (pH 8.0) 0.1M, MPD 40%
45. NH₄-sulphate 0.17M, PEG 4000 25.5%, Glycerol 15%
46. Ca-acetate 0.2M, Na-cacodylate (pH 6.5) 0.1M, PEG 300 40%
47. Ca-chloride 0.14M, Na-acetate (pH 4.6) 0.07M, Isopropanol 14%, Glycerol 30%
48. K-phosphate 0.04M, PEG 8000 16%, Glycerol 20%
49. tri-Na-citrate 1M, Na-cacodylate (pH 6.5) 0.1M
50. Na-chloride 0.2M, Na-cacodylate (pH 6.5) 0.1M, NH₄-sulfate 2M
51. Na-chloride 0.2M, HEPES (pH 7.5) 0.1M, Isopropanol 10%
52. Li-sulphate 0.2M, Tris (pH 8.5) 0.1M, NH₄-sulfate 1.26M
53. CAPS (pH 10.5) 0.1M, MPD 40%
54. Zn-acetate 0.2M, Imidazole (pH 8.0) 0.1M, PEG 3000 20%
55. Zn-acetate 0.2M, Na-cacodylate (pH 6.5) 0.1M, Isopropanol 10%
56. di-NH₄-phosphate 1M, Na-acetate (pH 4.5) 0.1M
57. Mg-sulphate 1.6M, MES (pH 6.5) 0.1M
58. BICINE (pH 9.0) 0.1M, PEG 6000 10%
59. Ca-acetate 0.16M, Na-cacodylate (pH 6.5) 0.08M, PEG 8000 14.4%, Glycerol 20%
60. Imidazole (pH 8.0) 0.1M, PEG 8000 10%
61. Cs-chloride 0.05M, MES (pH 6.5) 0.1M, Jeffamine M-600 30%
62. NH₄-sulphate 3.2M, Citric acid (pH 4.0) 0.1M
63. Tris (pH 8.5) 0.1M, MPD 20%
64. HEPES (pH 7.5) 0.1M, Jeffamine M-600 20%
65. Mg-chloride 0.2M, Tris (pH 8.5) 0.1M, Ethylene glycol 50%
66. BICINE (pH 8.5) 0.1M, MPD 10%

67. Succinic acid (pH 7.0) 0.8M
68. DL-Malic acid (pH 7.0) 2.1M
69. Na-malonate (pH 7.0) 2.4M
70. Na-malonate 1.1M, HEPES (pH 7.0) 0.1M, Jeffamine ED-2001 0.5%
71. Succinic acid 1M, HEPES (pH 7.0) 0.1M, PEG MME 2000 1%
72. HEPES (pH 7.0) 0.1M, Jeffamine M-600 30%
73. HEPES (pH 7.0) 0.1M, Jeffamine ED-2001 30%
74. Mg-chloride 0.02M, HEPES (pH 7.5) 0.1M, Polyacrylic acid 5100 22%, sodium salt
75. Co-chloride 0.01M, Tris (pH 8.5) 0.1M, Polyvinylpyrrolidone K15 20%
76. Trimethylamine N-oxide 0.2M, Tris (pH 8.5) 0.1M, PEG MME 2000 20%
77. Co-chloride 0.005M, Cadmium chloride 0.005M, Mg-chloride 0.005M, Nickel chloride 0.005M, HEPES (pH 7.5) 0.1M, PEG 3350 12%
78. Na-malonate (pH 7.0) 0.24M, PEG 3350 20%
79. Succinic acid (pH 7.0) 0.1M, PEG 3350 15%
80. DL-Malic acid (pH 7.0) 0.15M, PEG 3350 20%
81. K-thiocyanate 0.1M, PEG MME 2000 30%
82. K-bromide 0.15M, PEG MME 2000 30%
83. NH₄-sulphate 2M, Bis-Tris (pH 5.5) 0.1M
84. Na-chloride 3M, Bis-Tris (pH 5.5) 0.1M
85. Mg-formate 0.3M, Bis-Tris (pH 5.5) 0.1M
86. NH₄-sulphate 1M, Bis-Tris (pH 5.5) 0.1M, PEG 3350 1%
87. tri-Na-acetate (pH 4.5) 0.1M, Bis-Tris (pH 5.5) 0.1M, PEG 3350 20%
88. Ca-chloride 0.2M, Bis-Tris (pH 5.5) 0.1M, MPD 45%
89. NH₄-acetate 0.2M, Bis-Tris (pH 5.5) 0.1M, MPD 45%
90. NH₄-acetate 0.1M, Bis-Tris (pH 5.5) 0.1M, PEG 10,000 17%
91. NH₄-sulphate 0.2M, Bis-Tris (pH 5.5) 0.1M, PEG 3350 20%
92. Na-chloride 0.2M, Bis-Tris (pH 5.5) 0.1M, PEG 3350 20%
93. Li-sulphate 0.2M, Bis-Tris (pH 5.5) 0.1M, PEG 3350 20%
94. NH₄-acetate 0.2M, Bis-Tris (pH 5.5) 0.1M, PEG 3350 20%
95. Mg-chloride 0.2M, Bis-Tris (pH 5.5) 0.1M, PEG 3350 20%
96. NH₄-acetate 0.2M, HEPES (pH 7.5) 0.1M, MPD